Pulsed flow ultrafiltration in baffled tubular membranes

Finnigan, Sean Matthew

Award date:
1990

Awarding institution:
University of Bath

PULSED FLOW ULTRAFILTRATION IN BAFFLED TUBULAR MEMBRANES

submitted by

Sean Matthew Finnigan

for the degree of PhD
of the University of Bath

1990

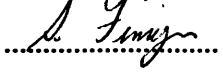

ProQuest LLC
789 East Eisenhower Parkway
P.O. Box 1346
Ann Arbor, MI 48106-1346

DEDICATION

"We are not permitted to choose the frame of our destiny. But what we put into it is ours. He who wills adventure will experience it--according to the measure of his courage. He who wills sacrifice will be sacrificed--according to the measure of his purity of heart" from "Markings" by Dag Hammarskjöld

TO MY FAMILY

ACKNOWLEDGEMENTS

I wish to thank Professor John A Howell for his helpful supervision and friendship during my time at Bath, especially in this final writing up stage where his comments, criticism, encouragement and lucidity have been invaluable.

I am also very grateful for the technical help and advice I have received from people in different departments here at the university. Within the School of Chemical Engineering, I would like to thank John Hubble and particularly Robert Field for their help and advice; John Bishop for his technical assistance and Fernando Acosta for his help with the HPLC. I also would like to thank the Science Schools Workshop staff, especially Jeff Venn, Alan Shave and Mike Lock for their work on the construction of the test apparatus, and the staff in the Photography department, especially Colin Wilson and Trew Mehaffy for their help with the flow visualization work.

I also want to thank my colleagues here in the department for their help and friendship, especially Pierre(in my first year), Neil, Mark, Andy, Fang Ming and Dengxi Wu and in this last year, Mary and Susan; and my friends outside the department, especially Julian and Mario, up in Statistics.

I would like to thank the Commonwealth Scholarship Commission for their financial support which made my stay in Britain possible and also the financial contribution made towards this work by the Membrane Applications Centre.

Finally, I would like to thank my friends here in England and all over the world and especially my family for just being there, physically or in spirit.

CONTENTS

INDEX OF TABLES

INDEX OF FIGURES

ABSTRACT

Concentration polarization and fouling are the major bottlenecks preventing the large scale industrial implementation of membrane technology. One of the common approaches taken to combat concentration polarization and fouling is to improve the hydrodynamic conditions at the membrane surface. This is achieved most simply by operating with turbulent cross-flow or by modification of the channel geometry.

An alternative approach has been taken in this study based on the vortex mixing technique developed by Mackley for enhanced mixing. The feasibility of using periodically spaced baffles of a disc and doughnut shape alone and in combination with pulsed flow in a tubular membrane system has been investigated using a 10-25 gl^{-1} solution of Bipro, a purified 95% whey protein isolate, and FP100 ultrafiltration membranes. Transmembrane pressures up to 5.5 bar and Reynolds numbers corresponding to laminar and turbulent cross-flow rates were investigated using a "snapshot" technique. The fluxes obtained within the baffled systems were compared with a conventional system operating under identical conditions.

A significant improvement in flux was observed with the baffled systems under both steady and pulsed flow conditions. The relative improvement reached a maximum in the Re range 750-2200 and 350-1550 at $C_b = 10$ and 25 gl^{-1} respectively. At a higher Reynolds number of 6450, fluxes were greater than or equal in magnitude to fluxes corresponding to fully turbulent flow conditions(Re = 16000-50000) in a conventional system. In pulsed flow, comparative fluxes could be obtained at relatively low net cross-flow velocities when the pulsed flow Reynolds number, $Re_p = 6450$, where Re_p is calculated from

the maximum velocity in pulsed flow. At P_{tm}=4 bar, fluxes varied from 60-70 $lm^{-2}h^{-1}$ for a conventional system at Re=16000-50000 to 75-95 $lm^{-2}h^{-1}$ for the different disc baffled systems. The "decoupling" of flux from net cross-flow velocity offers the opportunity for use of this system in a single pass, continuous mode of operation for thickening purposes or to avoid the pumping costs associated with recirculation.

The frequency and amplitude needed to be above certain minimum values for an optimum improvement in flux to be observed. At the same Re_p value, it was more effective to improve fluxes using short strokes rather than long strokes, as the frequency was higher in the former situation. In general, a greater improvement in mass transfer, mixing and flux was observed with "short, fast" strokes rather than "long, slow" strokes. Further improvements in flux were obtained by increasing Re_p(higher frequencies and/or amplitudes (lower St)) until the onset of pressure dependent behaviour.

Disc shaped baffles with a centre to centre baffle spacing of 1.6 times the tube diameter were found to give the best all-round performance of the baffled systems investigated. Baffles were shown to be dissipating energy more effectively than a conventional system. An optimum flux/power range was identified for the baffled systems corresponding to Re=700-1450. Within this range, the power consumption was a maximum of 1 Wm^{-2}. Fluxes of similar magnitude could be obtained in a conventional system but only at a much greater power consumption of approximately 20 and 45 Wm^{-2} at P_{tm}=2 and 4 bar respectively.

Flow visualization was used to study the flow patterns in the conventional and baffled systems under pulsed and steady flow conditions. In steady flow, baffles increased local mass transfer rates by promoting turbulence and interrupting development of the boundary layer. Vortex mixing occurred with pulsed flow in the baffled systems enhancing mass transfer and preventing the development of velocity and concentration boundary layers.

CHAPTER 1
INTRODUCTION

1.1 Fouling in Membrane Filtration:

Membrane filtration is a technique for the concentration of dissolved solutes(or suspended matter) and/or the purification of the solvent. Normally, the flow across the membrane surface is tangential. With all cross-flow membranes, the presence of either a suspension or a solution causes, at constant transmembrane pressure, a decline in permeate flux. Firstly, there is a rapid decline in flux followed by a slower change over a period of several hours. Secondly, particularly in cases of ultrafiltration, a limiting flux condition is reached. The limiting flux is independent of transmembrane pressure and is much smaller than the pure water flux that would be achieved under similar hydrodynamic conditions. Aimar and Sanchez(1985) attributed the existence of the limiting flux to variations of the physico-chemical properties and particularly the viscosity, in the boundary layer, superimposed on the osmotic pressure.

One of the dominant features associated with fouling is the well recognized phenomenon of **concentration polarization**. The flux of permeate through the membrane causes a convective flow of both permeate and retained material towards the membrane surface. The retained material close to the surface is at a concentration greater than the bulk concentration and so a diffusive back-flow is generated. Steady-state conditions are rapidly obtained; Howell and Velicangil(1982) have computed a time of no more than a few seconds. Thus, the convective flow towards the membrane and the associated transmembrane flux is limited by the magnitude of the back-diffusion. In other words, one factor

limiting permeate flux is the mass transfer of retained material back into the bulk flow. This transfer depends on the solution rheology and the hydrodynamics.

There is a considerable range of opinion on the nature of the flux decline process. Suki et al(1986) have shown that protein deposits on membranes are highly stratified with a dense layer at the membrane surface. Turker and Hubble(1987) consider that the initial layer on the membrane itself is denatured but caution against the assumption that all the bound material is denatured. Pore plugging, the formation of a slowly consolidating gelatinous layer on the membrane surface(Michaels, 1968), or protein polymerization(Velicangil, 1979) are other mechanisms that have been proposed. In this investigation, the material adjacent to the membrane responsible for this flux decline is considered to consist of three layers(Field and Finnigan, 1988):

a) a monolayer of adsorbed material at the membrane surface which forms rapidly and is relatively tightly bound;

b) an outer layer due to concentration polarization which forms rapidly but is not bound;

c) in between the two, a middle layer of accreted material which is gradually deposited upon the bound layer.

Whilst all three will modify the flux, only a) and c) can be called fouling layers. At low flux conditions, the middle layer may be absent and fouling greatly reduced.

A further implication of this flux decline is that the membrane itself seldom controls the separation process. Intrinsic membrane properties, in terms of flux and rejection, are relevant for only a very brief initial operational period. The relevant properties of the membrane are in the first place, mechanical and chemical resistance and chemical compatibility rather than filtration properties. Murkes and Carlsson(1988) state that these fouling layers, (a) and (c), sometimes referred to as a "secondary" or "dynamic" membrane, control the filtration process. In general, the flux declines and the rejection increases as the secondary membrane is formed. In addition to this reduction in throughput capacity and compromised separation capability, fouling results in increased power consumption, time consuming and expensive washing and cleaning operations and

reduced membrane service life. Murkes(1978) thinks that fouling is the major bottleneck preventing the large scale industrial implementation of membrane technology. Murkes and Carlsson(1988, pg 69-70) state "*The successful development of "better" membranes has, however, not been accompanied by a corresponding development of methods of combatting the fouling of these membranes*". Many membrane practitioners would agree with these statements.

Means of combatting membrane fouling and concentration polarization can be divided into three main categories:

a) improved hydrodynamics;

b) membrane modification;

c) feed pretreatment.

This investigation is a response to the challenge of Murkes and focuses on the hydrodynamic approach of combatting fouling. Consequently, these other categories are not discussed. Instead, common techniques used for membrane modification and feed pretreatment are summarized in Table 1.1.

1.2 Improved Hydrodynamic Conditions:

Before describing the nature of this work, different approaches that have been taken to improve the hydrodynamic conditions in membrane filtration systems are reviewed. The hydrodynamic approach to reducing fouling is based on increasing the wall shear rate and/or scouring the membrane surface. This is achieved most easily by simply increasing the cross-flow rate either directly, so that the flow changes from laminar to turbulent, or indirectly, by modification of the channel geometry. Prior to the 1960's, the principle geometric configurations of available membranes were flat sheet or tubular structures. The number of configurations has expanded since then to include spiral wound, hollow fibre, thin channels and plate and frame modules. For a discussion of these modules and their relative advantages and disadvantages, the interested reader is referred to Michaels(1968), Harper(1980), Bell(1985), Le and Howell(1985) and

Belfort(1988). The literature reviewed concentrates on other less conventional techniques for improving the hydrodynamic conditions.

Membrane Modification

1) Charged membranes: Hanemaaijer(1987), Reed and Dudley(1987), Gregor and Gregor(1978)

2) Membrane precoating: surfactants(Randerson, 1983, Fane et al, 1985); high MW polymers(Michaels et al, 1983); PEG(Le and Howell, 1983); Polyacrylonitrile or carbon coatings(Bauser et al, 1982)

3) Protective covers: Belfort and Marx(1979)

4) Langmuir-Blodgett layers: Speaker(1985)

5) Immobilized enzymes: Howell and Velicangil(1977, 1981); Wang et al(1980)

6) Electric Fields: Wakeman(1986), Bowen and Sabuni(1987)

7) Membrane electrets: Wallace and Gable(1974)

8) Piezoelectric membranes: Benzinger et al(1980)

Feed Pretreatment

1) pH adjustment: Muller et al(1973), Hayes et al(1974), Melling(1974)

2) Precipitation/Heat Treatment: Hayes et al(1974), Hickey et al(1980)

3) Demineralization: Delaney and Donnelly(1975), Merin and Cheryan(1980), Hiddink et al(1981)

4) Complexing Agents: Hayes et al(1974), Lee and Merson(1976), McGregor(1986), Melling(1974)

5) Filtering Aids: Fane(1983), Zahka et al(1985)

6) Clarification: de Wit et al(1978)

7) Prefiltration: Lee and Merson(1976), de Boer and Hiddink(1980)

8) Sterilization: Belfort(1977), Winfield(1986)

9) Adsorption: Belfort(1977), Winfield(1986)

Table 1.1: Common techniques used for membrane modification and feed pretreatment to improve filtration performance.

1.2.1 Turbulence/Convection Promoters:

Most attention has been devoted to fixed or static turbulence promoters. Static rods(Peri and Dunkley, 1971), wire spirals(Thomas and Watson, 1968), metal grills(Poyen et al, 1987) are examples of some of the many different types of turbulence promoters available. These alter the flow field in two ways: obstructing the flow increases the average flow velocity over that in an otherwise empty tube and the shear rate in the neighborhood of the membrane wall is increased. At sufficiently high Re numbers, secondary flows and turbulent eddies may be established which enhance mixing at the membrane surface and therefore reduce concentration polarization and/or fouling.

Some general conclusions concerning the use of turbulence promoters can be drawn from the literature studied:

a) the maximum increase in the rate of forced convection and the degree of flux enhancement is dependent upon Re. This dependency on Re is system and/or feed specific(Thomas and Watson(1968), Copas and Middleman(1974), Hiddink et al(1980)).

b) optimum spacing between promoters and optimum distance from the transfer surface depends on the particular flow configuration(Thomas and Watson, 1968).

c) most of the convection promoters studied occupy a sizeable volume fraction(typically 20-50%). This will increase the frictional pressure drop by factors as large as several hundred resulting in reduced volumetric flowrates. However, turbulence promoters generally produce the same flux as conventional units at a much lower velocity. Operation at this optimum velocity means for the same flux the frictional pressure drop may be of similar or even smaller magnitude for turbulence promoters compared with normal systems.

d) ideally such devices should introduce no stagnant regions, cause no damage to the membrane, act continuously and be economically justifiable in terms of energy, installation and maintenance costs.

1.2.2 Rotating Membranes:

A rotating module design represents another approach of minimizing the concentration polarization problem. The major advantage of a rotating unit is that the permeate flux becomes independent of the circulation flow, as the shear rate at the membrane surface is controlled by the rotational velocity. This means higher viscosity or concentrated feeds can be treated in single pass flow, reducing circulation pumping costs. Hallström and López-Leiva(1978) describe their own rotary module consisting of an external fixed pressure shell and an internal rotary perforated stainless steel tube which acts as the support for a semipermeable membrane. Between the external shell and the inner rotating tube a narrow slit is formed-this 0.7 mm wide annular space forms the holdup volume for the feed/concentrate. This width is typical of such devices and means scale-up to industrial filtration may be difficult. For the ultrafiltration of skim milk they found that significant flux improvements occurred as rotational speed increased. No limiting flux behaviour was observed within the experimental range of velocity gradients(up to 8000 ls^{-1}).

Rebsamen(1981) describes how the velocity gradient in the annular gap is determined by two important flow directions; namely, the field of vortices caused by the rotation of the inner cylinder and the flow forced by the axial pressure difference along the annular gap. The two overlying velocity fields are governed by stability criteria. An immediate transition to turbulence does not occur above a critical shearing intensity-instead the flow in the annular gap builds a regular three dimensional vortex field classified as laminar field, thus achieving radial mixing of the suspension. These **Taylor vortices**, as they are commonly known, form an ideal plug flow which prevents reverse flow or bypassing in the annular gap.

Long term tests have shown that as static residual layers are missing, the output capacity only decreases slightly. With this device, membranes may be located on both the outer stationary cylinder as well as the inner rotating drum.

Murkes and Carlsson(1988) state that this filter can be used for clarification, ultrafiltration and microfiltration purposes and also in thickening

operations. Kroner and Nissenen(1988) studied direct concentration(single pass thickening, constant flux) and compared it with recycle batch concentration(constant pressure) under similar conditions for Baker's yeast. The average flux after 90 min in the recycling mode was slightly higher at 160 $lm^{-2}h^{-1}$ compared with 150 $lm^{-2}h^{-1}$ for direct thickening. The flux rate for direct thickening remained stable over a 23 hr period with a slight increase in pressure of 0.5 bar. In their opinion, much longer operational times should be possible by using the internal back pressure generated by the centrifugal force from rotation to clean the membrane periodically.

1.2.3 Pulsed Flow:

In an excellent review article, Edwards and Wilkinson(1971) discuss how heat and mass transfer rates can be enhanced in laminar pipe flows by the imposition of a fluctuating pressure gradient. The studies discussed here concentrate on those that have investigated the use of pulsed flow for improving fluxes in membrane filtration. Kennedy et al(1974) summarized the main findings of Edwards and Wilkinson's work relevant to membrane filtration processes:
Pulsed flow in pipes will:

a) enhance mass and heat transfer;
b) modify the laminar/turbulent transition;
c) heighten the migration of solid particles away from the wall;
d) shift the maximum velocity under laminar flow conditions to the wall region.

They observed flux increases of up to 70% for pulsing frequencies up to 1 Hz in reverse osmosis of a 10 wt% sucrose solution. They attributed the gain in flux to a reduction in concentration polarization due to convection. Most of the experiments of this paper were in the turbulent or laminar-turbulent transition regimes.

Milisic and Bersillon(1986) investigated the use of pulsed flow as an anti-fouling technique in cross-flow filtration of a 0.1-1.0 gl^{-1} bentonite solution in a rectangular channel. Pulsations were produced by an air-driven valve located upstream from the filtration cell, fully automated for this purpose. Unlike

backflushing, neither filtrate nor much energy is required for this system to be operated. The flux was increased by as much as 5 times compared with the flux in a standard run and there is an optimum range of values for the frequency and pulse duration; higher fluxes being favoured by higher frequency and shorter pulse duration. Pulsed flow does not appear to solve the important problem of membrane clogging by colloids or macromolecular material likely to occur in natural water.

Bauser et al(1982) state that pulsed flow may be used to improve membrane performance under experimental conditions where a non-linear relationship between flux and wall shear rate exists. They applied a periodic sequence of pumping pulses keeping the mean flow constant by simultaneous adjustment of the frequency and amplitude. Results for the microfiltration of whey under conditions of constant transmembrane pressure showed 25% improvements in flux after one hour and 38% after 2-3 hours. Similar results have been obtained for blood serum filtration, the maximum gain in this case being about 30%.

Subsequently, Bauser et al(1986) took a different approach, applying a pulsatile negative pressure to the filtrate side of the test module. Gains of about 50% were achieved with feasible pressure amplitudes and frequencies for the ultrafiltration of whey. Long term tests over several days detected no membrane damage due to pulsed flow.

Pulsed flow may be induced by other means such as vibration of a porous plate above the membrane surface(Charm and Lai, 1971), pump vibration(Nakao, 1979) or ultrasound(Semmelink (1973), Fairbanks (1973), Lozier and Sierka (1985)). High frequency vibrations, both electrically and acoustically produced, (Hermann, 1982) have also been investigated for the mitigation of fouling with little if any success.

1.2.4 Dimpled/Furrowed Membranes:

Bellhouse et al(1973) rejected pulsed flow by itself as a means of improved mass transfer. Most of their work(1973-1987) has concentrated on the

development of membrane lungs for oxygen and carbon dioxide transfer between air and blood. These membranes consist of a large number of small, partly spherical dimples concave to the fluid channel(Dorrington et al, 1986). Alternatively they may be furrowed(Bellhouse et al, 1973). When pulsed flow is used in this system, significant improvements in gas permeation rates were observed. Sobey(1980) investigated the mechanism of mixing in the membrane oxygenator device of Bellhouse et al(1973). The dimensions chosen for the membrane oxygenator were shown to be near optimum in terms of mixing performance. It appears that in steady flow vortices form in the furrows, but remain trapped there, and little or no fluid exchange occurs between the vortices and the mainstream. For vortex mixing to be effective, the flow must be pulsatile and reversing. On flow reversal, these vortices are ejected from the furrows and immediately replaced by a set of counter-rotating vortices. It is this combination of vortex motion in the hollows and vortex ejection which was thought to eliminate fluid boundary layers and augment mass transfer.

In a practical mass transfer device there will be a mean flow superimposed on the oscillatory flow. Sobey(1980) also investigated the influence of the ratio of net forward to maximum flow, NFR(defined in equation (1.6)), on the flow patterns. When this ratio is small the basic mixing mechanism remains unaltered. Alternatively if this ratio is large, then the flow becomes unidirectional and no vortex ejection occurs. When both flow components are of the same order of magnitude, (NFR=0.4-0.6), the flow patterns become complicated and it is impossible to decide *a priori* whether high or low convective mixing would be obtained. These results were verified by Stephanoff et al(1980) using flow visualization.

A drawback of this technique was demonstrated by Abel et al(1981) in their haemodialyzer work. Pulsed flow enhanced diffusion in both the radial and axial directions. The latter is undesirable, as it reduces the mean concentration difference between blood and dialysate and raises the apparent resistance to transfer. This may be overcome by increasing mean velocities and increasing the dialyser flow path length-the utilization of long and narrow blood and dialysate channels is an effective means of achieving both changes together.

Wyatt et al(1987)successfully applied this technique to the harvesting of microorganisms using E.coli and a 0.2 micron polysulfone membrane. Volumetric efficiencies of the order of 300-400 $lm^{-2}h^{-1}$ were achieved with no pressure applied to the system. The application of low pressures to the retentate line also increased fluxes. An increase in pressure from 0-56 mm Hg increased the percentage of permeate obtained from 49-94% using repeated single pass filtration. Optimal permeate flux was achieved with a dimpled membrane with pulsed flow. Fluxes increased with increasing frequency over the range 2-5 Hz. With both flat and dimpled membranes, water fluxes after each experiment were the same, equalling about 25% of the initial clean water flux for no pulsing; with pulsing, the corresponding values were 51 and 75% respectively. They described a number of other potential applications: removal of cell debris; the harvesting of shear sensitive cells; prefiltration of water and media; ultrafiltration(eg. to separate enzymes); and the clarification of solvents.

Racz et al(1986)stated that the low flow rates and pulsating flow means the mechanism of vortex mixing is not directly applicable to reverse osmosis. They used self-made membranes with periodically spaced semi-cylindrical corrugations in a rectangular channel. Turbulence promotion was thought to be achieved by the fluid eddies following each other quickly, leaving insufficient length of channel through which the fluid can flow undisturbed thus reducing the buildup of a boundary layer at the membrane/salt solution interface. The membranes were self-made. They were cast on a polyester nonwoven support, had fluxes of about 30 $lm^{-2}h^{-1}$ and a retention of about 75% using feed containing 5 gl^{-1} Na_2SO_4 at P_{tm}=40 bar. These values are a different order of magnitude from those used by Bellhouse et al(1973-1987). Corrugations were shown to achieve the same mass transfer at much lower velocities than flat membranes. Pressure drop and pumping power were also reduced under these conditions. Further results were given for mass transfer and hydrodynamics by van der Waal and Racz(1989). Van der Waal et al(1989) applied this technique to polysulfone ultrafiltration membranes and obtained similar results. Corrugating these membranes improved the flux without changing the rejection behaviour. It appears that a critical distance between corrugations exists below which the presence of corrugations

results in decreased performance compared to a flat membrane. They concluded from these studies that the corrugations increase mass transfer in a more effective way than an increase in the flowrate. Racz also felt that this technique would be applicable to microfiltration and adaptable to tubular systems.

Several important features of the "ideal" membrane module and hydrodynamic conditions are illustrated by the literature already discussed and it is appropriate to pause at this stage and summarize these features.

The hydrodynamic conditions should:

a) generate high shear rates/scouring at the membrane surface;

b) produce good radial mixing avoiding stagnant regions;

c) produce minimal axial dispersion which is especially important for thickening operation where plug flow is desirable;

d) generate higher fluxes for the same energy consumption as a conventional system.

In addition:

e) it is desirable to operate at low net cross-flow velocities without a loss in flux, reducing circulation pumping costs;

f) the membrane should be able to tolerate the operating conditions, particularly pressure, typical of normal ultrafiltration and microfiltration applications;

g) any alterations to the module and/or the membranes must be acceptable in economic and hygienic terms.

Of the techniques discussed to date, only the rotating filter satisfies all these criteria. For practical reasons it was decided not to modify the membrane surface in any way. Production of dimpled, furrowed or corrugated membranes is expensive and painstaking. Racz et al(1986) found that their preparation procedure was not very reproducible and that corrugations will change the membrane morphological structure, thickness, surface area and performance. Bellhouse et al's membranes are ideally suited for the membrane oxygenator application. However, the low throughputs, operating pressures and delicate nature of the membranes are limitations that must be considered in ultrafiltration applications. Instead, this project has taken a different approach based on the

work of Mackley and his colleagues. The ensuing discussion shows how Mackley's approach satisfies the first three criteria above and possibly all seven.

1.3 Mackley's Approach: Vortex mixing in Baffled Systems:

Mackley(1987) looked at the combined effects of pulsed flow with suitable tube geometry on mixing. The channel used consisted of a right angled series of bends. The vortex mixing mechanism is similar to that described by Sobey(1980). Pulsatile, reversing flow in this channel provides a mechanism for forming eddies and of equal importance, a mechanism for convecting the eddy from the wall to the main body of the fluid. The overall result in the channel is a complex, well mixed eddy system with mean radial and axial velocity components of the same order of magnitude.

Brunold et al(1989) extended this work, showing that vigorous eddy mixing can be achieved in a tube by introducing periodically spaced, sharp edged, transverse baffles into the tube and applying a pulsatile, reversing flow. A baffle spacing of 1.5D, where D is the pipe I.D.(46mm) gives the most effective mixing over the greatest range of amplitudes. A baffle spacing of 1D seems particularly prone to large scale channelling of the flow through the middle of the tube with minimal separation and mixing. A spacing of 2D is too great for satisfactory eddy interaction to take place on flow reversal except within a closely defined range of amplitudes. This optimum amplitude range is about 3-7 mm. Under these conditions, the channelling problem is minimized.

Brunold et al modelled the energy losses in the system. The total energy losses were very low for the apparent high level of mixing observed from flow visualization studies. They showed that increasing the number of baffles causes only a small increase in the total energy lost in the system. There is however, a significant redistribution of the energy loss from viscous to eddy losses as the number of baffles increases. Increasing the amplitude of oscillation greatly increases the energy lost from the system.

The next four studies all used the same geometrical configuration, hereafter referred to as the baffled tubular system: sharp edged circular baffles having a flow area approximately 33% of the tube area and a baffle spacing of 1.5D. This "best" configuration is based on the work of Brunold et al(1989) described above and that of Howes(1988) who studied the flow patterns in the baffled tubular system using numerical simulation and flow visualization. Howes investigated circular baffles having a flow area of 20-80% of the tube area and a baffle spacing of 0.5-3D in steady flow. In pulsed flow, Howes concentrated on a 40% flow area, 1.5D spacing geometry. Howes results agree with those of Brunold and are discussed further in Section 1.4.2. Howes stated that other geometries, such as spiralled baffles and periodic central tube constrictions are likely to decrease dispersion when pulsed flow is superimposed on steady flow in these systems. The advantage of sharp edged baffles compared with smoother baffles is discussed in Section 1.4.2.

Dickens et al(1989) studied the residence time distribution(RTD) in the baffled tubular system. They found that for a fixed net cross-flow(Re=110) and fixed frequency of 3.5 Hz, an optimum amplitude of oscillation exists where near plug flow characteristics can be obtained. This optimum amplitude is approximately 1 mm in a 23 mm I.D. tube. This value is modest in magnitude and would reflect a very low power consumption for the device. The eddy mixing is generated primarily from the oscillatory motion. This means the mixing can be decoupled from any net cross-flow velocity that might be applied through the tube. If the objective is to achieve good mixing alone, then it would appear desirable to increase the amplitude above this optimum value. If plug flow characteristics are also required, then the device should be operated at this optimum value. In both situations, eddies of sufficient intensity are being generated to give good mixing between individual baffles but at higher amplitudes, larger scale eddies are being generated and these are responsible for strong axial dispersion along the length of the tube. For membrane filtration, Mackley(private communication, 1988) recommends operating at amplitudes greater than or equal to the optimum amplitude for minimal dispersion.

Mackley et al(1990) reported experimental heat transfer measurements for the flow of a lubricating oil on the tube side of a shell and tube heat exchanger for the baffled tubular system. Within the Re range investigated which corresponds to laminar flow conditions, they found that the pulsed flow had very little effect on the heat transfer in an empty tube. The incorporation of baffles increased the heat transfer coefficient up to a factor of 2.5 and 10 times in steady and pulsed flow respectively over the experimental range tested. The incorporation of baffles increases the heat conduction surface area and also modifies the flow pattern. They felt that the flow pattern modification is the dominant factor increasing heat transfer. The effectiveness of this technique would be better judged if the heat transfer coefficient obtained in baffled and/or pulsed flow could be compared with that in an empty tube under fully turbulent flow conditions.

Bradley et al(1989) studied the fouling behaviour of this tubular baffled system in the heating of a whey protein concentrate solution. They demonstrated that pulsed and steady flow in the baffled system reduced deposition rates compared with an empty tube when the deposit rate is primarily boundary layer controlled but when the fouling rate becomes mass transfer controlled, the deposition rates increase by between one to two orders of magnitude.

McKeever and Kemp(1986) conducted a preliminary investigation into the feasibility of using this baffled tubular system(but with a flow area of 67% of the tube area in this case) to improve fluxes in the ultrafiltration of reconstituted skim milk. They were unable to demonstrate any enhancement in fluxes due to the imposition of baffles under steady or pulsed flow conditions. The experimental conditions used by them correspond to Re=8600 and f=12.5 or 35 Hz for full strength skim milk and to Re=860 and f=18 Hz for $1/15^{th}$ natural strength skim milk. In both cases, the amplitude, X, was 1 mm. Their quoted frequency values are very high and it is possible they are in rpm and not Hz. Variations in membrane performance were generally more important than any variation in the imposed hydrodynamic conditions.

One further study illustrates the potential of this technique for membrane filtration applications. Colman and Mitchell(1990) investigated vortex mixing

generated by pulsed flow to enhance membrane performance. A system was designed in which 3 mm high baffles were spaced away from the surface of a flat sheet membrane in a 6 mm high rectangular channel. An interbaffle spacing of 12 mm was found to be optimal for mass transfer. The flow structure associated with pulsed flow in this baffled system shows the same sequence of vortex creation, expansion and ejection each cycle, as described by Sobey(1980) and Mackley(1987). As frequency is increased the flow becomes chaotic but this basic vortex mixing mechanism remains unchanged. The RTD was shown to exhibit plug flow characteristics with low axial dispersion. A mass transfer coefficient, measured at zero flux, equivalent to steady flow at Re>10000 in an empty channel was achieved by using pulsed flow in baffled channels when the net cross-flow rate is Re=100-200. Thus, the mass transfer coefficient can be made independent of the net cross-flow velocity and is relatively constant, provided flow reversal occurs. When there is no flow reversal, the effect of the superimposed oscillations diminishes and the mass transfer becomes mean flow dominated.

A flux, equivalent to that from turbulent cross-flow was achieved using this technique with pervaporation membranes. This technique was also applied to the ultrafiltration of a 1 wt% solution of Dextran T500(MW=500000) using DDS GR40 PP membranes(MWCO=100000). Dextran is a low fouling solute and no permanent fouling of the membrane was observed. Fluxes were enhanced by a factor of three when pulsed flow at a pulsed Reynolds number, Re_p, of 800 (defined in equation (1.2)), is superimposed on a low net cross-flow(Re=200) in a baffled channel relative to the flux in an unbaffled channel with steady flow(Re=200). The pulsed flow flux is equivalent to the flux for steady flow in the baffled channel at Re=1000 and greater than the flux in the unbaffled channel at the maximum cross-flow velocity attainable in the test rig(Re=3000). Limiting flux behaviour is demonstrated by each system and is reached at approximately 0.5 and 1.0 bar for the unbaffled and baffled systems respectively. By incorporating this technique into membrane module design, it will be possible to control mass transfer to the membrane surface independently of the net cross-flow and permeate driving force. No assessment of the power requirement was made.

The essential features of the vortex mixing technique in baffled systems relevant to ultrafiltration and microfiltration processes can now be summarized:
a) good radial mixing is achieved with the radial and axial velocity components being of similar magnitude;
b) near plug flow characteristics can be obtained with low axial dispersion thus maintaining axial concentration gradients along the length of the module;
c) the mixing effect, mass transfer and flux can be decoupled from the net cross-flow rate;
d) energy consumption within this system is expected to be small;
e) fluxes in pulsed flow in the baffled system are similar in magnitude to steady flow turbulent fluxes in an unbaffled tube;
f) the best geometrical configuration for a tubular system appears to be sharp edged circular baffles with a flow area approximately 33% of the tube area and a baffle spacing of 1.5D.

1.4 Theory:

The theoretical development presented here is restricted to material relevant to this investigation. It describes the hydrodynamic and geometric parameters used to characterize the baffled tubular membrane system under steady and pulsed flow conditions.

1.4.1 Hydrodynamics:

For a conventional tubular membrane system the Reynolds number, Re, which represents the ratio of inertial to viscous forces, is sufficient to fully describe the flow conditions existing within the membrane tube. This is defined as:

$$Re = \frac{\rho v D}{\mu} \qquad (1.1)$$

where D is the membrane I.D.; used in the experiment; v is the velocity based on the volumetric flow rate, Q, divided by the tube cross-sectional area, A_{et}.

However this is no longer true when baffles are present in the tube and/or pulsed flow is superimposed on the steady flow. Consequently several additional parameters have been defined to fully describe the hydrodynamic conditions existing within the tube.

The pulsed Reynolds number, Re_p, is defined as:

$$Re_p = \frac{\rho v_p D}{\mu} \tag{1.2}$$

where v_p is the maximum pulsed velocity defined as:

$$v_p = 2\pi f X \tag{1.3}$$

where X is the peak-centre amplitude(mm) and f is the frequency of oscillation(Hz). X is calculated from the volume displacement, V_p, divided by A_{et}.

The Strouhal number, St, is defined as:

$$St = \frac{fD}{2v_p} = \frac{D}{4\pi X} \tag{1.4}$$

The Valensi number, Va, is defined as:

$$Va = \frac{\rho(2\pi f)D^2}{4\mu} = \pi Re_p St \tag{1.5}$$

The Net to peak flow ratio, NFR, is defined as:

$$NFR = \frac{v}{v + v_p} = \frac{Re}{Re + Re_p} \qquad (1.6)$$

Re_p represents the ratio of inertial to viscous forces in pulsed flow(Sobey, 1980). Savvides and Gerrard(1984), who studied the flow patterns in pulsed flow in a tube with triangular corrugations, interpreted Re_p as governing the stages in the cycle at which separation takes place and determining convective transfer within the corrugation.

St is inversely proportional to the amplitude of oscillation. Savvides and Gerrard(1984) interpreted St as characterizing the relative axial motions of particles at different radii within their tubular system.

Va is proportional to frequency and describes the nature of the velocity profile in pulsed flow. Brunold et al(1989) state that a parabolic velocity profile is found for $Va<20$, a transition regime for $20<Va<70$ and plug flow for $Va>70$. The transition from laminar to turbulent flow is usually expressed in terms of critical Reynolds numbers. Two correlations are given by Ury(1962) and Sergeev(1966):

$$Re_{crit} = 180\,Va^{2/3} \qquad \text{(Ury)} \quad (1.7)$$

$$Re_{crit} = 700\,Va^{1/2} \qquad \text{(Sergeev)} \quad (1.8)$$

Savvides and Gerrard(1984) used a similar parameter called the Stokes number which is equal to the square root of Va. They state that the Stokes number represents the ratio of tube diameter to the distance that vorticity diffuses from the wall in one period of oscillation.

NFR is the ratio of net forward flow to maximum flow. The magnitude of this ratio affects the flow patterns within the tube as already described in Section 1.3(Sobey, 1980).

The definitions of Re_p and St are identical to those used by Mackley and his colleagues. These definitions are based on the tube cross-sectional area. Colman and Mitchell(1990) also used the same basis, evaluating corresponding hydrodynamic parameters using the channel height in their system. The same parameters are also defined by Sobey and colleagues but are based on the conditions at a constriction. Ralph(1987), who extended Sobey's work argued that it is best to base these definitions on the conditions at a constriction because most of the pressure drop and vorticity generation occurs at the constrictions. Defining a baffled pulsed Reynolds number, Re_{bp}, as:

$$Re_{bp} = \frac{\rho v_{bp} D_{hy}}{\mu} \tag{1.9}$$

$$v_{bp} = v_p \frac{A_{et}}{A_b} \tag{1.10}$$

where v_{bp} is the maximum velocity based on the cross-sectional area at the baffle, D_{hy} is the hydraulic diameter, and A_{et}/A_b is the baffle flow area ratio defined in equation (1.13); then it can be shown that:

$$\frac{Re_{bp}}{Re_p} = \frac{D}{D + d_o + d_i} \tag{1.11}$$

where d_i and d_o are the inner and outer diameters of the baffles used in these experiments. Note: $d_i = 0$ for disc shaped baffles. This shows that Re_{bp}/Re_p is always less than one. This ratio is also the same for steady flow conditions. Expressing the results on this basis does not facilitate a better understanding of the experimental results. Consequently, all results are expressed in terms of Re, Re_p, v_p, St and Va as defined in equations (1.1) to (1.5), based on the tube cross-sectional area. The definitions used in this work are summarized in Table 1.2 and compared with the definitions used by the other groups mentioned above.

Mackley	Sobey	Colman and Mitchell
Re_p	Re_o	Re_p
$\frac{\rho(2\pi fX)D}{\mu}$	$\frac{\rho(2\pi fX_o)h}{\mu}$	$\frac{\rho(2\pi fX)d}{\mu}$
St	St	Th
$\frac{D}{4\pi X}$	$\frac{h}{2\pi X_o}$	$\frac{X}{d}$
Va	α^2	PuRe
$\frac{\rho\pi fD^2}{2\mu}$	$\frac{\rho fh^2}{\mu}$	$\frac{\rho 2\pi fd^2}{\mu}$

Some additional symbols need to be defined. For Sobey: h is half the minimum channel width; X_o is the peak-centre amplitude evaluated at the point of minimum channel cross-sectional area; Re_o is the peak Reynolds number and α^2 is the pulsatile Reynolds number. For Colman and Mitchell: d is the channel height; Th is the Thomson number and PuRe is the Pulsatile Reynolds number.

Table 1.2: Comparison of the definitions of Re_p, St and Va used by Mackley and colleagues(including this work), Sobey and colleagues and Colman and Mitchell.

1.4.2 Effect of Re_p and St on the Flow Patterns:

The results discussed here are specific to the geometries investigated by Ralph and Howes and also strictly valid for NFR=0. Plotting the experimental results of this study on the same basis as Howes is not justified(see Section 6.4.4) but a qualitative understanding of the effect of Re_p, St and baffle geometry on the flow patterns can be gained from the ensuing discussion. Some final comments on the vortex mixing mechanism are also included.

Ralph(1985) extended the Re_p and St range investigated by Sobey(1980) for the "wavy-walled tube" geometry of the membrane oxygenator device using numerical simulation and identified eight different flow structures. Howes(1988), also used numerical simulation to characterize the flow patterns in the baffled tube geometry of Mackley for Re_p=5-640 and St=0.25-4 and identified seven different flow regimes. In both cases, the flow patterns predicted by the numerical simulation agreed reasonably well with those observed experimentally using flow visualization. Although no systematic experimental study was made, Howes observed that for Re_p>200, the observed flow patterns show increasing complexity which the numerical simulation was unable to predict. Both authors plotted their results on a Re_p/St diagram, where Re_p and St are defined in Table 1.2. The results are qualitatively similar and can be summarized as:

a) as Re_p is increased, the flow becomes more complicated. The vortex strength and disordered nature of the flow increases until a point is passed where the motion becomes chaotic. The flow was considered more complicated by Howes, when more vortices exist in each cell at flow reversal. The definition of a chaotic region adopted here is that an element of fluid will eventually visit every point within the region. Aref(1984) showed that chaotic regions can exist in extremely simple unsteady flows using a very simple stirred tank model and concluded that for unsteady flows in general one must expect to observe chaotic particle motion leading to efficient stirring.

b) the dependency on St is less straight forward but in very simplistic terms the graph can be divided into two regions where the vortex mixing process is inertia

dominated at low St and viscous dominated at high St. Howes stated that increasing St while keeping Re_p constant increases the complexity of the flow.

When Mackley's results are plotted on Ralph's Re_p/St diagram they lie in the viscous dominated region whereas Sobey(private communication, 1988) states Mackley's results appear to be due to inertial effects. Howes(1988) explains that the vortex mixing process is qualitatively similar in wavy-walled and baffled tubes but that the presence of a sharp edge introduces a fundamental difference. Best conditions in wavy-walled tubes correspond to oscillation stroke lengths greater than the wave period of the channel(low St) as the separation vortex is very weak in viscous dominated flows when the stroke is short. When a sharp edge exists this is not necessarily the case and in general vortex mixing is present in the baffled tube for stroke lengths considerably less than the baffle spacing(higher St). Hence, sharp edges shift the transition from inertial to viscous dominated flows to higher St values.

Ralph(1985) used a simple order of magnitude argument based on the time scale of the vortex ejection process to show that this process is predominantly a convective one although diffusive action is also involved. This agrees with Savvides and Gerrard(1984) who computed particle paths which showed that the vortex motion is convective rather than viscous. Howes(1988) stated that one mechanism in vortex mixing devices, also observed by Ralph(1986), is by the steady streaming caused by periodic vortex formation, growth and erosion. This causes fluid in the left of each cell to move anticlockwise from cycle to cycle while fluid in the right of each cell moves clockwise from cycle to cycle. This supports Sobey's comments(1985) that the actual mixing mechanism is more complex than the streamlines alone would suggest. Howes suggests it is possible that the dominant mechanism for transport from the tube wall to the bulk of the flow will be steady streaming when two vortices exist in each cell at flow reversal, while direct convection of fluid in the ejected vortices will be the major mechanism when only one vortex exists at flow reversal.

1.4.3 Geometrical Parameters:

The baffle geometry is specified in terms of the shape and the four parameters:

a) the interbaffle spacing ratio:

$$\frac{L}{D} \tag{1.12}$$

b) the amplitude ratio:

$$\frac{X}{L} \tag{1.13}$$

c) the baffle flow area ratio:

$$\frac{A_b}{A_{et}} \tag{1.14}$$

d) the Keulagen Carpenter number, K_c:

$$K_c = \frac{X}{r} \tag{1.15}$$

where X is the peak-centre amplitude in mm, L is the centre to centre distance between adjacent baffles in mm, r is the radius of curvature at the baffle tip in mm, and A_b and A_{et} are the flow area of the baffle and empty tube respectively.

Only the Keulagen Carpenter number requires an explanation. K_c represents the dependence of separation on the amplitude of oscillation and radius of the geometrical insert. Separation is obtained when $K_c \geq 3$. K_c provides a theoretical basis for using sharp edged baffles.

1.5 Scope of this Study:

1.5.1 Objectives:

Mackley's approach has been applied to a tubular membrane system by fitting geometrical inserts of a doughnut or disc shape to create a periodically grooved channel. Membrane performance for these baffled systems alone and in combination with pulsed flow has been investigated and the results compared with a conventional unbaffled or empty tube system operating under the same conditions of cross-flow velocity and transmembrane pressure.

1.5.2 Experimental Design:

The filtration experiments have been divided into two main stages. The preliminary studies were carried out in Stage 1(Chapter 3) under laminar flow conditions and transmembrane pressures up to 2.4 bar to establish the feasibility of using baffles and/or pulsed flow for improving membrane filtration performance. In Stage 2(Chapter 4), a number of different baffled systems were investigated and the operational range was expanded to include turbulent flow conditions and higher transmembrane pressure values. Chapters 5 and 6 describe the evaluation of the system power consumption and the flow visualization results respectively. A "snapshot" technique was used for most of the experiments. The development of this technique and its validation was an ongoing process throughout both stages and is discussed in Appendix A1.

1.5.3 Parameter Space Investigated:

(A) Hydrodynamics:

The values of Re_p, St and Va are listed in Table 1.3 for Stages 1 and 2.

Stage	Re_p	St	Va
1	0-950	0.22-1.24	100-650
2	0-6450	0.033-0.63	110-670

Table 1.3: Values of Re_p, St and Va for Stages 1 and 2 of the filtration experiments.

The criteria of Ury and Sergeev have only been applied to the empty tube situation. For all values of Va in Table 3.1, $Re_p < Re_{crit}$, according to both correlations (1.8) and (1.9). Hence, in an empty tube, the fluid should be in laminar plug flow for all conditions of pulsed flow used in these experiments.

(B) Geometry:

Two circular inserts have been designed based on the recommendations of Mackley. These consist of sharp edged, disc and doughnut shaped circular baffles, ideally with $A_b/A_{ct}=0.4$, $L/D=0.2\text{-}3.2$ and $K_c \geq 3$. The final geometrical parameters differ slightly from these values due to practical considerations. In order to avoid any contact of the doughnut shaped baffle with the membrane, the outside diameter has been made slightly smaller than the membrane internal diameter leaving a small annular gap between the membrane and the wall. Full details of the baffle specifications are given in Table 2.1.

CHAPTER 2

APPARATUS AND EXPERIMENTAL METHODS

2.1 Materials:

FP100 membranes supplied by Paterson Candy International Ltd, Whitchurch, Hampshire, England were used throughout this work. These were made from polyvinylidene fluoride(PVDF) and are available in the form of 12.5 mm tubes rated as allowing 100% passage of 100K dextran.

The feed solution used in most of this work was a purified 95% whey protein BiPro(BIO-ISOLATES Plc., Swansea, U.K.) and was used as a solution of 5-25 gl^{-1} Bipro at 25-30°C and pH 7.0. This solution needs no additional buffering under the experimental conditions used. It is comprised primarily of alpha-lactalbumin and beta-lactoglobulin with smaller amounts of IgG and BSA and a small amount of salt and lactose.

The other feed material used in the concentration experiments was a 93% soya protein isolate, Ardex D, supplied by The British Arkady Company Ltd., Manchester. This is manufactured from selected defatted soya flakes by a precipitation process for separation from the non-protein components and has a pH of 7.0. This was used at concentrations in the range 2-100% and the viscosity and density information is presented along with the corresponding information for Bipro(3-150 gl^{-1}) in Table 4.2 of Section 4.2.3(C).

The cleaning chemicals used were Terg-A-Zyme enzyme detergent(Alconox Inc.) and Ultrasil, a caustic detergent supplied by Henkel.

All solutions were made up using distilled water.

2.2 Apparatus

2.2.1 Cross-flow Ultrafiltration Unit:

A schematic diagram and photograph of the experimental system are shown in Fig 2.1 and 2.2 respectively. The cross-flow ultrafiltration unit consists of two tubular membranes each 360 mm long and 12.5 mm I.D. contained within two perforated stainless steel tubes, 376 mm long and assembled in a U-tube arrangement to facilitate the superposition of a pulsed flow on the net forward flow. Rubber gaskets hold the membranes in place inside the stainless steel tubes and seal the unit. Each membrane unit is housed within a perspex tube of 1" I.D. which collects the permeate and drains it out continuously from one end into two conical flasks seated on an Avery model 1763 balance. Two flasks were used to collect the permeate from each tube separately in order to monitor any variation in membrane permeability and to detect any anomalous permeation behaviour that may occur if the unit is not properly sealed. For most experiments the feed volume is 2 l and the permeate is periodically returned to the feed vessel after 250-300 ml has been collected. This 15% reduction in feed volume means the feed concentration increases as the flasks fill as very little protein goes through the membranes. This change in concentration was not observed to have any effect on flux for the experimental conditions used. Hence, the system can be assumed to be operating under constant volume conditions.

The feed solution was pumped via a centrifugal pump(Stuart Turner Ltd 302X, Henley on Thames, England) through a non-return valve(NRV) and through the membrane unit with the retentate being recycled to the feed vessel, passing through a fine needle control valve and calibrated rotameter(GEC Elliott Process Instruments Ltd, England Metric 10S). Ideally, the NRV should prevent any backflow through the inlet leg due to the superposition of pulsed flow on steady flow at the two Tee positions shown in Fig 2.1. The pump was rated for 54.5 and 11.4 $l.min^{-1}$ at a head of 3 and 13.7 m respectively. A variable transformer(Zenith Electric Co Ltd, Milton Keynes, England) was used to control the pump speed. Alteration of the pump speed and the control valve constriction

allowed the transmembrane pressure and cross-flow velocity to be set to the desired values. The inlet and outlet pressures were measured using PDCR 810 absolute pressure transducers(Druck Ltd, Leicester) interfaced to an Opus PC via an A to D interface(Linkon). The feed solution was kept at a constant temperature of 25°C by a stainless steel coiled heat exchanger positioned inside the cylindrical perspex feed vessel. The piping between the NRV and the rotameter consisted of Stainless steel tubing of 0.5" I.D. connected by Swagelok fittings. Rigid tubing was used here to avoid any contraction/ expansion of the tubing due to the pulsed flow. The remainder of the pipework consisted of clear reinforced PVC tubing of variable diameter. The hold-up volume was deliberately kept as small as possible. A drain line and valve was fitted immediately after the NRV.

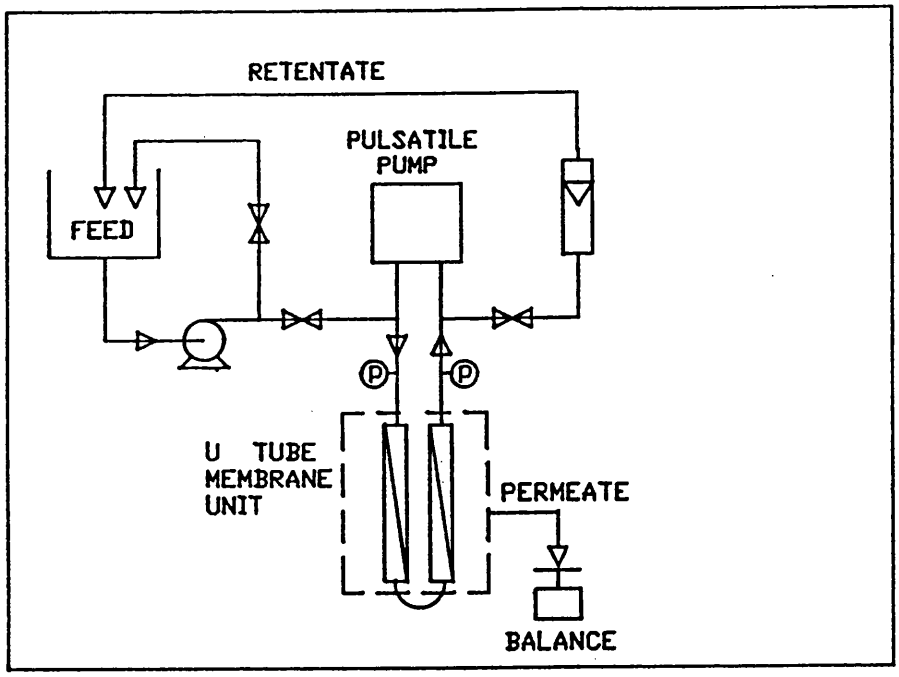

Fig 2.1: A schematic diagram of the experimental system.

The pulsed flow was produced by a dual head Metripump(MPL E3B/PG10L, MPL Ltd, Slough, England) with a maximum capacity of 9.6 lh^{-1}. The pumpblock was redesigned as shown in Fig 2.3. The conventional inlet and outlet ports are now used as liquid drain and air bleed valves respectively. A central circular opening has been machined out of the perspex block, aligned on

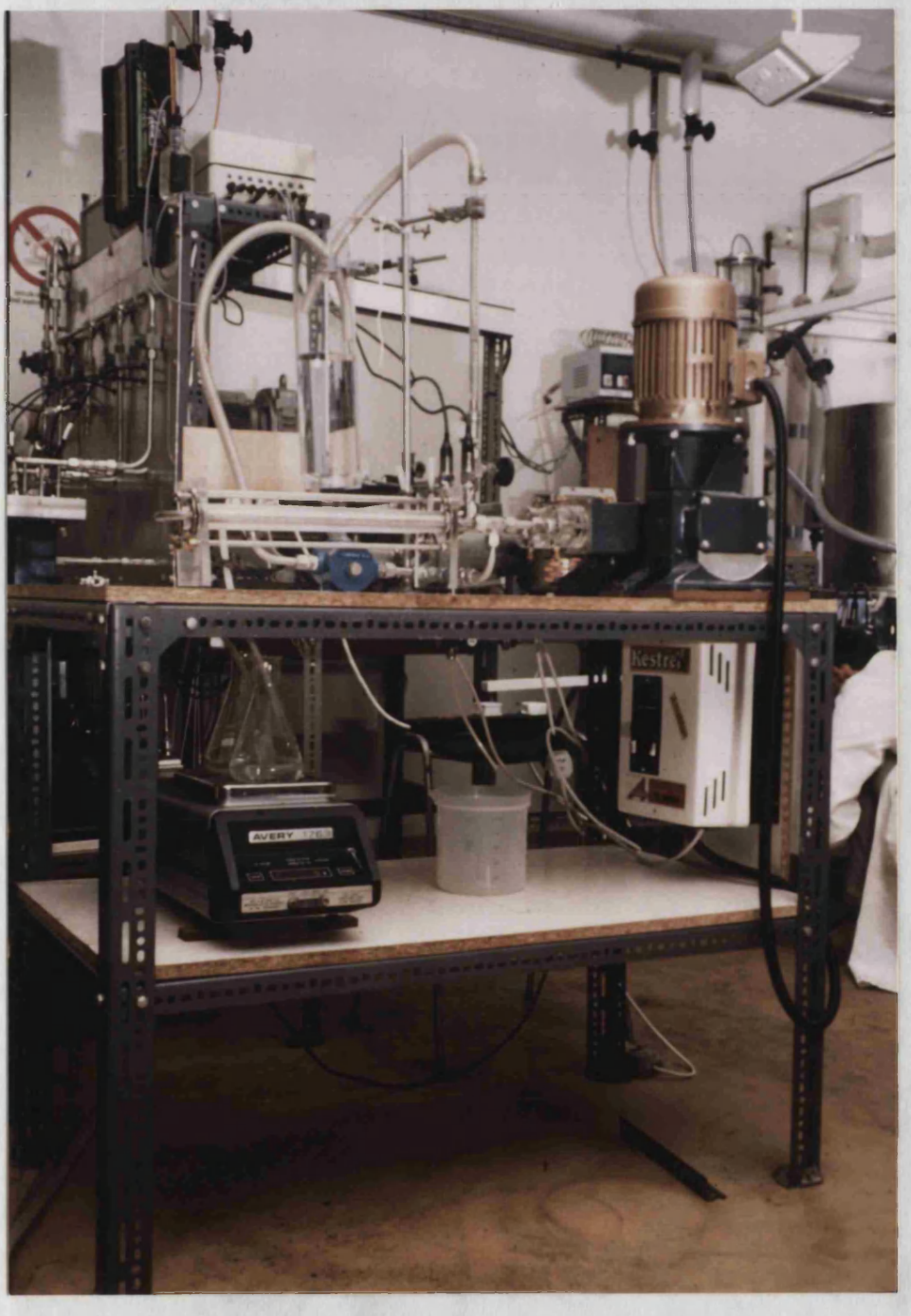

Fig 2.2: The experimental system used in Stage 1 of the experiments.

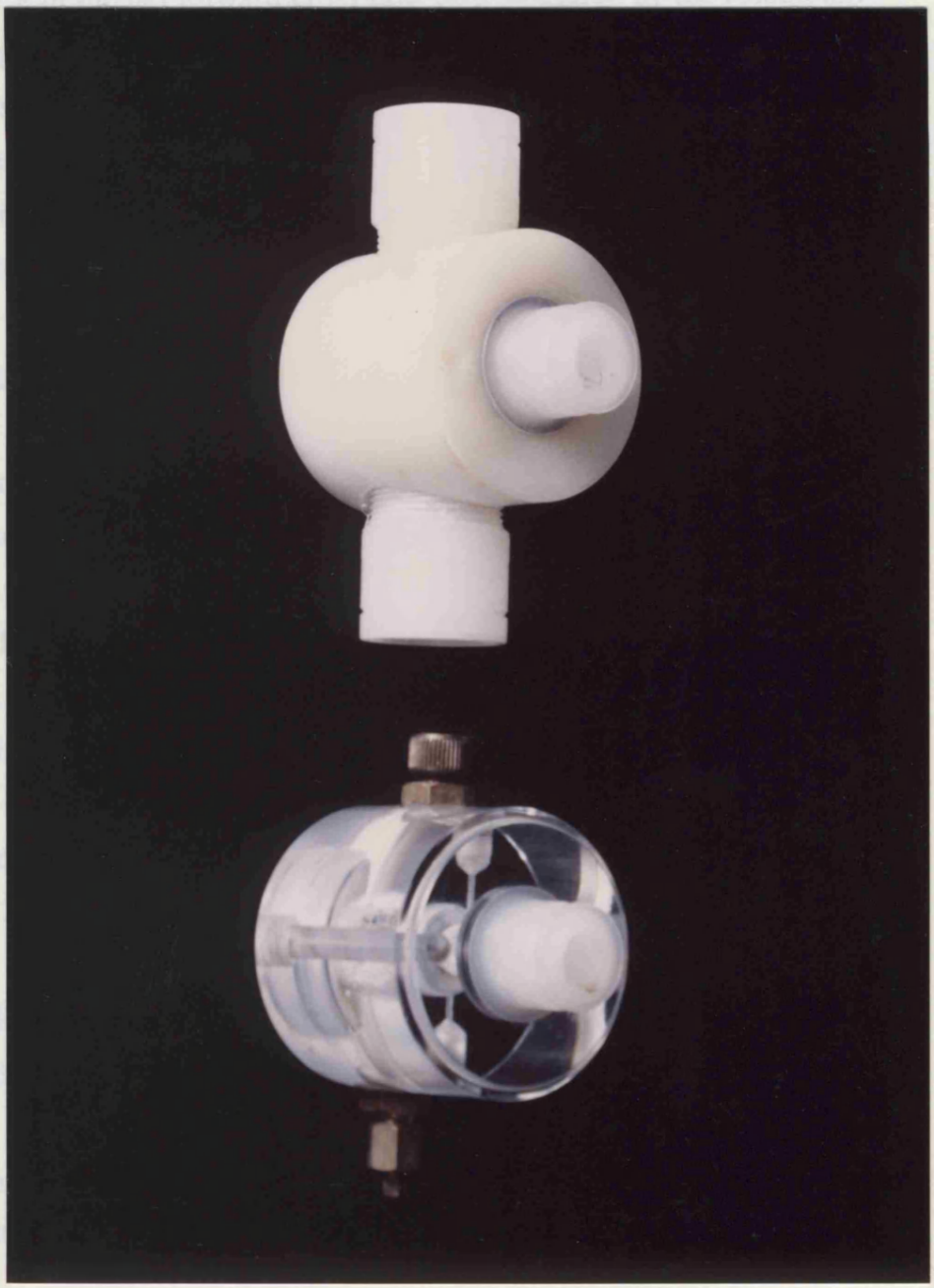

Fig 2.3: The original(top) metering pumphead and redesigned(bottom) pumphead for producing pulsed flow. A similar modification was made to the diaphragm pumphead in Stage 2.

the same axis as the plunger assembly. Connecting these two plungers in antiphase means that the fluid is pushed backwards and forwards through the circular opening to create the pulsed flow without any change in the system volume and hence in the net forward cross-flow rate measured by the rotameter. A Kestrel Whisper Control Model 2150 AC Invertor(Allspeeds Ltd, Lancashire, England) was used to control the frequency of oscillation in the range 0-2.5 Hz and the peak-peak amplitude could be manually adjusted between 0-14.2 mm. As the tubular membrane has a larger diameter than the plunger pumphead, the maximum attainable peak-centre amplitude in the tubes was 4.6 mm.

2.2.2 Stage 2 Modifications:

Several modifications were made to the apparatus in Stage 2 in order to achieve the experimental objectives. The centrifugal feed pump was replaced by a Verder V096.07/2030 gear pump which made it possible to investigate P_{tm} up to 5-5.5 bar although the maximum Reynolds number that could be reached at these pressures was reduced to 2200.

To reach cross-flow rates in the turbulent regime the membrane rig was connected to a rotary trilobe pump(SSP Pumps Ltd, Size AP12.5/BS) capable of reaching a head of 8.5 bar. To measure the higher flow rates achieved with this pump a Metric 24P rotameter(Rotameter Mfg. Co Ltd) with a maximum capacity of 20.9 ls^{-1} was used.

The E3B/PG10L plunger pumpheads were also replaced with E2B(short stroke)/D50P diaphragm pumpheads. The maximum capacity of these was 68 lh^{-1} compared with 9.6 lh^{-1} for the former, meaning that flow reversal could always be achieved for the Re range investigated. The maximum attainable amplitude in this case was 30.5 mm.

2.2.3 Baffles:

These are pictured in Fig 2.4. The designation adopted here is made up of two parts; a letter code **ET** or **DO** or **DI** referring to an empty tube(the

conventional or unbaffled system) doughnut or disc shape respectively and a number X.X. This number refers to the ratio L/D, defined in equation (1.12), where L is the centre-centre distance between adjacent baffles, and D is the membrane internal diameter(12.5 mm). An extra letter code **P** means that pulsed flow was used in this instance; hence **DO**2.2 and **DO**2.2**P** refer to steady and pulsed flow respectively for the doughnut baffles with an L/D ratio of 2.2.

Two types of baffle inserts were constructed for Stage 1: a doughnut or ring shape(**DO**2.2) and a disc shape(**DI**1.6). The specifications for these inserts appear in Table 2.1 below. The first doughnut baffles were made from perspex rod which placed a practical limit on the minimum thickness of 2 mm. These were glued to three perspex rods spaced equidistantly around the perimeter of each doughnut. All other baffles were made from stainless steel(SS) or brass as specified in Table 2.1. The **DO**1.5 baffles were silver soldered on opposite sides to two stainless steel rods. The disc baffles were silver soldered to a central rod 3.2 mm in diameter.

Baffles	I.D.(mm)	O.D.(mm)	L(mm)	t(mm)	A_b/A_{et}	Material
Stage 1:						
DO2.2	5.6	11.5	27.6	2.0	0.35	Perspex
DI1.6	---	9.7	19.4	0.8	0.4	SS
Stage 2:						
DI0.8	---	9.7	9.7	0.8	0.4	Brass
DI1.6	---	9.7	19.4	0.8	0.4	SS
DI3.2	---	9.7	38.8	0.8	0.4	Brass
DO1.5	7.9	11.5	18.8	0.8	0.55	SS

Table 2.1: Specifications of the different baffles used in Stages 1 & 2. t is the baffle thickness; A_b/A_{et} is the baffle flow area ratio as defined in equation (1.14); SS refers to stainless steel.

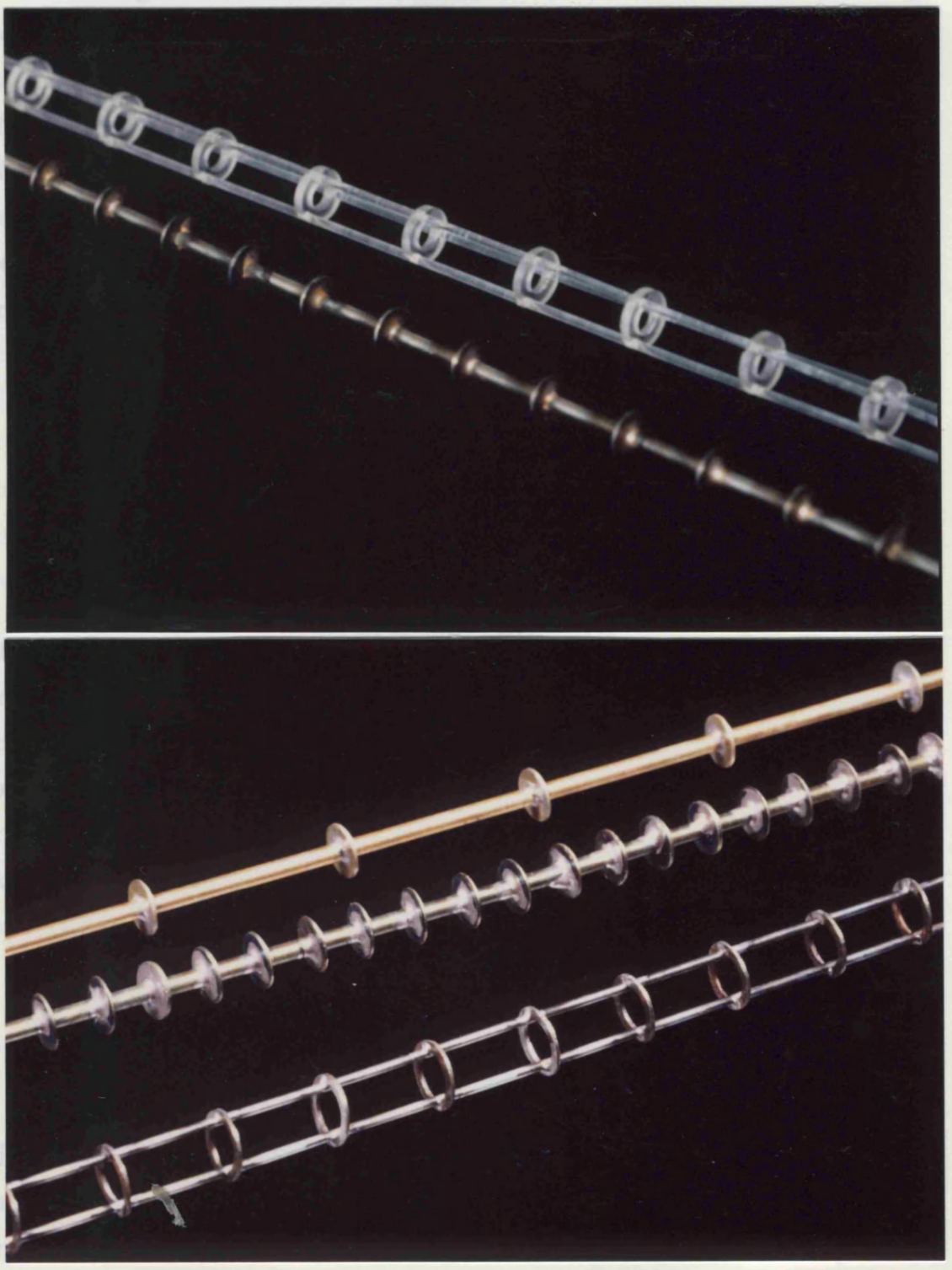

Fig 2.4: The disc and doughnut shaped baffles used in a) Stage 1 and b) Stage 2 of the experiments. From top to bottom, the baffles are a) **DO**2.2, **DI**1.6, b) **DI**3.2, **DI**0.8 and **DO**1.5.

For fitting inside the membrane tube, end connections were soldered or glued onto the axial support rod(s) so that the baffles rested securely against the rubber gaskets holding the membrane in position to prevent any axial motion of the baffles which could possibly damage the membrane. Gaskets at one end of both tubes had to be shortened to ensure the baffles did not move. This reduced the membrane length and area available for permeation to 347 mm and 274.9 cm^2 respectively for **DO2.2**. For the other baffled systems, the corresponding parameters were 350 mm and 272.5 cm^2 respectively.

2.3 Methods:

2.3.1 Flux measurement:

Fluxes were measured from the change in mass of permeate collected in the flasks. For most of Stage 1 experiments this data was recorded manually at intervals of 20-30s. The purchase of a top loading electronic balance(L2200P) from Sartorius Ltd, Epsom, Surrey, England and RS232/423 computer link data output to replace the Avery balance enabled the flux data to be logged by a BBC microcomputer onto disc and then transferred to an IBM PC using a file transfer package(Kermit) to allow analysis and plotting. As described in Section A1.3, the error in flux values is estimated to be 5%.

2.3.2 Transmembrane Pressure, P_{tm}:

Logging software that has been developed within the department allowed the inlet and outlet pressures measured by the transducers to be recorded at user defined intervals of 20s. The transmembrane pressure, P_{tm}, was evaluated as the average of the inlet and outlet pressures. These values could then be averaged within the program over longer periods of time to provide smoothed data. The maximum error in P_{tm} values is estimated to be 5% and 10% for steady and pulsed flow respectively.

2.3.3 Reynolds Number, Re :

The net cross-flow rate measured by the rotameter was used to calculate the Reynolds number, Re, defined in equation (1.1). The maximum error in Re is 10% and Re values have been rounded accordingly in the text to reflect this accuracy.

Note: The raw and rounded Re values are found in Appendix A2. The raw Re values have been used in all calculations.

A further rotameter was purchased from Platon Flowbits Ltd, Basingstoke, England(50520-200/GI/0.25"S) with two interchangeable tubes(No 22112 and 22112) to measure flows in the range 20-280 and 50-800 $ml.min^{-1}$ respectively. Connecting this rotameter in parallel with the GEC rotameter increased the system flexibility as small flowrates could now be measured accurately and the range of flowrates that could be measured was greater.

2.3.4 Pulsed Reynolds Number, Re_p :

To evaluate the pulsed Reynolds number, Re_p, defined in equation (1.2), the peak-centre amplitude, X(mm), and frequency of oscillation, f(Hz), are needed. These were evaluated directly from the percentage amplitude of the pulsing pump and frequency controlled setting respectively after calibration of this equipment. The amplitude in mm differs in Stages 1 and 2 at the same percentage amplitude due to the different capacity of the plunger and diaphragm pumpheads respectively.

2.3.5 Cleaning:

In Stage 1, the membranes were chemically cleaned under steady flow conditions for 1 hr at 55°C using a 3 gl^{-1} solution of Terg-A-Zyme enzyme detergent. In Stage 2, the cleaning cycle was modified to improve the efficiency of cleaning under the harsher operating conditions used in Stage 2(see Section A1.5) and because of the smaller flow capacity of the pump(see Section 2.2.2).

A 2.5 gl^{-1} solution of Ultrasil, a caustic detergent, was added to the Terg-A-Zyme solution used in Stage 1 and pulsed flow was superimposed on the steady flow. In all experiments, on the completion of cleaning, the membranes were rinsed until the pH of the permeate was approximately 6.0 and the water flux was then measured as described in Section 2.3.6.

2.3.6 Membrane Resistance, R_m :

The membrane resistance was measured immediately prior to an experiment and after rinsing with distilled water on the completion of an experiment. With all membranes used in these experiments a linear relationship between water flux and transmembrane pressure existed up to at least two bar. Above this point some deviation from linearity did occur. Consequently it was decided to evaluate R_m at P_{tm}=1-1.2 bar.

The water flux was then measured over a 5 min period using fresh distilled water and a logging period of 20-30s. An average water flux value was calculated from these readings and corrected to 20°C by applying a 2.5% correction/°C temperature difference to account for the variation in viscosity of water with temperature. The membrane resistance was then calculated using:

$$R_m = \frac{3.593 * 10^{14} \, P_{tm}}{J} \qquad (2.1)$$

where R_m is in m^{-1}, J is in $lm^{-2}h^{-1}$ and P_{tm} is in bar.

2.3.7 Rejection:

The composition of the permeate samples was determined using HPLC analysis on a Gilson Holochrome UV-Detector(Anachem Ltd) at 280 nm fitted with a Tosoh TSKgel G3000 SW XL column. A 0.1N phosphate buffer/0.1N sodium sulphate/0.5% sodium azide solution was circulated throughout the system with 20 microlitre samples being injected every 20-30 min. The permeate

concentration and hence the membrane rejection for the 4 main proteins in Bipro was determined by comparison of the peak heights with those of a standard 1 gl^{-1} solution of Bipro.

The membrane resistance and rejection results are described in Section A1.8.

2.3.8 Protein Concentration:

The concentration of the retentate/feed solutions was determined for concentration experiments using 2 of 3 methods:

a) mass balance: based on the feed volume and the total volume of permeate collected.

b) HPLC: after appropriate dilution of the sample to be in the 1 gl^{-1} protein range.

c) UV Absorption: The amount of protein in a clear solution was estimated by measuring the UV absorption at 278 nm. Each sample was diluted to a maximum concentration of 1 gl^{-1} and duplicate samples read in a Cecil CE272 spectrophotometer using a quartz cell with a 1 cm path length. The concentration was calculated from a standard curve of absorbance versus concentration. The Ardex solutions were not completely homogeneous and constant readings could not be obtained with a conventional cell. Hence a flow cell was used for these samples.

2.3.9 Kinematic Viscosity:

The kinematic viscosity of different concentration solutions of Bipro and Ardex D was measured using a combination of Canon-Fenske viscometers(No's 100 and 150) and U-tube reverse flow viscometers(No's 4, 5, 6 & 7) at 25°C.

CHAPTER 3
STAGE ONE FILTRATION EXPERIMENTS

3.1 Introduction:

Preliminary studies have been carried out in Stage 1, investigating the feasibility of incorporating periodically spaced baffles of a doughnut and disc shape(described in Table 2.1) within the membrane tubes to improve the membrane filtration performance under steady and pulsed flow conditions. The objectives were:

a) to compare the fluxes obtained in the baffled systems with a conventional system at the same conditions of P_{tm} and Re for steady and pulsed flow.

b) to investigate the performance of these systems under laminar flow conditions (Re=0-3300) and over the P_{tm} range 0-2.5 bar.

c) to determine if a threshold Reynolds number has to be exceeded before baffles improve the flux compared with a conventional system.

d) to investigate the effect of frequency and amplitude on filtration performance.

e) to carry out a series of long term fouling experiments concentrating on the operating conditions where the most interesting snapshot results were obtained.

3.2 Experimental Design:

3.2.1 Doughnuts(DO2.2):

In order to assess quickly the feasibility of the pulsed approach for improving membrane filtration performance, a "snapshot" technique was used to

obtain flux data for a 25 gl^{-1} solution of Bipro at 25°C under varying conditions of transmembrane pressure and cross-flow velocity for each system as summarized in Table 3.1 for the empty tube(**ET**) and baffled(**DO2.2** & **DO2.2P**) systems. In this technique, after allowing sufficient time for the initial rapid flux decay to have stabilized, many operating conditions are each used over a short period of time, called a frame, and the resultant fluxes measured. The conditions are randomly selected. The initial operating conditions are returned to at the end of an experiment and if the extent of long term fouling is less than 15%, the results are considered acceptable as variations based on the major parameters of influence are greater than 300%. This technique is fully described in Section A1.2. A feed concentration of 25 gl^{-1} was chosen in order to obtain limiting flux conditions for the conventional system under these operating conditions. The pulsed flow conditions were determined by the capacity of the metering pump. For the Re/P_{tm} experiments an amplitude of 100%(4.6 mm) and frequency of 2.5 Hz were selected which correspond to $Re_p=950$($v_p=7.3$ $cm.s^{-1}$) and $St=0.22$.

The long term fouling behaviour at $Re=1050$ and $P_{tm}=1.2$ bar was also investigated for **ET, DO2.2** and **DO2.2P.** A further "snapshot" experiment was carried out at $Re=350$ and 1050 at the different amplitudes and frequencies tabulated in Table 3.1.

3.2.2 Discs(DI1.6):

These membranes were replaced when the doughnut baffles were exchanged for the disc baffles. The snapshot technique was again used to obtain flux data under the conditions of P_{tm} and Re tabulated in Table 3.1 for **ET, ETP, DI1.6** and **DI1.6P** in Stages 1B and 1C. Several snapshot experiments were carried out in Stage 1C at $Re=10$, 50, 100 and 200 at $C_b=25$ gl^{-1} at the amplitudes and frequencies tabulated in Table 3.1.

A series of long term fouling experiments of 2 hours duration concentrating on $Re=350$ and 700 were also carried out. Further long term fouling experiments were carried out with the recycle valve completely closed. At the end of the 2 hour time period the flow conditions were changed from

pulsed to steady flow or conversely from steady to pulsed flow for a further 10 min of operation.

1A) **DO2.2**	v ($cm.s^{-1}$)	4.1	8.1	12	22		
	Re	500	1050	1550	2800		
	P_{tm} (bar)	0.4	0.8	1.2	1.6	2.0	2.3
	Re	350		1050			
	f (Hz)	0.4		1.4		2.5	
	X (mm)	0.8		2.6		4.6	
1B) **DI1.6**	v ($cm.s^{-1}$)	2.7	5.4	9.4	12	26	
	Re	350	700	1200	1550	3300	
	P_{tm} (bar)	0.4	0.8	1.2	1.8	2.2	
1C) **DI1.6**	v ($cm.s^{-1}$)	0.4	0.7	1.4	2.7		
	Re	50	100	200	350		
	P_{tm} (bar)	0.4	0.8	1.2	1.8	2.4	
	Re	10	50	100	200		
	f (Hz)	0.4		1.4		2.5	
	X (mm)	0.8		2.6		4.6	

Table 3.1: The experimental conditions investigated in each of the snapshot filtration experiments, where for every Re value, all combinations of f and X or every P_{tm} value was investigated.

Finally, the first long term fouling experiment was repeated to determine if the membrane performance had changed in any way. A variation of 19% in steady state flux values had occurred and this was judged to be satisfactory.

3.3 Results:

3.3.1 Terminology:

The following terminology is used to describe the filtration results. At a constant Reynolds number, Re; at low transmembrane pressure, P_{tm}, the flux, J, increases with increasing P_{tm} until a threshold pressure value, P_{th}, is reached. Any further increase in P_{tm} will not result in an increase in flux-this flux is called the limiting flux. The region of increasing flux is known as the pressure dependent region; the plateau flux region as the pressure independent or limiting flux region.

The experimental data from Stage 1 has been plotted in Fig 3.1-3.7 and the Reynolds numbers corresponding to each set of data are shown in the legend. In Fig 3.1-3.3, the data is represented as a vertical bar representing the raw average plus and minus one standard deviation. Calculation of the raw average and standard deviation is described in Section A1.3. The results are expressed in terms of a change(usually an improvement) in flux, relative to ET, unless otherwise stated.

3.3.2 Summary:

These experiments demonstrated the feasibility of using baffles and/or pulsed flow for improving membrane filtration performance.

Pulsed flow(**ETP**) resulted in a small flux improvement for Re≤350. This coincided with the conditions under which flow reversal occurred.

Both sets of baffles improved fluxes at the same Reynolds number. The extent of improvement reached a maximum in the Re range 350-1550 where concentration polarization was most severe for **ET**. With **DI1.6**, a Reynolds number of approximately 200 had to be exceeded before any improvement in flux was observed relative to **ET**.

For both baffled systems a further improvement in flux occurred with pulsed flow when the baffled systems were operating under limiting flux conditions. For **DI1.6**, the net cross-flow velocity had to be increased beyond Re = 150 for the improvement in flux with pulsed flow to be maximized. Between this point and the position of flow reversal, the flux became decoupled from the cross-flow velocity and was of similar magnitude to the steady flow flux in the baffled system when the steady flow velocity was similar in magnitude to the pulsed flow velocity($Re = Re_p$). For **DI1.6**, there was no advantage of using pulsed flow once the point of flow reversal was passed.

Limiting flux behaviour did not appear to be reached for either baffled system in steady flow($Re \geq 350$) and in pulsed flow within the experimental range investigated. The fluxes under steady and pulsed flow conditions were significantly greater than for **ET** at the highest Re used in these experiments of 3300.

In the variable frequency and amplitude experiments, fluxes were increased for $f \geq 1.4$ Hz and $X \geq 2.6$ mm($Re_p \geq 300$, $St \leq 0.38$). For the same Re_p value, fluxes were consistently higher at f=2.5 Hz and variable amplitude than at X=4.6 mm and variable frequency.

The results of long term fouling experiments supported the snapshot experiments.

It has been suggested that pulsed flow in a baffled system could be used in a single pass continuous system either for thickening purposes or to avoid the pumping costs associated with recirculation.

3.3.3 Flux and Pressure:

In these experiments, with pulsed flow, the frequency and amplitude are 2.5 Hz and 4.6 mm respectively which corresponds to $Re_p = 950$ and $St = 0.22$.

(A) Doughnuts(DO2.2):

Fig 3.1(a)-(d) compares the "snapshot" results for **ET**, **DO2.2** and **DO2.2P** at Re=500, 1050, 1550 and 2800 respectively. For **ET**, limiting flux behaviour begins in the region 0.8-1.2 bar for all Reynolds numbers investigated. **DO2.2** increases fluxes for Re=500, 1050 and 1550(Fig 3.1a, 3.1b, 3.1c). At Re=2800(Fig 3.1d) a smaller flux improvement was observed, especially within the pressure dependent region.

When pulsed flow is used with the baffled system a further improvement in flux occurs for all P_{tm} at Re=500 and at $P_{tm} > 1.2$ bar at Re=1050. The improvement in flux, relative to **DO2.2**, is greatest at Re=500, the only case where flow reversal occurs(NFR=0.36).

With **DO2.2** in steady and pulsed flow, limiting flux behaviour is not occurring at $P_{tm} < 1.6$bar. In fact, it is uncertain whether a flux plateau has been reached at 2.2 bar or if the slight upward trend shown by the data points at all Reynolds numbers is genuine.

(B) Discs(DI1.6):

Fig 3.2(a)-(h) compares the "snapshot" results for **ET**, **ETP**, **DI**1.6 and **DI1.6P** at Re=50, 100, 200, 350, 700, 1200, 1550 and 3300. In Fig 3.2d, the data is represented by different symbols and smoothed curves. This was done as two independent sets of data from Stages 1B and 1C corresponding to Re=350 have

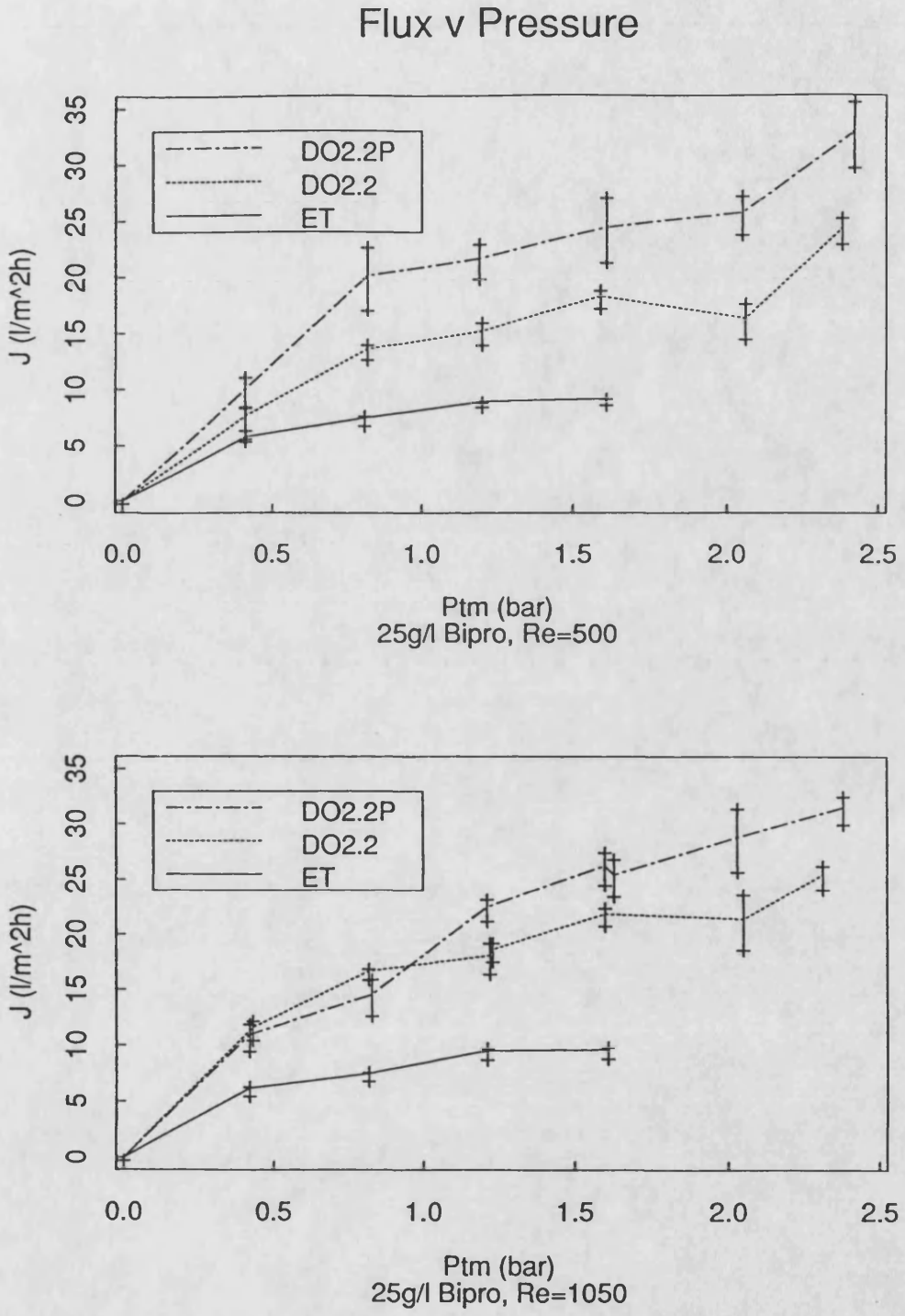

Fig 3.1: Comparison of "snapshot" ultrafiltration fluxes for **ET**, **DO**2.2 and **DO**2.2**P** at Re= a) 500 and b) 1050. NFR=0.36 and 0.53 respectively. Re_p=950 and St=0.22 for pulsed flow.

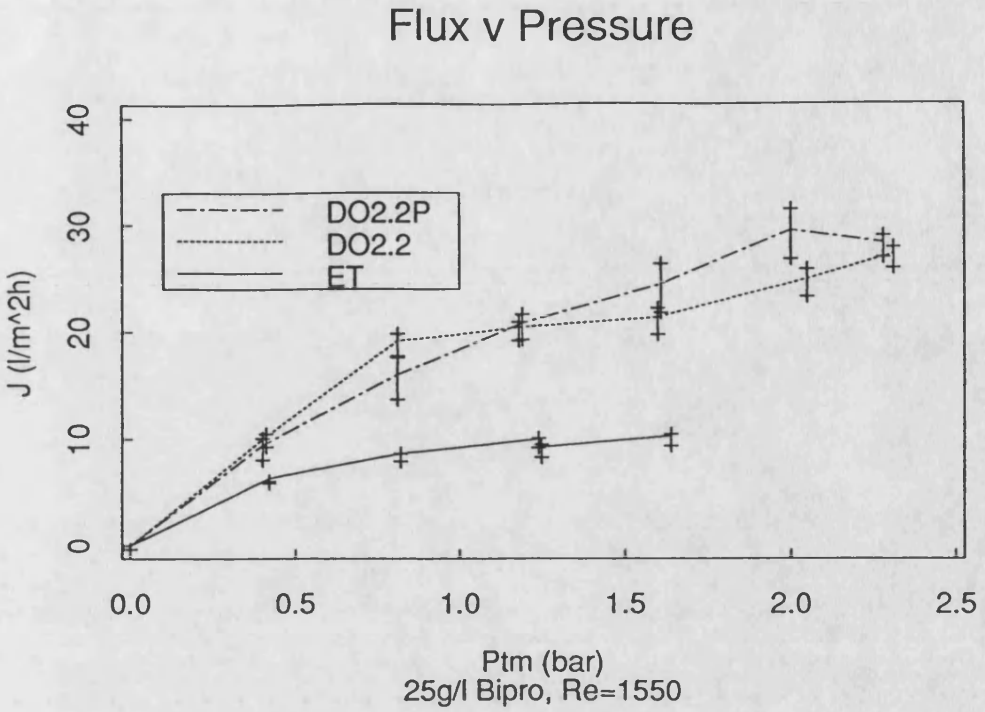

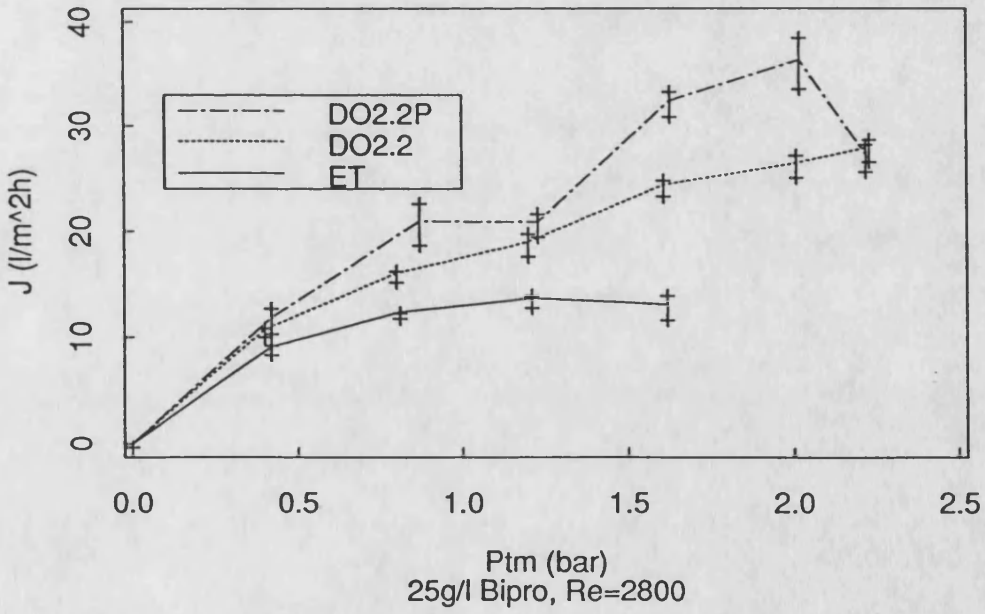

Fig 3.1: Comparison of "snapshot" ultrafiltration fluxes for **ET**, **DO2.2** and **DO2.2P** at Re= c) 1550 and d) 2800. NFR=0.63 and 0.75 respectively. Re_p=950 and St=0.22 for pulsed flow.

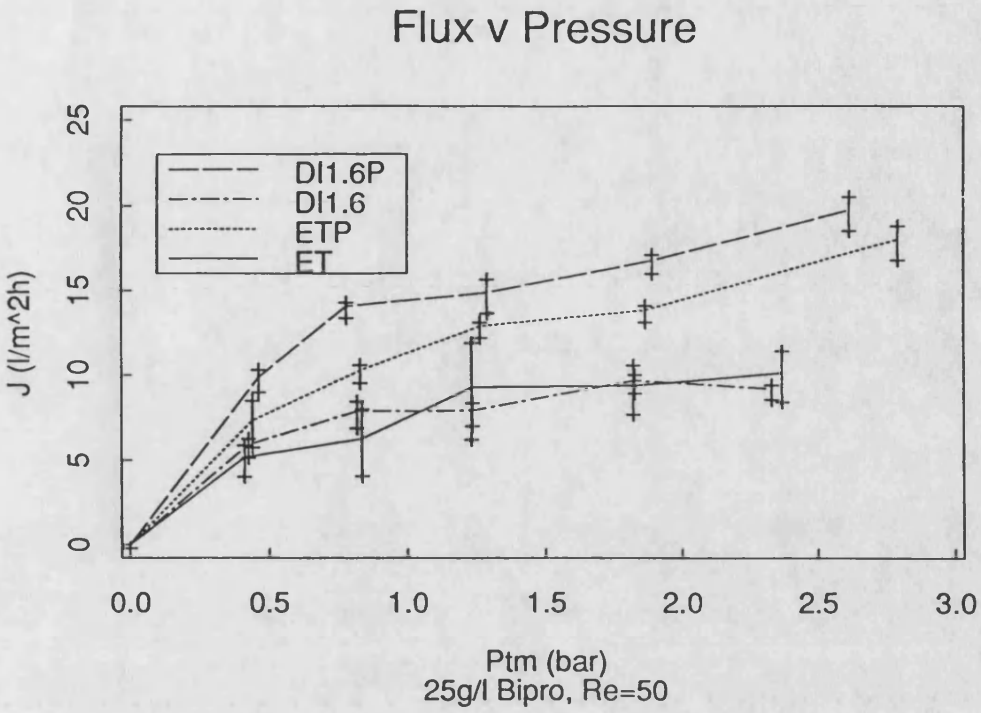

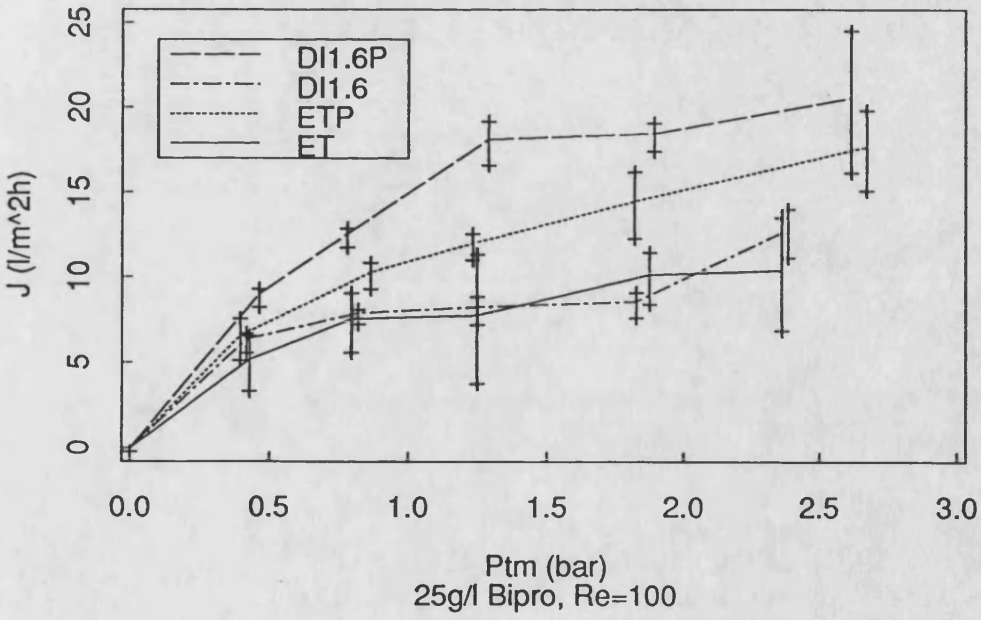

Fig 3.2: Comparison of "snapshot" ultrafiltration fluxes for **ET**, **ETP**, **DI**1.6 and **DI**1.6**P** at Re = a) 50 and b) 100. NFR = 0.04 and 0.09 respectively. Re_p = 950 and St = 0.22 for pulsed flow.

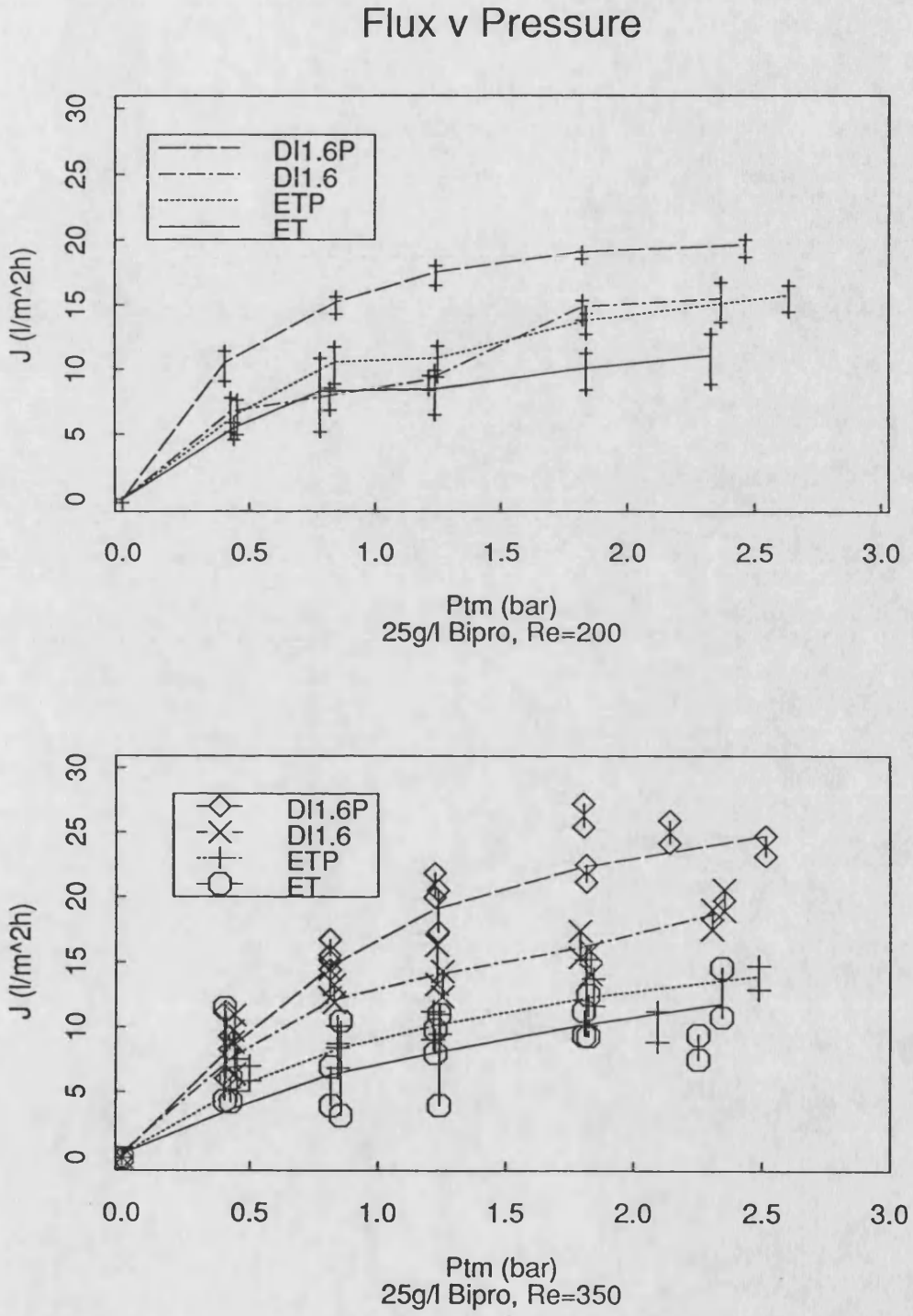

Fig 3.2: Comparison of "snapshot" ultrafiltration fluxes for **ET**, **ETP**, **DI**1.6 and **DI**1.6**P** at Re= c) 200 and d) 350. NFR=0.16 and 0.27 respectively. Re_p=950 and St=0.22 for pulsed flow.

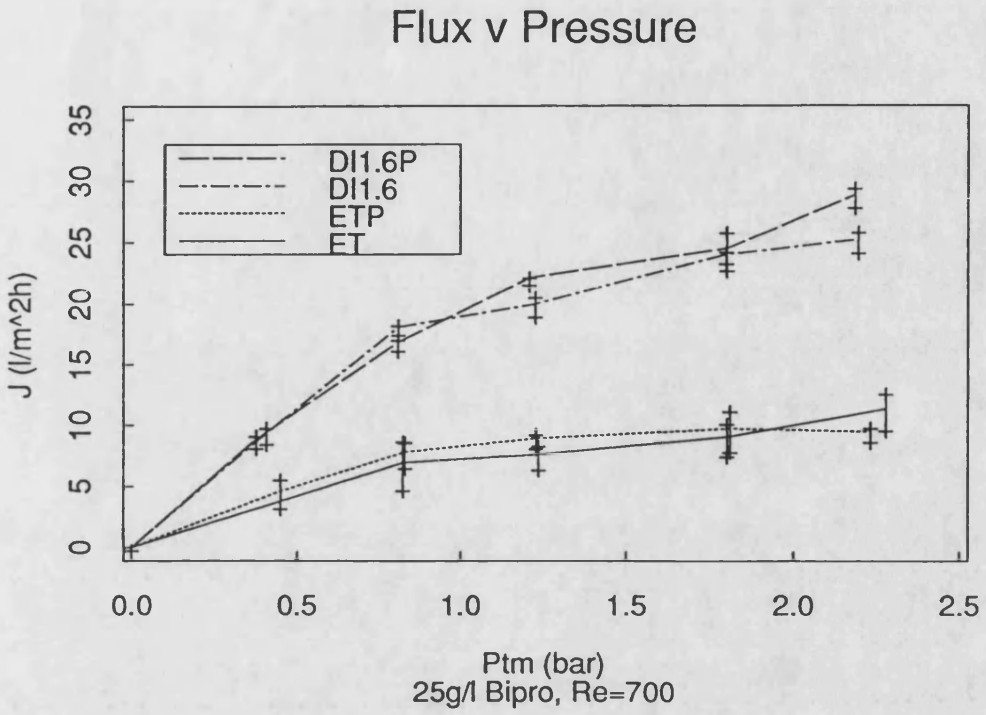

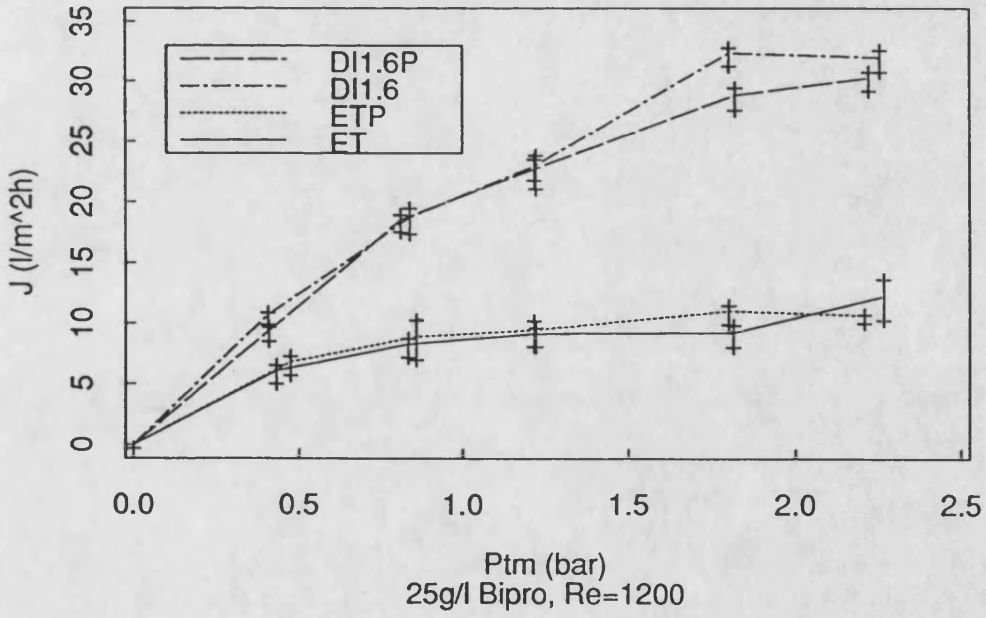

Fig 3.2: Comparison of "snapshot" ultrafiltration fluxes for **ET**, **ETP**, **DI**1.6 and **DI**1.6**P** at Re= e) 700 and f) 1200. NFR=0.43 and 0.56 respectively. Re_p=950 and St=0.22 for pulsed flow.

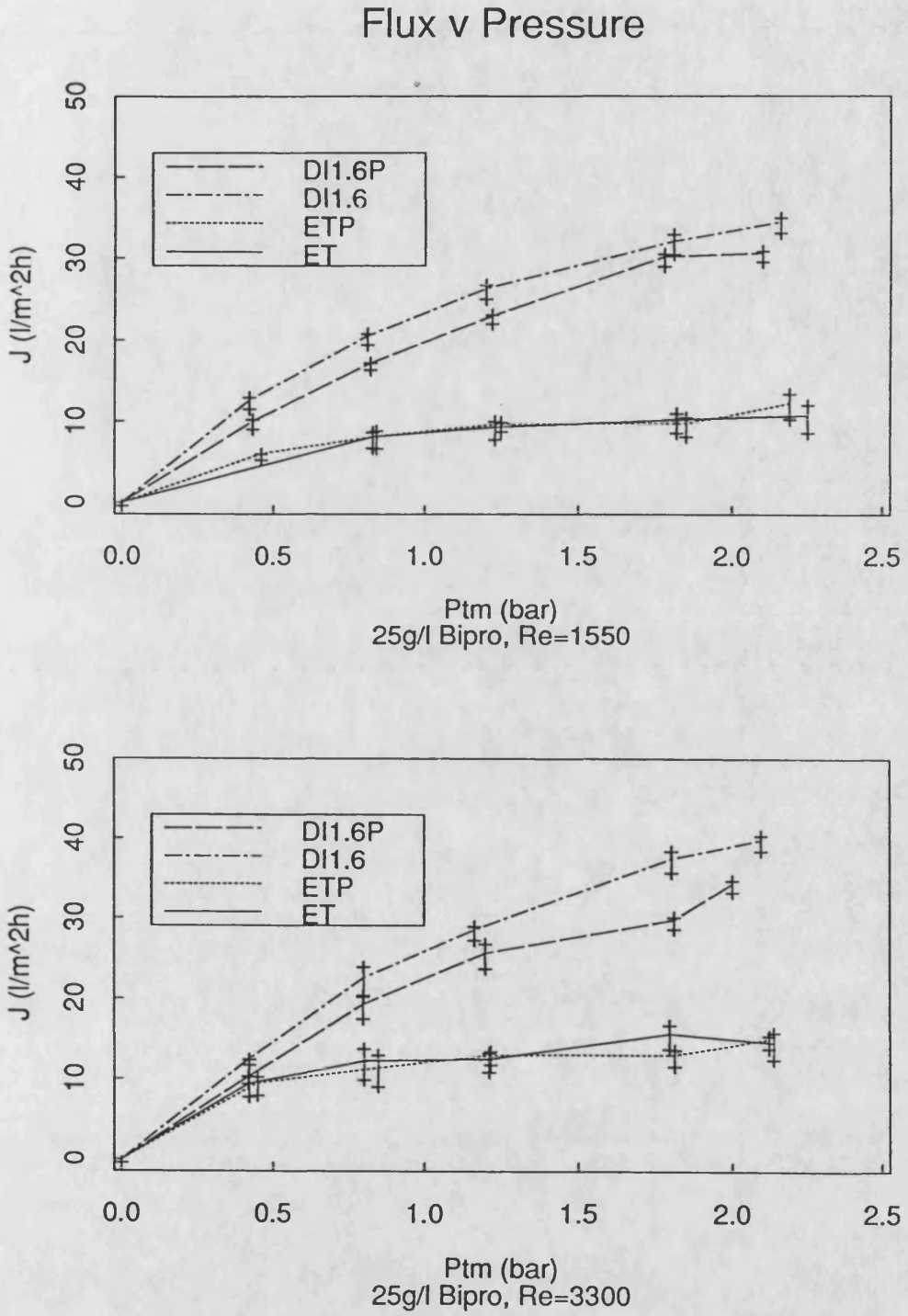

Fig 3.2: Comparison of "snapshot" ultrafiltration fluxes for **ET**, **ETP**, **DI**1.6 and **DI**1.6**P** at Re = g) 1550 and h) 3300. NFR = 0.62 and 0.78 respectively. Re_p = 950 and St = 0.22 for pulsed flow.

been plotted here. The agreement between the 2 sets of data is excellent. Fig 3.2 shows:

Pulsed flow(**ETP**) improves fluxes for Re≤350. The extent of improvement is reduced as Re is increased until at Re≥700, fluxes obtained with **ET** and **ETP** are the same.

A threshold Reynolds number, Re_t, of approximately 200 must be exceeded before **DI**1.6 has a beneficial effect on flux. At Re=50 and 100, the **ET** and **DI**1.6 fluxes are identical. At Re=200 there is a flux enhancement effect above 1.6 bar and at Re=350 over the entire P_{tm} range. This is consistent with Wyatt et al(1987) who observed that in steady flow, the flux through both dimpled and flat membranes is approximately the same at low P_{tm} and Re.

For Re≥350, the improvement in flux is significant and reaches a maximum in the Re range 350-1550. At Re=3300, the relative improvement is slightly smaller as the **ET** fluxes have increased from Re=1550.

When pulsed flow is used, a further improvement in flux occurs for **DI**1.6**P** relative to **DI**1.6 at Re=50-350 over the entire P_{tm} range. Flow reversal occurs at these low Re values: NFR= 0.04-0.27. At Re=700-1200(NFR=0.43-0.56) the **DI**1.6 and **DI**1.6**P** fluxes are the same. For Re=1550-3300(NFR=0.62-0.78) the **DI**1.6**P** fluxes are less than the **DI**1.6 fluxes.

For **DI**1.6 at Re≥350, limiting flux behaviour is not occurring for P_{tm}<1.6 bar. As with **DO**2.2, it is not certain whether a flux plateau has been reached at P_{tm}=2.2 bar for **DI**1.6(Re≥700) and for **DI**1.6**P**(at all Re) or if further increases in flux are possible.

3.3.4 The Effect of Amplitude and Frequency:

Fig 3.3(a)-(b) shows the snapshot results for the effect of frequency and amplitude on flux for **DO**2.2 at Re=350 and 1050 respectively. The numbers indicate the random order in which the experimental conditions were changed for the snapshot experiments. The fluxes at points 1 and 11 agree as the vertical bars representing the raw average plus and minus one standard deviation overlap. These points represent the initial and final data points which correspond to the

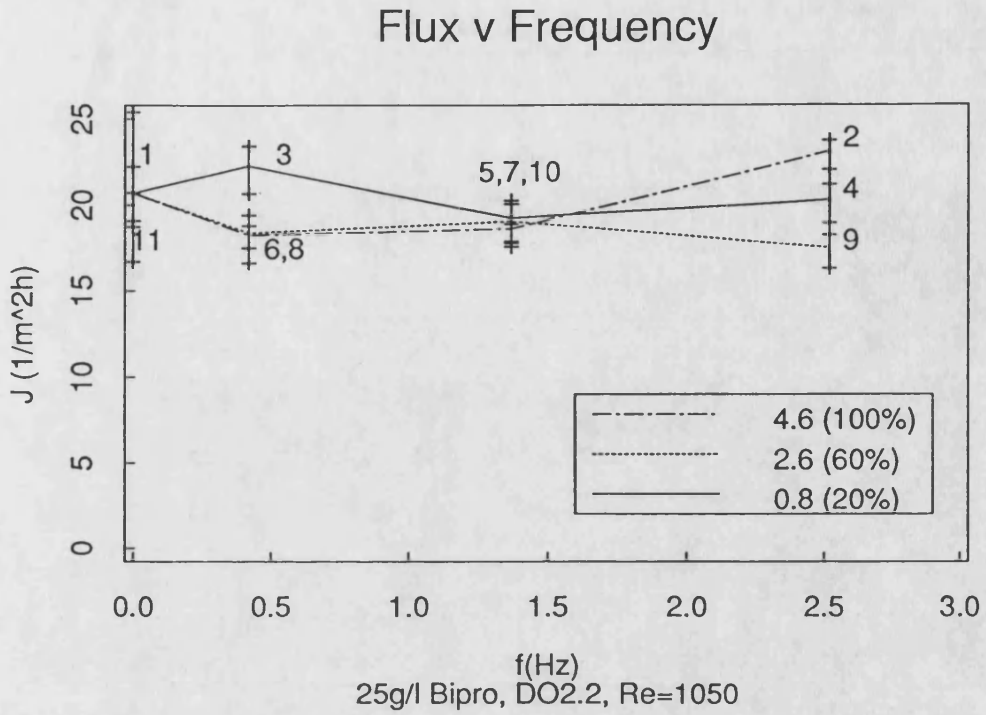

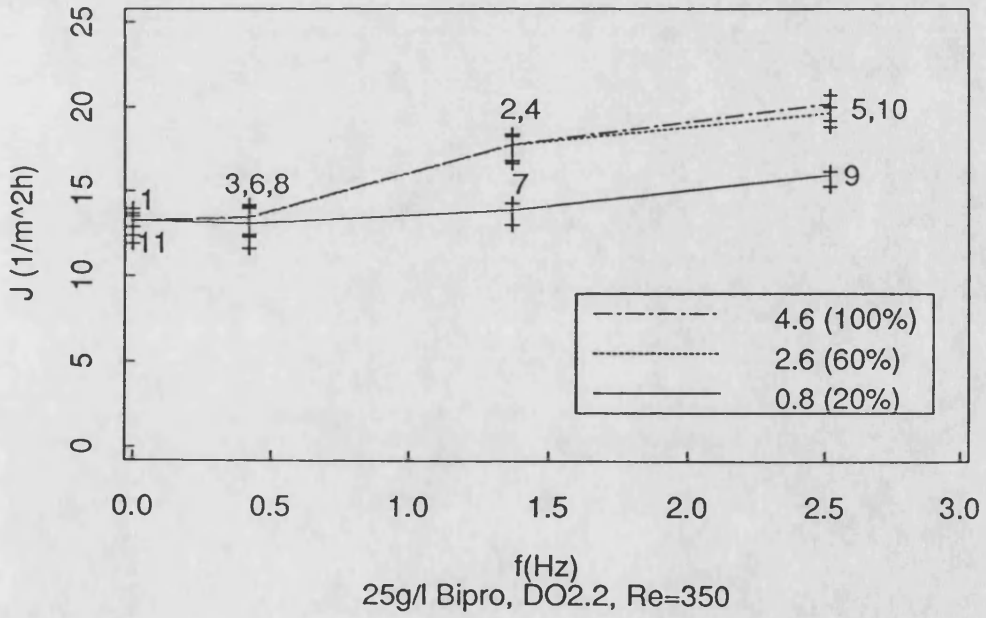

Fig 3.3: The effects of frequency and amplitude on "snapshot" ultrafiltration fluxes for **DO**2.2 at P_{tm} = 1.2 bar and Re = a) 1050 and b) 350.

same operating conditions. This agreement shows that the extent of long term fouling occurring during each experiment is insignificant.

At Re=1050(Fig 3.3a) there is no improvement in flux as the amplitude and/or the frequency is increased. The variation in fluxes illustrated here is due to experimental error. At Re=350(Fig 3.3b), for f=0.4 Hz, there is virtually no effect of amplitude on flux. As the frequency increases to 1.4 and then 2.5 Hz this results in a moderate improvement in flux of similar magnitude for amplitudes of 2.6 mm(60%) and 4.6 mm(100%) but no significant improvement at 0.8 mm(20%). Flow reversal only occurs at positions 5, 10 and 4 in Fig 3.3b.

The **DI**1.6 results at Re=10, 50, 100 and 200 are not presented here on a flux v f/X basis as they show exactly the same trends as Fig 3.3b; the only difference being the positions where flow reversal occurs. Instead, the **DI**1.6 fluxes corresponding to a) X=4.6 mm(100%), variable frequency and b) f=2.5 Hz, variable amplitude, have been plotted together with the **ET**, **DI**1.6 and **DI**1.6**P**

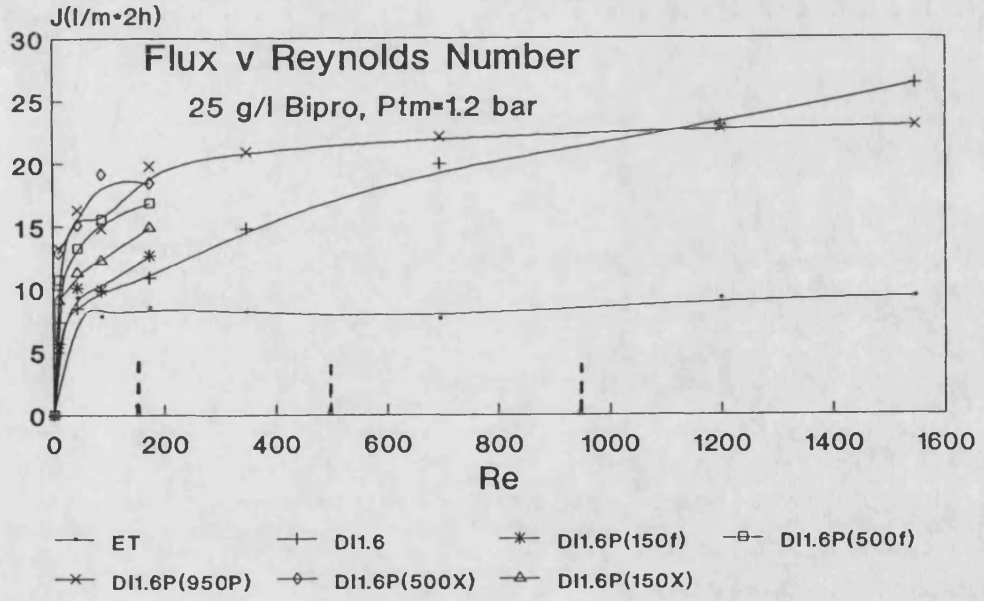

Fig 3.4: A comparison of the "snapshot" ultrafiltration fluxes for **ET** and **DI**1.6 with **DI**1.6**P** fluxes at P_{tm}=1.2 bar and Re_p=150, 500 and 950. The suffix, X or f, in the legend indicates the dependent variable for each set of pulsed flow data. For variable f, X=4.6 mm(St=0.22); for variable X, f=2.5 Hz.

snapshot data from Fig 3.2 in Fig 3.4 against Re. Each set of data corresponds to a particular Re_p value, tabulated in the legend of Re_p=150, 500 and 950(f=0.4, 1.4 and 2.5 Hz at X=4.6 mm and X=0.8, 2.6, and 4.6 mm at f=2.5Hz respectively). The letter, X or f, in the legend indicates the dependent variable for each set of data. The dashed line indicates the point of flow reversal for each Re_p value in Fig 3.4. At Re_p=150, the **DI1.6** and **DI1.6P** fluxes are similar. At the higher Re_p values, fluxes increase rapidly with Re until a plateau level is reached around Re=200. These fluxes are significantly greater than the **DI1.6** fluxes at the same Re. Once this plateau level is reached the flux becomes independent of the net cross-flow velocity and of similar magnitude to the flux obtained in steady flow for **DI1.6** at a velocity similar in magnitude to the pulsed flow velocity. As the point of flow reversal is passed there appears to be no flux advantage to be gained by using pulsed flow.

These fluxes are significantly greater than the **ET** fluxes which remain relatively constant over this range. For the same Re_p value, the limited amount of data points show that the fluxes at f=2.5 Hz and variable amplitude are consistently higher than those at X=4.6 mm and variable frequency.

3.3.5 Long Term Fouling Experiments:

In this section, the results of long term fouling experiments for **DO2.2** and **DI1.6** under steady and pulsed flow conditions are presented. The flux data has been exponentially smoothed using a=0.2 as described in Section A1.3.

In Fig 3.5 and 3.6, the long term fouling steady state fluxes are consistent with snapshot fluxes corresponding to identical operating conditions from Sections 3.3.3. and 3.3.4. A more quantitative comparison of corresponding long term and snapshot fluxes is made in Section A1.4. Each graph shows that the period of rapid initial flux decay is virtually complete after 30 min for each system. The flux continues to decline gradually. The implications of this gradual flux decay on the validity of the snapshot technique is discussed in Section A1.4.

(A) Doughnuts(DO2.2):

Fig 3.5 shows the results of the long term fouling experiments for **ET**, **DO**2.2, and **DO**2.2**P** at Re = 1050 and P_{tm} = 1.2 bar. The steady state flux for **DO**2.2 is 93% greater than for **ET** . There was no significant difference in flux behaviour between **DO**2.2 and **DO**2.2**P**.

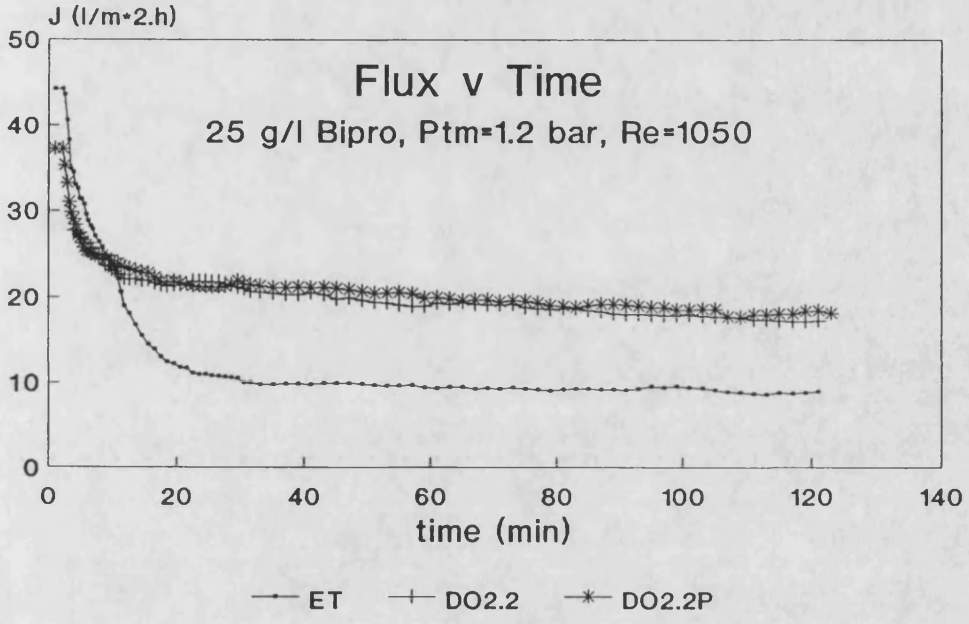

Fig 3.5: Long term flux behaviour of the **ET**, **DO**2.2 and **DO**2.2**P** systems at Re = 1050. Re_p = 950 and St = 0.22 for pulsed flow.

(B) Discs(DI1.6):

Fig 3.6(a)-(b) shows the results of the long term fouling experiments for **ET**, **ETP**, **DI**1.6 and **DI**1.6**P** at P_{tm} = 1.2 bar and at the Re values indicated in the legend. In Fig 3.6a at Re = 700, the **DI**1.6 steady state flux is approximately 150% greater than the **ET** flux. The steady state fluxes are virtually the same for **ET** and **ETP** and also for **DI**1.6 and **DI**1.6**P**. Fig 3.6b shows that at Re = 350, pulsed flow improves the fluxes for **ET** and **DI**1.6; the ratio of the steady state fluxes for pulsed/steady flow is approximately 1.45 for both **ET** and **DI**1.6.

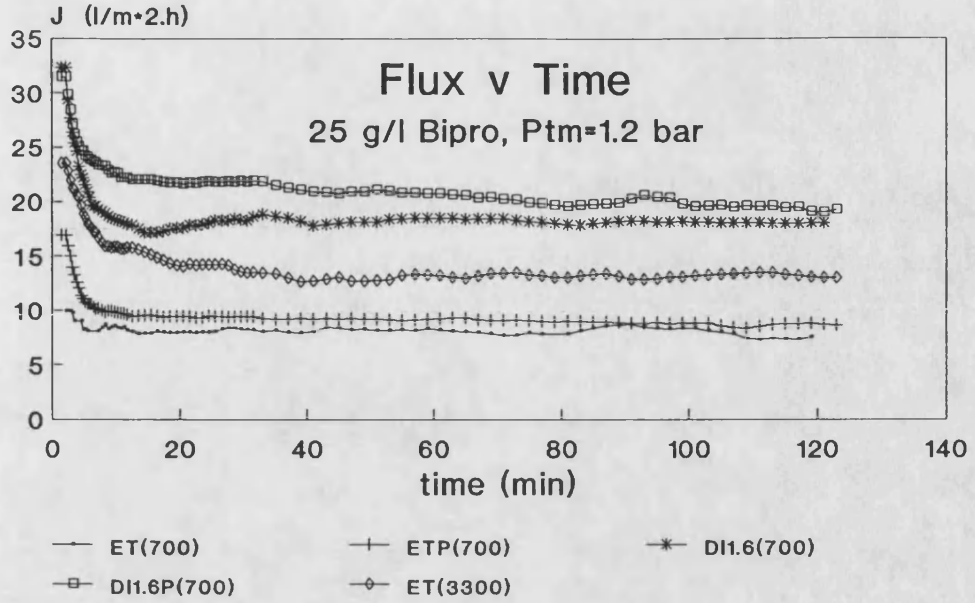

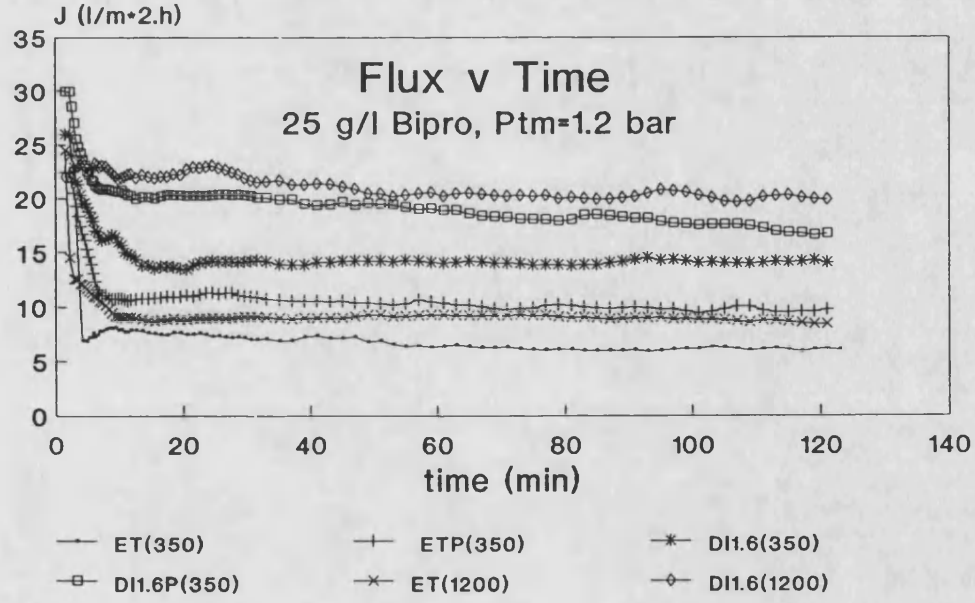

Fig 3.6(a-b): Long term flux behaviour of **ET**, **ETP**, **DI**1.6 and **DI**1.6**P** at the Re values indicated in the legend. Re_p=950 and St=0.22 for pulsed flow.

Results for Re=1200 are also included in Fig 3.6b. At Re=1200, the steady flow velocity in the tube is similar to the pulsed flow velocity for Re=350 (Re_p=950). For **ET** the steady state flux is slightly greater at 950P than at 1200 while with **DI1.6**, the converse is true.

The fluxes of the baffled systems at Re= 350, 700 and 1050(Figs 3.6b, 3.6a & 3.5 respectively) are greater than for **ET** at Re=3300(Fig 3.6a).

(C) Closed Outlet Valve Experiments and the Effect of Switching Between Steady and Pulsed Flow:

For long term fouling experiments with the retentate outlet valve closed steady state fluxes were obtained over the last 60 min of operation. At the end, the flow conditions were changed from steady to pulsed flow or vice-versa and filtration continued for a further 10 min and average fluxes were calculated. These results are shown in Table 3.2 and the flux/time behaviour shown in Fig 3.7. Each symbol shown in Table 3.2 and Fig 3.7 refers to a particular experiment; the code shown in Table 3.2(eg. **ET**) is used to indicate whether the flow is steady or pulsed and changes in the final 10 min period of operation(in Table 3.2, **ET** becomes **ETP**, etc). The symbols shown in Fig 3.7 remain the same.

The 2 hour time period results are described first. The **DI1.6** and **ET** flux behaviour is identical. The **ETP** and **DI1.6P** steady state fluxes are 30 and 191% greater than the **ET** flux respectively. Pulsed flow should promote better mixing when the system is operated in this mode which will help to alleviate concentration polarization particularly in the end region of the membrane module where the highest concentrations in the module will be reached in steady flow.

The steady state fluxes calculated over the last 10 min agree with corresponding 2 hour values within plus or minus one standard deviation, as shown in Table 3.2 except for **DI1.6P** where the difference is significant. On the completion of this experiment the retentate valve was reopened and a sample of the retentate taken to determine the degree of concentration that had been

	First 2 hours			Last 10 min		
Expt	Code	J_{ss}	σ	Code	J_{ss}	σ
•	**ET**	5.6	0.5	**ETP**	8.9	0.8
+	**ETP**	7.3	0.6	**ET**	4.1	0.7
*	**DI**1.6	4.9	0.3	**DI**1.6P	9.5	0.5
□	**DI**1.6P	16.2	1.0	**DI**1.6	5.5	0.5

Table 3.2: Steady state fluxes calculated over the two hour long term fouling period and 10 min at the end for the disc baffles system. J_{ss} is the steady state flux calculated over the last 60 min of operation for the initial period and also over the last 10 min of operation when the flow conditions were changed. σ is the standard deviation.

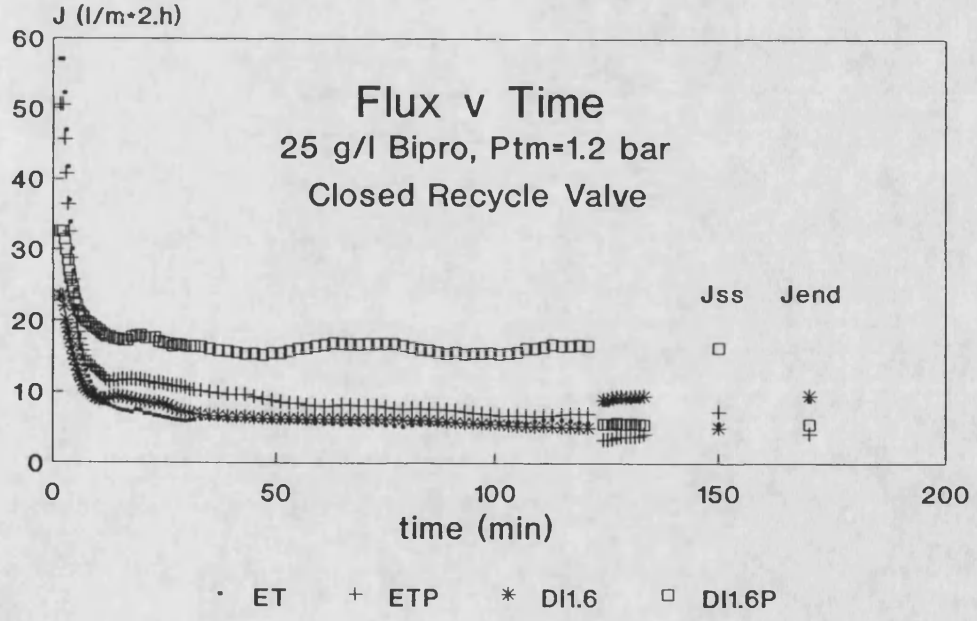

Fig 3.7: Long term fouling behaviour of the **ET**, **ETP**, **DI**1.6 and **DI**1.6**P** systems. $Re_p = 950$ and $St = 0.22$ for pulsed flow. The retentate outlet valve was completely closed for these experiments.

reached in the module for the **DI**1.6 and **ETP** experiments. These were found to be 4.7 and 5.4 for lactoglobulin and 3.4 and 4.3 for lactalbumin respectively.

3.4 Discussion:

These results are related to the power consumption and flow patterns in each system in Chapters 5 and 6 respectively.

3.4.1 Empty Tube(**ETP**):

For **ETP**, pulsed flow(Re_p=950) increases fluxes to a small extent for Re≤350 where flow reversal occurs. The pulsed fluxes over the Re range 50-3300 are equal in magnitude to steady flow fluxes for Re=700-3300. Hence the **ETP** fluxes are comparable in magnitude to **ET** fluxes when the pulsed flow velocity is similar in magnitude to the steady flow velocity($Re=Re_p$). Long term fouling experiments at P_{tm}=1.2 bar support this as fluxes were similar for **ETP** at Re=350 (Re_p=950) and Re=1200 for **ET**. The occurrence of flow reversal and the magnitude of the maximum velocity in the tube are two observations that help to explain these results. The actual mechanism is not well understood but some insight can be gained from similar work, which is described in more detail in Section 1.2.3.

One possible mechanism is the Richardson's effect which occurs in laminar pipe flows. Edwards and Wilkinson(1971) explained that for Newtonian fluids with pulsed flow at low frequencies, the velocity profile is nearly parabolic with the maximum at the tube axis. As the frequency increases this maximum increases in amplitude and moves towards the tube wall. This velocity overshoot is known as the Richardson's effect. The actual mechanism will be more complicated in filtration processes due to the presence of a flux through the membrane. Milisic and Bersillon(1986) stated that this velocity overshoot is believed to affect the shear stress at the surface of the filtration cake, helping to stabilize its thickness. Most of the experiments of Kennedy et al(1974) were

carried out in the laminar-turbulent transition or turbulent regimes and consequently, the Richardson's effect can not be used to explain these results. Instead, Kennedy et al attributed the improvement in flux to a reduction in concentration polarization due to greater convection in pulsed flow compared with steady flow. Bauser et al(1986) partly attributed the improvement in flux they observed for pulsed flow to greater convection like Kennedy. In addition, they stated that a reduction in the protein deposits could have occurred due to shear forces in pulsed flow. As the maximum in the velocity profile increases in amplitude and moves towards the wall with increasing frequency, this will result in greater convection of fluid in the wall region and an increase in the local shear rate, resulting in a reduction in the boundary layer thickness. The occurrence of flow reversal may also have a significant effect on local shear. These effects may be more significant in microfiltration applications where fouling occurs via a different mechanism.

3.4.2 Baffles:

Both sets of baffles improve fluxes relative to **ET** at the same Re value. The relative improvement is most significant in the Re range: 350-1550, where concentration polarization is most severe for **ET**.

Intuitively, addition of periodically spaced baffles will not only increase turbulence in the bulk fluid stream but will also interrupt development of the boundary layer at the membrane surface. Both these effects will tend to reduce concentration polarization. This is discussed further in Section 6.4.3.

3.4.3 Baffles and Pulsed Flow:

For both baffled systems, a further improvement in flux occurs with pulsed flow(Re_p=950, St=0.22) when the baffled systems are operating under limiting flux conditions. This corresponds to low Re values where flow reversal occurs. One mechanism causing this improvement will be vortex mixing as described by Sobey(1980), Mackley(1987) and Colman and Mitchell(1990). The maximum

fluxes with pulsed flow in the Re range 50-3300 are equivalent to the **DI**1.6 fluxes at Re=700-1200 and greater than the **ET** fluxes at Re=3300. Hence, as in the **ET** case, the **DI**1.6**P** fluxes are similar in magnitude to **DI**1.6 fluxes at $Re=Re_p$. This is supported by the long term fouling experiments where fluxes of similar magnitude were obtained at Re=350(Re_p=950) and Re=1200 for **DI**1.6. At Re≥700, the system is also approaching pressure dependent behaviour so that any further improvement in flux will be nominal. These observations are consistent with the results of Colman and Mitchell(1990) who found that fluxes in pulsed flow(Re=200, Re_p=800, St=0.11) were similar to those in steady flow in the baffled channel(Re=1000) and greater than those in steady flow in an unbaffled channel at Re=3000. It is surprising that McKeever and Kemp(1986) observed no flux improvement in steady and pulsed flow in their baffled system. Assuming their stated values of frequency are correct, their experimental conditions correspond to Re_p=2700 and 1400(f=35 and 18 Hz respectively; X=1 mm, St=0.99) for Re=8600 and 860 respectively. The relatively large magnitude of the net cross-flow rate, especially at Re=8600, and high St value compared with the Stage 1 experiments and the results of Colman and Mitchell, may explain why they observed no improvement with pulsed flow in their system. This still does not explain why McKeever and Kemp observed no flux improvement at all for steady flow in their baffled system at Re=860-8600, as this contrasts with the flux improvements observed for steady flow in a baffled system in this study and in Colman and Mitchell's work at moderate Re values.

3.4.4 Frequency and Amplitude:

As stated in Section 3.4.3, pulsed flow only causes an increase in flux when the baffled systems are operating under limiting flux conditions. This explains why no improvement in flux was observed at Re=1050 in Fig 3.3a, as under these conditions(P_{tm}=1.2 bar and Re=1050) Fig 3.1b shows **DO**2.2 is only beginning to demonstrate limiting flux behaviour and, in fact, there is very little difference in the **DO**2.2 and **DO**2.2**P** fluxes shown in Fig 3.1b. Whereas, at Re=350 for **DO**2.2 and Re=10-200 for **DI**1.6, inspection of Fig 3.1a and 3.2a-d shows that each

baffled system is operating under limiting flux conditions and an improvement in flux should be observed with pulsed flow. This is true as Fig 3.3b and 3.4 show for **DO2.2** and **DI1.6** respectively. Both these graphs show that fluxes increase with increasing amplitude for X≥2.6 mm(60%) and f≥1.4 Hz.

The rapid increase in flux observed at low Re values, shown in Fig 3.4, suggests that the net cross-flow velocity must be above a certain minimum value for pulsed flow to be effective. It is possible that if the residence time in the module is too long, then an axial concentration gradient will develop. For higher Re values, but still within the range where flow reversal occurs, the flux becomes decoupled from net cross-flow velocity and of similar magnitude to the steady flow flux at $Re=Re_p$.

3.4.5 Closed Outlet Valve Experiments and the Effect of Switching Between Steady and Pulsed flow:

Some interesting results were obtained in these experiments. Changing the operating conditions from steady to pulsed flow or vice-versa showed that the flux behaviour was reversible except for changing from **DI1.6** to **DI1.6P**. This may be due to fouling being greater for steady flow compared with pulsed flow for **DI1.6** when operated in this mode.

More importantly, the flux of 16.2 $lm^{-2}h^{-1}$ is comparable with the **DI1.6** flux at Re=700 at the same P_{tm} value of 1.2 bar(see Fig 3.2e) and quite high concentration factors were reached within the module. These observations are **significant** and suggest that it is possible to operate the baffled module in continuous single pass mode with pulsed flow for thickening purposes or to avoid the pumping costs associated with recirculation. Colman and Mitchell(1990) made a similar suggestion on the basis of their pervaporation results. Kroner and Nissenen(1988) showed that this approach was feasible with the rotating filter. Murkes and Carlsson(1988, pg 80-81) discuss in more detail the practical ways of controlling the intermittent opening and closing of the outlet valve. Another option is to operate at a sufficiently low net cross-flow velocity to give the desired outlet concentration. One possible advantage of the former approach compared

with the latter is that dissipation of the pulse is less likely to occur(see Section 4.1.3(C)). According to Dickens et al(1989) and Colman and Mitchell(1990), the RTD will exhibit plug flow characteristics with minimum axial dispersion by appropriate choice of the amplitude. In this mode of operation an axial concentration gradient will develop due to the residence time in the module. The valve opening interval and cross-flow velocity must be chosen to balance the desired outlet concentration with flux considerations.

CHAPTER 4
STAGE 2 FILTRATION EXPERIMENTS

In Stage 1(Chapter 3), the feasibility of using baffles alone and in combination with pulsed flow for improving membrane filtration performance has been demonstrated. Stage 2 extends this work, investigating the filtration performance of four different baffled systems. Higher P_{tm} values up to 5-5.5 bar are investigated and the hydrodynamic conditions are extended to include fully turbulent flow conditions. Re_p is also increased to 6450 so that flow reversal can be achieved over a much wider range of operating conditions. This chapter has been divided into four sections. Section 4.1 deals with characterization of the system. Section 4.2 describes the "snapshot" filtration experiments for four different baffled systems. Section 4.3 investigates the effect of frequency and amplitude on flux for the disc baffled systems. Section 4.4 describes the filtration experiments for variable concentration and two different feed solutions.

4.1 System Characterization:

4.1.1 Introduction:

Two additional parameters have been defined in order to help explain the filtration results. These are:

a) the pulsed velocity waveform, $V_p(t)$. The pulsed velocity waveform is the "trace" which shows how the volume displacement of the fluid in pulsed flow varies as a function of time and percentage amplitude. It is important to

characterize the waveform as its nature and magnitude could affect the filtration results.

b) the pulsing pressure, P_p. In pulsed flow the pressure measured by the inlet and outlet transducers changes with time in a similar manner to the volume displacement. The peak-centre amplitude of the pressure pulse is defined as the pulsing pressure, P_p.

The objectives in this section were:

a) to determine the waveform, $V_p(t)$, as a function of amplitude and time.

b) to determine the magnitude of P_p as a function of P_{tm} at X=30.5 mm(100%) and f=2.5 Hz.

4.1.2 Materials and Methods:

(A) Characterization of the Waveform, $V_p(t)$:

The waveform is a characteristic of the pump drive and not the type of pumphead. Hence although two different pumpheads were used in Stages 1 and 2:(plunger and diaphragm respectively); the waveform was exactly the same shape for each pumphead, the only difference being the actual amplitude of the wave due to the different capacities of the 2 pumpheads. Consequently, a simple method was used to measure the volume displacement, V_p, as a function of time and amplitude for the larger capacity E2B(short stroke)/D50P diaphragm pumpheads only. The metering pump was disconnected from the filtration module and the "volume displacement" circuit connected to each pumphead as shown in Fig 4.1. The "volume displacement" circuit consisted of two 10 ml pipettes mounted side by side and connected independently via flexible tubing to the inlet and outlet pumpheads. The plug valve enabled the system to be filled using distilled water at 18°C with the seal cap on the pumphead being opened to allow air to escape from the system. The water levels in each manometer could be adjusted independently allowing a common zero to be set corresponding to zero displacement.

The rotating disc attached to the drive shaft of the metering pump was graduated at 45° intervals allowing the liquid level in each pipette to be measured at each of 8 positions on the disc for amplitudes ranging from 10-100%.

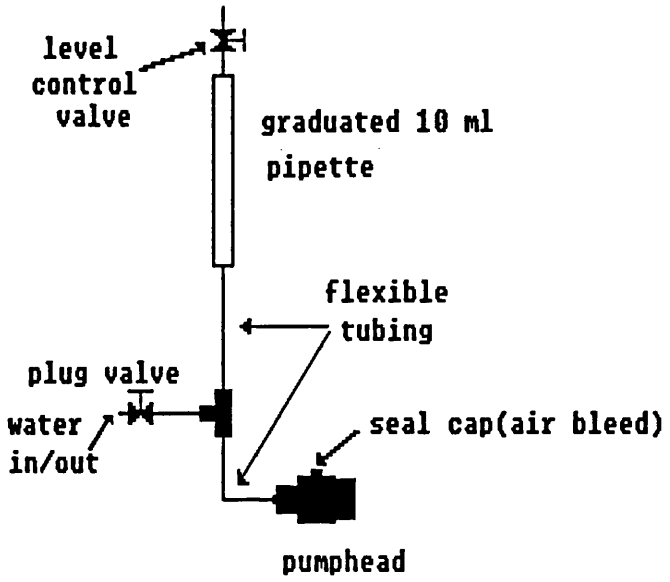

Fig 4.1: Schematic diagram of the "volume displacement" circuit.

(B) Measurement of the Pulsing Pressure, P_p:

P_p was measured using the same 2 PDCR absolute pressure transducers used for measuring P_{tm}. These were connected to a U/V trace recorder(Type S.E. 3006 manufactured by S.E. Laboratories Ltd, Middlesex, England). Traces of pulsing pressure using distilled water at 18°C for both inlet and outlet sides were obtained at different P_{tm} values. P_p was measured from these traces directly in mm as the peak-centre amplitude and converted to P_p in bar by correcting for the signal amplification and using the transducer calibration data. When a transmembrane pressure is applied this causes the trace to be offset from zero. P_{tm} was evaluated directly from the voltage applied to correct this offset and converted to P_{tm} in bar in the same manner as P_p.

4.1.3 Results and Discussion:

(A) Summary:

The pulsed velocity waveform has been described as being truncated triangular in nature, where truncated means that as the amplitude is decreased below 100%, there are increasingly larger proportions of the cycle over which no motion occurs.

The pulsing pressure increased with P_{tm}, reaching a maximum value of approximately 1.6 bar for all systems at P_{tm}=4 bar.

(B) Waveform, $V_p(t)$:

Fig 4.2 shows the nature of the pulsed flow at different amplitudes for two complete cycles for the inlet(top) and outlet(bottom) pumpheads. Each wave begins at the point of maximum volume displacement for the outlet plunger (minimum for the inlet) and has been offset so that the zero position on Fig 4.2 corresponds to the position of zero displacement(maximum forward velocity for inlet; maximum reverse for outlet). Fig 4.2 shows that the waveform is "triangular" rather than sinusoidal. As the amplitude is decreased the waveforms consist of progressively smaller fractions of the full wave observed at 100% until at 10% only the very top fraction of the 100% wave is seen. Hence, the waveform is periodic but truncated. As the amplitude is decreased below 100%, the truncation of the pulsed waveform results in an increasingly larger proportion of the cycle over which no motion occurs. These are the horizontal sections of each waveform. In further discussion, the waveform is referred to as being truncated triangular.

This behaviour can be explained by considering how the amplitude is altered: the displacement of the pumphead is controlled by an eccentric mechanism. Hence as the eccentric rotates the plunger or diaphragm rod is pushed forward to the position of maximum displacement; its motion being

controlled by a spring on the backward movement. As the amplitude is reduced, the rod is pushed forward so that a gap occurs between the eccentric and the rod resulting in a larger proportion of the cycle over which no rod motion occurs.

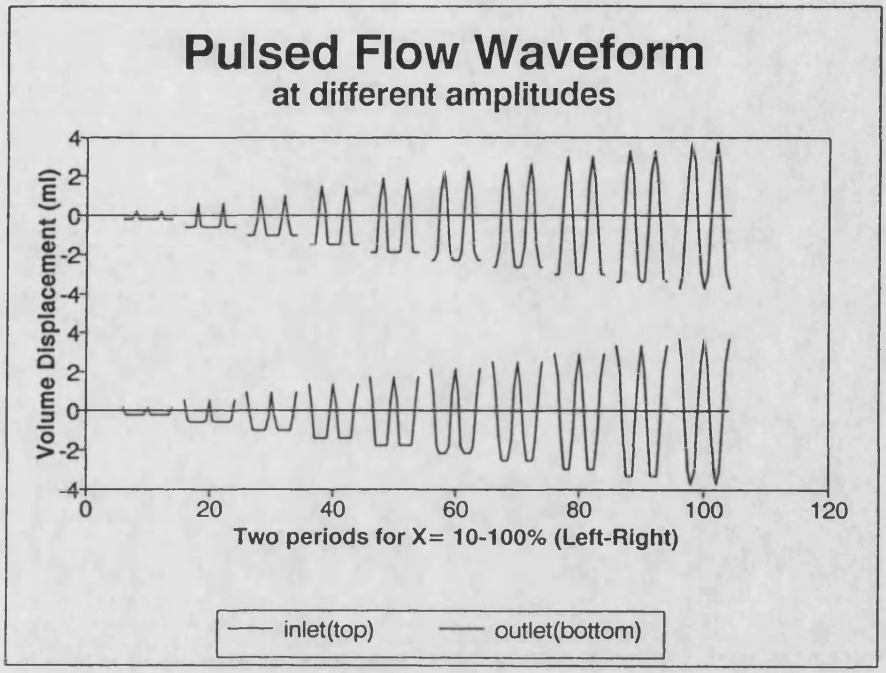

Fig 4.2: The volume displacement as a function of amplitude and time. Two complete periods are shown for X=10-100%. The inlet and outlet waveforms are shown at the top and bottom respectively.

(C) Pulsing Pressure, P_p:

For each system, at $P_{tm}=0$, a small but finite P_p exists. As P_{tm} is increased, P_p also increases, especially above 1.5 bar. Maximum values of P_p are approximately 1.5 and 1.7 bar for the inlet and outlet sides respectively for all systems at P_{tm}=3-4 bar. The error in P_{tm} under pulsed flow conditions is estimated to be 10% from experimental observations. The outlet pulsing pressure is greater than the inlet for all systems except **ET**.

Wyatt(1988) noted that when oscillatory flow was used, the rotameter bob, measuring the cross-flow, dropped and also vibrated up and down. Vibration of the rotameter bob was also observed in these experiments. This is due to the

flow around the bob being disturbed and possibly due to an increase in the pressure drop. It is to be expected that as P_{tm} increases the pressure drop across the retentate control valve will rise and this may explain the increasing magnitude of P_p with P_{tm}. The vibrations mean some of the pulsed flow is being dissipated down the outlet tubing.

On the inlet side some dissipation of the pulsed flow due to backflow through the non-return valve is also occurring and this may explain why the pulsing pressure was greater for the outlet side compared with the inlet. In future, it may be possible to purchase a pulsed flowmeter such as a Gould Statham Flowmeter which employs electromagnetic probes and is typically used in medical applications to measure the pulsed flow in situ. This will give a more accurate measurement of the pulsed flow velocity and will enable the extent of pulse dissipation to be determined.

4.2 Filtration Experiments:

4.2.1 Introduction:

The objectives were:

a) to investigate the filtration performance of 4 different baffled systems, described in Table 2.1, using pulsed or steady flow. The performance is to be compared with a conventional system operating under the same conditions of cross-flow velocity and transmembrane pressure. It is hoped to determine the optimum baffle configuration and the best operating conditions.

b) the P_{tm} range is extended to 5-5.5 bar to investigate whether the slight upward trend in the flux data at P_{tm}=2.2 bar that was observed in Stage 1, is indicative that higher fluxes can be obtained at higher P_{tm} values or alternatively, that limiting flux behaviour will be demonstrated. The flow regime is also extended to cover fully turbulent flow conditions to compare the fluxes with pulsed flow with steady flow fluxes for the ET and baffled systems.

c) Re_p is increased to 6450 to investigate if the decoupling of flux from cross-flow velocity observed in Stage 1 means it is possible to obtain fluxes similar to those in turbulent operation, through the use of pulsed flow of sufficient magnitude but at relatively low cross-flow velocities. For pulsed flow of this magnitude, flow reversal can be achieved over a much wider range of Re values.

4.2.2 Experimental Design:

In Stage 2 several modifications were made to the apparatus(see Section 2.2.2) and snapshot technique used in Stage 1 in order to achieve these objectives. The snapshot modifications are described here.

In Stage 2A, the "snapshot" technique was used to obtain flux data under the various conditions of cross-flow velocity and transmembrane pressure for 4 different baffle systems as shown in Table 4.1. A lower feed concentration of 10 gl^{-1} was chosen to obtain limiting flux conditions for the conventional system under these operating conditions. The pulsed flow conditions were determined by the pump capacity. For the P_{tm}/Re snapshot experiments an amplitude of 30.5 mm(100%) and frequency of 2.5 Hz were used which corresponds to Re_p=6450 (v_p=0.48 ms^{-1}) and St=0.033.

2A) **ET, DI**0.8,	v($cm.s^{-1}$)	0.7	2.7	5.4	11	16	20
DI1.6, **DI**3.2,	Re	100	350	750	1450	2200	2750
DO1.5							
	P_{tm} (bar)	1	2	3	4	5-5.5	
2B) **ET, DI**1.6,	v($cm.s^{-1}$)	5.4	11	48	48	120	
DI3.2	Re	750	1450	6450	6450P	16000	
	P_{tm} (bar)	1	2	3	4	5-5.5	

Table 4.1: The experimental conditions investigated in each stage of the snapshot filtration experiments, where for every Re value every P_{tm} value was investigated.

For reasons explained in Section A1.5, the "snapshot" technique was modified as follows:

a) the initial period was extended from 20 to 60 min.

b) the logging period was also changed from 20 to 30s.

c) with each set of baffles two experiments were carried out under steady flow conditions consisting of 17 frames, a frame being a 6 min interval where the operating conditions were maintained constant(see Section A1.2). These two experiments were combined to give the overall flux/pressure relationship, the first experiment used Re = 100, 750 and 2200; the second 350, 750, 1450 and 2750 for P_{tm} up to approximately 5 bar. Identical starting and end conditions were chosen for each part and a single frame corresponding to pulsed flow was included in the steady flow snapshot experiment.

At least two snapshot experiments for each set of baffles using pulsed flow conditions were also carried out consisting of 14 frames. These followed the same form as the above experiments and included a single steady flow frame. In this case the effect of cross-flow velocity over the range Re = 100-1450 and amplitude(4.8, 17.7 and 30.5 mm) was investigated at different P_{tm} up to approximately 5 bar.

In Stage 2B, further "snapshot" experiments were carried out under the conditions of cross-flow velocity shown in Table 4.1 for **ET**, **DI**1.6 and **DI**3.2.

4.2.3 Results:

(A) Summary:

Baffled systems improved local mass transfer rates in steady flow over the entire Re range investigated: Re = 100-50000. The relative improvement reached a maximum over the range: Re = 750-2200.

It has been suggested that a threshold number, Re_t , exists ($Re_t < 100$) in steady flow, below which no improvement in flux is observed for the baffled systems relative to **ET**.

DI1.6 consistently gave the highest fluxes in this optimal range and at Re≥6450, the **DI**1.6 fluxes were greater than the **DI**3.2 fluxes. In pulsed flow there was no significant difference in the fluxes between the **DI** systems. In both pulsed and steady flow the **DO**1.5 fluxes were lowest of all the baffled systems. The **DI**1.6 baffles are considered to be the best configuration of the baffles studied.

It would be impractical to operate **DI**1.6 and **DI**3.2 at Re≥16000 because the pressure drop becomes excessive in this Re range, causing a drop in P_{tm}, which reduces any improvement in flux that would be observed.

Limiting flux behaviour was not demonstrated within the experimental range in steady flow for Re≥6450 and 16000 for (**DI**1.6 and **DI**3.2) and **ET** respectively and in pulsed flow(Re_p=6450) for all baffled systems.

High fluxes, similar in magnitude to steady flow fluxes in the baffled system at Re=6450 and greater than **ET** fluxes at Re=16000-50000 were obtained with pulsed flow(Re_p=6450) in the **DI** systems at very low cross-flow velocities, providing further support for the use of pulsed flow in a baffled system in a single pass, continuous mode of operation.

For **ET**, the flux in steady flow at Re=6450 was significantly greater than in pulsed flow(Re_p=6450).

(B) Effect of Re and P_{tm} on Flux for each System:

The results for Stages 2A and 2B have been presented together in Fig 4.3 and 4.4 for both pulsed and steady flow. **DI**0.8 and **DO**1.5 were not used in Stage 2B for reasons explained in Section 4.2.4 and consequently, no data is shown for these systems for Re≥6450. In Fig 4.3 and 4.4, smoothed curves have been used to represent the trends shown by the experimental data as explained in Section A1.6. The legend in each graph refers to Re and the suffix **P** indicates this data

corresponds to pulsed flow. The same terminology is used to describe the filtration results as defined in Section 3.3.1. The results are expressed in terms of a change(usually an improvement) in flux relative to **ET**. With pulsed flow, the frequency and amplitude are 2.5 Hz and 30.5 mm(100%) respectively which corresponds to Re_p=6450 and St=0.033.

Fig 4.3(a)-(e) compare the flux performance for each system at different Re and P_{tm} values. For each system, limiting flux behaviour is observed with the magnitude of the limiting flux and P_{th} increasing with Re. Fluxes also increase within the pressure dependent region as Re increases. The dependence of flux on Re is weak for **ET** within the range 100-2750. With each of the baffled systems, there is a strong dependence of flux on Re. Little further improvement in flux is observed for **ET** and (**DI**1.6 & **DI**3.2) for Re>16000 and 6450 respectively and limiting flux behaviour is not demonstrated within the experimental range at these Re values.

The magnitude of the pressure drop and ratio of the mass of permeate collected from the inlet to the outlet sides of the module($m_{i/o}$) shows that it is not practical to operate at Re>6450 for the baffled systems as any improvement in fluxes that may occur at Re=16000 and 26000 is reduced by a drop in P_{tm}. At Re=26000 the pressure drop is approximately 4.8 and 4.0 bar for **DI**1.6 and **DI**3.2 respectively and $m_{i/o}$ is 1.5-2.0. At Re=16000, the corresponding pressure drops are 1.9 and 1.5 bar respectively and $m_{i/o}$ is 1.1-1.3. At Re=6450, the pressure drop, is 0.43 and 0.40 bar respectively and the fluxes are the same from each side.

The pulsed flow data is also included in Fig 4.3. There was **no dependence of flux on the net cross-flow velocity** for all systems over the range: Re=100-1450. The **ETP** flux(Re_p=6450) is worse than the **ET** flux at Re=6450. With **DI**1.6 and **DI**3.2, examining the data scatter and the smoothed curves for Re_p=6450 and Re=6450 shows that in both cases the flux behaviour is similar, although the 6450 fluxes are greater than the 6450**P** fluxes for **DI**1.6. In addition, for each baffled system, the fluxes obtained under steady flow conditions at the maximum Re values used in Stage 2A of Re=2200 and 2750 are similar to the pulsed fluxes up to around P_{tm}=2-3 bar. It is only above 3 bar that the fluxes are greater in pulsed flow than in steady flow.

The variability with the snapshot results is much greater in the case of pulsed flow than with steady flow, especially for $P_{tm} \geq 3$ bar. There are several reasons for this:

a) the degree of concentration polarization is reduced and hence fluxes are more sensitive to variations in membrane resistance(fouling) and/or operating conditions.

b) the pulsing pressure, P_p, increases the error in the measured P_{tm} value(see Section 4.1.3(C)) and may affect the flux directly if the system is operating in the pressure dependent region. P_p reaches a maximum of approximately 1.6 bar for $P_{tm} = 4$ bar.

In the variable amplitude(4.8, 17.7 and 30.5 mm) experiments the only consistent difference in flux behaviour occurred at $P_{tm} > 3.5$ bar where the flux at X=4.8 mm(20%) was lower than the fluxes at 17.7 mm(60%) and 30.5 mm(100%). The X=17.7 and 30.5 mm fluxes were similar in magnitude.

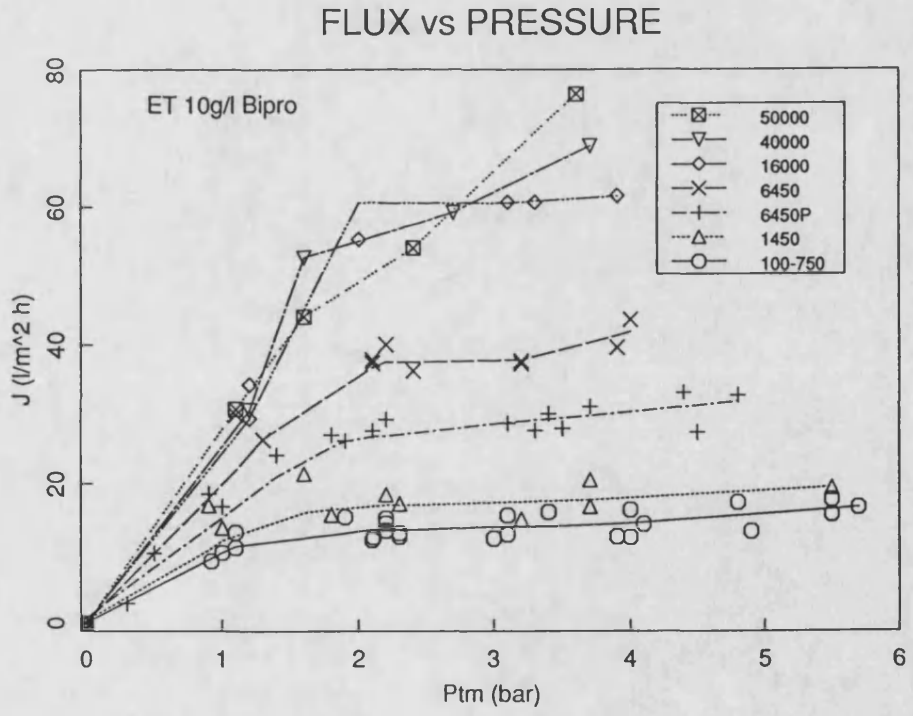

Fig 4.3: Comparison of "snapshot" ultrafiltration results for a) ET for Stage 2.

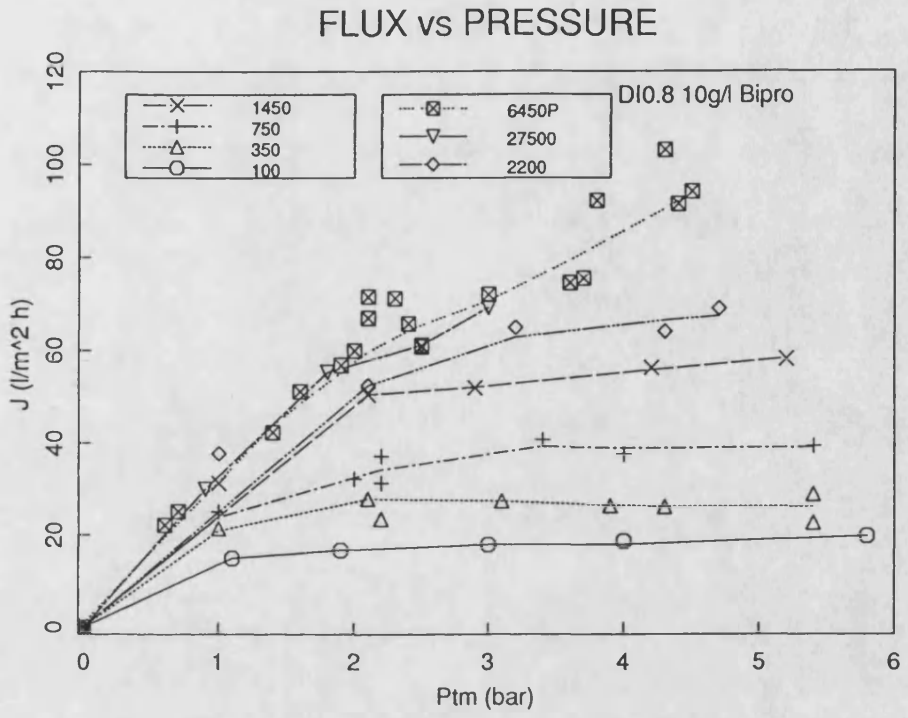

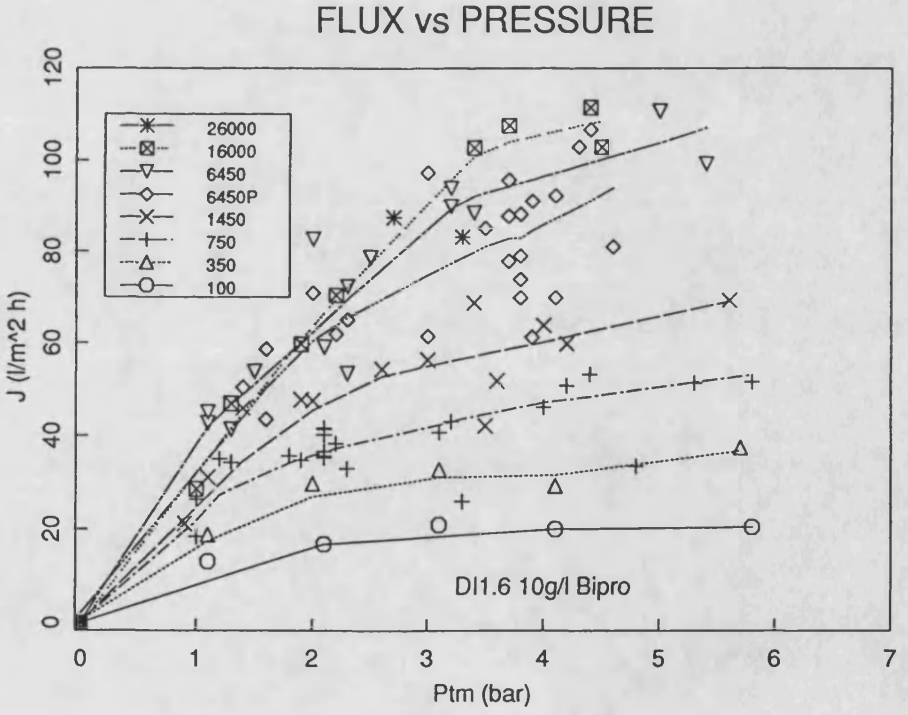

Fig 4.3: Comparison of "snapshot" ultrafiltration results for b) **DI**0.8 and c) **DI**1.6 for Stage 2.

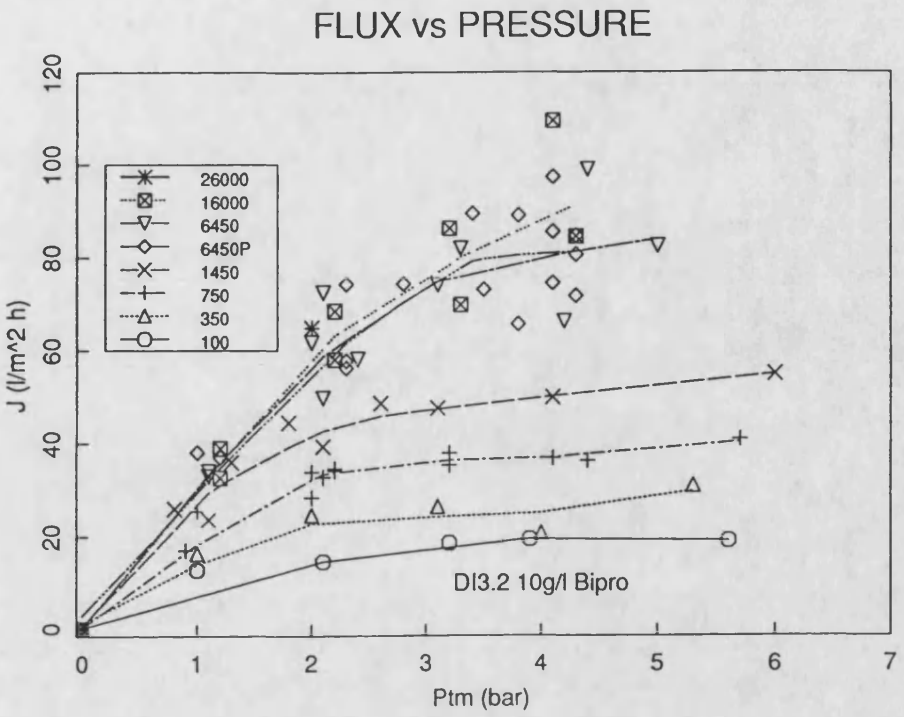

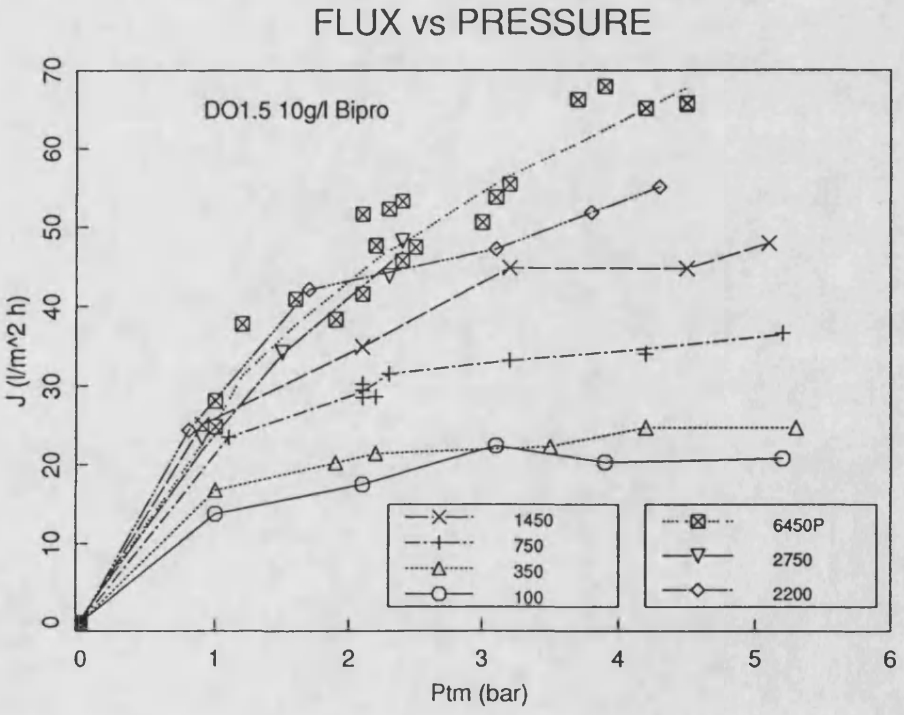

Fig 4.3: Comparison of "snapshot" ultrafiltration results for d) **DI**3.2 and e) **DO**1.5 for Stage 2.

(C) Comparison of Different Systems:

Fig 4.4(a)-(i) compare the performance of each system for particular values of Re. For each baffled system the extent of flux improvement increases with Re in both the pressure dependent and independent regions, this improvement reaching a maximum in the range Re=750-2200. **DI**1.6 and **DO**1.5 consistently give the highest and lowest fluxes for Re=350-2200 respectively. At Re≥6450, the **ET** fluxes have increased significantly and the difference in fluxes between **ET** and the disc baffled systems is much smaller than at Re=6450.

These observations also apply to the pressure dependent region except no significant difference was observed in the flux between different baffled systems and under fully turbulent flow conditions, **ET** fluxes are approximately equal to **DI**1.6 and **DI**3.2 fluxes.

Fig 4.4i plots the pulsed flow data from Stage 2A for each system together with the **ET** data for Re=16000-50000. The pulsed fluxes for the **DI** systems are greater than the **ET** and **DO**1.5 fluxes. At P_{tm}=4 bar, the flux varies from 60-70 $lm^{-2}h^{-1}$ for **ET** and **DO**1.5 to 75-95 $lm^{-2}h^{-1}$ for the **DI** systems. Limiting flux behaviour does not begin within the experimental range of P_{tm} values for the baffled systems.

4.2.4 Discussion:

These results are related to the power consumption and flow patterns in each system in Chapters 5 and 6 respectively.

(A) Baffles:

In steady flow, the observed improvement in flux over the entire range:Re=100-50000 shows that the baffled systems increase local mass transfer rates and that this improvement is more effective than simply increasing the velocity in **ET** to fully turbulent flow conditions(Re=50000). The occurrence of an optimum Re range of 750-2200 for the relative improvement in flux is

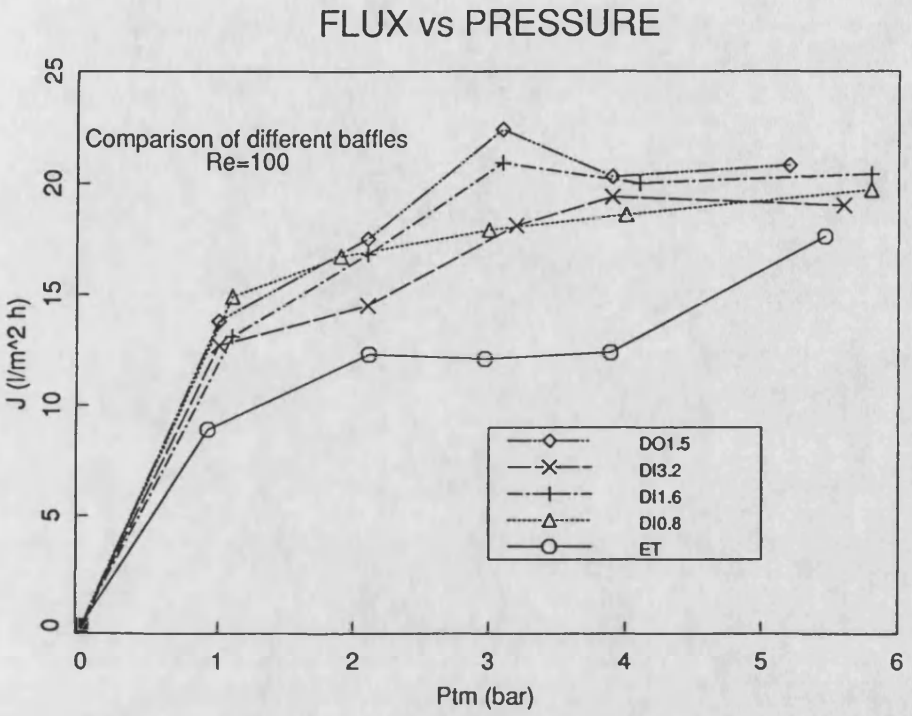

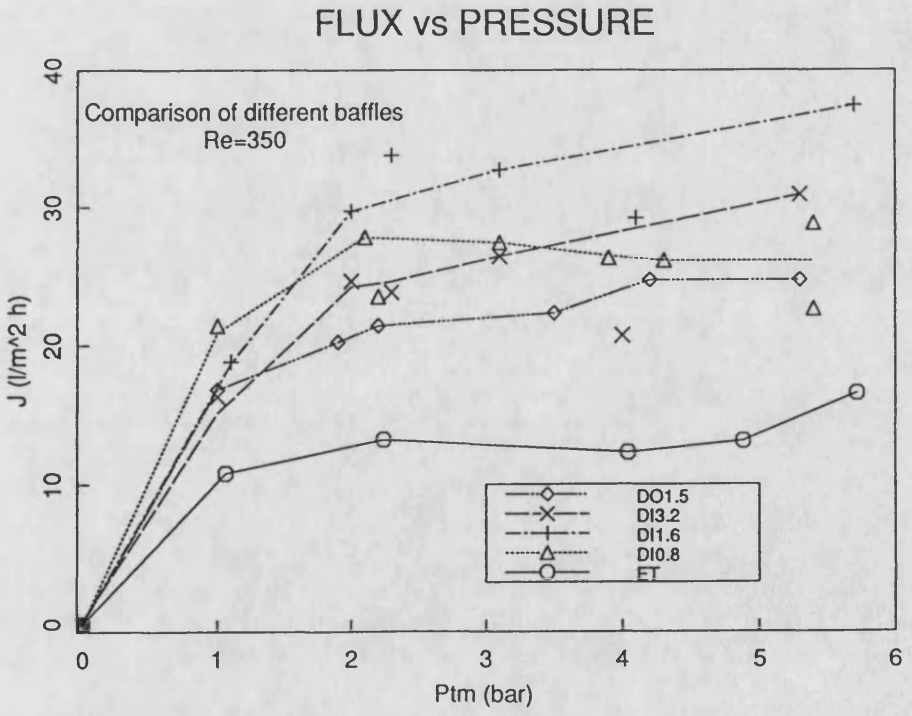

Fig 4.4: Comparison of "snapshot" ultrafiltration fluxes for **ET**, **DI**0.8, **DI**1.6, **DI**3.2 and **DO**1.5 at Re= a) 100 and b) 350.

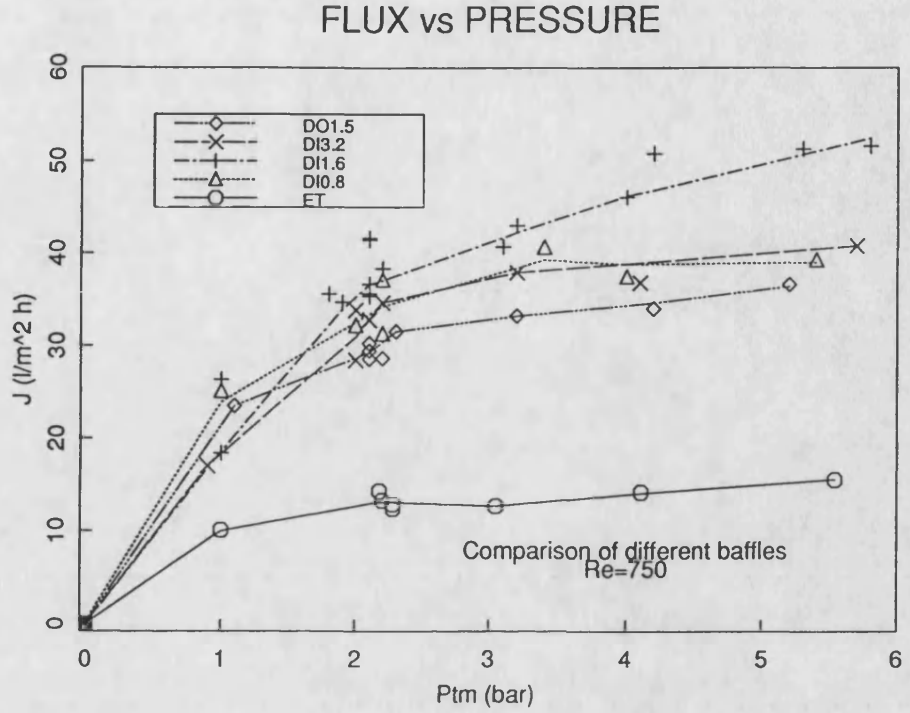

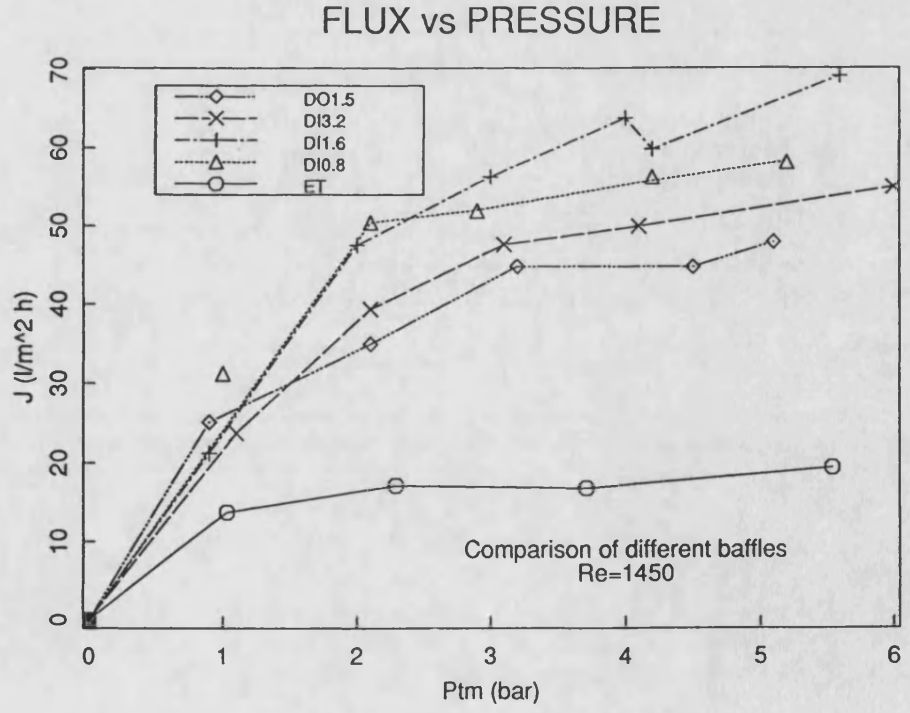

Fig 4.4: Comparison of "snapshot" ultrafiltration fluxes for **ET**, **DI**0.8, **DI**1.6, **DI**3.2 and **DO**1.5 at Re= c) 750 and d) 1450.

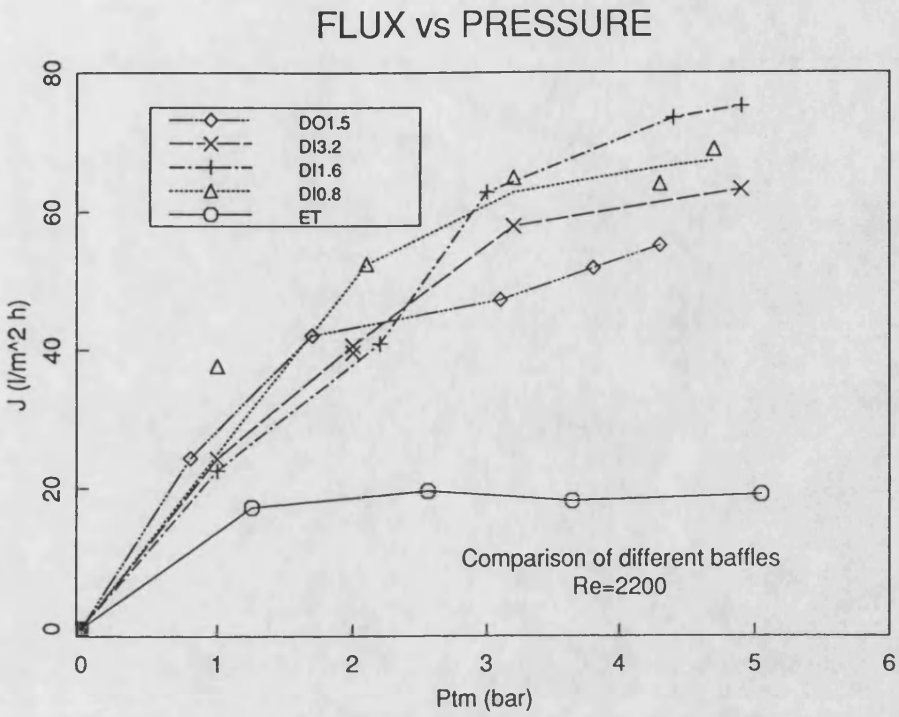

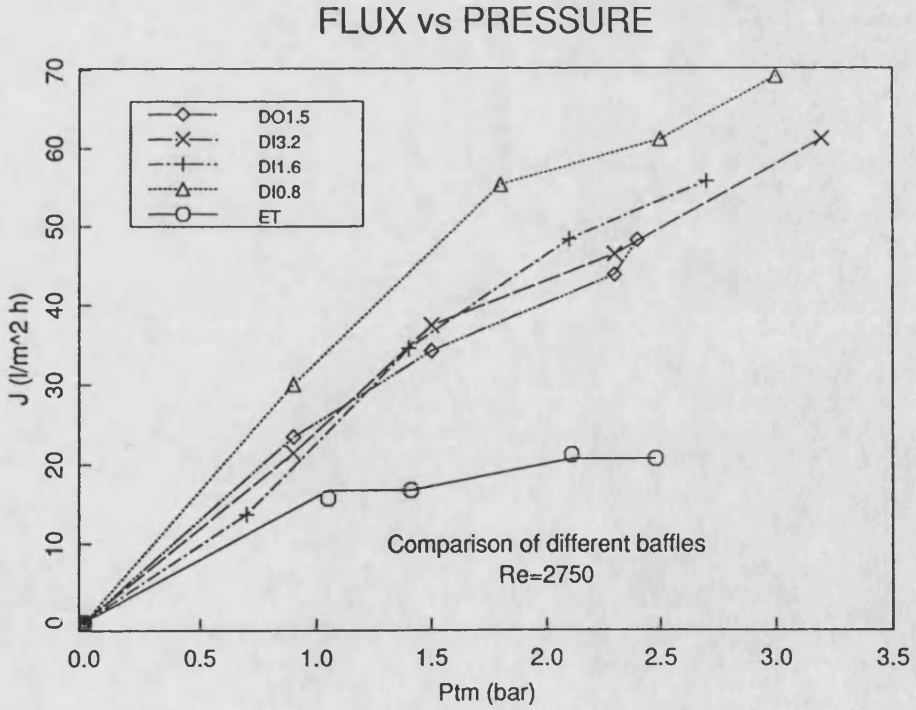

Fig 4.4: Comparison of "snapshot" ultrafiltration fluxes for **ET**, **DI**0.8, **DI**1.6, **DI**3.2 and **DO**1.5 at Re = d) 2200 and e) 2750.

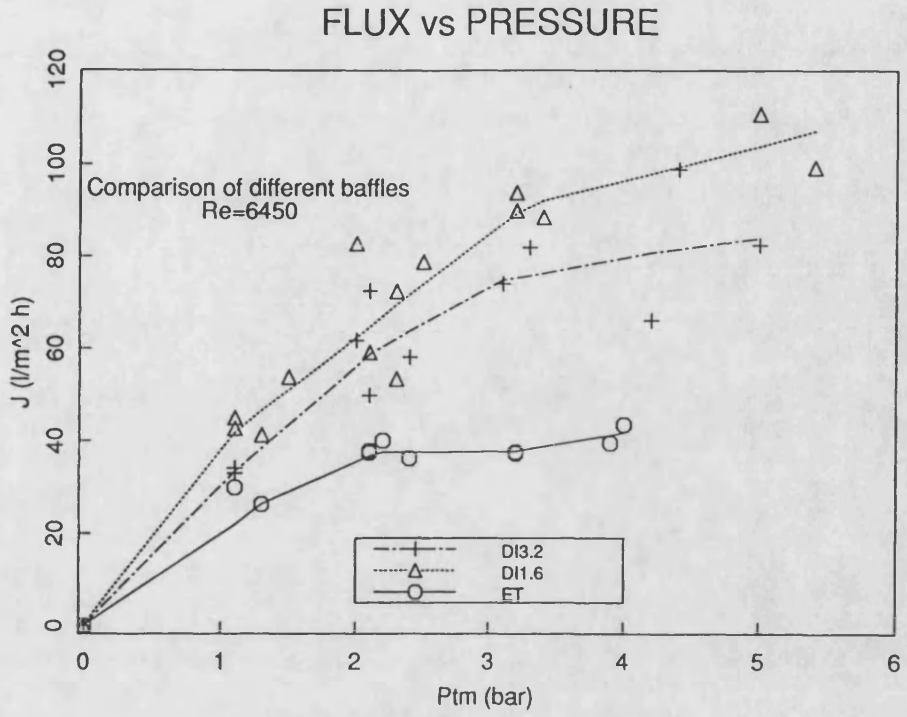

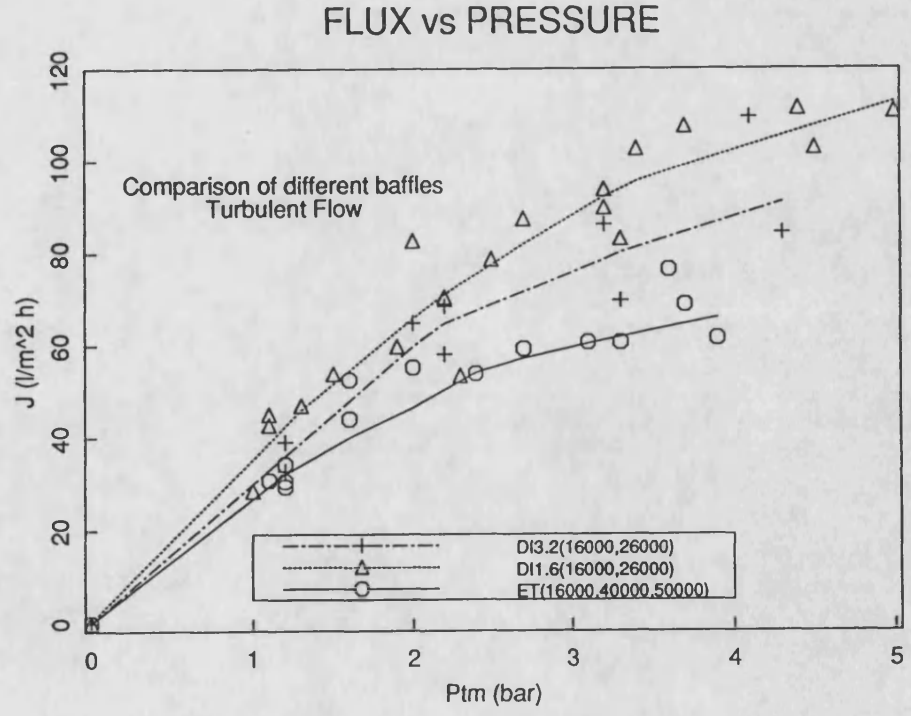

Fig 4.4: Comparison of "snapshot" ultrafiltration fluxes for **ET**, **DI**0.8, **DI**1.6, **DI**3.2 and **DO**1.5 at Re= g) 6450 and h) ≥16000.

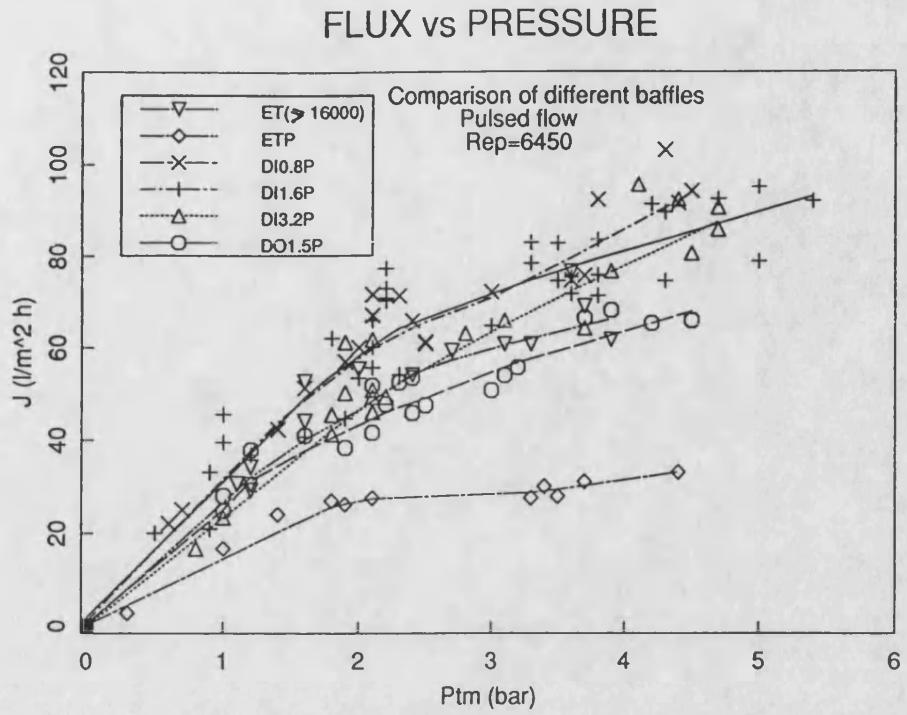

Fig 4.4i: Comparison of "snapshot" ultrafiltration fluxes for **ET**, **DI**0.8, **DI**1.6, **DI**3.2 and **DO**1.5 at Re=6450**P**(all systems) and 16000-50000 for **ET**.

consistent with Stage 1 results(see Section 3.3.2). The fluxes are quite high in this range indicating high local mass transfer rates can be achieved at relatively low Re values.

At Re=100, the lower limit of the Re range investigated, fluxes were greater for the baffled systems compared with **ET** over the entire P_{tm} range. This contrasts with the Stage 1 results where a threshold number, $Re_t=200$, existed for **DI**1.6 below which no improvement in flux was observed relative to **ET**. Two observations suggest that Re_t does exist at Re<100 for Stage 2:

a) the relative improvement in flux is smallest at Re=100.

b) no difference was observed in **DO**1.5 fluxes at Re=100 and 350(Fig 4.3e).

This suggests that Re_t is a function of C_b and Re.

(B) Optimum Baffle Configuration:

In steady flow the **DI**1.6 fluxes are consistently best in the Re range:350-2200. With the pulsed flow data it is impossible to distinguish which baffled system gives better performance although the **DO**1.5 fluxes are worse than the **DI** fluxes. **DO**1.5 was not used in subsequent experiments because of their inferior filtration performance and also for practical reasons. The **DI** baffles are much easier to manufacture, install, fix in position, remove and are less likely to come into contact with the membrane surface. **DI**0.8 was also eliminated because the pressure drop increased much more rapidly with Re for **DI**0.8(see Section 5.1.2) compared with **DI**1.6 and **DI**3.2 without any compensatory flux advantage being demonstrated. Experiments were continued with the **DI**1.6 and **DI**3.2 systems. The former gave better fluxes in steady flow for Re values up to 16000 while the fluxes were approximately equal with pulsed flow. There was no dependence of flux on frequency or amplitude for the **DI** systems as discussed in Section 4.3.4. On the basis of these results, it is concluded that **DI**1.6 gives the best performance.

(C) Pulsed Flow:

The pulsed flow fluxes in the baffled systems are independent of the net cross-flow velocity over the range:Re = 100-1450, which corresponds to NFR = 0.01-0.18. Sobey(1980) observed that when NFR is small, the basic mechanism in the furrowed membrane oxygenator of Bellhouse et al(1973) remains unaltered from pure pulsed flow and this is discussed further in Section 6.4.4. The magnitude of these pulsed fluxes is similar to the steady flow flux at $Re = Re_p$ and greater than(for **DI** systems) or equal to(for **DO**1.5) **ET** fluxes at Re = 16000-50000. Hence, fluxes typical of turbulent operation can be obtained at very low cross-flow velocities. These results are consistent with Stage 1(see Section 3.3.2) and support the use of this system in a continuous, single pass mode of operation.

For **ET**, the flux in steady flow is significantly greater than in pulsed flow at $Re = Re_p = 6450$. This result is related to the flow patterns in Section 6.4.2.

When pulsed flow was used, the feed solution became much cloudier; returning to steady flow resulted in the solution slowly clearing. The membrane was observed to expand and contract in pulsed flow within the stainless steel housing. The permeate chamber gradually filled with froth until this reached the midpoint of the permeate housing. No foam was produced in a steady flow experiment.

These observations suggest that denaturation due to air(cloudiness) in the feed solution may have occurred. Perhaps as the membrane expands and contracts, this draws air into the space between the membrane and the stainless steel support and possibly into the membrane module itself. This air will be in intimate contact with the protein in the permeate stream. These conditions will favour an interaction between the protein, air and permeate liquid to produce this foam. This "backflushing" can be tolerated by microfiltration membranes and in many cases, is highly desirable. However, with ultrafiltration membranes it should be avoided. This problem should be eliminated by flooding the permeate collection chamber.

4.3 The Effect of Amplitude and Frequency:

4.3.1 Introduction:

The objectives were:

a) to determine the effect of frequency and amplitude on flux for the different **DI** systems.

b) to determine if there is a relationship between flux and the ratio of amplitude to baffle spacing(X/L).

c) to determine for a baffled system, if the pulsed flow flux is similar in magnitude to the steady flow flux when $Re = Re_p$.

4.3.2 Experimental Design:

The conventional snapshot technique has been changed in these experiments. The P_{tm} and Re values were held constant throughout each experiment at 3.8-4.1 bar and 100-250 respectively. Under these conditions there is a significant difference in fluxes between steady flow(Re = 100-250 corresponds to limiting flux conditions) and pulsed flow(at f = 2.5 Hz and X = 30.5 mm limiting flux behaviour is only just beginning). This means that any effect of amplitude and frequency on the flux should be clearly demonstrated. Only one parameter(frequency or amplitude) is changed in each experiment while the other conditions are held constant and the snapshot conditions are varied in a systematic rather than random manner. For variable frequency, X = 30.5 mm(100%) while for variable amplitude, f = 2.5 Hz. The dependent variable(f or X) was decreased systematically from frame to frame from its maximum value to zero, and then back to the maximum value. Between each change in conditions, the dependent variable was increased momentarily to its maximum value before setting it at the desired value for that particular frame.

DI1.6 and **DI**3.2 were used in the variable frequency experiments. In the variable amplitude experiments **DI**0.8 was also used to determine if there is a relationship between flux and X/L.

4.3.3 Results:

(A) Summary:

The effects of frequency and amplitude on flux were similar for all the **DI** systems. Frequencies needed to be above 1.4 Hz at X = 30.5 mm($Re_p \geq 3500$, St = 0.033) and amplitudes above 5 mm at f = 2.5 Hz($Re_p \geq 1100$, $St \leq 0.20$) for an optimal improvement in flux to be observed. Increasing f or X above these values resulted in nominal further improvement in flux due to the onset of pressure dependent behaviour. It is possible that the pulsed flow fluxes achieved in

Section 4.2.3(Re_p=6450) could be achieved at much lower Re_p values of 3500 or possibly even 1100.

At Re_p<1000, the fluxes were significantly greater at low X and high f(2.5 Hz) experiments than at low f and high X(30.5 mm, 100%). This means, that at the same Re_p value, **short** strokes are better than **long** strokes as the frequency is higher in the former case. It has been suggested that, in general, a greater improvement in mass transfer and flux, and minimum axial dispersion will be observed using "short, fast" strokes rather than "long, slow" strokes. If minimum axial dispersion is not a requirement, further improvements in flux can be obtained by increasing Re_p(higher f and/or X(lower St)) until the onset of pressure dependent behaviour.

No relationship between flux and X/L was demonstrated for the **DI** systems investigated.

Most importantly, the flux in pulsed flow in the baffled systems was equivalent to the flux in steady flow when the steady flow velocity was of similar magnitude to the pulsed flow velocity, further supporting the use of this system in a single pass, continuous mode of operation.

(B) The Effects of Frequency and Amplitude:

Fig 4.5a and 4.5b show the flux behaviour as a function of frequency and amplitude respectively for the **DI** systems. The same trends are shown in both graphs. The high P_{tm} value of 3.8-4.1 bar maintained throughout each experiment resulted in greater fouling than was observed with earlier snapshot experiments so that there is a hysteresis effect and the flux behaviour is not reversible. The systematic approach was used to compensate for this greater extent of fouling as it is easier to separate the effects of fouling and frequency/amplitude on flux when the operating conditions are varied in a systematic rather than random manner.

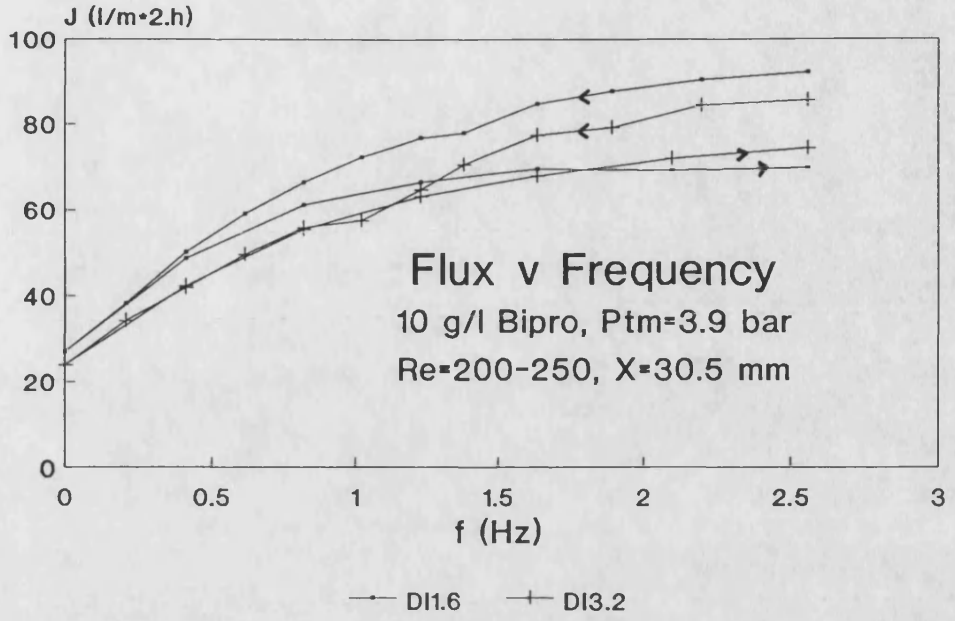

Fig 4.5a: The effect of frequency on flux for **DI**1.6 and **DI**3.2 at P_{tm}=3.9 bar and Re=200 and 250 respectively.

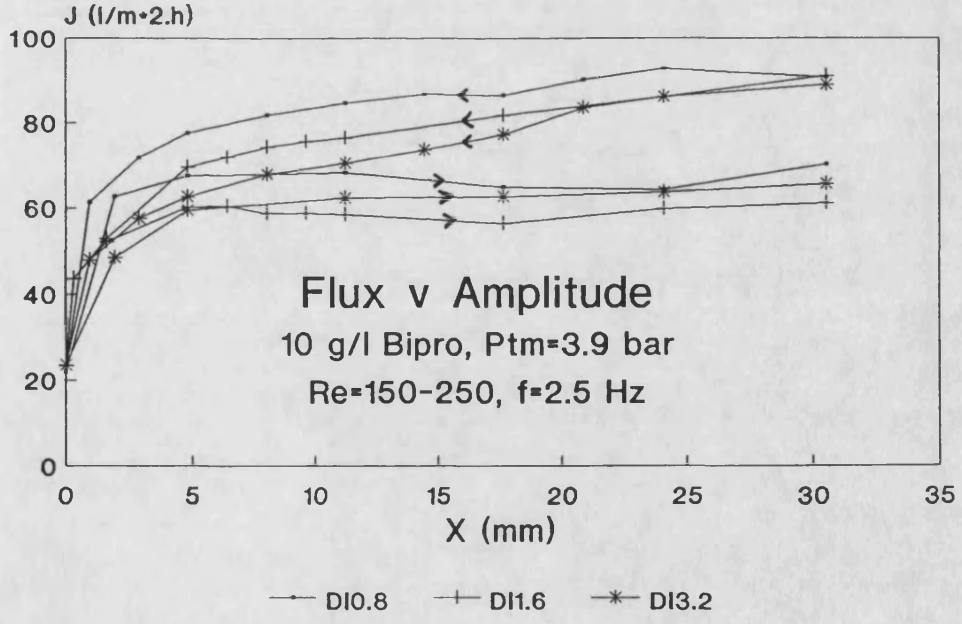

Fig 4.5b: The effect of amplitude on flux for **DI**0.8, **DI**1.6, and **DI**3.2 at P_{tm}=3.9 bar and Re=100, 150 and 250 respectively.

Both **DI**1.6 and **DI**3.2(Fig 4.5a) show the same response of flux to frequency. Between 1.4-2.5 Hz(Re_p>3500), there is very little dependence of flux on frequency. As the frequency is decreased below 1.4 Hz, a gradual deterioration in flux occurs, until at f=0 Hz, the flux is equal in magnitude to the corresponding steady flow flux value for this P_{tm} and Re. On increasing the frequency again, this process is reversed but full flux recovery is not achieved due to the fouling that has occurred.

The effect of amplitude on flux is shown in Fig 4.5b. At X=30.5 mm there is no difference in fluxes between each system which is consistent with the earlier snapshot results of Section 4.2.3. As the amplitude was decreased the flux first appears to drop for **DI**3.2 at X=20 mm(St=0.05). A more significant drop in flux occurs for <u>each</u> baffled system at an amplitude of 5 mm(Re_p=1100, St=0.20) and on the return cycle as the amplitude is increased only this second change in flux with amplitude was repeated. Significant fouling has occurred and increasing the amplitude above 16 mm(Re_p>3400, St=0.06) results in negligible further improvement in flux.

<u>(C) Comparison with Steady Flow at $Re=Re_p$:</u>

In Section 3.3.2 and 4.2.3, it was stated that for pulsed flow in a baffled system, the flux is of similar magnitude to the flux in steady flow in the baffled system when the latter is operating at a velocity similar in magnitude to the pulsed flow velocity(v_p). This observation is supported in Fig 4.6a and 4.6b for **DI**1.6 and **DI**3.2 respectively. In each graph, the variable amplitude and frequency data is plotted together with the snapshot data from Stage 2B(Section 4.2.3) against Re_p and Re respectively. Re_p is evaluated from f and X using equation (1.2). The suffix, f or X, in the legend indicates the <u>dependent variable</u> for each set of data.

A qualitative comparison of the variable f/X and steady flow flux data can only be made due to the greater extent of fouling that occurred in the former experiments compared with the latter. The fluxes in pulsed flow(at Re_p) are almost identical to the steady flow flux(at Re) for variable frequency experiments

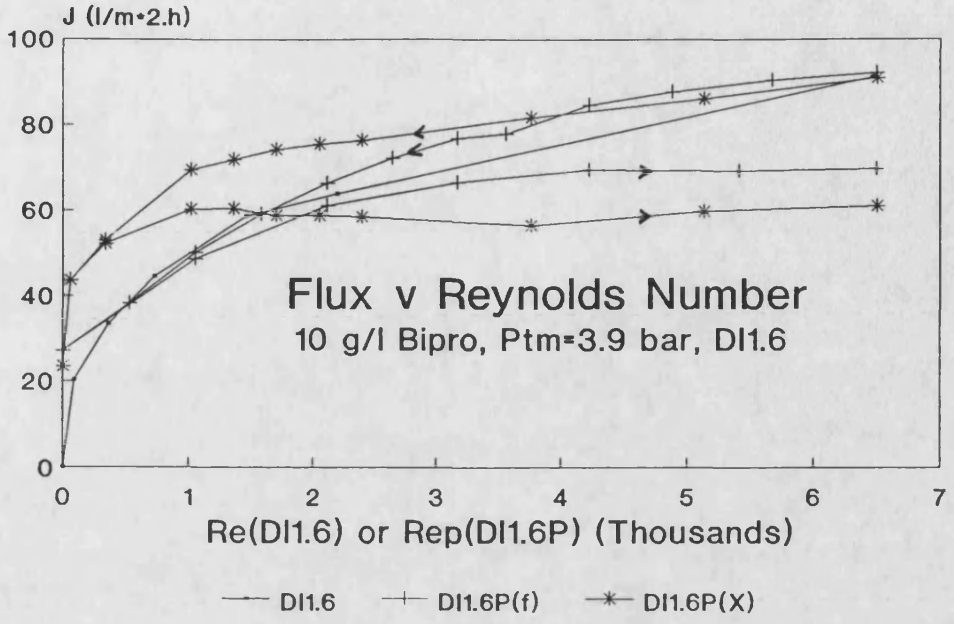

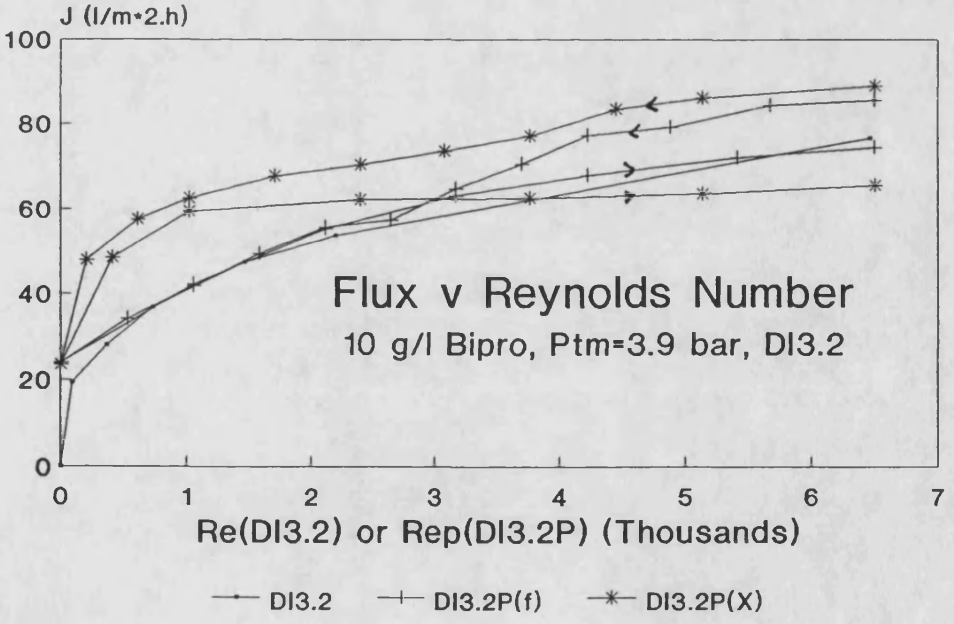

Fig 4.6: Comparison of Fluxes for a) **DI**1.6 and b) **DI**3.2 for steady flow(plotted against Re) with pulsed flow (plotted against Re_p). Two sets of pulsed flow data are shown; the suffix, f or X, indicates the parameter varied in each case.

over the entire Re(Re_p) range. With variable amplitude experiments, the fluxes are similar in magnitude for $Re_p > 3000$ while at $Re_p < 1000$, the flux is significantly greater for low X, high f(2.5 Hz) compared with low f, high X(30.5 mm, 100%) and steady flow fluxes.

Each graph can be split into two sections as done in Fig 4.5. The dividing line between each section corresponds to $Re_p = 1200$ and 3500 approximately for variable X and f experiments respectively which is consistent with the critical Re_p values determined in Fig 4.5.

4.3.4 Discussion:

These results are related to the flow patterns in Section 6.4.4.

The effects of frequency and amplitude on flux are similar for all the **DI** systems. Frequencies need to be above 1.4 Hz at X=30.5 mm($Re_p \geq 3500$, St=0.033) and amplitudes above 5 mm at f=2.5 Hz($Re_p \geq 1100$, $St \leq 0.20$) for an optimal improvement in flux. Increasing f or X above these values results in nominal further improvement in flux. This is consistent with the earlier observations made in Section 4.2.3(B) that fluxes were similar in magnitude for each baffled system at X=17.7 and 30.5 mm at f=2.5 Hz. This flux plateau is due to the system entering the pressure dependent region so that any further improvement in flux is not expected. It is possible that the pulsed flow fluxes achieved in Section 4.2.3 2($Re_p = 6450$) could have been achieved at much lower Re_p values of 3500 or possibly even 1100.

At $Re_p < 1000$, the fluxes are significantly greater at low X and high f(2.5 Hz) than at low f and high X(30.5 mm, 100%). This means that at the same Re_p value, **short** strokes are better than **long** strokes for improving fluxes, as the frequency is higher in the former situation. Rephrasing this important concept, at the same Re_p value, it is more effective to improve fluxes by increasing the frequency rather than the amplitude, while decreasing the other variable to maintain Re_p constant. Hence, provided the frequency is fast enough, short strokes are not deleterious, as shown by the low amplitude value of 5 mm that

must be exceeded to observe an optimal improvement in flux. In general it is suggested that the combination of "short, fast" strokes is more effective than "long, slow" strokes. Further improvements in flux can be obtained until the onset of pressure dependent behaviour by increasing Re_p, either by increasing the amplitude(at constant frequency) or the frequency(at constant amplitude) or increasing both simultaneously.

Howes(1988) explains that best conditions in "wavy walled" tubes correspond to stroke lengths greater than the wave period(L) of the channel(low St). With sharp edged baffles in the system, separation occurs at much lower amplitudes and in general, vortex mixing is present in the baffled tube for stroke lengths considerably less than the baffle spacing(high St). This is supported by Brunold et al(1989) who found that the optimal amplitude range is about 3-7 mm in a tube of I.D.=46 mm and for L/D=1-2. Colman and Mitchell(1990) do not directly discuss the effects of amplitude and frequency in their work. However, f and X values can be calculated from values of the Thomson number, Th, and pulsatile Reynolds number, PuRe, used by them to describe the hydrodynamic conditions in their system and defined in Table 1.2. For their mass transfer experiments, the mass transfer coefficient increases over the range X=2.16-7.2 mm(Th=0.36-1.2 in their Fig 3) and f=4.8 and 9.6 Hz(PuRe=640 and 1280 in their Fig 4)in a 6 mm high rectangular channel. The frequencies and amplitudes used by them in their pervaporation and ultrafiltration experiments correspond to(f,X)=(18.7 Hz, 1.1 mm) and (8.3 Hz, 4.2 mm) respectively. These studies support the use of "short, fast" strokes rather than "long, slow" strokes for improving mass transfer and flux. Colman and Mitchell's work and the results presented here, also show that further increases in mass transfer and flux will be observed by increasing Re_p(higher frequencies and/or amplitudes) until the onset of pressure dependent behaviour. More work is needed to test these hypotheses.

Colman and Mitchell state that if there is a requirement for minimum axial dispersion in a membrane system, for which there is an optimum at relatively low X, this must be balanced with the requirement of good mass transfer, favoured by high f and X(high Re_p and low St). It is obvious that "short, fast" strokes will meet both of these requirements but "long, slow" strokes will increase the axial

dispersion. Otherwise, as Mackley(private communication, 1988) recommended, the amplitude selected for membrane filtration should be greater than or equal to the optimum value for minimum dispersion.

Most importantly, the flux in pulsed flow in the baffled systems is equivalent to the flux in steady flow when the steady flow velocity is of similar magnitude to the pulsed flow velocity. This means the flux can be decoupled from the net cross-flow velocity supporting the use of this system in a single pass, continuous mode of operation.

There appears to be no relationship between flux and X/L for the **DI** systems investigated. This result is possibly a consequence of the truncated nature of the waveform for amplitudes less than 100%. As explained in Section 4.1.3(B), as the amplitude is decreased below 100%, there are significantly greater proportions of the cycle over which no motion occurs. In these experiments, only one of the parameters, f or X, were changed at the same time, the other being maintained at its maximum value: 2.5 Hz for frequency and 100%(30.5 mm) for amplitude. Maintaining the amplitude at 100%, while frequency is varied eliminates this truncated effect as the waveform is continuous at X=100%. Maintaining the frequency at 2.5 Hz as the amplitude is varied should ensure that although the truncated nature of the pulse becomes greater as the amplitude is decreased, the actual time taken to complete a cycle is so short that any effect this has on the filtration behaviour is minimal. Ideally, the pulsed velocity waveform should be continuous at all amplitudes so that the effects of X, X/L and St on flux can be clearly resolved. An arrangement similar to that used by Dickens et al(1989) where different cams were used to produce different amplitudes may be more suitable for future experiments.

4.4 Concentration Experiments:

4.4.1 Introduction:

Based on the superior performance of **DI**1.6 compared with **DI**3.2 under steady flow conditions it was decided to use **DI**1.6 only in the concentration experiments. The objectives were:

a) to investigate the effect of feed concentration on flux for two feed solutions: Bipro and Ardex D.

b) to compare the flux performance for **ET**, **DI**1.6 and **DI**1.6**P** under the different operating conditions described in Section 4.4.2.

4.4.2 Experimental Design:

In this section, flow conditions are expressed in terms of velocities as the changing physical properties of the feed solution with changing bulk concentration causes a corresponding change in Re and Re_p. Re and Re_p can be calculated from these velocities using the viscosity data in Table 4.2 and equations (1.1) and (1.2) respectively or evaluated graphically from Fig 4.10.

Two concentration experiments using $P_{tm}=1.2$ bar and $v=0.014$ ms^{-1} were carried out for 2 l of 25 gl^{-1} Bipro using **DI**1.6 under conditions of steady and pulsed flow($v_p=0.073$ ms^{-1}) in Stage 1C. These were supplemented in this stage with two further concentration experiments at $P_{tm}=1.2$($C_b=25$ gl^{-1}) and 3.8 bar ($C_b=10$ gl^{-1}) and $v_p=0.48$ ms^{-1} for **DI**1.6.

Concentration experiments were carried out for **ET**, **DI**1.6 and **DI**1.6**P** at $P_{tm}=2$ bar and $v=2.9$, 0.48 ms^{-1} and $v_p=0.48$ ms^{-1} respectively using Bipro and Ardex D feed solutions. These cross-flow velocities were deliberately chosen to give the same pressure drop of 0.43 bar in each system. Beginning with 2 l of 10 gl^{-1} feed solution, ultrafiltration was carried out for 30 min under approximately constant volume conditions. The concentration of the original solution was then incrementally increased to 25, 50, 100 and 150 gl^{-1} and then progressively diluted to near the original concentration with a further 20 min of ultrafiltration being

carried out at each stage. With the Ardex D solution the maximum concentration reached was 100 gl^{-1} as the fluxes were very low at this point. The concentration of the feed solution at the end of each stage was determined accurately using UV absorbance spectrophotometry. Measurement of the kinematic viscosity of the feed solution at different concentrations enabled Re to be calculated using equation (1.1) as a function of C_b and hence the hydrodynamic conditions to be determined at each stage of the experiment. Between each stage, the system was rinsed twice for 5 min using 2l of distilled water at minimal P_{tm} and maximum cross-flow velocity prior to measuring the membrane resistance using distilled water for 5 min at 1-1.2 bar. Average flux values were calculated using the last 10 min of data for each stage.

4.4.3 Results:

(A) Summary:

The mass transfer coefficient for $v_p = 0.48$ ms^{-1} was greater than at $v_p = 0.073$ ms^{-1} by a factor of approximately three. The **ET** and **DI1.6** fluxes were similar in magnitude for Bipro over the entire concentration range while with Ardex D, **ET** gave higher fluxes than **DI1.6**. The **DI1.6** fluxes were greater than the **DI1.6P** fluxes in the pressure independent region for both feed solutions. One explanation for these results and especially the improved performance of **ET** relative to **DI1.6**, concerned the difference in the power consumption in each system, as the power consumption ratio for **ET:DI1.6:DI1.6P** was 12:2:1 at $v = 2.9$ ms^{-1}, $v = 0.48$ ms^{-1} and $v_p = 0.48$ ms^{-1} respectively. These results were also attributed to the increasing magnitude of viscous effects as Re and Re_p decreased with increasing C_b.

The **ET**, **DI1.6** and **DI1.6P** fluxes agreed with corresponding snapshot fluxes from Section 4.2.3 within the pressure dependent region($C_b < 33$ gl^{-1}).

The flux behaviour was reversible on increasing the concentration from its initial to maximum value and then decreasing it to near the initial concentration for both feed solutions.

(B) Effect of v_p:

Fig 4.7 plots the results of five concentration experiments carried out in Stages 1 & 2 including the **DI**1.6**P** data plotted in Fig 4.8(a). The **DI**1.6 data at $v=0.014$ ms^{-1}($Re_0=200$, where Re_0 is the Re value at the start of the experiment) and with no pulsed flow, has been included to provide a basis for comparison. The $v_p=0.48$ ms^{-1}($Re_{p0}=6450$) data in Fig 4.7 suggests that a flux plateau is being reached at low concentrations although no firm conclusions can be made. At higher C_b, fluxes decrease with increasing concentration and a line can be fitted to the experimental data in accordance with the film model. The slope of this

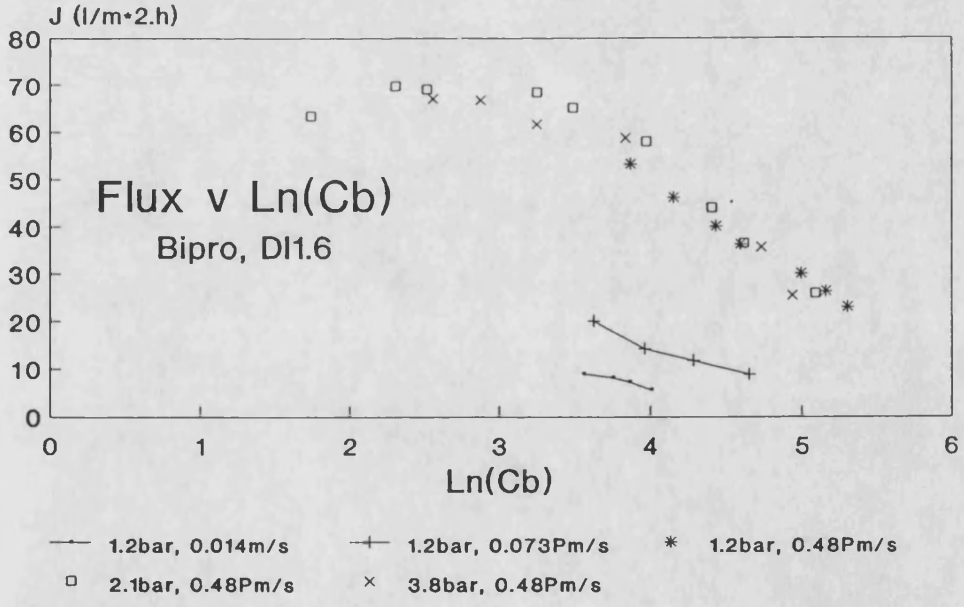

Fig 4.7: Flux v Ln(C_b) for five concentration experiments from Stages 1 and 2 for **DI**1.6.

line is equal to the mass transfer coefficient. This region corresponds to pressure independent behaviour as the similarity of the fluxes at P_{tm}=1.2, 2.1 and 3.8 bar demonstrates.

Fluxes increase with pulsed flow relative to **DI1.6** at v_p=0.073 ms^{-1} (Re_{p0}=950) and especially at v_p=0.48 ms^{-1}. The slope of the graph, and hence the mass transfer coefficient for the latter data is approximately 3 times greater than for the former data.

(C) Comparison of the Different Systems:

Fig 4.8(a)-(b) summarizes the six concentration experiments for the Bipro and Ardex D feed solutions respectively. The data has been plotted against Ln(C_b) and subdivided into 2 sections corresponding to increasing and decreasing(shaded symbols) concentration. The flux behaviour appears to be reversible on increasing and then decreasing the concentration as both sets of data for increasing and decreasing concentration for each system agree with one exception. This is the final data point for **DI1.6P**(Ardex D) where a big flux drop occurs. Problems experienced with the feed pump in this run meant that the total run time was 50 min longer than for **ET** and **DI1.6**. Consequently, this flux decay may be due to some time dependent behaviour of the feed solution. These observations are supported in Fig 4.9 which plots the membrane resistance, R_m, at the end of each stage after rinsing with distilled water. The change in R_m during an experiment is generally small especially after the maximum concentration is reached except in the final experiment. Here, R_m continues to increase especially in the last 20 min period.

For Bipro(Fig 4.8a), there is very little difference in behaviour in flux over the entire concentration range between **ET**, **DI1.6** and **DI1.6P** although at high concentrations the flux is smaller for **DI1.6P** than for **ET** and **DI1.6**. With Ardex D(Fig 4.8b), the response is different and a much clearer distinction exists between each system. Unlike Bipro, this "solution" was not completely homogeneous especially at high concentrations. The magnitude of the flux is

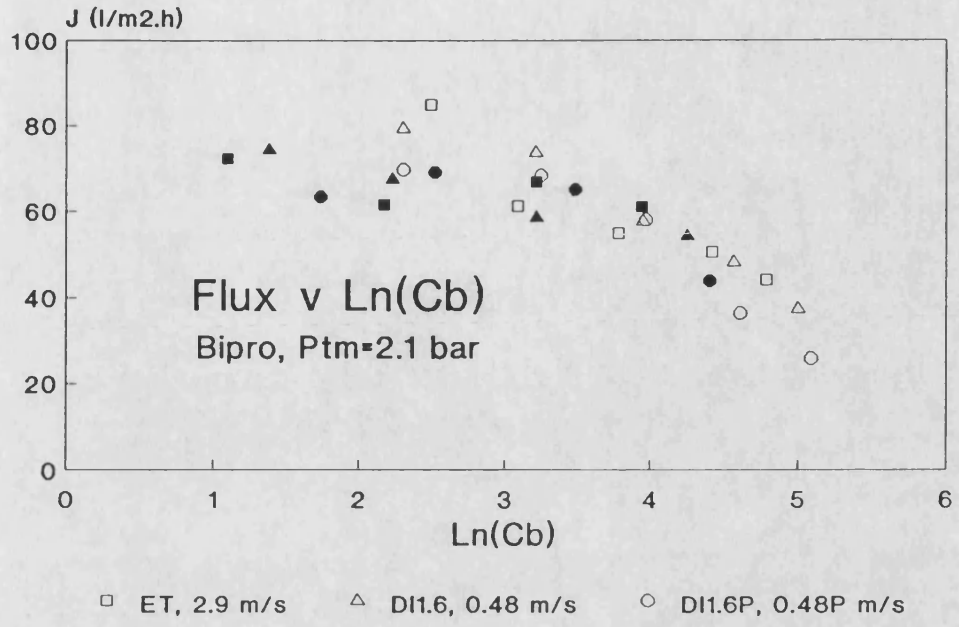

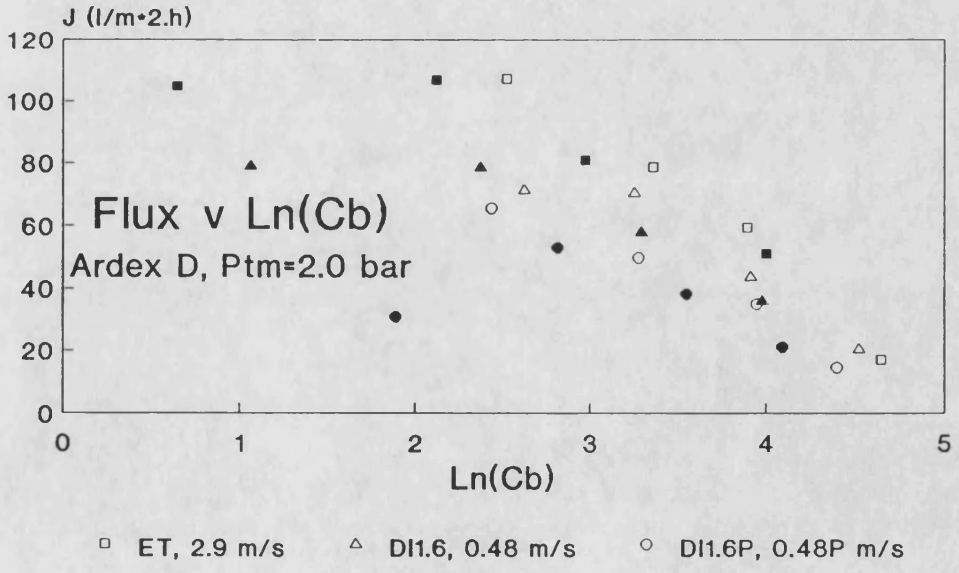

Fig 4.8: Flux v Ln(C_b) for a) Bipro and b) Ardex D.

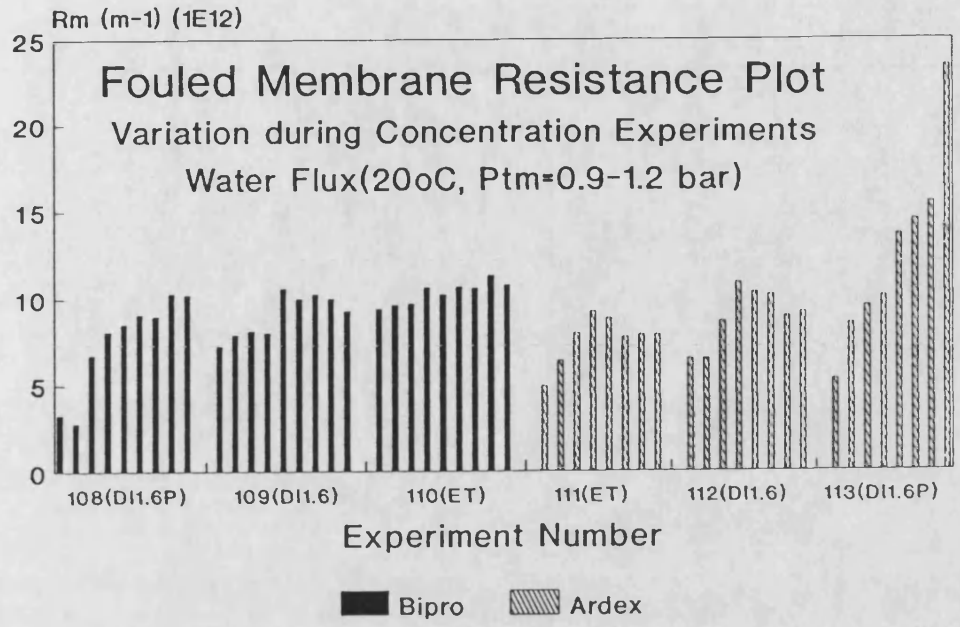

Fig 4.9: Membrane resistance, R_m, at the end of each stage for the Bipro and Ardex D concentration experiments.

greater over the entire concentration range in the order **ET**, **DI**1.6 and **DI**1.6**P**.

(D) Determination of the Flow Regime:

Fig 4.10 plots Re against C_b for **ET** and **DI**1.6 respectively for Bipro and Ardex D. Values of the density and kinematic viscosity are shown in Table 4.2 for Bipro and Ardex D. These have been included here for completeness and also because there is a dearth of such data in the literature.

The dependence of Re on C_b is much stronger for Ardex D than for Bipro. For Bipro, a dramatic drop in Re occurs for $C_b > 180$ gl^{-1}, due to a 2 order of magnitude change in kinematic viscosity that occurs in the range 180-230 gl^{-1}. Adopting the criteria that laminar flow is established at Re = 2000, this means that for **ET** and **DI**1.6 the critical C_b values for laminar flow conditions to be established are 225 and 190 gl^{-1} for Bipro and 84 and 34 gl^{-1} for Ardex D respectively. For all the experimental data, 1 and 3 data points, corresponding

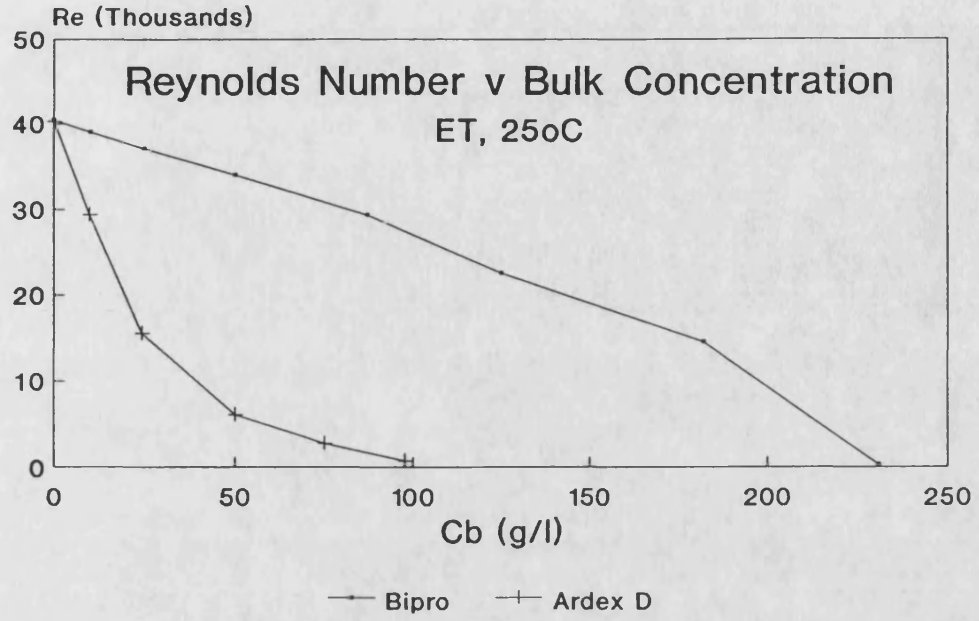

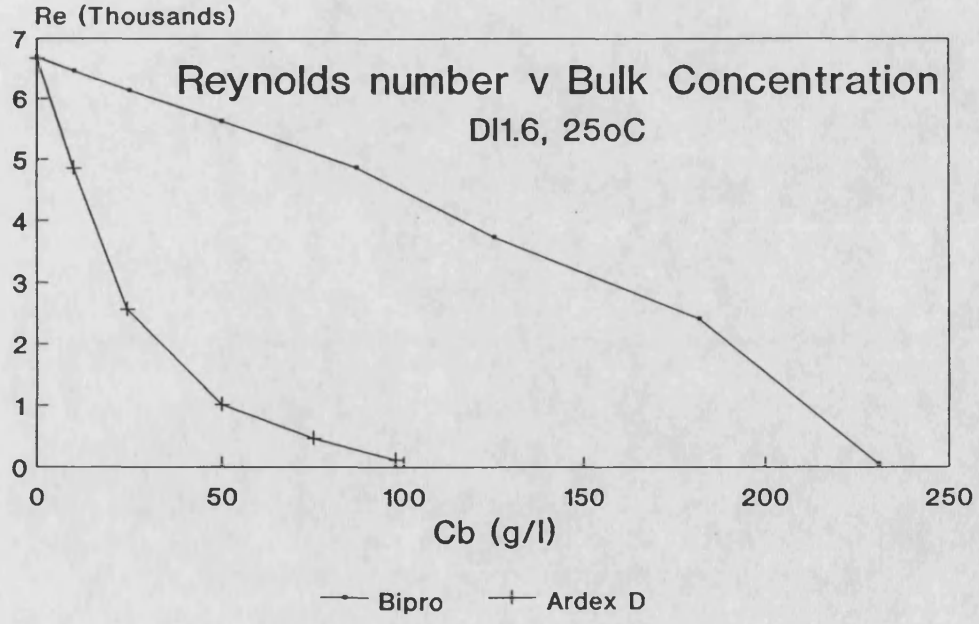

Fig 4.10: Re against C_b for a) **ET** and b) **DI**1.6 for Bipro and Ardex D.

C_b (gl^{-1})	Viscosity (cSt)	Density ($kg.m^{-3}$)	ET Re	DI1.6 Re
0	0.90	997	40440	6690
10	0.93	999	39040	6460
25	0.98	1003	37080	6140
50	1.07	1008	34020	5630
87	1.23	1016	29390	4870
125	1.61	1027	22580	3740
182	2.49	1039	14560	2410
231	114	1051	320	50
364	283	1079	130	20
		Ardex D		
0	0.90	997	40280	6670
10	1.23	999	29380	4860
24	2.34	1000	15490	2560
50	5.93	996	6120	1010
75	12.88	993	2820	470
98	49.88	987	730	120

Table 4.2: Measured values of the kinematic viscosity(cSt), and density($kg.m^{-3}$) for Bipro and Ardex D at different concentrations. Re values are calculated for ET and DI1.6 ($v=2.9$ and $0.48\ ms^{-1}$ respectively) at each concentration at 25°C.

to the highest concentrations, satisfy this criteria for **ET** and **DI**1.6 respectively for the Ardex D feed solution only.

4.4.4 Discussion:

The number of concentration experiments carried out is relatively small compared with the snapshot experiments and the results are not as well understood, especially for Ardex D, as no other experiments were carried out using this feed solution.

The Bipro fluxes for **ET**, **DI**1.6 and **DI**1.6**P** at low concentration ($C_b < 35$ gl^{-1}) are consistent with corresponding data at $C_b = 10$ gl^{-1} from the snapshot experiments of Stage 2B(see Section 4.2.3).

Considering the **ET** and **DI**1.6 results first. The **ET** and **DI**1.6 fluxes were similar in magnitude for Bipro over the entire concentration range while with Ardex D, **ET** gave higher fluxes than **DI**1.6. The improved fluxes obtained with **ET** compared with the snapshot experiments of Section 4.2.3, is partly attributed to a six-fold increase in power consumption relative to **DI**1.6 as the velocities used in each case were 2.9 and 0.48 ms^{-1} respectively while the pressure drop was the same for each system.

The increasing magnitude of viscous effects as the bulk concentration increases and the consequent decrease in Re may also explain these results and especially the differences between Ardex D and Bipro. Viscous effects become more important at a lower C_b value for **DI**1.6 than for **ET** due to the six-fold difference in velocity and hence Re. This is particularly true for Ardex D where the dependence of Re on C_b is much stronger than for Bipro. This statement needs to be qualified as the transition from laminar to turbulent flow occurs at a lower Re for **DI**1.6 than for **ET**(see Section 6.4.1) which will compensate to some degree for this difference in velocity. However, as significant increases in viscosity occur, this may change the nature of the flow patterns. In Section 4.2.4, it was suggested that Re_t is dependent on C_b. It may be possible that separation of the flow does not occur until very high Re values in viscous solutions.

Now, considering the **DI1.6** and **DI1.6P** results, where $v=v_p=0.48$ ms^{-1}. The fluxes were greater in steady flow compared with pulsed flow at high concentration for both feed solutions. The ratio of flux for **DI1.6**:**DI1.6P** reaches a maximum of 1.4:1 for Ardex D and Bipro but the corresponding power consumption ratio is 2:1(see Section 5.2). Hence the **DI1.6P** system performance is better than **DI1.6** when the results are expressed on a power consumption basis.

The increasing magnitude of viscous effects may explain these results and also the difference in flux and mass transfer coefficient observed for **DI1.6P** at $v_p=0.073$ and 0.48 ms^{-1}, as viscous effects will be more significant in the former case. Sobey(1980) stated that in order to have vortex mixing, Re_p must be sufficient in magnitude to cause an equivalent steady flow to separate. For $C_b=10\text{-}25$ gl^{-1}, $v_p=0.073$ and 0.48 ms^{-1} correspond to $Re_p=950$ and 6450 respectively. The difference in the flux/concentration behaviour at these 2 Re_p values apparently contradicts the statement made in Section 4.3.4 based on the f/X results that it may be possible to achieve the same flux in pulsed flow at $Re_p=6450$ at a much lower Re_p values of 3500 or possibly even 1100. One explanation for the apparent contradiction is that the wall viscosity may be more sensitive to <u>increasing bulk viscosity</u> than to <u>decreasing cross-flow velocity</u>. This will result in laminar flow conditions being established within the boundary layer at higher Re_p values for increasing viscosity compared with decreasing velocity.

These conclusions are preliminary <u>only</u>. Flow visualization studies, additional to those described in Chapter 6 would need to be carried out investigating the effects of viscosity in steady and pulsed flow on the flow patterns to test these hypotheses.

CHAPTER 5
POWER CONSUMPTION

The incorporation of baffles within the tubular membrane system increases the pressure drop and hence at a given Reynolds number the power consumption will be greater than in a conventional system. The use of pulsed flow further increases power consumption. In this chapter, the power consumption of the conventional and baffled systems under steady and pulsed flow conditions is compared to determine whether the filtration performance of the baffled systems is superior to that of a conventional system at the same power input.

This chapter is divided into two sections. Section 5.1 describes the evaluation of two further parameters needed to be able to calculate the power consumption of each system for the experimental conditions used. These parameters are the steady flow pressure drop, dP, and the pulsed flow pressure drop, dP_p. Section 5.2 explains the power consumption calculation. The power consumption has been expressed in terms of the power dissipated within the membrane module and on a unit area basis to make scaleup to larger industrial units easier. The equations used to calculate the power consumption are developed and applied to the data for steady and pulsed flow conditions.

5.1 Measurement of The Pressure Drop:

5.1.1 Introduction:

The pressure drop in a conventional system is primarily due to friction at the wall. These losses are known as viscous losses. With baffles in the tube for

steady flow the fluid accelerates and decelerates as it moves around or through each baffle for the disc and doughnut systems respectively and eddies are generated in the wake of each baffle. The pressure drop is made up of both viscous and eddy losses in this case. The viscous losses are due to both friction at the wall and at the baffle as the fluid moves past it. With pulsed flow in a conventional system, the acceleration, deceleration and change of direction of the fluid produces inertia losses. With baffled systems and pulsed flow viscous, eddy and inertia losses add to produce the total pressure drop in the system. This simplistic description illustrates why the theoretical evaluation of the power consumption under the different operating conditions used in this project is not easy.

The parameters measured in this section are the pressure drop in steady flow, dP, and the pulsed flow pressure drop, dP_p. The pressure drop, dP, is defined as the difference between the inlet and outlet pressures. This is the pressure drop through the membrane module as distinct from P_{tm}.

With pulsed flow, the pressure drop changes in a periodic fashion with time with the same frequency as the pulsed flow. The peak-centre amplitude of this wave is defined as the pulsing pressure drop, dP_p. ϕ is defined as the phase difference between dP_p and the amplitude of the pulsed flow rate, Q_p. Positive values of ϕ imply that dP_p is ahead of Q_p.

An empirical equation relating the pressure drop, dP, to the Reynolds number, Re, can be evaluated using linear regression from the experimental data. This steady flow regression equation can be used to estimate dP_p at $Re = Re_p$. By comparing the values of dP_p calculated using this equation with the experimentally measured values, the contribution of inertial losses to the pressure drop can be assessed.

The objectives of this section were:

a) to measure the steady flow pressure drop(dP) as a function of Re for the different systems over the experimental range.

b) to determine the transition from laminar to turbulent flow for each system.

c) to determine the pulsing pressure drop(dP_p) at an amplitude of 30.5 mm(100%) and f=2.5 Hz and to investigate if there is any dependence of dP_p on P_{tm} and Re.

d) to investigate if there is a phase difference, ϕ, between Q_p and dP_p for each system.

e) to compare dP_p with dP at $Re=Re_p$ to assess the contribution of inertial losses to dP_p.

5.1.2 Materials and Methods:

The steady flow pressure drop, dP was measured using distilled water at 18°C by water and Hg manometers for the ET and baffled systems respectively over the Re range 0-2500 in Stage 2A. No measurements of the pressure drop were made for **DO2.2** as these baffles had been damaged during storage and were no longer usable. The manometer was connected at the same location as the pressure transducers thus measuring the total pressure drop through the membrane module. In Stage 2B, the Re range was much higher and dP was measured using the Hg manometer for **ET, DI1.6** and **DI3.2.**

dP_p was estimated at $Re=Re_p$ from the empirical relationship between dP and Re for each system, obtained using linear regression on the experimental data from Stages 2A(**DI0.8** and **DO1.5**) and 2B(**ET, DI1.6** and **DI3.2**):

$$dP(Pa) = BRe + CRe^2 \qquad (5.1)$$

dP_p was measured using distilled water at 18° C by a wet/wet differential transducer(Type PDCR 120/WL manufactured by Druck Ltd) connected to the inlet and outlet pressure tappings. This was connected to the U/V Trace recorder used for measuring P_p(see Section 4.1.2(B)). Traces of dP_p as a function of amplitude, Re and P_{tm} were obtained for each system. dP_p was evaluated directly from these traces in mm as the peak-centre amplitude and converted to dP_p(bar) after correcting for the signal amplification and using the transducer calibration data.

The phase difference, ϕ, was measured from the traces as the distance between the positive peak of the dP_p curve and middle of the displacement blip.

The middle of the displacement blip corresponds to the point of zero displacement.

5.1.3 Results:

(A) Summary:

dP increased much more rapidly for the baffled systems compared with **ET**. **DI**0.8 and **DO**1.5 had the strongest and weakest dependency of dP on Re respectively while the dP/Re behaviour was similar for **DI**1.6 and **DI**3.2.

The dP/Re behaviour suggested that the laminar/turbulent transition occurred at a much lower Re value for the baffled systems than for **ET**.

The measured and predicted values of dP_p agreed well for the **DI** systems but not for **DO**1.5 and especially **ET**. No conclusions were reached about the contribution of inertial effects to dP_p. Hence, for evaluating the power consumption in pulsed flow, measured values of dP_p should be used for **ET** and **DO**1.5 while the empirical dP/Re equation can be used to predict dP_p for the **DI** systems. The dP_p waveform was more triangular than sinusoidal and a phase difference existed between Q_p and dP_p that is dependent on system geometry.

(B) Steady Flow Pressure Drop:

Fig 5.1 shows the steady flow pressure drop as a function of Re for each system for Stages 2A(Fig 5.1a) and 2B(Fig 5.1b). All the data has been presented on two graphs for Stages 2A and 2B rather than individually to illustrate the significant differences in the pressure drop response of each system. In Fig 5.1a the pressure drop increases much more rapidly with Re for the baffled systems compared with **ET**. The rate of increase in dP with Re is smaller for **DO**1.5 compared with the disc baffled systems. The increase in dP with Re for **DI**0.8 is

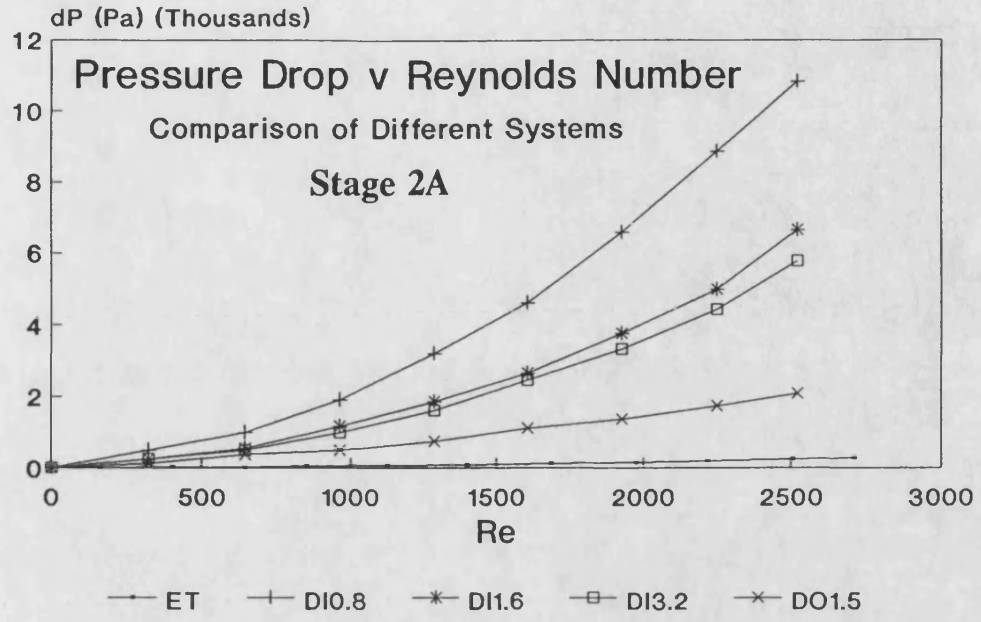

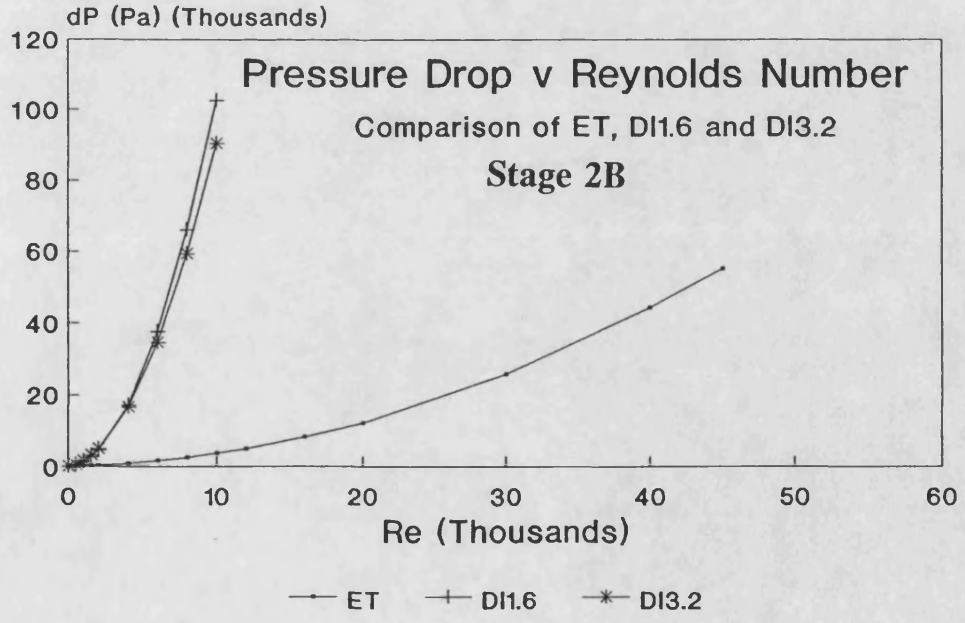

Fig 5.1: The pressure drop as a function of Re for the different systems from Stage a) 2A and b) 2B.

substantially higher than **DI1.6** and **DI3.2**, both of which show a similar dependence on Re.

In Stage 2B(Fig 5.1b), the experimental range was extended to much higher Reynolds numbers. The increase in dP with Re is very similar for both baffled systems while dP only begins to increase significantly for **ET** at Re>20000.

The Re range for transition from laminar to turbulent flow was estimated graphically from individual curves for each system and is tabulated in Table 5.2. The transition range was assumed to be the Reynolds number "band" corresponding to the lower and upper Re bounds where a distinct change of slope of the graph occurs, presumably, as the flow changes from being laminar to turbulent in nature. The transition occurs at a much lower Re range for the baffled systems compared with **ET**. The transition band is compared with that estimated from the flow visualization studies in Section 6.4.1.

An empirical relationship between dP and Re was evaluated using equation (5.1) for each system. Values of the coefficients, B and C, in equation (5.1) for each system are tabulated in Table 5.1. The agreement of the regression values with the experimental data is excellent: the regression coefficient varies between 0.997-0.999 for each system.

System	Stage	B	C	regn. coeff.
ET	1, 2A	0.030420	0.000027	0.9984
	2B	0.122331	0.000025	0.9998
DI1.6	1, 2A	0.195491	0.000938	0.9979
	2B	0.316219	0.000993	0.9997
DI3.2	1, 2A	0.158287	0.000857	0.9976
	2B	0.896663	0.000814	0.9976
DI0.8	1, 2A	0.496971	0.001530	0.9987
DO1.5	1, 2A	0.367868	0.000182	0.9970

Table 5.1: Values of B and C from equation (5.1) for each system.

(C) Pulsing Pressure Drop:

Values of dP_p and ϕ, were measured from the U/V trace recorder and are tabulated in Table 5.2. ϕ is expressed as a fraction of the period. Under these conditions, the dP_p waveform is more triangular than sinusoidal. There was no dependency of dP_p on Re or P_{tm} within the range 0-1250 and 1-5 bar respectively. The error in dP_p is estimated to be 10% from experimental observations.

The predicted values of dP_p using equation (5.1) are compared with experimental values in Table 5.2. Table 5.2 shows that the values agree well for the **DI** systems while with **ET** and **DO1.5** the experimentally measured values are 670 and 75% greater respectively.

	ET	**DI0.8**	**DI1.6**	**DI3.2**	**DO1.5**
		a) regression			
dP_p (bar)	0.015	0.52	0.34	0.31	0.08
		b) experiment			
dP_p (bar)	0.10	0.50	0.34	0.27	0.14
ϕ	0.45	0.25	0.25	0.25	0.35
		c) transition to turbulence:Re range			
lower	3000	700	800	900	1400
upper	7000	1400	1500	1600	2000

Table 5.2: For each system: a) predicted values of dP_p at Re_p=5700 using equation (5.1); b) measured values of dP_p and ϕ at X=30.5 mm(100%) and f=2.5 Hz(Re_p=5700); c) estimated Re band for the transition from laminar to turbulent flow.

5.1.4 Discussion:

Two explanations are put forward to explain the difference in the dP/Re behaviour for **DI**0.8 compared with **DI**1.6 and **DI**3.2. The first is based on an analogy with the pressure recovery in orifice type meters(Coulson and Richardson, 1977). A certain distance downstream from the throat of such devices, a final recovery pressure is reached, which naturally, is less than the upstream throat pressure. It is possible that with **DI**0.8, but not **DI**1.6 and **DI**3.2, insufficient distance exists between adjacent baffles for the final recovery pressure to be reached. Secondly, the likelihood of channelling of the fluid, which will increase the pressure drop, is greater for **DI**0.8 than for the other **DI** systems as Brunold et al(1989) commented on. This is discussed further in relation to the flow patterns in the **DI** systems in Section 6.4.3.

The existence of a phase difference, ϕ, between Q_p and dP_p is acknowledged by Edwards and Wilkinson(1971) and Ralph(1985). The definition of ϕ is somewhat arbitrary. Consequently although the general trend of the effect of geometry on ϕ is qualitatively correct, the quantitative accuracy is suspect. In some cases, the dP_p waveform was not symmetric which made it more difficult to measure ϕ.

The difference in the measured and predicted values of dP_p is significant for **DO**1.5 and especially **ET**. These results suggest that inertial effects are insignificant for the **DI** systems, relatively important for **DO**1.5 and dominate dP_p for **ET**. This is thought to be false. Hence, the only conclusion that can be reached is that the empirical dP/Re equation, (5.1), can be used to predict dP_p for the **DI** systems but measured values should be used for **ET** and **DO**1.5.

5.2 Power Consumption Evaluation:

The power consumption has been expressed in terms of the power dissipated within the membrane module only and on a unit area basis to make scaleup to larger industrial units easier. It does not include the power required

to generate the transmembrane pressure. This approach was used as, in a commercial unit, about 80% of the retentate is recycled around a high pressure loop. In the experimental rig, all of this flow is returned to the feed vessel losing pressure energy. These losses and associated losses in the pipework are ignored if only the power dissipated in the membrane module itself is calculated, which can be scaled between the two rigs. Section 5.2.1 explains the development of the equations and the evaluation of the parameters needed to calculate the power consumption. The results are presented and discussed in Section 5.2.2 and 5.2.3 respectively. The objectives were:

a) to evaluate the power consumption for each system under steady and pulsed flow conditions.

b) to assess which of the baffled systems give the best performance when the fluxes for each system are expressed on a power consumption basis and whether this performance is better than for ET.

5.2.1 Evaluation of The Power Consumption:

In steady flow, the measured values of the pressure drop, dP, and volumetric cross-flow rate, Q, were combined to calculate the power(E) consumed in the module on a unit area basis. This represents a specific power consumption in Wm^{-2}:

$$E = \frac{QdP}{A_m} \qquad (5.2)$$

where A_m is the membrane area.

In pulsed flow, the total power dissipated is the sum of 2 terms: one due to the pulsing flow alone, E_p, and the second due to the net forward flow, E_n. The pulsed flow component was evaluated by assuming that the pulsing flowrate, $Q_p(t)$, and pulsing pressure drop, $dP_p(t)$ are sinusoidal functions with the same

frequency of oscillation and are in phase. Hence, the equations for $Q_p(t)$ and $dP_p(t)$ are:

$$Q(t) = Q + Q_p \sin(\omega t)$$

$$dP(t) = dP + dP_p \sin(\omega t)$$

Integrating over one period gives:

$$E = E_n + E_p = \frac{QdP + 0.5 Q_p dP_p}{A_m} \quad (5.3)$$

The pulsed flow term, E_p, in equation (5.3) represents the average power dissipated per cycle. There is a direct analogy between this quantity and the average power dissipated within an A.C. resistive circuit with Q_p and dP_p being analogous to electrical current and resistance respectively. Hence E_p can be thought of as the product of the r.m.s. values of the amplitude of the pulsing flow rate and pulsing pressure drop.

5.2.2 Evaluation of the Parameters:

a) Q was measured directly by the rotameter(see Section 2.3.3).

b) dP was evaluated using equation (5.1).

c) Q_p was evaluated as the product of the pulsed velocity, v_p, defined in equation (1.3) and A_{et}, the area of the empty tube.

d) In Stage 1, dP_p was evaluated using equation (5.1) for **DI1.6** substituting $Re=Re_p=950$ in equation (5.1). Equation (5.1) was also used to evaluate dP_p for **ET** as no experimental data was available. This is in spite of the conclusion reached in Section 5.1.3 that measured dP_p values should be used for **ET**.

In Stage 2 $Re=Re_p=6450$ was substituted in equation (5.1) for the disc baffled systems. The measured values of dP_p for **ET** and **DO1.5** were used after

correcting for the difference in the kinematic viscosity between distilled water at 18°C and Bipro at 25°C where Re_p=5700 and 6450 respectively.

In earlier papers(Finnigan and Howell, 1989A, 1989B, 1989C), evaluation of the power consumption included the power required to generate the transmembrane pressure except for one(Finnigan and Howell, 1989D) where the power consumption was expressed on the same basis as used here. In all cases, the pressure drop was evaluated from the absolute transducer readings for **ET**, **DI**1.6 and **DO**2.2. The pressure drop results obtained with the manometer method described in Section 5.1.2 are more accurate than these earlier measurements. For this reason, only these later results have been presented here. Comparison of the two sets of results shows that the trends in each case remain the same and hence the conclusions reached previously are qualitatively correct but the earlier results are not quantitatively valid.

5.2.3 Results:

(A) Summary:

Baffles have been shown to dissipate energy more effectively than turbulence in an empty tube(**ET**). An optimum flux/power range has been identified for the baffled systems. The fluxes were greater for the baffled systems than for **ET** within this optimum range. This optimum range corresponded to Re=700-1200 and 750-1450 for Stages 1 and 2 respectively. Within this range the power consumption was a maximum of 1 Wm^{-2}. These Re values are consistent with the earlier conclusions of Chapters 3 and 4. Comparative fluxes can be obtained for **ET** but only at a much higher power consumption of approximately 20 and 45 Wm^{-2} at P_{tm}=2 and 4 bar respectively.

DI1.6 gave the best performance when the flux results were expressed on a power consumption basis.

In the baffled systems, fluxes in pulsed and steady flow were of similar magnitude for the same power consumption. Once flow reversal no longer occurred, there was no advantage from a flux and power viewpoint of using pulsed flow. It has been suggested that in order to be operating in the optimum flux/power range, the pulsed flow velocity should be chosen so that Re_p=700-1500.

(B) Power Consumption:

The power consumption for each system over the experimental Reynolds number range is tabulated for Stages 1 and 2 in Table 5.3. The **DO2.2** results are not included here as no pressure drop measurements were obtained for this system. For Stage 1, the pulsed flow power consumption, E_p, corresponds to Re_p=950 in Table 5.3 and is used to calculate the fraction of the total power consumption due to pulsed flow, E_p/E, shown in Table 5.3. For Stage 2, Re=100-1450 for pulsed flow at Re_p=6450. Examination of the power data in Table 5.3 shows that the power consumption at Re=1450 is 1-3% of the pulsed power consumption at Re_p=6450. Consequently, the steady term, E_n, in equation (5.3) is neglected for all Stage 2 data.

For both Stages, the power consumption has been evaluated for Re≥350 as at smaller Re values the pressure drop measurements are considered to be inaccurate and the power consumption is insignificant.

The flux v power results for Stage 1 at P_{tm}=0.4, 1.2 and 2.2 bar are shown in Fig 5.2(a)-(c) and for Stage 2 at P_{tm}=2 and 4 bar in Fig 5.3(a)-(d). Both graphs are discussed together. Data from Stages 2A and 2B has been plotted together in Fig 5.3. The fluxes were determined graphically from the Stage 2 flux/P_{tm}/Re graphs in Section 4.2.3 at P_{tm}=2 and 4 bar over the Re range:Re≥350. Two graphs have been drawn at each P_{tm} value. This has been done to display the trends in the data better for low values of the power consumption. Fig 5.3a and 5.3c plot the steady flow data for Re≤2200 and Re≤6450 for the baffled and **ET** systems respectively. Fig 5.3b and 5.3d plot all the data from Stages 2A and 2B except the fluxes corresponding to Re≥40000 for

ET and Re=16000 for the **DI** systems as the power consumption becomes prohibitive in these systems at these Re values without any significant flux improvement(see Section 4.2.3(B)).

	Specific Power Consumption (Wm^{-2})					
Re	**ET**	**ETP**	E_p/E	**DI**1.6	**DI**1.6**P**	E_p/E
Stage 1						
350	0.002	0.010	0.82	0.022	0.17	0.87
700	0.008	0.016	0.49	0.14	0.29	0.52
1200	0.032	0.040	0.20	0.66	0.82	0.19
1550	0.061	0.069	0.12	1.37	1.53	0.09
3300	0.46	0.47	0.02	12.5	12.7	0.01
950**P**	0.008			0.15		
Stage 2	**ET**	**DI**0.8		**DI**1.6	**DI**3.2	**DO**1.5
350	0.002	0.047		0.024	0.021	0.019
750	0.009	0.29		0.16	0.14	0.089
1450	0.050	1.94		1.11	1.00	0.45
2200	0.14	6.15		3.60	3.25	1.22
2750	0.26	11.7		6.90	6.26	2.16
6450**P**	12.7	71.2		46.2	42.2	18.0
6450	3.89	--		92.3	84.4	--
16000	45.4			1410	1210	
40000	613					
50000	1123					

Table 5.3: The specific power consumption as a function of Re for the different systems in Stages 1 and 2. The suffix P refers to pulsed flow. E_p/E is the fraction of the total power consumption due to pulsed flow.

For all systems, each graph shows there is a flux/power optimum range, centred about the sharp inflection point in the flux/power graph. For power consumptions greater than this optimum, a flux plateau is reached, and further increases in flux are relatively small and do not compensate for the much higher power consumption required to achieve them. This flux plateau corresponds to the system moving into the pressure dependent region. The magnitude of the flux and power consumption in this optimum range increases with increasing P_{tm} and decreasing concentration.

The fluxes for the baffled systems are much higher than for **ET** in this optimum range for the same power consumption except at P_{tm} = 0.4 bar where **ET** and **DI**1.6 are both operating in the pressure dependent region. As P_{tm} increases to 1.2 and 2.2 bar(Fig 5.2) and in Fig 5.3, from 2 to 4 bar, the relative difference in fluxes between the baffled systems and **ET** is greater. Fluxes of similar magnitude can be obtained for **ET** but only at a much higher power consumption than the optimum power consumption for the baffled systems. Fig 5.3 shows that as the power consumption is increased beyond the levels reached in Stage 1(Fig

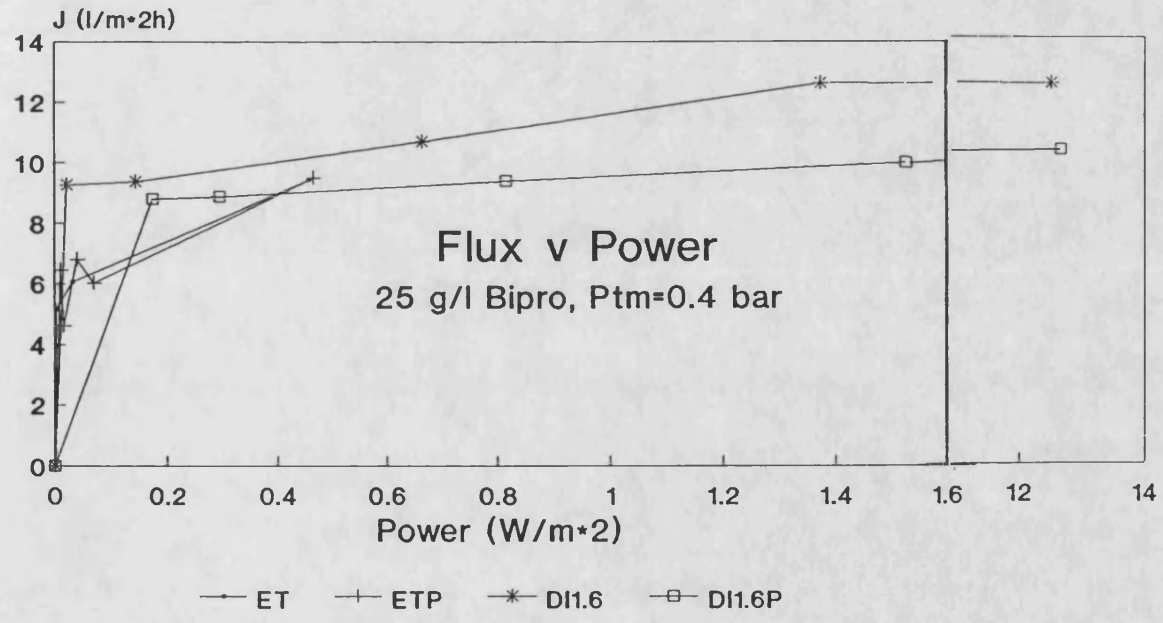

Fig 5.2: Flux v Power Consumption for Stage 1 at P_{tm} = a) 0.4 bar for **ET**, **ETP**, **DI**1.6 and **DI**1.6**P**.

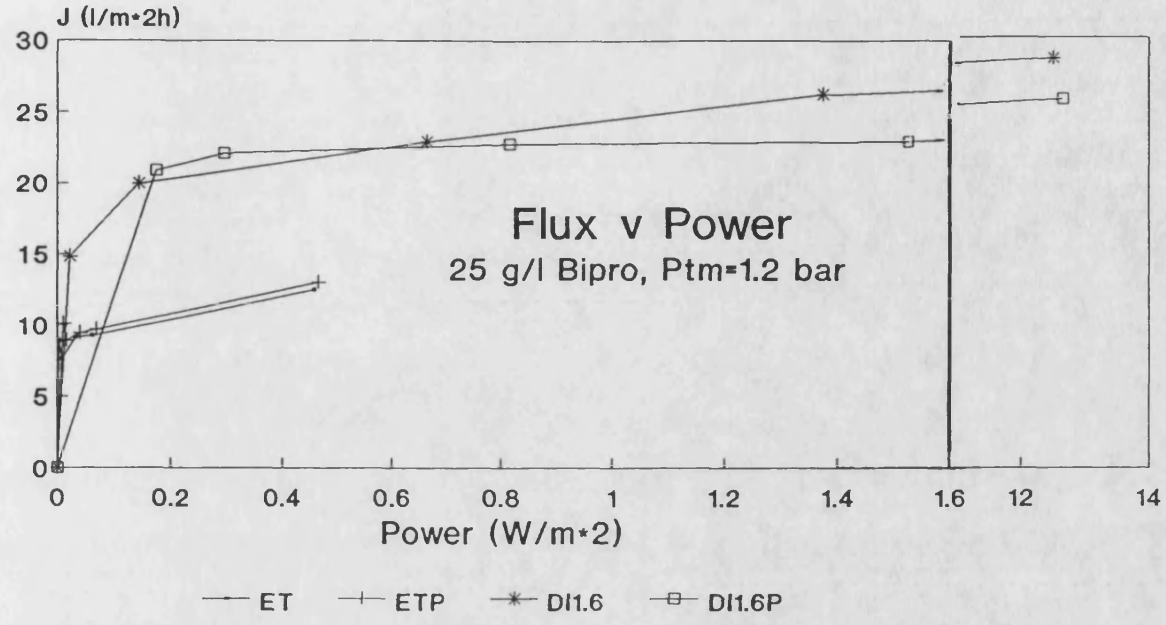

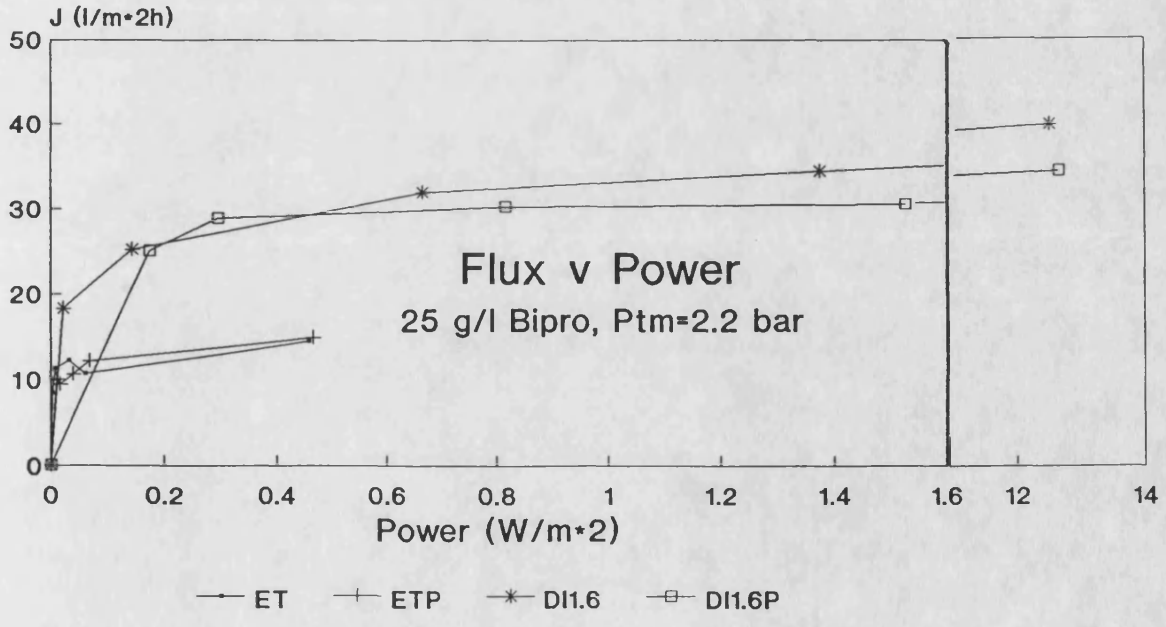

Fig 5.2: Flux v Power Consumption for Stage 1 at P_{tm} = b) 1.2 and c) 2.2 bar for **ET, ETP, DI**1.6 and **DI**1.6**P.**

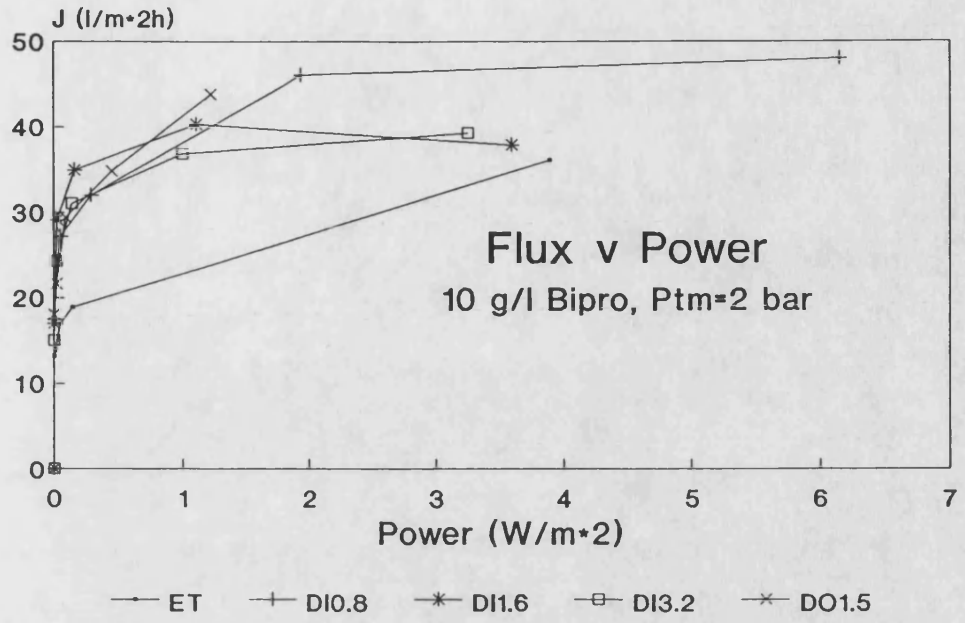

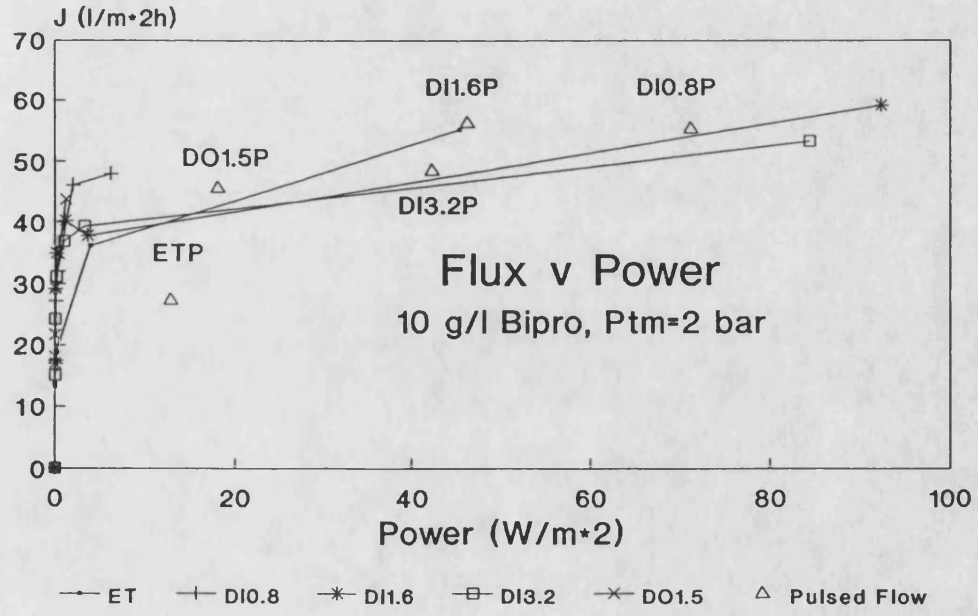

Fig 5.3: Flux v Power Consumption for Stage 2 at P_{tm}=2 bar for **ET** and the baffled systems. The same graph is shown in a and b, except that fewer data points are plotted in a as explained in the text.

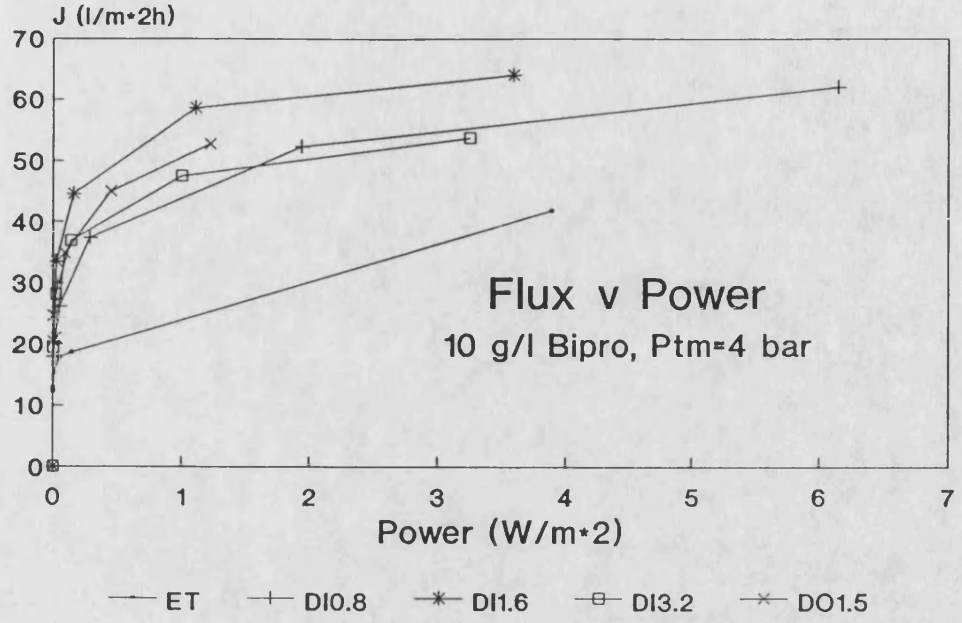

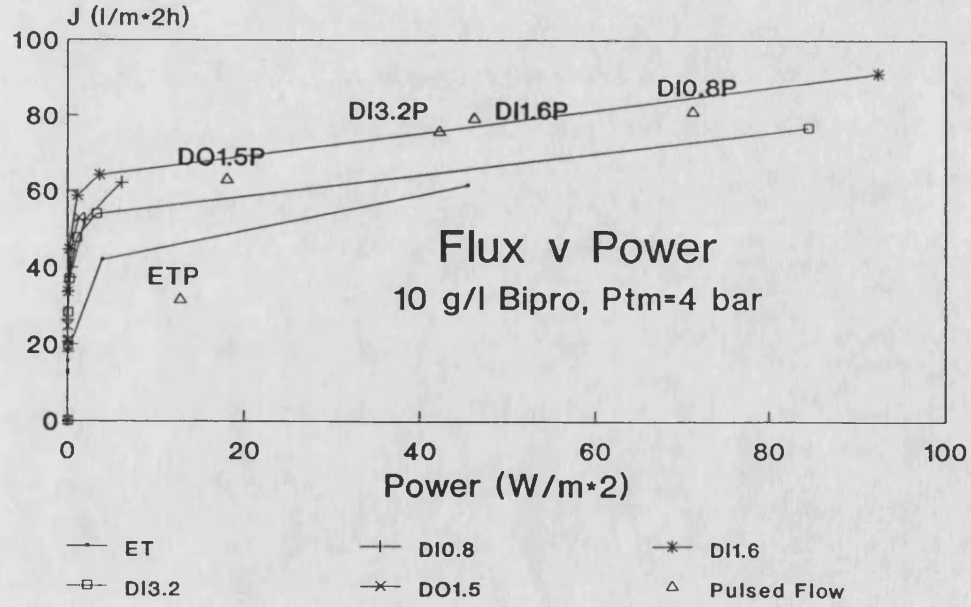

Fig 5.3: Flux v Power Consumption for Stage 2 at P_{tm}=4 bar for **ET** and the baffled systems. The same graph is shown in c and d, except that fewer data points are plotted in c as explained in the text.

5.2), little further improvement in flux occurs for the baffled systems, while for **ET**, fluxes do increase. At P_{tm}=2 bar, the **ET** fluxes approach(Fig 5.3a) and surpass(Fig 5.3b) the baffled system fluxes. At P_{tm}=4 bar, this observation is also true except in this case, the **ET** fluxes are always less than in the baffled systems even when the fluxes at Re=40000 & 50000 for **ET** and Re=16000 for **DI**1.6 & **DI**3.2 not shown in Fig 5.3 are compared.

Fig 5.3 shows that for each baffled system, the fluxes are similar in magnitude in steady flow at the same power consumption. Although the pressure drop dependence on Re is weakest for **DO**1.5 of all the baffled systems, the flux performance is still better for the **DI** systems on a power consumption basis. Similarly, for **DI**0.8, the stronger dependence of dP on Re than for **DI**1.6 and **DI**3.2 means the power consumption increases more rapidly for the former system compared with the other 2 **DI** systems. **DI**1.6 fluxes are consistently greater than **DI**3.2 over the entire range in pulsed and steady flow. It is concluded that **DI**1.6 gives the best performance on this basis.

For all systems, the fluxes in pulsed flow are similar in magnitude to the steady flow fluxes at the same power consumption. Fig 5.2(Stage 1, Re_p=950) shows that this observation is true for **ET** and **ETP**(all data) and for **DI**1.6 and **DI**1.6**P**(for E<0.5Wm^{-2}). For E>0.5Wm^{-2}, where flow reversal no longer occurs, the **DI**1.6 fluxes are greater than the **DI**1.6**P** fluxes. Fig 5.3(Stage 2, Re_p=6450) shows for the same power consumption, the fluxes in pulsed flow are greater than or equal to steady flow fluxes for all systems except **ETP**. There is some doubt as to whether the power consumption values are accurate for **ETP** due to the uncertainty in the values of dP_p used(see Section 5.1.3).

5.2.4 Discussion:

Baffles are dissipating power more effectively than turbulence in an empty tube(**ET**). An optimum flux/power range has been identified for the baffled systems. The fluxes are greater for the baffled systems than for **ET** within this optimum range. Comparative fluxes can be obtained for **ET** but only at a much higher power consumption than for the baffled systems. Inspection of Fig 5.2 and

5.3 and Table 5.3 shows that this optimum range corresponds to Re=700-1200 and 750-1450 for Stages 1 and 2 respectively. This is consistent with the optimum Re range of 350-1550 and 750-2200 determined in the filtration experiments in Stages 1 and 2 respectively(see Section 3.3.2 and 4.2.3(A)). Table 5.3 shows that within this optimum range the power consumption is a maximum of 1 Wm^{-2}. Fig 5.3 shows that to obtain comparative fluxes for ET requires a power consumption of approximately 20 and 45 Wm^{-2} at P_{tm}=2 and 4 bar respectively. The average total power consumption of large units using similar membranes are of the order of 120 Wm^{-2} owing to the higher Reynolds numbers which are required in the conventional systems. Some high velocity units are even operated at 1 kWm^{-2}. It is clear that power consumptions of the baffled systems are in fact quite small when operated at these moderate velocities. This conclusion is consistent with the work of Brunold et al(1989) and Dickens et al(1989) who stated that the power consumption in pulsed flow should be very low compared with conventional systems.

In the baffled systems, fluxes in pulsed and steady flow are of similar magnitude for the same power consumption. Once flow reversal no longer occurs there is no advantage from a flux and power viewpoint of using pulsed flow. The pulsed velocity is possibly too large in Stage 2 at Re_p=6450, as the power consumption is becoming large and lies beyond the flux/power optimum. In Sections 3.3.2 and 4.2.3(A), it was stated that in the baffled systems, fluxes in pulsed flow are of similar magnitude to those in steady flow when $Re=Re_p$. It is suggested that in order to be operating in the optimum flux/power range, the pulsed flow velocity should be chosen so that Re_p=700-1500.

The major advantage of pulsed flow is the "decoupling" of the net cross-flow velocity from the flux. It may be possible to have a single pass system, avoiding the pumping costs associated with recirculation. However, the use of pulsed flow requires additional capital expenditure for the purchase of the "pulse production unit", whether this be a pump, pneumatic valves or a cam arrangement.

It is also important to measure the actual power consumed by the pulsing pump and compare this with the power consumption predicted by the E_p term in

equation (5.3). The approach used in equation (5.3) is semi-theoretical in nature, uses experimentally determined parameters and is felt to give a reasonable estimate of the pulsed flow power consumption. The assumptions made in predicting E_p were that Q_p and dP_p are sinusoidal functions and in phase; neither of which are correct. Q_p and dP_p are both triangular rather than sinusoidal in nature(see Section 4.1.3 and 5.1.3 respectively) and a phase difference, ϕ, exists between Q_p and dP_p. Ralph(1985) also found that the dP_p waveform was not sinusoidal and that there was a phase difference between $Q_p(t)$ and $dP_p(t)$. Ralph evaluated the power consumption in a similar manner to equation (5.3) but included an extra term $\cos(\phi)$ in the pulsed power expression to account for the phase difference between $Q_p(t)$ and $dP_p(t)$:

$$E_p = Q_p(rms)\,dP_p(rms)\cos(\phi) \qquad (5.4)$$

$$= 0.5 Q_p\,dP_p\cos(\phi)$$

where rms denotes root mean square quantities. This expression only differs from the E_p term in equation (5.3) by the $\cos(\phi)$ term, which has not been included in equation (5.3) because of the doubts raised about the quantitative accuracy of ϕ in Section 5.1.4. Hence, the pulsed flow power term, as presented in this chapter, will be a maximum value.

CHAPTER 6
FLOW VISUALIZATION

Flow visualization has been carried out under the same conditions of steady and pulsed flow used in the filtration experiments to determine the flow patterns in the ET and baffled systems. There are a number of essential requirements for a flow visualization system. In this chapter these are discussed in Section 6.1, using examples of flow visualization studies similar in nature to the present work. The materials and methods used for this particular application are described in Section 6.2 and the results presented in Section 6.3. These are discussed in Section 6.4 and related to the filtration results of Chapters 3, 4 and 5. The objectives were:

a) to determine the flow patterns in each system under the same conditions of steady and pulsed flow used in the filtration experiments.

b) to relate the flow patterns to the experimental filtration results.

6.1 Introduction:

The essential requirements for a flow visualization system relate to the particles and the apparatus:

a) Merzkirch(1974) states that in selecting particles, a rule of thumb is that they should be as small as possible and at least one order of magnitude smaller than the fine structure of the flow under study. The particle size is also important relative to that of the test geometry. Stephanoff et al(1980) used polystyrene particles of diameter 15-125 micron and stated that some errors will be introduced by using particles between 0.1-0.2 the minimum channel gap. Generally a low

concentration of particles is used so that the fluid flow is not disturbed by the particle's presence. Particles should also be neutrally buoyant and highly reflecting. Of these criteria all but the last help to ensure that the particle motion follows that of the streamlines.

b) The walls of the test section and the working fluid itself can act as a strong lens preventing more than a fraction of the illuminated plane being held in focus simultaneously. This can be avoided if the working fluid and material have similar refractive indices and if the exterior cross-section of the model is rectangular. It is also important that the working fluid has a similar density and viscosity to that of the ultrafiltration test fluid. Perspex and glass both have refractive indices of approximately 1.5 whereas most liquids that are not excessively viscous are considerably less refractive. If water is used as the test fluid its physical properties can be modified by adding glycerol, as done by Ralph(1985). Another possibility is to use oil of turpentine which has a refractive index of 1.47 and is not excessively viscous.

For a tubular system, fulfilling this second criteria is not possible. However, Ralph(1985) overcame this problem by fitting a small rectangular box around each test section and filling this with the working fluid. This also reduces the lens effect of light waves travelling from the camera through air/material/ water mediums as the refractive indices of air and water are 1.0 and 1.33 respectively.

c) There are three major considerations concerning construction of the test section. It must be easy to remove flow visualization particles from the walls of the model; a sufficient number of baffles should be incorporated to render entrance effects negligible and if the geometry is scaled up, similarity of flow must be maintained. Ralph(1985) found that for a test section consisting of five hollows and a further 50 mm of unformed tube on each end of the shaped section the flow patterns observed in the central three hollows were indistinguishable from each other. Stephanoff et al(1980) found that it was simpler to scale up the membrane oxygenator geometry for flow visualization purposes. However in unsteady flow this procedure is not as useful as in order to keep the two governing parameters constant if h, half the minimum channel width, is increased

by a factor, f, then the velocity and frequency must be increased by factors of 1/f and $1/f^2$ respectively. In order to avoid very low operating frequencies a scale factor of two was used in their studies.

d) The permitted range of frequencies may also be limited by constraints on the photographic exposure time. Stephanoff et al(1980) found that exposure of one side of the film occurred before the other as the shutter blind moved across the film, this problem being worse at an exposure time of 1/125s than at 1/60s. Ralph(1985) states that this problem may be avoided by using exposure times of 1/30-1/60s. This choice represents a compromise between the requirement of achieving an adequate exposure level which imposes a lower limit on exposure time and the desirability of using as short an exposure time as possible. This latter requirement arises because in oscillatory flow, particle paths do not generally coincide with streamlines but if the exposure times are small compared with the time scale for significant changes in the streamline pattern, there will be approximate coincidence. Such a compromise places restrictions on the parameter range which can be investigated.

e) For pulsed flow, it is important to synchronize the initiation of each exposure with the flow cycle if a comparison is to be made with numerical results corresponding to different phases of the flow cycle.

6.2 Materials and Methods:

Taking the above considerations into account, the following materials and methods were used for flow visualization purposes.

a) A dilute suspension(2.5 gl^{-1}) of fine Hostalen 415 GUR polyethylene particles was used as tracer. These particles were kindly supplied by Dr M. Mackley of the Department of Chemical Engineering, Cambridge University. They are highly reflecting and almost neutrally buoyant. A few drops of dishwashing liquid were added to wet the particles.

b) Distilled water at 18°C was used as the test fluid in a tubular glass test section. The viscosity and density of water at this temperature are $1056*10^{-6}$

$kg.m^{-1}s^{-1}$ and 998.5 $kg.m^{-3}$ respectively. The difference in physical properties between Bipro at 25 and 10 gl^{-1} at 25°C compared with distilled water at 18°C means for the same values of v and v_p, the Re and Re_p values differ by a maximum of 13%. A rectangular box was built that could be fitted around the tubular test section and filled with water. This was not used as preliminary photographs taken without this box in position were satisfactory.

c) Precision bore glass tubing of 12.2 mm I.D., slightly smaller than the membrane I.D. of 12.5 mm was used to make 2 flow visualization tubes 376 mm in length with flanges at each end. These test sections are identical to the stainless steel membrane support tubes. Having the same geometry has two main advantages:

1) the same geometrical inserts can be used for flow visualization and filtration purposes.

2) the actual modules are interchangeable and can be mounted in the same rig.

d) Flow visualization photographs have been taken using a F3 Nikon SLR camera with 105 mm lens and motor drive. Ilford 35 mm FP4 film was used. The exposure times and aperture settings were determined for steady and pulsed flow in a preliminary series of photographs and are tabulated in Table 6.1. A 150

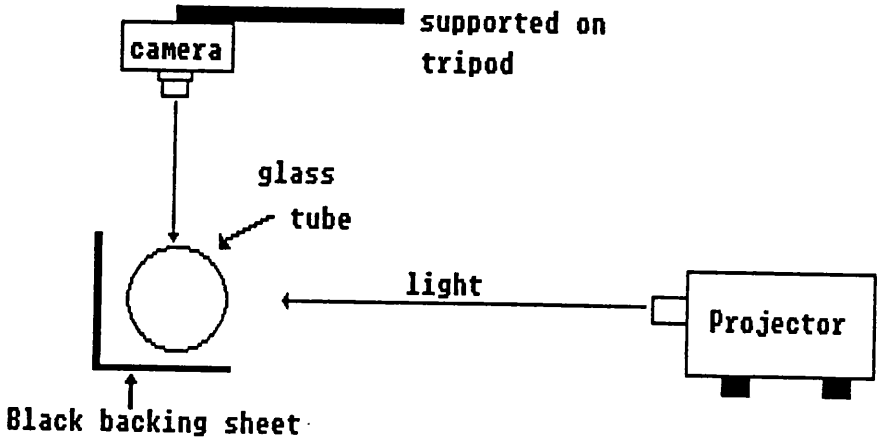

Fig 6.1: A Schematic diagram showing the Flow Visualization Setup.

W Pradovit R150 slide projector was used as a light source. Slides with a narrow slit cut in them were made so that light from the projector illuminated a thin horizontal diametric cross-section of the tube. A black backing sheet was used to give a dark background. The camera was positioned above the flow visualization unit as illustrated in Fig 6.1.

e) No attempt was made to synchronize the camera shutter with the phase of oscillation although a method has been devised and the equipment designed and built to do this.

Steady Flow:

Stage	Re	t(s)	F
2A	150-300	1	22,32
	650-950	1/8	11,22
	1300-1950	1/15	8,11
2B	2100	1/15	8,11
	3850-5700	1/30	5.6,8
	9450-31000	1/60	5.6,8

Pulsed flow:

X(mm)	f(Hz)	NFR	t(s)	F
30.5	0.4	0	1/8,1/15	5.6,8
30.5	1.4	0	1/15,1/30	5.6,8
30.5	2.5	0	1/30,1/60	5.6,8
17.7	2.5	0	1/30,1/60	5.6,8
4.8	2.5	0	1/30,1/60	5.6,8
30.5	0.4	0.34	1/8,1/15	5.6,8
30.5	0.4	0.52	1/8,1/15	5.6,8
30.5	0.4	0.62	1/8,1/15	5.6,8

Table 6.1: Exposure times(t) and aperture settings(F) used for flow visualization photographs.

6.3 Results:

6.3.1 Summary:

The flow patterns for **ET** showed a gradual change from laminar flow($Re<2000$), where a distinct fluid boundary layer existed, to turbulent flow($Re>6000$). With pulsed flow(**ETP**), laminar, plug flow existed for all values of frequency and amplitude($Re_p \leq 5700$).

For the baffled systems in steady flow, 3 distinct flow patterns were identified for **DI**1.6 and **DI**3.2, differentiated by the number of vortices present in each cell and the laminar/turbulent nature of the flow patterns. With **DI**0.8 and the **DO** systems, only 1 flow pattern was observed. With all systems, increasing Re resulted in better mixing, enhanced mass transfer and interrupted development of the boundary layer. The transition to turbulence occurred at much lower Re values than for **ET.** The mixing pattern appeared to "fill" the cell better for **DI**1.6 than **DI**3.2 while channelling of the fluid along the wall region was particularly strong for **DI**0.8. For **DO**1.5, the flow was generally less chaotic than in the **DI** systems at identical Re values, with most of the bulk flow moving through the middle of the tube.

For the baffled systems in pulsed flow, a vortex mixing mechanism was observed, which enhanced mass transfer and prevented the development of velocity and concentration boundary layers at the membrane surface. For all systems, the "instantaneous" flow pattern resembled the steady flow pattern at $Re=Re_p$. The overall flow pattern was very similar to pure pulsed flow and steady flow for $NFR<0.2$ and $NFR>0.8$ respectively. The flow was generally more chaotic for the **DI** systems compared with **DO**1.5.

Good mixing has been shown to be a function of amplitude, frequency and baffle geometry. Increasing frequency increased the degree of chaos while increasing amplitude increased the strength of the vortices and proportion of each

cell occupied by the vortex motion. In Stage 1, the frequency and amplitude needed to be at least 1.4 Hz and 2.6 mm(60%) respectively to achieve effective mixing, while in Stage 2, little difference was observed in the flow patterns for X=17.7 mm(60%) and 30.5 mm(100%) at f=2.5 Hz. For f>1.4 Hz at X=30.5 mm and for X>5 mm at f=2.5 Hz, chaotic fluid motion was observed. Sharp edges promote separation at relatively low amplitudes so that "short, fast" strokes achieved good mixing provided the f and X criteria for good mixing were satisfied.

These flow visualization results were used to explain many of the observations made in the filtration experiments, illustrating the usefulness of this technique, even though the effect of the permeation flux through the membrane on the flow patterns can not be accounted for.

6.3.2 General Observations:

The observations and flow visualization photographs have been presented together for each system. Each photograph shown corresponds to a horizontal cross-section of the tube with the flow moving from right to left. Photographs were taken of a mid-section of the inlet tube to minimize any end effects on the flow patterns. Two series of photographs were taken corresponding to Stages 2A and 2B. These differ in size. Some photographs from Stage 2A were developed on 2 separate occasions and differ in magnification. This explains the different size and magnification of some of the photographs in the text. For Stage 1, only visual observations and sketches of the flow patterns were made for **DI1.6** and **DO2.2** for a vertical cross-section of the tube. Due to the lens effect of the glass water interface and the parallax due to the camera position, the baffle spacing to tube diameter ratio, L/D, is not correct in the photographs.

Observations were made for pulsed flow looking at the effects of amplitude, frequency and net cross-flow velocity on the flow patterns. The frequency and amplitude observations were made with no net cross-flow. The retentate valve was closed to prevent any dissipation of the pulse in the retentate line in this case. Unless otherwise stated the frequency was varied from 0.4, 1.4

to 2.5 Hz at an amplitude of 100% for each system. As the frequency increases it was observed that the flow patterns remain the same but the intensity of motion increases. The increasingly chaotic nature of the flow at higher frequencies makes it difficult to resolve the flow phenomena and for this reason the observations for pulsed flow described here correspond to f=0.4 Hz unless otherwise stated.

The amplitude was varied between 100%, 60% and 20% and observations were made at 0.4 Hz unless otherwise stated in the text. These percentage amplitudes correspond for Stage 1 to amplitudes of 4.6, 2.6 and 0.8 mm and for Stage 2 to 30.5, 17.7, and 4.8 mm respectively. The actual amplitude is expressed in mm in the text. Percentage values are only stated where relevant for explaining a certain feature of the flow. The Stage 2 results are described first with the Stage 1 observations being included in Section 6.3.6 for the baffled systems.

6.3.3 Empty Tube(ET):

(A) Steady flow:

The steady flow patterns in Fig 6.2(a-g) show a gradual change from laminar flow in Fig 6.2(a-d)(Re<2000) to turbulent flow in Fig 6.2(e-g)(Re>6000). At all flowrates within the laminar range, there is a boundary layer near the wall where the fluid is relatively slow moving. This is particularly prominent for Re<650.

The quality of the second series of photographs(Fig 6.2(e-g)) corresponding to Re≥3850 is poor. The flow patterns were more chaotic in nature but this is difficult to tell from the photographs. The transition to turbulent flow could only be predicted roughly and occurs in the range 2000-6000.

(B) Pulsed flow:

Laminar plug flow exists for all values of frequency and amplitude ($Re_p \leq 5700$). No radial or axial dispersion was observed. When a net cross-flow

A) Re =

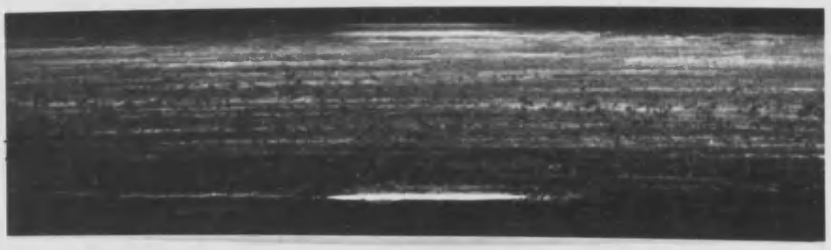

B) Re = 650

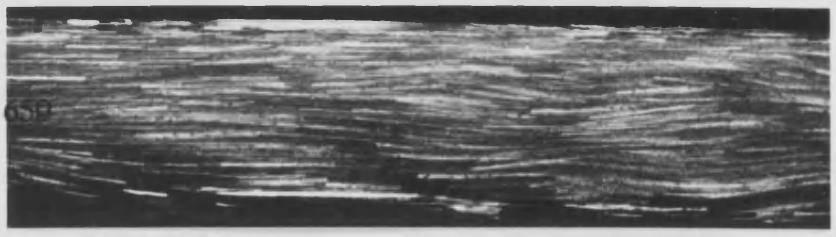

C) Re = 1300

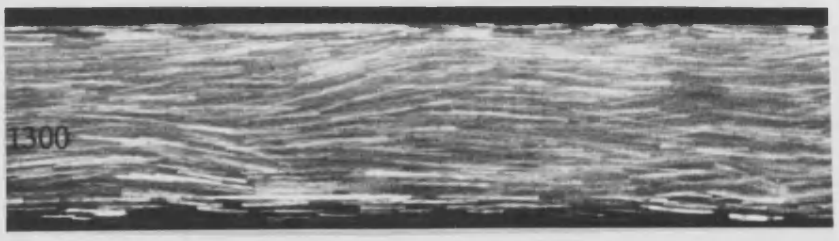

D) Re = 1950

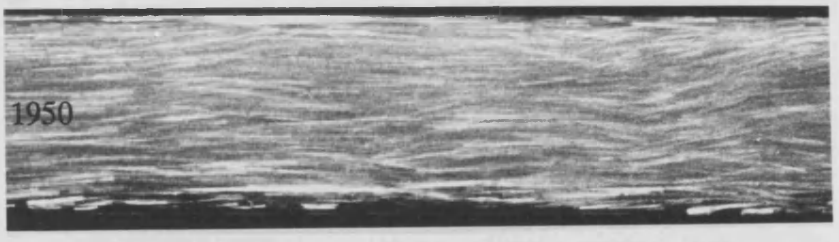

E) Re =

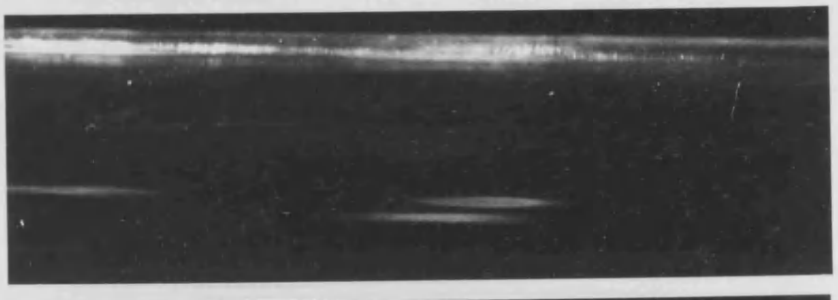

F) Re =

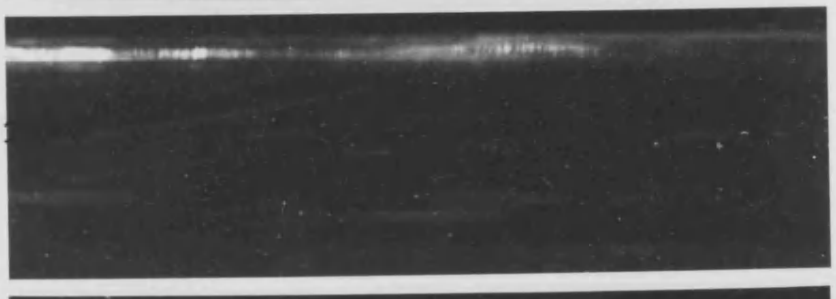

G) Re = 31000

Fig 6.2: Steady flow patterns for ET for Stages 2A and 2B

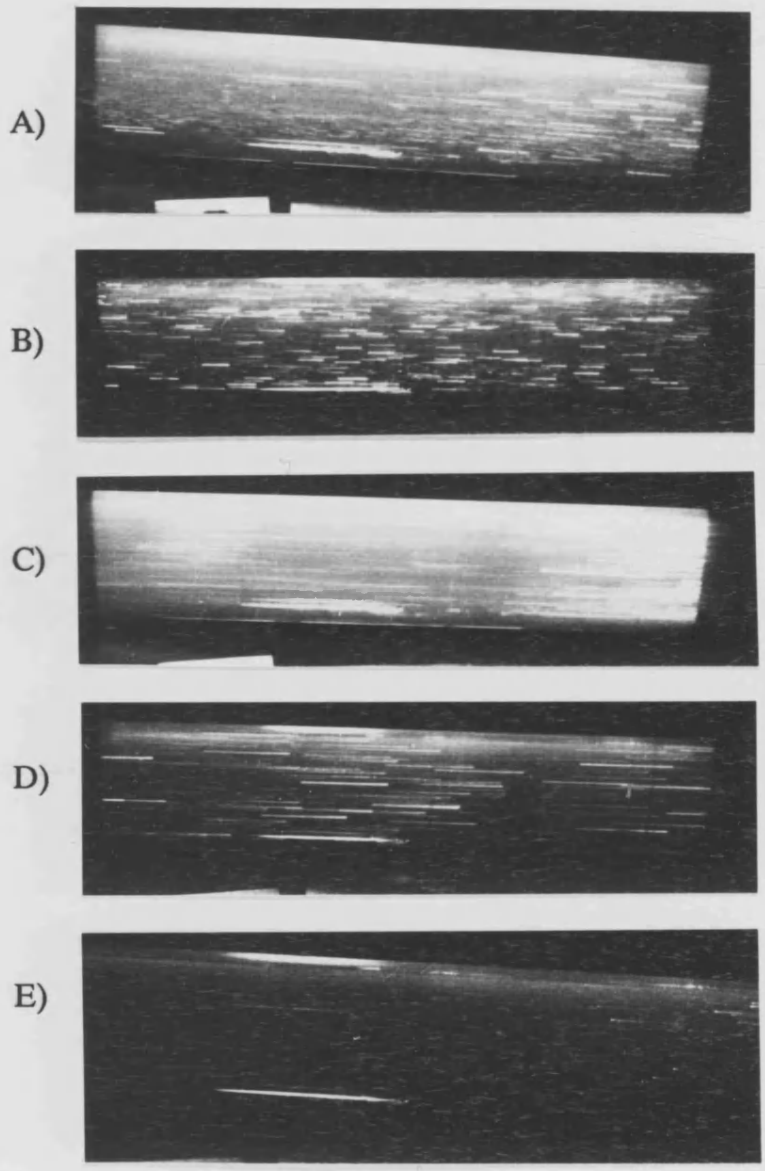

Fig 6.3: Pulsed flow patterns for **ETP** with no cross-flow for X=30.5 mm(100%) and for variable frequency: a) 0.4 Hz; b) 1.4 Hz; c) 2.5 Hz; and for f=2.5 Hz and variable amplitude: d) 17.7 mm(60%); e) 4.8 mm(20%).

velocity is superimposed on the pulsed flow, the plug flow remains intact and

moves forward with the cross-flow in a shunting fashion. Increasing frequency and amplitude increases the speed and extent of the motion respectively. Fig 6.3(a-e) captures the pluglike nature of the flow well but does not illustrate the effects of frequency and amplitude on the flow patterns.

6.3.4 Disc(DI) Baffles:

(A) Terminology:

The nomenclature used throughout this discussion for the disc shaped baffles is summarized here. Up to 2 vortices were observed in flow visualization. These are labelled as **VA** and **VB** in the figures. **VA** occupies a certain proportion(x) of the distance between adjacent baffles, L. Each interbaffle spacing is called a cell. It is said to occupy xL. The mainstream flow is referred to as the bulk flow. Flow is said to be chaotic when an element of fluid will eventually visit every point within the region(see Section 1.4.2). When the streamlines detach or attach to the tube wall or the central support rod this is referred to as separation. The flow is said to be laminar when the bulk flow retains its streamline nature and turbulent when these streamlines become disordered. With pulsed flow, laminar flow refers to unsteady laminar flow where the flow maintains its laminar character over the accelerational and decelerational phases of the cycle; turbulent flow refers to the flow being chaotic over most of the cycle.

(B) Steady Flow:

DI1.6 and DI3.2: The flow patterns are similar for both these baffled systems. Three distinct flow regimes exist. These are referred to as Type 1, 2 and 3 and are illustrated schematically in Fig 6.4-6.7. Photographs of these flow patterns are shown in Fig 6.4(a-g) and 6.5(a-g) for Stage 2A for **DI**1.6 and **DI**3.2 respectively.

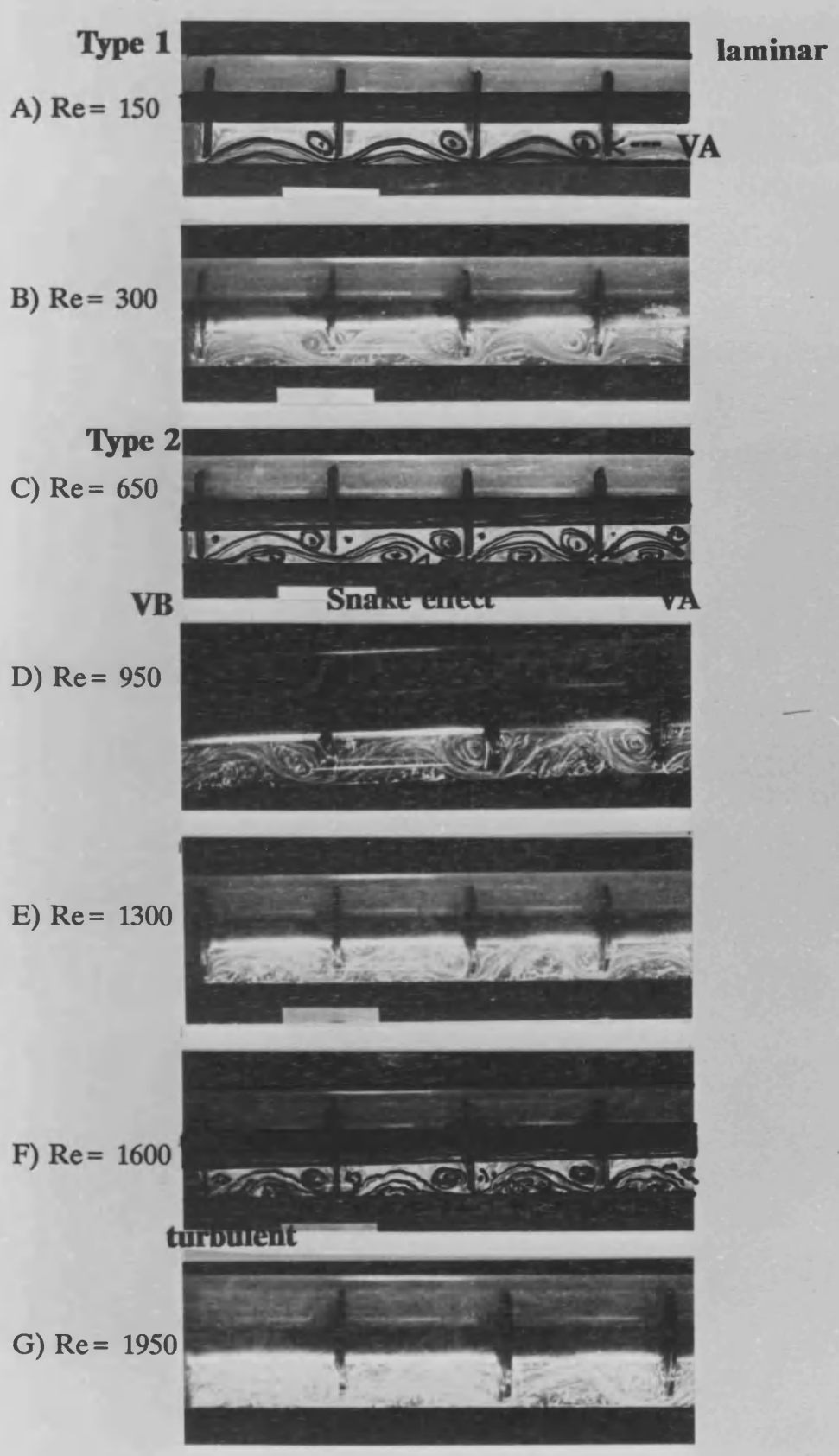

Fig 6.4: Steady flow patterns for **DI**1.6 for Stage 2A.

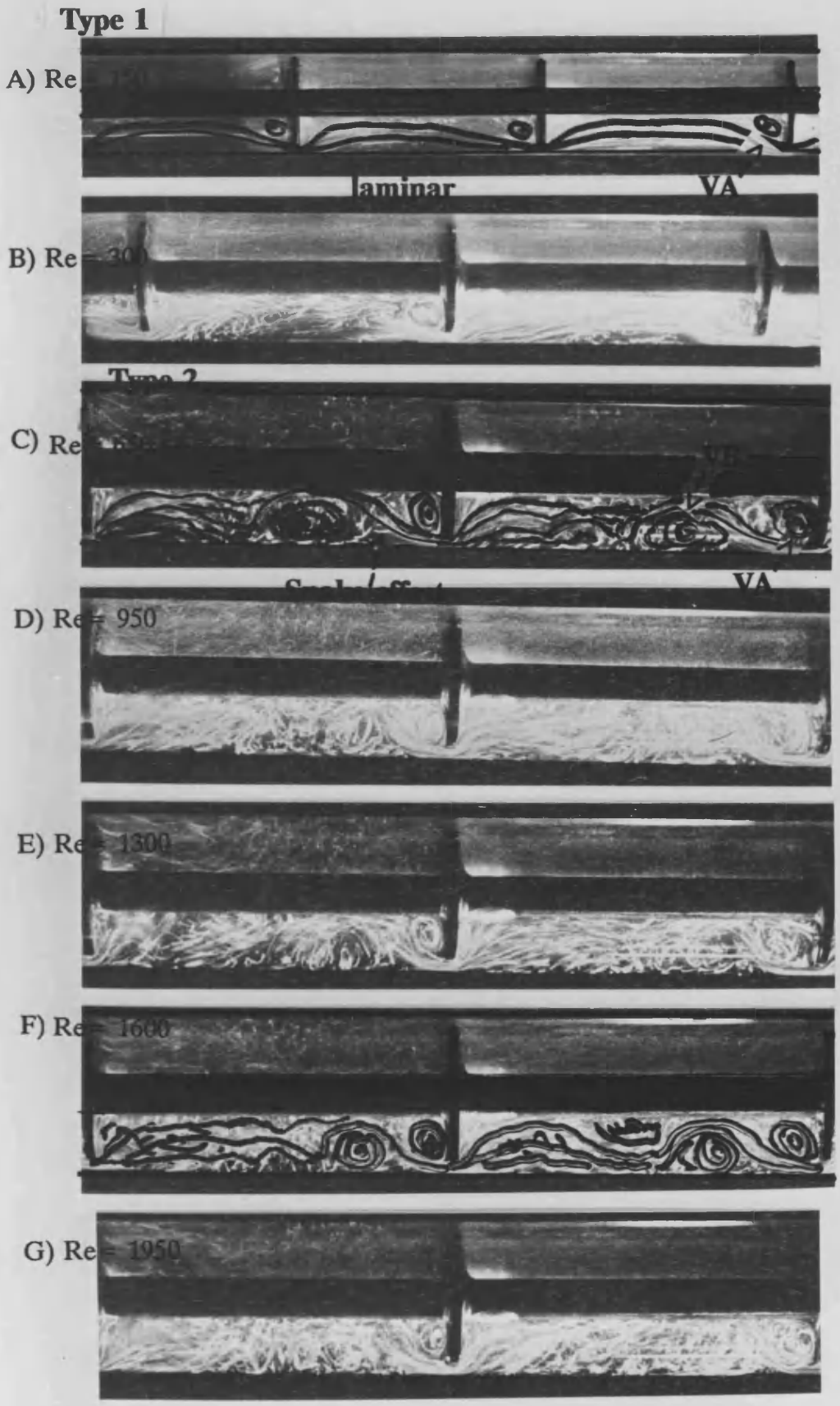

Fig 6.5: Steady flow patterns for DI3.2 for Stage 2A.

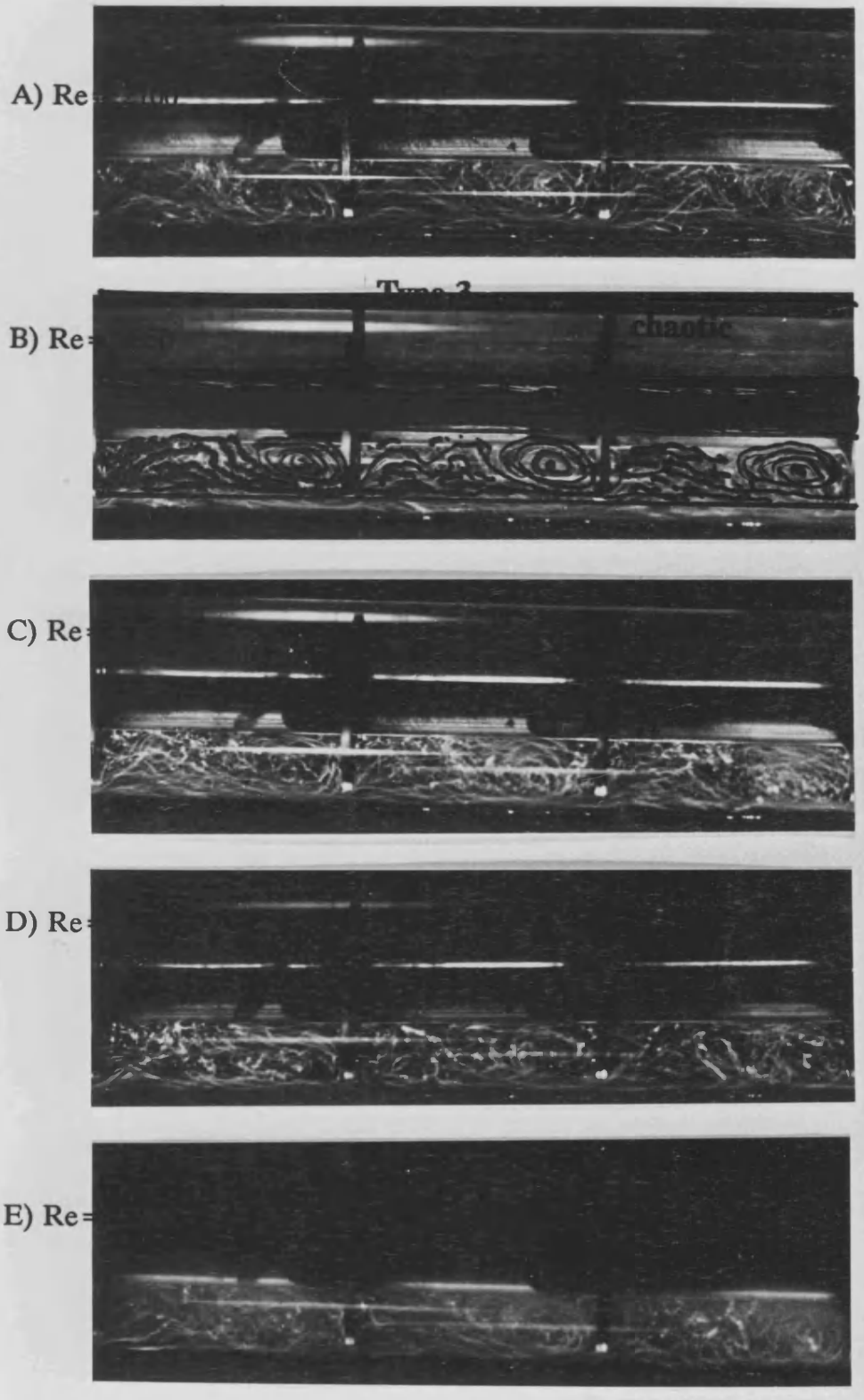

Fig 6.6: Steady flow patterns for **DI**1.6 for Stage 2B.

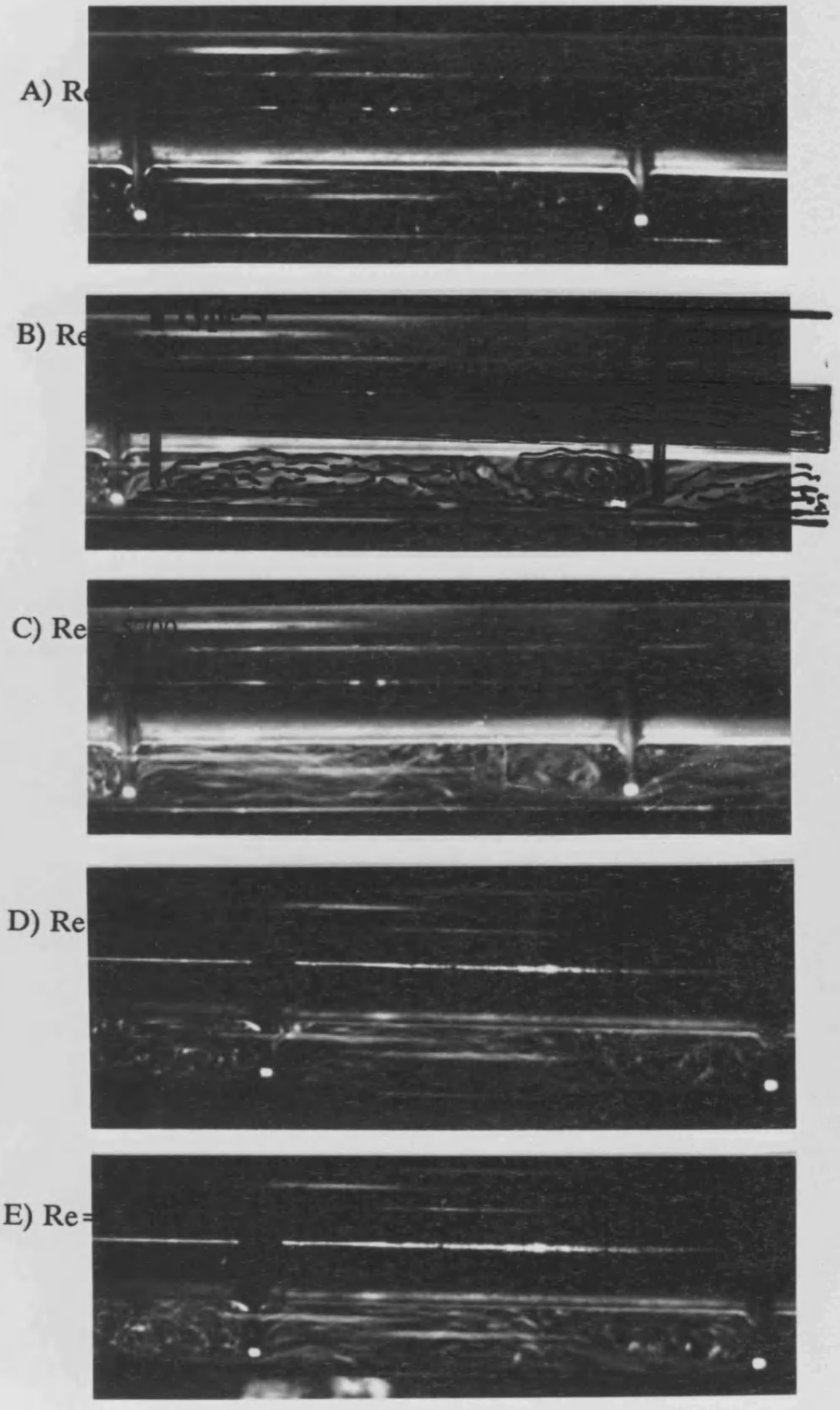

Fig 6.7: Steady flow patterns for DI3.2 for Stage 2B.

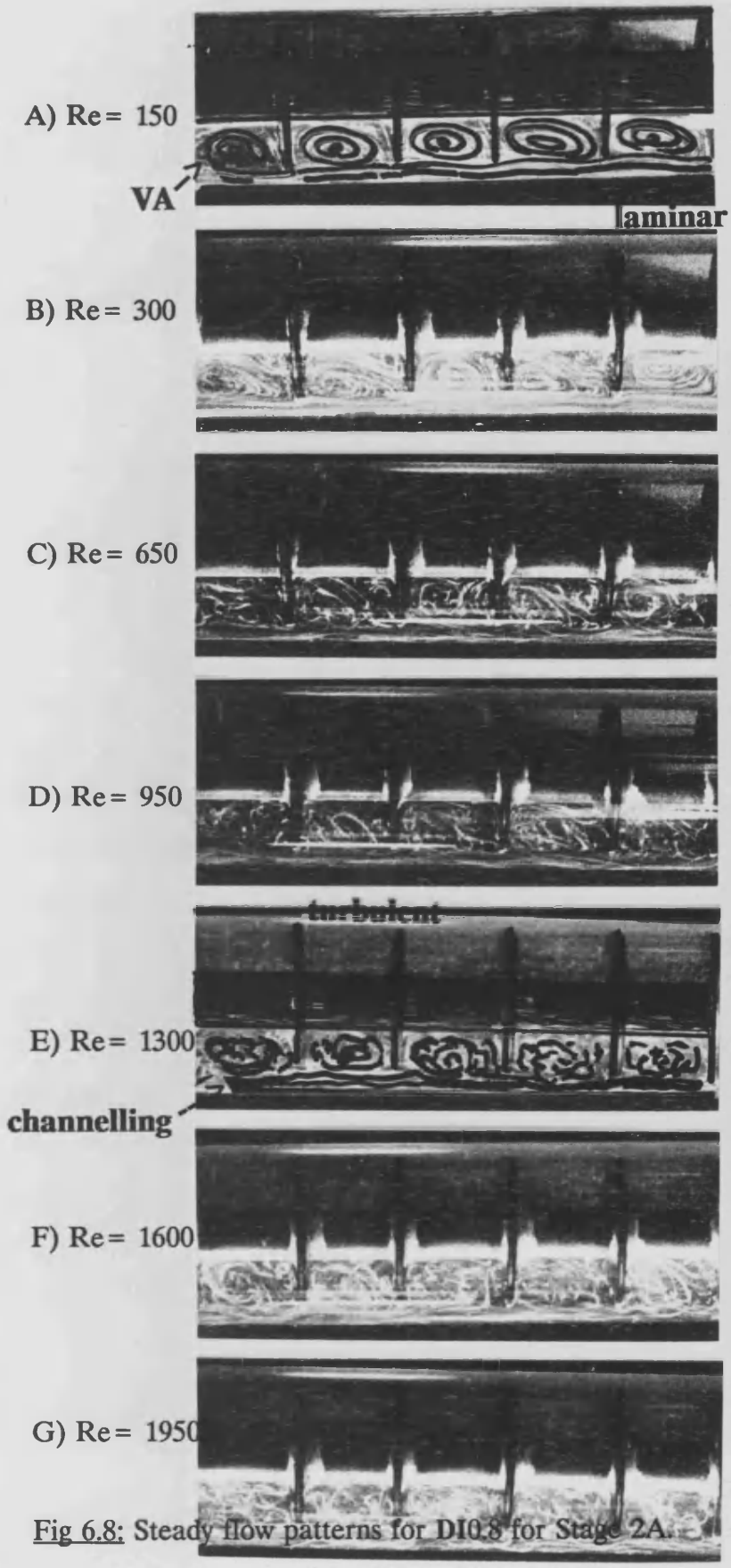

Fig 6.8: Steady flow patterns for DI0.8 for Stage 2A.

Type 1 flow exists for Re=150 (Fig 6.4a, 6.5a) where the flow is almost entirely laminar with only one vortex, **VA**, forming immediately downstream of the baffle. Separation of the streamlines from the tube wall and central support rod occurs but most of the streamlines remain relatively parallel to the central rod. Flow is relatively slow moving in the wall region as particles gradually accumulate at the top of the tube and form a "semi-stagnant" region where material moves slowly from one cell to the next.

Type 2 flow exists for Re=300-1950. At Re=300(Fig 6.4b, 6.5b) a weak vortex, **VB**, has formed at the wall and the semi-stagnant region has disappeared. The bulk flow moves between these 2 vortices in a convoluted fashion which is referred to as the snake effect. This snake effect is the dominant feature of Type 2 flow which is well established at Re=650(Fig 6.4c, 6.5c). As Re is increased further(Fig 6.4d, 6.5d) the bulk flow loses its streamline nature and it is difficult to accurately identify where separation occurs. The estimated laminar-turbulent transition range is Re=950-1200 and 1050-1300 for **DI**1.6 and **DI**3.2 respectively. As Re increases to 1950(Fig 6.4(e-f) & 6.5(e-f)) the streamlines become more turbulent in nature and the general flow pattern becomes more chaotic. **VA** and **VB** remain approximately the same size over this Re range but grow in strength with increasing Re. For **DI**1.6 the snake motion seems to fill the cell better than for **DI**3.2. For **DI**3.2, **VB** is more unstable and the flow pattern is generally more disordered downstream of **VA** than for **DI**1.6.

Fig 6.6(a-e) and 6.7(a-e) presents the Stage 2B photographs for **DI**1.6 and **DI**3.2 respectively. Type 3 flow is established at Re=2100. Vortex **VB** has disappeared and no separation occurs. **VA** is larger than in Stage 2A(Fig 6.4 and 6.5) and channelling of the bulk flow along the wall region is more prominent, especially for Re≥3850. As Re is increased further(Fig 6.6(c-e), 6.7(c-e)) the flow becomes more chaotic.

DI0.8: The flow patterns are shown in Fig 6.8(a-g) for Stage 2A for **DI**0.8. These baffles were more difficult to make than the other 2 sets of disc baffles. Fig 6.8(a-g) show that L varies between 8-10 mm and some of the baffles are skew. Despite this, the flow pattern is relatively uniform and remains unchanged

over the Re range. At Re=150(Fig 6.8a), a weak vortex, **VA**, forms occupying the entire cell. As Re increases, **VA** becomes stronger and then unstable and chaotic in nature. This is clearly shown at Re=650(Fig 6.8c). The estimated laminar-turbulent transition range is Re=500-800. Channelling of the bulk flow along the wall is stronger for **DI0.8** compared with the other **DI** systems.

(C) Pulsed Flow:

DI1.6 and DI3.2: The flow patterns in pulsed flow are similar for these two baffled systems. These observations were made at an amplitude of 30.5 mm and f=0.4 Hz. In pulsed flow, vortices **VA** and **VB** form and grow in strength as the flow accelerates. During deceleration, this flow pattern breaks up and on flow reversal, these vortices are ejected into the bulk flow. This cycle is then repeated in the opposite direction. The overall sequence is a see-saw motion from one side of the baffle to the other. The flow pattern during acceleration and deceleration resembles Type 2 flow. This mechanism of vortex mixing remains unchanged as the frequency is increased but the flow becomes more chaotic in nature and it is not possible to distinguish individual stages of this cycle.

As the amplitude is decreased the snake motion still occurs but **VA** and **VB** are weaker and smaller. There is a greater proportion of each cycle over which no motion occurs. The snake motion occupies a smaller proportion of each cell as the amplitude is decreased as tabulated in Table 6.2, although there is little difference between the flow patterns at X=30.5 and 17.7 mm.

X (mm)	4.8	17.7	30.5
DI0.8	0.5	1.0	1.0
DI1.6	0.5	0.65	0.7-0.8
DI3.2	0.2	0.4-0.5	0.5-0.6

Table 6.2: The proportion, x, of each cell occupied by the snake motion at f=0.4 Hz. For **DI0.8**, only **VA** is present.

DI0.8: For **DI**0.8, the flow pattern is qualitatively the same except in this case only one vortex, **VA** is present. The vortex mixing mechanism occurs and the strength and size of **VA** increases with increasing frequency and amplitude. The proportion of each cell occupied by **VA** is tabulated in Table 6.2. Once the cell is filled, **VA** can not grow further in size.

Fig 6.9(a-e), 6.10(a-f) and 6.11(a-e) show the flow patterns for **DI**1.6, **DI**3.2 and **DI**0.8 respectively at X=30.5 mm at f=0.4(a), 1.4(b) and 2.5 Hz,(6.9c, 6.10(c-d), 6.11c) and f=2.5 Hz at X=17.7 mm(6.9d, 6.10e, 6.11d) and 4.8 mm(6.9e, 6.10f, 6.11e). The observations made above are not clearly captured in these photographs, primarily because each photograph corresponds to an arbitrary stage of the flow cycle and direct comparison of the intensity of the flow between different photographs is misleading. In addition, the variable amplitude photographs correspond to f=2.5 Hz, where the flow is more chaotic than at 0.4 Hz, where the visual observations were made. This was done deliberately as this frequency reflects the conditions used in the filtration experiments where the amplitude was varied between 0-100% at f=2.5 Hz. However, several salient features can be noted from the photographs:

a) Fig 6.9(a-b) and Fig 6.10(c-d) capture "opposite ends" of the see-saw effect as they are approximately half a cycle apart.

b) The flow is less chaotic at X=4.8 mm(Fig 6.9e, 6.10f, 6.11e) than at X=17.7 mm(Fig 6.9d, 6.10e, 6.11d) and X=30.5 mm(Fig 6.9c, 6.10(c-d), 6.11c). There is little difference in the flow patterns at X=17.7 and 30.5mm.

c) Fig 6.10(a-b) are near the point of flow reversal and show how the vortices have broken up.

d) Fig 6.11c shows the chaotic nature of the flow for **DI**0.8 at f=2.5 Hz and X=30.5 mm.

NFR: The effect of NFR on the flow patterns was investigated over the Re range 0-1950 at X=30.5 mm for **DI**1.6. The following observations and photographs(Fig 6.12(a-g)) were made at 0.4 Hz. At low NFR(0-0.2) the flow patterns are almost identical to pulsed flow. Three stages of a flow cycle that

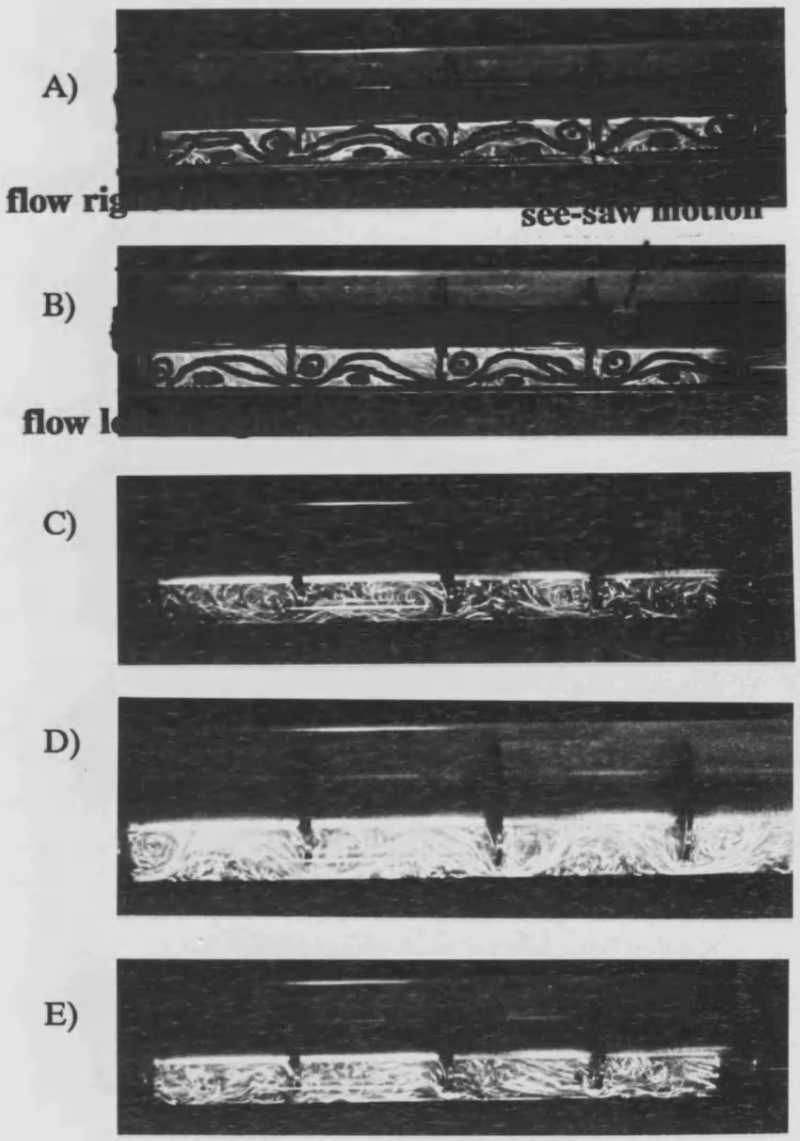

Fig 6.9: Pulsed flow patterns for **DI**1.6 with no cross-flow for X=30.5 mm(100%) and for variable frequency: a) 0.4 Hz; b) 1.4 Hz; c) 2.5 Hz; and for f=2.5 Hz and variable amplitude: d) 17.7 mm(60%); e) 4.8 mm(20%).

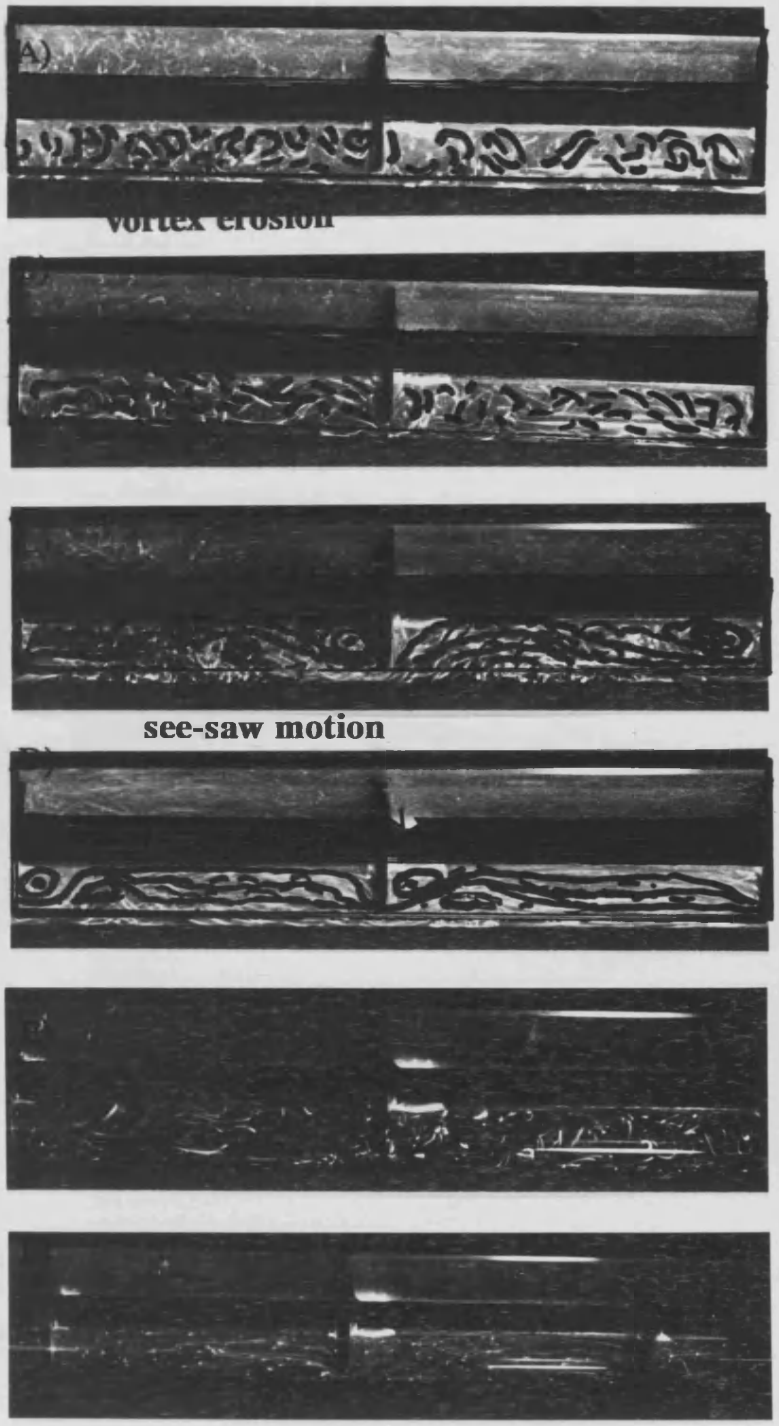

Fig 6.10: Pulsed flow patterns for **DI**3.2 with no cross-flow for X=30.5 mm(100%) and for variable frequency: a) 0.4 Hz; b) 1.4 Hz; c) 2.5 Hz(flow right to left); d) 2.5 Hz(flow left to right) and for f=2.5 Hz and variable amplitude: e) 17.7 mm(60%); f) 4.8 mm(20%).

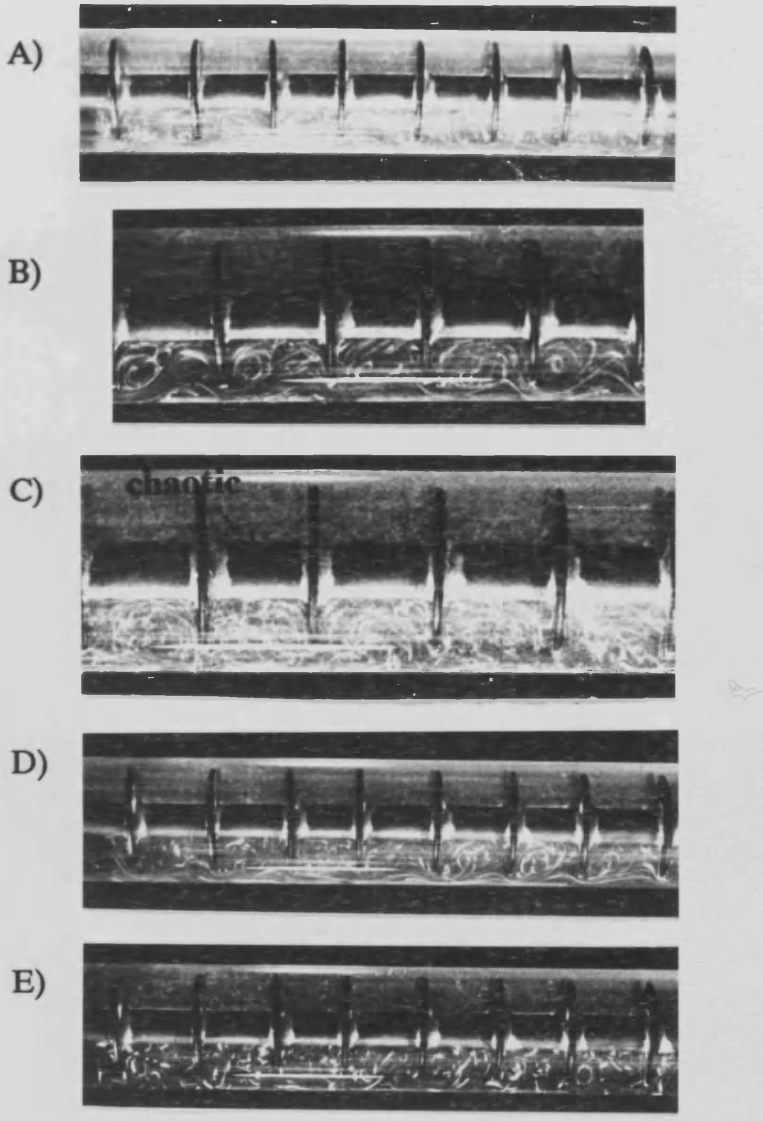

Fig 6.11: Pulsed flow patterns for **DI**0.8 with no cross-flow for X=30.5 mm(100%) and for variable frequency: a) 0.4 Hz; b) 1.4 Hz; c) 2.5 Hz; and for f=2.5 Hz and variable amplitude: d) 17.7 mm(60%); e) 4.8 mm(20%).

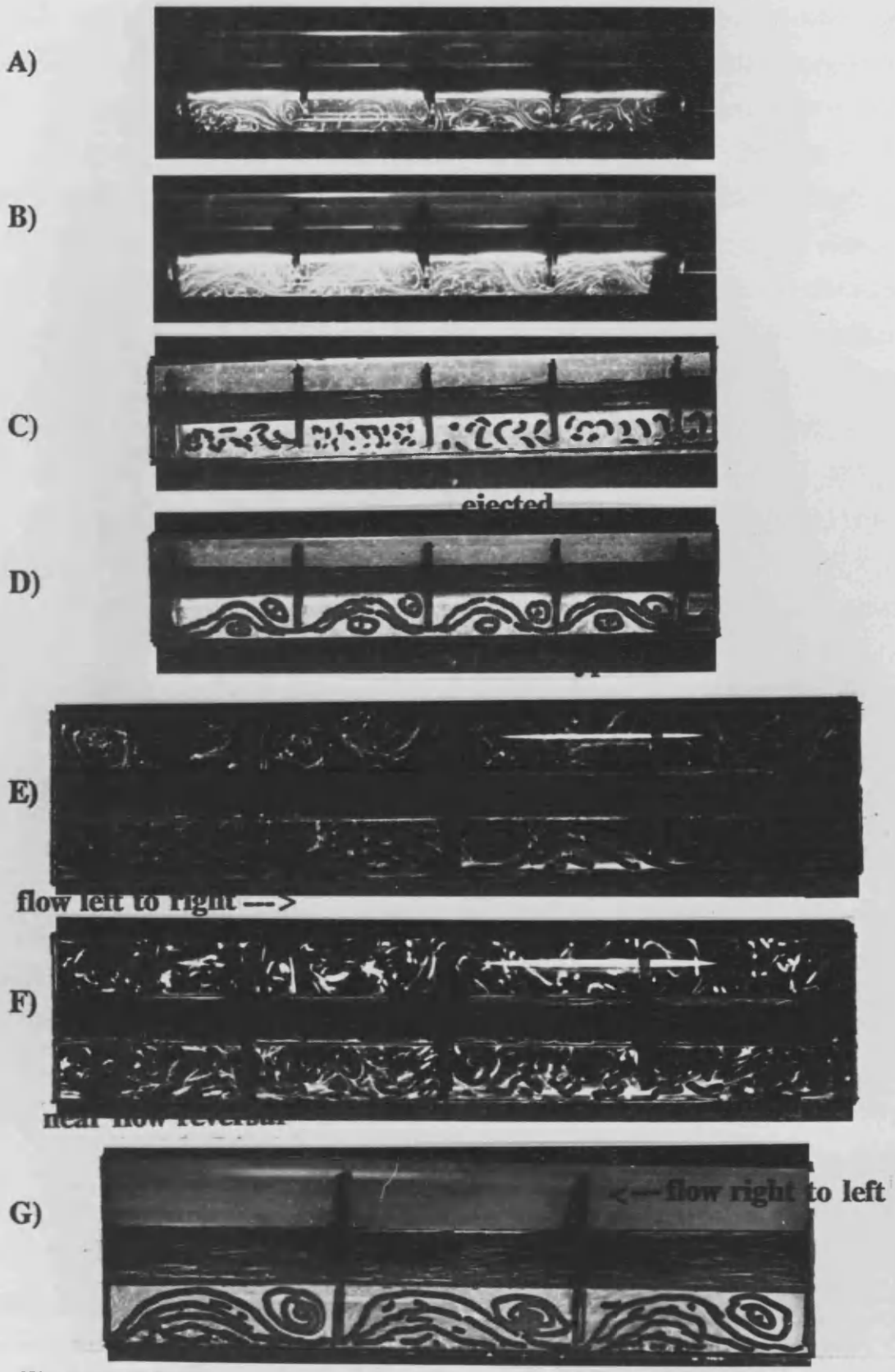

Fig 6.12: Pulsed flow patterns for DI1.6 at X=30.5 mm(100%) and f=0.4 Hz for NFR= a) 0.34; b) 0.52 flow from left to right(L-R) c) 0.52(near flow reversal(FR); d) 0.62. At NFR=0; e) flow L-R; f) near FR; g) flow R-L.

occurs at NFR<0.2 are shown in Fig 6.12(e-g) for 2.5 Hz and X=30.5 mm. Fig 6.12e shows flow moving in the direction left to right; 6.12f is near the point of flow reversal and 6.12g shows flow moving in the opposite direction: right to left. Fig 6.12a captures the forward phase of the cycle for NFR=0.34. As Re is increased further the forward motion becomes stronger(Fig 6.12b), the reverse weaker and of shorter duration. At NFR=0.52, flow reversal no longer occurs; the flow momentarily stops each cycle and the vortex is ejected into the bulk flow(Fig 6.12c) but does not move to the other side of the baffle as with pulsed flow. As NFR is increased the flow becomes unidirectional(Fig 6.12d) and resembles the steady flow pattern, especially for NFR>0.8. The "instantaneous" flow pattern is Type 2 in both the accelerational and decelerational phases, resembling the corresponding steady flow pattern at $Re=Re_p$, and becomes more chaotic with increasing frequency.

The effect of NFR on flow patterns described here applies equally well to the other baffled systems under the flow conditions of both Stages 1 and 2.

6.3.5 Doughnut(DO) Baffles:

(A) Steady flow:

DO1.5: The flow patterns shown in Fig 6.13(a-g) for **DO**1.5 are very different when compared with the **DI** baffles. The **DO**1.5 baffles were difficult to make. L varies; some of the baffles are slightly bent and it was difficult to mount them vertically. The gap between the outer edge of the baffle and the glass wall also varies so that 2 distinct situations were observed; namely, when particles can and can not flow between the outer edge of the baffle and the wall. The best position for flow visualization to be carried out was found to be with the supporting rods at approximately a 45° angle to the horizontal so that neither rod is in the same plane as the projector or camera.

Only one flow pattern was observed over the Re range investigated. At Re=150(Fig 6.13a) the flow is laminar with the bulk flow going through the middle of the tube. There is a large semi-stagnant region extending almost the

entire length of each cell along the top of the tube. Viewed in the horizontal plane, this region is a weak vortex, **VB**, in cells where there is no gap between the baffle and the wall. Otherwise it is a region of very slow moving forward flow. At Re=300(Fig 6.13b) there is increased flow between the outer edge of the baffle and the wall where this is possible. At Re=650(Fig 6.13c) the streamlines are becoming wavier and there is more interaction between the bulk flow and the wall region. Particles in the wall region are accelerated by the bulk flow as they near the wall/bulk flow boundary. If not captured by the bulk flow these particles remain in the wall region and move in a chaotic fashion along the wall until merging with the rest of the wall flow. The stagnant region has almost disappeared. Where there is a baffle/wall gap a small vortex, **VA**, forms immediately downstream of the baffle. This vortex is the only discernible difference in the flow patterns for the 2 types of cell for Re>650(Fig 6.13(d-g)). The flow pattern becomes more chaotic as Re is increased and the estimated laminar-turbulent transition range is Re=1300-1600. At identical Re values, the flow patterns are generally less chaotic than in the **DI** systems.

DO2.2: No photographs were taken of the flow patterns for the baffles used in Stage 1. These are sketched in Fig 6.14(a-d). The overall motion is similar to **DO1.5**. The clearance between the baffle and the wall is more significant in this case and the baffles are 2 mm thick compared with 0.8 mm for **DO1.5**. The flow patterns are slightly different from those observed with **DO1.5** for Re≥300. Here(Fig 6.14b), the interaction between the bulk flow and that around the outside of the baffles results in a strong vortex, **VA**, forming immediately downstream of the baffle. As these 2 sets of streamlines meet this causes a disturbance in the flow resulting in a strong mixing effect. These streamlines flow around region **VB** which forms at the wall and either through or around the outside of the next baffle. A chaotic movement of the fluid is occurring in **VB**. Increasing Re above 600(Fig 6.14d) does not alter the flow patterns-the degree of turbulence increases and **VB** becomes smaller. The estimated laminar-turbulent transition is Re=600-800.

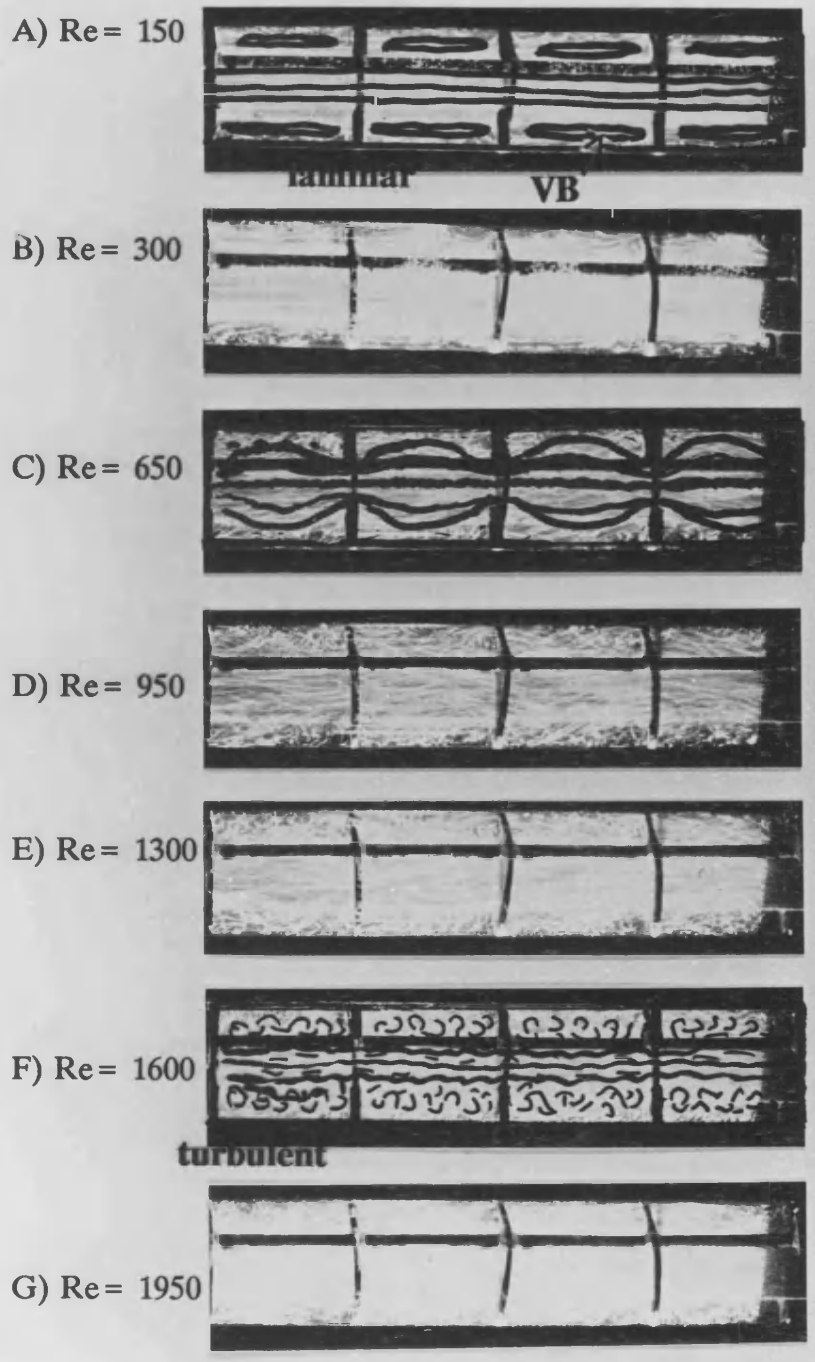

Fig 6.13: Steady flow patterns for DO1.5 for Stage 2A.

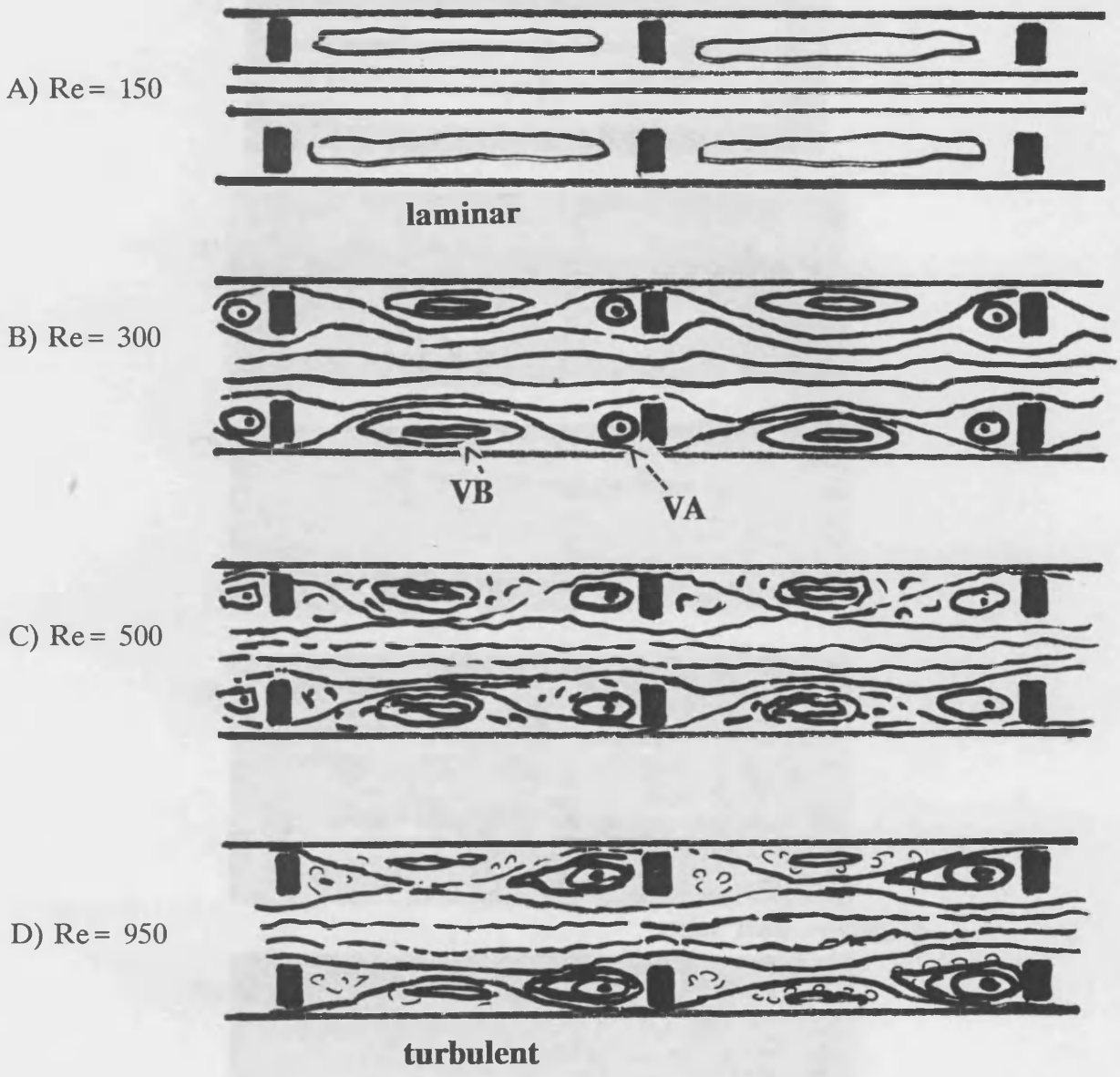

Fig 6.14: Steady flow patterns for **DO2**.2 for Stage 1.

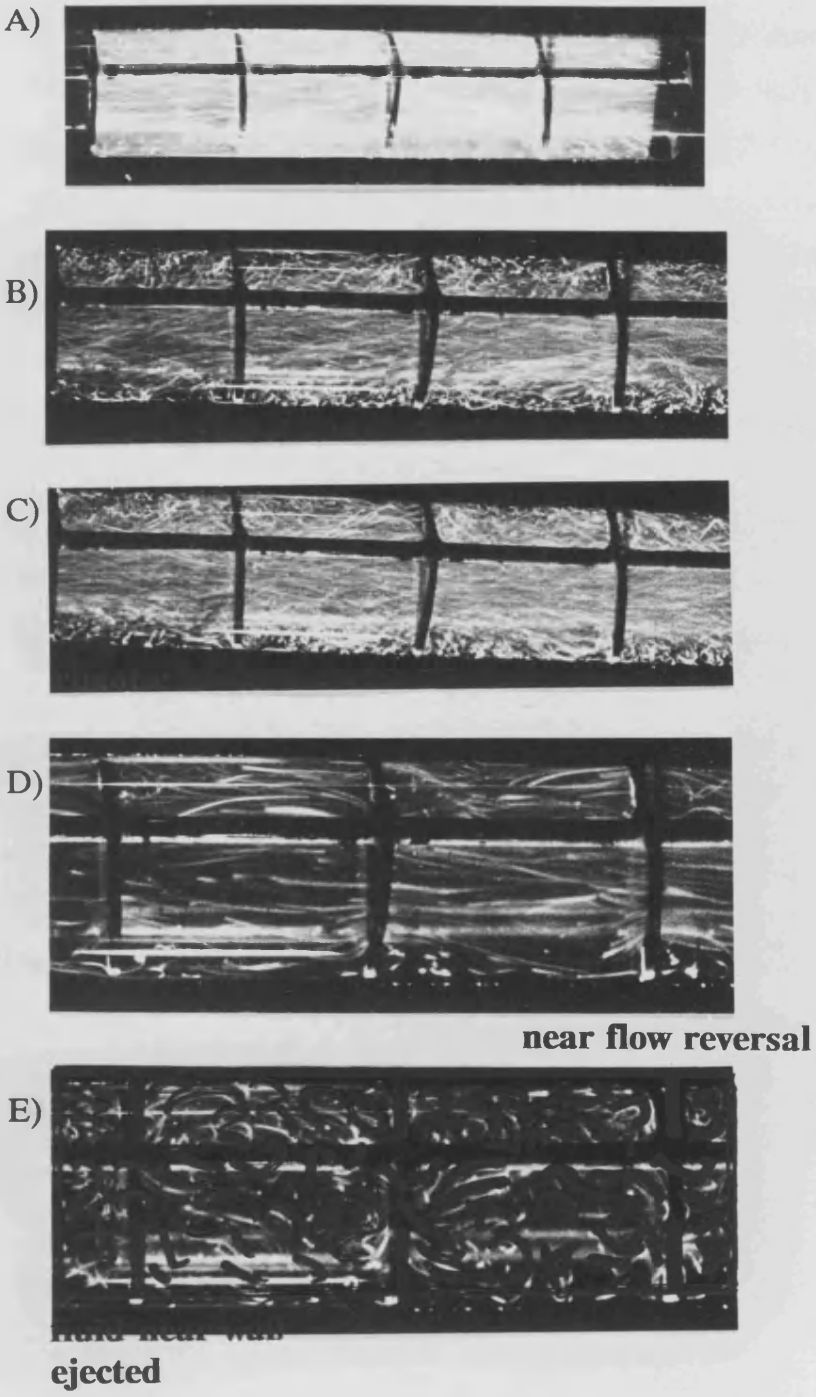

Fig 6.15: Pulsed flow patterns for **DO**1.5 with no cross-flow for X=30.5 mm(100%) and for variable frequency: a) 0.4 Hz; b) 1.4 Hz; c) 2.5 Hz; and for f=2.5 Hz and variable amplitude: d) 17.7 mm(60%); e) 4.8 mm(20%).

(B) Pulsed Flow:

DO1.5: These observations apply to f=0.4 Hz and X=30.5 mm. In pulsed flow, the flow pattern is similar to steady flow with most of the bulk flow going through the middle of the tube. The see-saw motion extends 3-4 cells in each direction. As the fluid decelerates, a vortex forms at the end of this motion which is quickly eroded as the flow changes direction, resulting in the ejection of fluid from the wall region of each cell. The vortex mixing mechanism remains the same as frequency is increased but individual stages of the cycle can not be distinguished as the flow becomes more chaotic. The flow pattern is generally less chaotic than in the **DI** systems for identical pulsed flow conditions.

As the amplitude is decreased to 17.7 mm and then to 4.8 mm there is virtually little difference from the 30.5 mm motion except that the see-saw effect extends around 3 and 1-2 cells in each direction respectively and there is a greater proportion of each cycle over which no motion occurs.

Fig 6.15(a-e) shows the flow patterns for X=30.5 mm at f=0.4(6.15a), 1.4(6.15b) and 2.5 Hz(6.15c) and f=2.5 Hz at X=17.7(6.15d) and 4.8 mm(6.15e). The visual observations are not captured very well in these photographs. However, several salient features can be noted:

a) Fig 6.15(a-c) show the increasingly chaotic nature of the flow as the frequency is increased. The resemblance to the steady flow patterns(Fig 6.13) is clear.

b) Fig 6.15e shows the ejection of fluid from the wall region on flow reversal.

6.3.6 Stage 1:

For both systems, it was observed that the frequency and amplitude need to be at least 1.4 Hz and 2.6 mm respectively for effective mixing.

(A) DI1.6:

The smaller amplitude of the pulsed flow in Stage 1 compared with Stage 2 reduces the size and strength of the vortex motion. At f=0.4 Hz and X=0.8

mm, fluid near the baffle moves backwards and forwards but does not move around the edge of the baffle and a large semi-stagnant region forms at the top of each cell. As the amplitude is increased, a vortex, **VA**, forms; the see-saw motion begins and the semi-stagnant region decreases in size. At X=4.6 mm, **VA** occupies approximately 0.2L. Hence, there is a large proportion of each cell where the fluid is unaffected by the vortex motion and moves backwards and forwards in a laminar fashion. As the frequency is increased, a secondary vortex, **VB**, is formed and the snake effect begins at 0.6 and 1.4 Hz respectively. At 1.4 Hz it occupies 0.5L and at 2.5 Hz, the motion is chaotic.

(B) DO2.2:

At f=0.4 Hz and X=0.8 mm, the see-saw motion occupies approximately 0.25L and there is a large proportion of the cycle over which no motion occurs at all. A very large semi-stagnant region forms which is still prominent at 1.4 Hz but has virtually disappeared at 2.5 Hz. At X=2.6 mm and 4.6 mm the motion is more continuous and the see-saw motion occupies 0.5-0.7L. As the frequency increases, at 1.5 Hz, these stagnant regions have disappeared and at 2.5 Hz the motion is chaotic.

6.4 Discussion:

This discussion focuses on relating the flow visualization results to the filtration results of Chapters 3 and 4 and the pressure drop results of Chapter 5. **It must be emphasized that all these mentions of vortex ejection in Section 6.3 are hard to verify.** This is discussed further in Section 6.4.4 and 6.4.5.

6.4.1 Transition from laminar to turbulent flow:

The Re range for transition from laminar to turbulent flow for each system, estimated from the flow visualization and pressure drop(see Section 5.1.3)

studies, are compared in Table 6.3. The agreement is satisfactory. The flow visualization results are considered to be more accurate and are used in further discussion.

	dP	FV
ET	3000-7000	2000-6000
DI0.8	700-1400	500-800
DI1.6	800-1500	950-1200
DI3.2	900-1600	1050-1300
DO1.5	1400-2000	1300-1600
DO2.2	------	600-800

Table 6.3: Comparison of Re range for transition from laminar to turbulent flow estimated from pressure drop(dP) and flow visualization(FV) studies.

6.4.2 Empty Tube(ET):

For **ET**, there was very little dependence of flux on Re for Re<2000. Significant improvements in flux only occurred at Re>2700. These results can be related to the changing nature of the flow from laminar to turbulent over the range 2000-6000, resulting in increased shear at the membrane surface and a reduction in concentration polarization.

It was difficult to identify the transition range using the particle tracer technique. Brunold et al(1989) also found this and discuss how for turbulent flow in a tube, the particle trajectory is in general only a few degrees different from the laminar flow trajectory parallel to the tube wall and hence the overall optical effect of the two flow regimes is similar. The absence of the boundary layer and a slight difference in the flow patterns between the two regimes can be used to detect the transition.

With pulsed flow, the fluid moves in laminar plug flow for all values of f and X, which is consistent with the calculated values of Va and Re_{crit} in Section

1.5.3(A).

The flux in steady flow is significantly greater than in pulsed flow at $Re=Re_p=6450$(see Section 4.2.3). The different nature of the flow patterns in steady and pulsed flow(turbulent versus laminar plug flow respectively) at $Re=Re_p=5700$ will result in more effective mixing in the former case and hence better fluxes.

6.4.3 Steady flow in the Baffled Systems:

Section 3.3.3 indicates that a threshold Reynolds number, $Re_t=200$, has to be exceeded for DI1.6 for an improvement in flux to be observed relative to **ET** at $C_b=25$ gl^{-1}. Section 4.2.4 indicates that $Re_t<100$ at $C_b=10$ gl^{-1} for all systems. At these low Re values, the flow is Type 1 for **DI**1.6 and **DI**3.2 and laminar in all baffled systems. The existence of a semi-stagnant region for all systems, except **DI**0.8, implies that fluid near the wall is relatively slow moving and mass transfer will be poor. These semi-stagnant regions have disappeared at $Re=350$ for **DI**1.6 and **DI**3.2, but not for **DO**1.5, which is consistent with fluxes being the same for **DO**1.5 at $Re=100$ and 350 while an improvement in flux was observed for the **DI** systems over the same range(see Section 4.2.4).

Fluxes continue to increase with increasing Re, the improvement relative to **ET**, reaching a maximum in the range $Re=350$-1500 and 750-2200 at $C_b=25$ and 10 gl^{-1} respectively. Over this range, which corresponds to Type 2 flow for **DI**1.6 and **DI**3.2, the flow patterns change from laminar to turbulent in all the baffled systems. Within each regime, the vortices present in the **DI** systems increase in strength and the interaction between the wall and bulk flow becomes stronger for the **DO** systems. These effects result in better mixing, enhanced mass transfer and interrupt the development of the boundary layer.

DI1.6 consistently gives the best fluxes over this optimum Re range. The flow patterns appear to fill each cell most effectively for **DI**1.6 compared with **DI**0.8 and **DI**3.2 over this Re range and in general. The steady streaming of fluid between the 2 vortices in the snake motion ensures good radial mixing and mass transfer. For **DI**3.2, this snake motion still occurs but occupies approximately

0.67L. For **DI**0.8, channelling of the fluid is much stronger than for the other **DI** systems and radial mixing is not as good. Brunold et al(1989) also found that a baffle spacing of L/D=1 was more prone to channelling than L/D=1.5 and 2. This may explain the greater dependency of dP on Re for **DI**0.8 compared with **DI**1.6 and **DI**3.2(see Section 5.1.4).

DO1.5 consistently gave the worst fluxes over this optimum Re range. This can be attributed to most of the bulk flow going through the middle of the tube. The flow is generally less chaotic at the same Re value than in the **DI** systems and it is only when the annular flow becomes more prominent that better radial mixing occurs for **DO**1.5.

Experimentally, no flux improvement was observed for Re≥6450 for **DI**1.6 and **DI**3.2. The flow patterns show that Type 3 flow is established at Re=2100. Channelling of the fluid along the wall region is quite prominent in this regime. The flow appears to be chaotic which suggests that there is little flux advantage to be gained from increasing Re above 3850.

6.4.4 Pulsed Flow in the Baffled Systems:

For the **DI** systems, the vortex creation, growth and ejection stages of each cycle ensure good fluid mixing. For the **DO** systems, good fluid mixing is achieved via a similar mechanism as the vortex formation and erosion motion that occurs on deceleration of the flow and flow reversal causes ejection of fluid from the wall region. A proviso must be added that with the flow visualization system used, these vortex mixing mechanisms are difficult to verify as discussed further in Section 6.4.5. This mechanism of vortex formation, growth and ejection is similar to that described by Sobey(1980), Mackley(1987) and Colman and Mitchell(1990). This enhances mass transfer and destroys velocity and concentration boundary layers at the membrane surface. The vortex mixing process appears to be convective in nature although steady streaming may also be occurring as Howes(1988) suggests, especially for **DI**1.6 and **DI**3.2 where, under most conditions of pulsed flow, two vortices are present in each cell.

The filtration results in Chapters 3 and 4 showed that fluxes in pulsed flow

in a baffled system can be made independent of the net cross-flow velocity and of similar magnitude to the steady flow flux at $Re=Re_p$. There is no advantage in using pulsed flow once the point of flow reversal is passed. These three observations can be related to the flow patterns. For all systems, the "instantaneous" flow pattern in pulsed flow resembles the steady flow pattern at $Re=Re_p$. Very little change in the overall flow pattern occurs for $NFR<0.2$ from that observed for pulsed flow alone and for $NFR>0.8$, very little change occurs from the steady flow pattern. No dramatic change in flow patterns occurs between $NFR=0.2$ and 0.8. These are qualitatively the same during the acceleration and deceleration stages of each cycle. The major difference is that the flow is bidirectional for $NFR<0.5$ and includes a flow reversal stage while for $NFR>0.5$, it is unidirectional.

The flow patterns also show that good mixing is a function of X, f and baffle geometry. Increasing frequency increases the degree of chaos while increasing the amplitude increases the strength of the vortices and the proportion of each cell occupied by the pulsing motion. The flow is generally more chaotic for the **DI** systems than for **DO**1.5 at f=2.5 Hz and X=30.5 mm. Four parallels with the filtration results can be drawn immediately:

a) In Section 4.2.3(C), there was no significant difference in the fluxes at f=2.5 Hz and X=30.5 mm($Re_p=6450$, St=0.033) for the **DI** systems while the **DO**1.5 fluxes were slightly smaller.

b) In Section 3.3.4, an improvement in flux was only observed for $f\geq1.4$ Hz and $X\geq2.6$ mm($Re_p\geq300$ and $St\leq0.38$) which correspond to the observed values of f and X which must be exceeded to avoid the formation of semi-stagnant regions and to ensure that vortex mixing occurs(see Section 6.3.6).

c) In Section 4.2.3(B), the fluxes were similar in magnitude at X=17.7 and 30.5 mm at f=2.5 $Re_p\geq3770$, $St\leq0.056$) in each baffled system. The flow patterns are very similar at both these amplitudes.

d) In Section 4.3.3, f and X need to be above 1.4 Hz(at X=30.5 mm) and 5 mm (at f=2.5 Hz) respectively for an optimal improvement in flux. These conditions correspond to $Re_p\geq3500$, St=0.033 and $Re_p\geq1100$, $St\leq0.20$ respectively. These are conditions for which chaotic fluid motion is observed.

These observations can be related qualitatively to the results of Howes(1988) discussed in Section 1.4.2. The flow patterns for **DO**1.5 in steady and pulsed flow have some features similar to those observed by Howes(1988) who carried out numerical and flow visualization studies for this particular cross-section. However, in this study the annular flow between the baffle edge and the wall significantly alters the flow patterns from those observed by Howes(see Section 6.3.5 and 6.3.6).

Ignoring the differences in geometry for **DO**1.5 and especially the **DI** systems, the Re_p and St values noted in observations(a), (c) and (d) correspond to the "chaotic" flow regime identified by Howes in his work which exists at $Re_p = 640$ and all St values investigated in the range 0.25-4. $Re_p = 300$ and $St = 0.38$ in (b) correspond to a region of time asymmetric flow identified by Howes with 2 eddies being present at one flow reversal and 3 at the other. Excellent fluid mixing and mass transfer is occurring in both these regimes.

The observed flow patterns show that with sharp edges, separation of the flow occurs at relatively low amplitudes. Vortex mixing is present in the tube for amplitudes significantly smaller than the centre-centre baffle spacing, L. Hence "short" strokes are not deleterious and good mixing can be achieved, provided the frequency is fast enough. From a membrane filtration viewpoint, good mixing does not necessarily equate with good fluxes and it is better to take the approach already discussed in Section 4.3.4 based on 3 criteria:

a) at the same Re_p value, a greater improvement in flux can be obtained with short strokes than long strokes as the frequency is faster in the former case.

b) in general, for sharp edged baffles, "short, fast" strokes are more effective for improving mass transfer and fluxes and achieving minimum axial dispersion than "long, slow" strokes.

b) if minimum axial dispersion is not a requirement, further improvements in flux can be achieved by increasing Re_p(higher frequencies and/or amplitudes(lower St)) until the onset of pressure dependent behaviour.

In Section 4.3.4, an optimum X/L value could not be identified from the filtration results for the **DI** systems. The truncated nature of the waveform was suggested as a possible explanation for this. The visual observations made here

confirm that as the amplitude is decreased below 100%, significantly greater proportions of each cycle exist over which no motion occurs.

6.4.5 General Remarks:

These flow visualization experiments do not account for the effect of the permeation flux through the membrane on the flow patterns. This may be significant, especially in microfiltration applications, where the flux constitutes a larger fraction of the net cross-flow velocity and the particles being filtered are typically at least an order of magnitude larger than in ultrafiltration applications. Nevertheless, the flow visualization experiments facilitate a greater understanding of the filtration results by shedding light on the mechanisms by which an improvement in flux is occurring.

Many of the photographs for pulsed flow failed to capture the important flow features. This means the mentions of vortex ejection are difficult to verify, imparting a subjective nature to the experimental observations. In future work, the technique used could be improved by synchronizing the camera shutter with the phase of oscillation. Another possibility is to use a high speed cine camera. These improvements will make the observations more objective by helping to identify the finer features of the flow that can not be detected via visual observation and will facilitate a greater understanding of the vortex mixing mechanism.

In addition, no RTD studies were carried out in this work. The flow visualization apparatus could easily be adapted to measure the residence time distribution for different baffled geometries under different conditions of pulsed flow.

In the preliminary stages of this study, the FLUENT fluid flow software package was used to predict the flow patterns in the baffled systems under conditions of pulsed and steady flow. It was hoped that after verifying the accuracy of the FLUENT results by comparison with flow visualization results, that this package could be used to determine the most promising geometrical configurations and flow conditions which could then be investigated

experimentally. Howes(1988) found that for $Re_p > 200$, the observed flow patterns showed increasing complexity which the numerical simulation was unable to predict. This observation of Howes also applies to this study. As an optimum improvement in flux was found to occur for Re and Re_p values significantly greater than 200 the FLUENT package was no longer used and the results are not presented here. Numerical simulation does have some advantages. It can provide a useful first estimate of the flow patterns and is a valuable tool for assessing the velocity, shear and vorticity distributions for a particular geometry. As FLUENT is a licensed, commercially available fluid flow simulation package, access to the source code is not possible. It is recommended that further work in this area should begin with development of a numerical code and not the use of a commercial package.

CHAPTER 7
CONCLUDING REMARKS

7.1 Summary and Conclusions:

The feasibility of using sharp edged baffles of a disc or doughnut shape for improving filtration performance alone and in combination with pulsed flow has been demonstrated.

Pulsed flow by itself(**ETP**) at $Re_p = 950$ has been shown to improve fluxes to a small extent relative to **ET** within the laminar range for $Re \leq 350$. This coincided with the conditions under which flow reversal occurred. There was no advantage in using pulsed flow(**ETP**) once turbulent flow conditions were established as fluxes at $Re = 6450$ were significantly greater than at $Re_p = 6450$.

With steady flow in a baffled system, an improvement in flux was observed relative to **ET**. Stage 1 showed that at $C_b = 25\ gl^{-1}$, a threshold Reynolds number, $Re_t = 200$, had to be exceeded for **DI**1.6 before any flux improvement was observed. The relative improvement reached a maximum in the Re range 350-1550. Stage 2 showed for all the baffled systems at $C_b = 10\ gl^{-1}$ that $Re_t < 100$ and an improvement in flux was observed over the entire Re range: Re = 100-16000 relative to **ET**(Re = 100-50000). The relative improvement reached a maximum in the Re range: Re = 750-2200, and fluxes were quite high within this range.

When these results were expressed on a power consumption basis, the baffled systems were shown to dissipate energy more effectively than turbulence in an empty tube(**ET**). An optimum flux/power range was identified for the

baffled systems which corresponded to Re=700-1200 and 750-1450 for Stages 1 and 2 respectively. Within this range, the energy consumption was $\leq 1 W/m^2$. Fluxes of similar magnitude could be obtained for **ET** but only at a much higher power consumption of approximately 20 and 45 Wm^{-2} at $P_{tm}=2$ and 4 bar respectively.

The baffled systems promoted better mixing and increased turbulence within the membrane tubes at much lower Re values than for **ET**. This increased local mass transfer rates and fluxes by interrupting development of the boundary layer which reduced concentration polarization and delayed the onset of limiting flux behaviour.

Fluxes in pulsed flow within the baffled systems were similar in magnitude to steady flow fluxes at $Re=Re_p$. Stage 1 showed that for $Re_p=950$, the net cross-flow velocity had to be above Re=150 for an optimal improvement in flux to be observed. There was no advantage in using pulsed flow once the point of flow reversal was passed. Within this range, fluxes were greater than for **ET** at the highest Re value used in Stage 1 of Re=3300. Stage 2 showed that for $Re_p=6450$, there was no dependency of flux on net cross-flow velocity within the range Re=100-1450 and fluxes were greater(for all **DI** systems) or equal(for **DO**1.5) to **ET** fluxes under fully turbulent flow conditions at Re=16000-50000.

Within the optimum flux/power range, fluxes were of similar magnitude in steady and pulsed flow in the baffled systems at the same power consumption. It was suggested that the pulsed flow conditions should be chosen to lie within this optimum range so that $Re_p=700-1500$.

The "decoupling" of mass transfer and flux from the net cross-flow velocity provides the opportunity for use of pulsed flow in a baffled system in a single pass, continuous mode of operation; avoiding recirculating pumping costs, with a high concentration ratio from inlet to outlet and a lower hold-up volume with less complicated pipework.

The pulsed flow conditions should be carefully selected. Stage 1 showed that an improvement in flux was observed if the frequency and amplitude were

above 1.4 Hz and 2.6 mm respectively($Re_p \geq 300$, $St \leq 0.38$). Stage 2 showed that frequencies needed to be above 1.4 Hz at X=30.5 mm($Re_p \geq 3500$, St=0.033) and amplitudes above 5 mm at f=2.5 Hz($Re_p \geq 1100$, $St \leq 0.2$) for an optimal improvement in flux. At $Re_p < 1000$, fluxes were significantly greater at low X, high f(2.5 Hz) than at low f, high X(30.5 mm, 100%).

Vortex mixing occurred with pulsed flow in the baffled systems, enhancing mass transfer and preventing the development of velocity and concentration boundary layers at the membrane surface. Good mixing was found to be a function of amplitude, frequency and baffle geometry. Increasing the frequency increased the degree of chaos while increasing the amplitude increased the strength of the vortices and the proportion of each cell occupied by the vortex motion. Sharp edges promoted the occurrence of separation at relatively low amplitudes.

It has been suggested that a greater improvement in mixing, mass transfer and flux will be observed in general, with "short, fast" strokes rather than "long, slow" strokes. Provided the frequency was high enough, short strokes were not deleterious as in general, vortex mixing is present in sharp edged baffled tubes for amplitudes significantly less than the baffle spacing(Howes, 1988). In fact, at the same Re_p value, it was more effective to use short strokes rather than long strokes for an optimal improvement in flux as the frequency was faster in the former case. This is particularly important when minimum axial dispersion is required for which an optimum exists at relatively low amplitude values(Mackley, 1987). If minimum axial dispersion is not required, further improvements in mass transfer and flux can be obtained by increasing Re_p(higher frequencies and/or amplitudes(lower St)) until the onset of pressure dependent behaviour.

The **DI**1.6 system is considered to give the best all-round performance of the baffled systems investigated on a flux and power consumption basis. **DI**1.6 consistently gave the best fluxes in steady flow within the optimum Re ranges of Stage 1 and 2 and for $Re \geq 6450$, the **DI**1.6 fluxes were greater than the **DI**3.2 fluxes. In pulsed flow there was no significant difference in the fluxes observed between the **DI** systems. In both pulsed and steady flow, the **DO**1.5 fluxes were

lowest of all the baffled systems and these baffles were rejected because of this and also for practical reasons. With **DI**0.8, the pressure drop increased much more rapidly with Re than for the other **DI** systems. The flow pattern appeared to fill the cell more effectively for **DI**1.6 than for **DI**3.2 while channelling of the fluid along the wall was particularly strong for **DI**0.8.

The flow visualization experiments were able to explain many of the observations made in the filtration experiments illustrating the usefulness of this technique even though the effect of the flux through the membrane can not be accounted for.

The snapshot technique has been validated with average flux values obtained from any frame of a snapshot experiment being representative of steady state fluxes from long term fouling experiments performed under identical operating conditions.

7.2 Recommendations:

The only published work apart from that based on this work(Finnigan and Howell, 1989A, 1989B, 1989C, 1989D) using this technique in ultrafiltration is that of Colman and Mitchell(1990). Consequently, there are many areas one could explore in future work. This discussion focuses specifically on two areas; namely the weaknesses of this study and the areas where the most potential is seen for future work.

This technique has considerable potential for use in ultrafiltration and microfiltration applications in a single pass, continuous mode of operation for thickening purposes or to avoid the costs of recirculation. In microfiltration, fouling occurs via a different mechanism. It will be interesting to see what effect this technique has on fluxes and whether the pulsing nature of the flow will disrupt the formation and growth of the cake that forms on the membrane

surface. The rejection should also be monitored closely in microfiltration experiments to determine if any change in the fractionation of proteins between the feed and permeate occurs with pulsed flow. The expansion and contraction of the membrane and presence of air(cloudiness) that occurred in pulsed flow is another potential advantage as it suggests some "backflushing" is occurring. Backflushing should be avoided with ultrafiltration membranes but can be tolerated by microfiltration membranes and is generally desirable. With microfiltration, the effect of pulsed flow alone(ETP) may be more significant than in ultrafiltration. Edwards and Wilkinson(1971) discuss how pulsed flow enhances the tubular pinch effect which is a well documented phenomenon in microfiltration applications.

All of the snapshot experiments were carried out under constant concentration(volume) conditions and using the same feed material and membranes. Consequently, these results are specific to this system. This work needs to be extended to other feed solutions and membranes than those investigated here.

A systematic investigation using this technique for concentration and thickening purposes should be made. The few concentration experiments carried out suggest that the pulsed flow technique may not be as successful when viscous effects become more significant than in the snapshot experiments. Further experiments investigating different feed materials under a wide range of operating conditions are needed to test this hypothesis. Flow visualization studies should also be carried out investigating the effect of viscosity on the flow patterns.

This work investigated two baffle configurations of a disc and doughnut shape and a limited range of L/D values. Other geometries such as spiralled, aerofoil, or propeller shaped baffles may be suitable. This technique is also applicable to rectangular channel systems as the work of Colman and Mitchell(1990) demonstrates. It avoids the need to use thin channels in order to generate high shear rates at the membrane surface.

In this work, a constant baffle flow area ratio was used based on the recommendations of Mackley. The baffle flow area ratio may become more significant in thickening applications as the local shear rate will reach a maximum at the baffle tip and the pressure drop may increase to the point where flow around the edge of the baffle will not occur.

Ideally, the pulsed waveform should be continuous over the entire range of amplitudes investigated. The truncated nature of the pulsed waveform for amplitudes less than 100% is a major weakness of this study and may explain why no relationship between flux and X/L was observed. An arrangement similar to that used by Dickens et al(1990) may be more suitable in future work so that the effects of St, X/L and X on flux can be clearly resolved.

More work is needed to investigate the effect of frequency and amplitude on mass transfer and fluxes. It has been suggested that:

a) short, fast strokes are more effective than long slow strokes for improving mixing, mass transfer and fluxes;

b) the pulsed flow fluxes achieved in Stage 2 at Rep=6450 could have been achieved at Re_p=3500 and possibly Re_p=1100, by suitable choice of the frequency and amplitude.

These hypotheses need to be investigated further.

The pulsed flow rate, Q_p, was calculated from measurements of frequency and amplitude. A pulsed flow meter, such as a Gould Statham Flowmeter, which measures the pulsed flow velocity in situ should be used in future to give a more accurate measurement of the pulsed flow velocity. A device like this will also enable the extent of pulse dissipation to be determined.

The increase in pulsing pressure, P_p, with P_{tm} is due to the pressure drop across the retentate recycle valve. With the present system, it is difficult to eliminate this effect. This is a problem that should be considered in the practical scale-up of this device.

The approach used to evaluate the pulsing power consumption, E_p, is semi-theoretical in nature and gives a reasonable estimate of the pulsed power consumption. However, this calculation is based on the assumptions that Q_p and dP_p are sinusoidal functions and in phase, neither of which are correct. In future, it is important to measure the power consumed by the pulsing pump and compare this with the calculated value.

Many of the flow visualization photographs failed to capture the important flow features in pulsed flow. In future work, the initiation of each exposure should be synchronized with the flow cycle or a high speed cine camera could be used to obtain better quality photographs.

No measurement of the RTD was made in this work. The flow visualization rig could be adapted quite easily to determine the RTD and the dependence of axial dispersion on amplitude and frequency.

APPENDIX A1
SNAPSHOT VALIDATION

A1.1 Introduction:

The "Snapshot" technique has been devised to assess quickly the feasibility of the baffled/pulsed approach for improving membrane filtration performance. In this technique, many operating conditions are each used over a short period of time(frame) and the resultant fluxes measured. The conditions are randomly selected. The technique generates a lot of information on the filtration performance of a system for several sets of operating conditions in a single experiment. To be valid, this information must be representative of the system filtration behaviour when operated in a conventional manner. The major aim in this section is to validate the snapshot technique. To be valid the following criteria must be satisfied:

a) stability of the flux within any frame, where a "frame" is defined in Section A1.2 below.

b) negligible long term fouling occurring over the duration of an experiment.

c) no dependence of snapshot fluxes on the initial operating conditions.

d) the initial operating period is of sufficient length for fluxes to stabilize after the initial period of rapid flux decline before the first change of the operating conditions. The conditions should be changed once the flux decline over a 6 min period is negligible, although some further flux decline may in fact occur.

If these conditions are satisfied, flux values will be consistent between different snapshot experiments and should be representative of fluxes obtained from long term fouling experiments performed under identical operating conditions.

These points are discussed below. The format used in this section is to present the methods, results and discussion together as the development of the snapshot technique was an ongoing process. The snapshot technique is first described in Section A1.2. Section A1.3 addresses (a) above and describes how an "average" flux value was evaluated for each frame of a snapshot experiment. A statistical analysis has been used to see if the "average" chosen realistically represents the data and an estimate of the experimental error in the flux is made. (b)-(d) are addressed in Section A1.4 where snapshot results are compared with fluxes from long term fouling experiments obtained under identical operating conditions. Section A1.5 describes the modification of the snapshot technique to check directly that fluxes from different snapshot experiments are consistent. Section A1.6 describes the smoothing procedure used to generate a curve to represent the pulsed flow data for each system from different snapshot experiments. Section A1.7 describes some weaknesses of the snapshot technique. Section A1.8 describes how the membrane itself is a potential source of error and may result in inconsistent flux data being obtained in different snapshot experiments. The main points are then summarized in Section A1.9.

A1.2 The Snapshot Technique:

A set of operating conditions of P_{tm} and Re for Stage 1B are summarized in Table A1.1. This table will be used to explain the "snapshot" technique more fully.

Each pair of operating conditions was assigned a number(No.) and the numbers placed in random order. The first pair of values of P_{tm} and Re were imposed on the system and ultrafiltration initiated. The conditions initially selected were P_{tm}=1.2 bar and Re=1200(No.13 in Table A1.1). The initial operating conditions were maintained for 20-30 min after which time the flux decline over a 5 min period was negligible. P_{tm} and Re were then changed according to the random ordering to eliminate the time dependent flux decline as a systematic variable and the corresponding flux was measured over a 5-6 min

Re	v	P_{tm} (bar)				
	$cm.s^{-1}$	0.4	0.8	1.2	1.8	2.2
350	2.7	21	16	11	6	1
700	5.4	22	17	12	7	2
1200	9.4	23	18	13	8	3
1550	12	24	19	14	9	4
3300	26	25	20	15	10	5

Table A1.1: The experimental conditions used for "snapshot" ultrafiltration experiments with **DI1.6** in Stage 1B. Each number corresponds to a particular transmembrane pressure and cross-flow velocity.

period or frame using a logging interval of 20s as illustrated in Fig A1.1. Each data point corresponds to the flux value for a particular 20s interval and the data points are grouped together in 6 min intervals(frames). The number above each 6 min set of data refers to the operating conditions as summarized in Table A1.1. For instance, after frame one(No.13: P_{tm}=1.2 bar, Re=1200); pulsed flow was used in frame 2(No.P13) at the same conditions of P_{tm} and Re. In frame 3, steady flow was again used at P_{tm}=1.2 bar and Re=700(No.12). The remainder of Fig A1.1 and Table A1.1 can be interpreted in this manner. The experimental loop was completed by returning to the initial operating conditions to determine how much long term fouling had occurred. If the decline over the series of experiments was less than 15% the results were considered acceptable as variations based on the major parameters of influence were greater than 300%. Average flux values were then calculated for each operating condition, as described in Section A1.3, and used to plot a graph of flux versus transmembrane pressure. A typical curve is shown in Fig A1.2 and is based on the data in Fig A1.1.

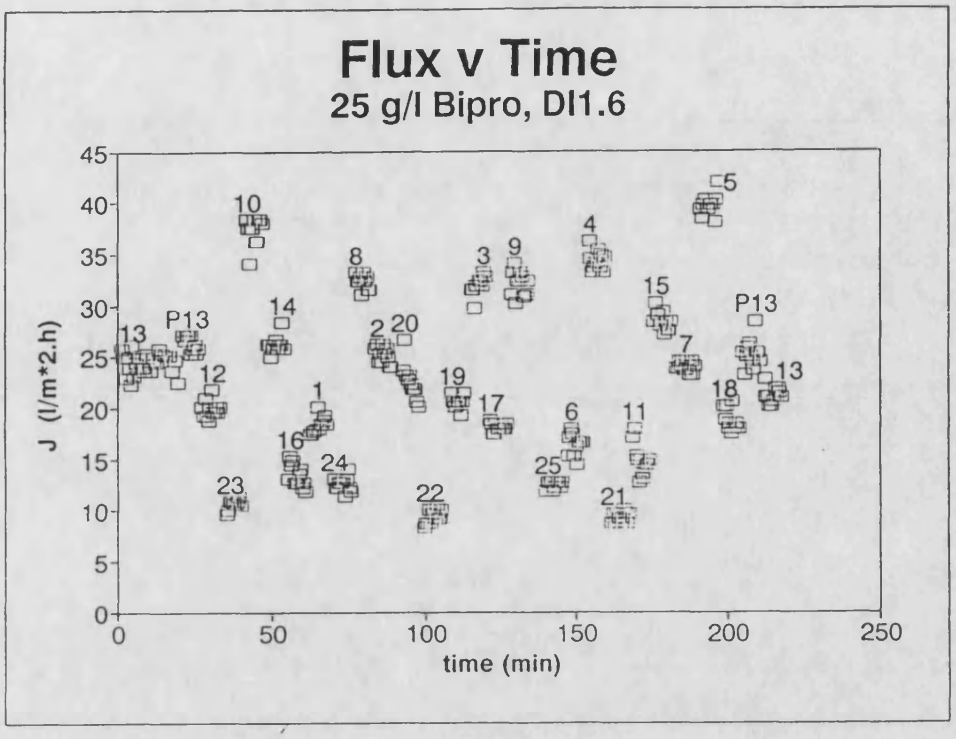

Fig A1.1: A typical "snapshot" ultrafiltration experiment for **DI**1.6. The numbers refer to the operating conditions of Table A1.1.

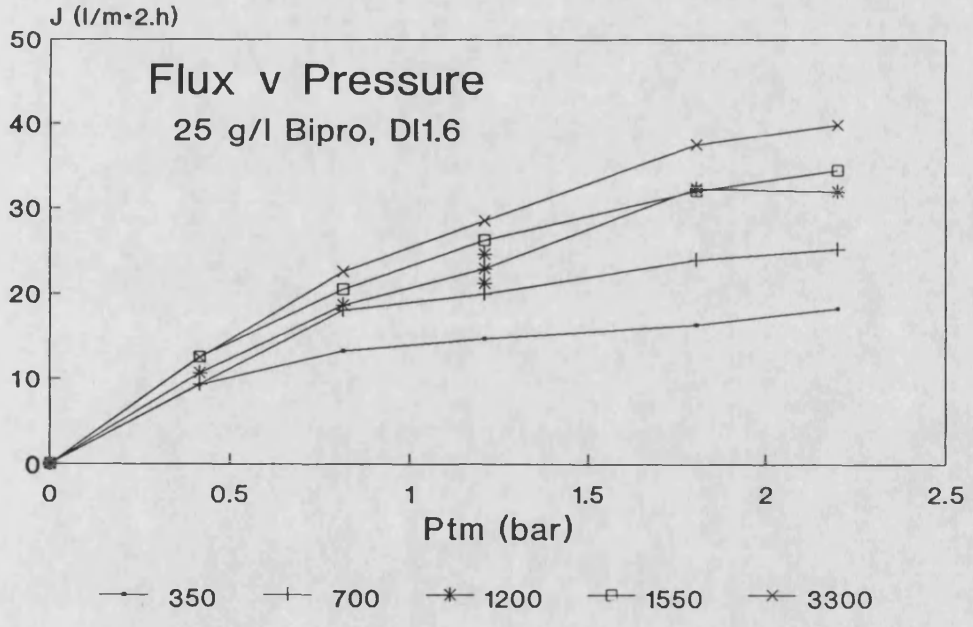

Fig A1.2: The "snapshot" ultrafiltration flux curve for **DI**1.6 constructed from Fig A1.1 at the Re values indicated in the legend.

A1.3 Single Frame Data Analysis:

An "average" flux value needs to be evaluated for each frame. This is possible if the flux data shows no systematic decline or rise within the frame. In the snapshot experiments, 2-5 min were allowed after changing the operating conditions between each frame for fluxes to stabilize before beginning data logging. There should also have been negligible flux decline within any 6 min frame. Examination of the experimental data shows that this was true.

The method adopted here to obtain an "average" flux value is one of the simplest and involved calculating the average flux value from the raw data for each frame and its sample standard deviation after rejecting any obvious spurious values. The data was sometimes quite scattered resulting in large values of the standard deviation. The data scatter was primarily due to:

a) not maintaining constant operating conditions for the duration of a frame.

b) if the flux was low the 20s logging interval was too short resulting in the permeate flow from the collection chamber to the weighing flasks being more erratic than at higher fluxes.

A statistical analysis has been used to assess if the average flux realistically represents the data. Two approaches were used:

a) leaf and stem analysis and data summaries.

b) exponential smoothing.

These are described below.

A1.3.1 Leaf and Stem Analysis:

(A) Method:

Leaf and Stem displays are a visual data display technique(Tukey, 1977), which show:

a) separation of the data into groups;

b) about where the data values are centred;

c) the data spread;

d) appearance of unexpectedly popular or unpopular values;

e) unsymmetric trailing off of data(going further in one direction than the other).

While leaf and stem analyses reveal details, data summaries are also needed to reveal the trends. A three number summary was chosen using the "median" and the two "hinges". The median, is the middle number and is more sensitive than the average for small data sets with a high degree of granularity, where the granularity is a measure of the data spread(Cloake, 1988, pg 154) The hinges, are the numbers located halfway between the median and the extreme data points. It is relatively simple to evaluate these three parameters from a leaf and stem display. In addition to these criteria the trimean was calculated. This is defined as:

$$Trimean = \frac{hinges + 2\,median}{4} \qquad \textbf{(A1.1)}$$

The trimean will differ from the median if the data is not symmetrically distributed about the median.

(B) Results:

The data from three experiments from Stage 1C was analyzed using this approach. The fluxes measured in these experiments were in the range 7-38 and 5-24 $lm^{-2}h^{-1}$ at 5 and 25 gl^{-1} respectively. These fluxes are low and hence the data is quite scattered as explained in Section A1.3. Two of these three experiments (Expts 46 and 47, C_b=25 gl^{-1}) exemplified the typical spread of the data while the third experiment(Expt 34, C_b=5 gl^{-1}) represented a worst case. A sample leaf and stem analysis is shown below for the worst case(Expt 34).

Note: The 5 gl^{-1} results have not been presented in the main text as subsequent experiments at 25 gl^{-1} show the same trends as at 5 gl^{-1} in a clearer fashion.

Sample Leaf and Stem Analysis

The following data corresponds to 20s flux values($lm^{-2}h^{-1}$) from a single 6 min frame(No.5) of Expt 34:

15.7, 15.89, 16.42, 17.01, 17.14, 17.21, 18.19, 18.26, 18.32, 18.39, 18.52, 18.65, 18.98, 19.05, 19.24, 20.49, 20.49, 21.28.

Each line in Table A1.2 is a stem, each piece of information on a stem is called a leaf. For the above data in the form AB.XY the stem is AB and the leaf is XY and the corresponding leaf and stem display is shown in Table A1.2. Hence, the flux 15.7 has a stem of 15 and leaf of 70 and appears on the bottom line of Table A1.2. The stems are chosen to cover equal data intervals. In this case each data interval is 1(eg. the stem 15 covers all data in the range 15.00-15.99, 16 covers 16.00-16.99 etc). The data is presented in ascending order from bottom to top. The right hand column is a cumulative tally of the number of data points on each line beginning at the bottom and counting upwards. This is referred to as the count. In this case, the total count, N, is 18.

To evaluate the median and hinges, the depth of these parameters is first calculated from the count, N, as described below. The depth refers to the position of these parameters in the leaf and stem display.

Depth of median = 0.5(1+N)=9.5 (written as 9h)

Depth of hinges = 0.5(1+depth of median) = 0.5(1+9) = 5

Stem(AB)	Leaf(XY)	Count
21	28	18
20	49 49	17
19	05 24	15
18	19 26 32 39 52 65 98	13
17	01 14 21	6
16	42	3
15	70 89	2

Table A1.2: Leaf and stem display for the experimental data from Expt 34.

The median and hinges can now be read from the display. In this case, the median is the average of the 9^{th} and 10^{th} data points(9h); the lower and upper hinges are obtained by counting to the 5^{th} point from the bottom(the 5^{th}) and 5^{th} from the top(the 14^{th}) respectively.

Median (M) = 0.5(18.32+18.39) = 18.36
Lower hinge (L) = 17.14
Upper hinge (H) = 19.05
Trimean (T) = 0.5(2M+L+H) = 18.22

These parameters are tabulated in Table A1.3 along with the raw average and sample standard deviations for all the data from this experiment.

(C) Discussion:

The agreement between the average, median and trimean is satisfactory as in all but 3 cases, the % diff, defined in Table A1.3 is less than 5% and typically 1-2%. Thus, the raw data average is a valid criterion for data representation despite the relatively large magnitude of the standard deviation that was calculated in some cases. All Stage 1 flux data has been plotted using raw average flux values. The Stage 1 results are presented in Section 3.3.

A1.3.2 Smoothing:

(A) Method:

The leaf and stem form of statistical analysis is tedious and time consuming. It does not affect the graphical display of the flux v time data. This is not important with the snapshot experiments as normally only the flux v pressure graph, which is obtained from the flux v time data, is presented. However, for displaying the long term fouling results it is important to improve the graphical data display. Consequently, a second statistical approach has been

			Flux Values ($lm^{-2}h^{-1}$)						
No.	P_{tm}	Re	avg	σ	M	L	H	T	%diff
1	2.3	50	18.0	2.4	18.2	16.7	20.2	18.9	5
2		100	23.5	1.9	23.2	22.1	24.2	23.2	1
3		200	18.0	3.8	18.4	16.5	19.1	18.2	2
4		350	21.2	2.5	21.5	19.6	23.2	21.5	1
5	1.8	50	18.3	1.6	18.4	17.1	19.1	18.2	1
6		100	19.2	1.8	19.4	18.5	20.4	19.4	1
7		200	20.3	2.7	20.1	17.9	21.9	20.6	2
8		350	20.6	1.9	21.0	20.1	21.9	21.0	2
9	1.2	50	12.5	0.8	12.4	12.0	13.3	12.5	1
10		100	13.7	1.6	13.8	12.4	15.1	15.6	14
11	Start	200	17.3	1.8	17.0	16.0	18.7	17.2	2
11	End	200	14.7	3.1	14.7	12.1	16.9	14.6	1
12		350	17.6	3.4	17.7	14.6	20.5	17.6	1
13	0.8	50	11.2	1.3	10.9	10.4	11.6	11.0	3
14		100	10.6	2.9	10.8	8.6	12.6	10.7	2
15		200	9.5	1.7	9.2	8.0	10.8	9.3	2
16		350	15.5	1.9	15.5	14.4	16.8	15.5	0
17	0.4	50	10.0	0.9	9.4	8.9	10.7	9.6	4
18		100	8.8	7.6	7.0	4.1	14.1	8.1	20
19		200	8.1	1.1	8.0	7.3	8.8	8.0	1
20		350	9.5	6.6	7.4	4.2	13.5	8.1	22

Table A1.3: Summary of experimental data from Expt 34 showing the median(M), upper(U) & lower(L) hinges, trimean(T), average(avg) and standard deviation(σ). %diff is diff/avg*100% where diff is the absolute value of maximum [avg-M, avg-T].

taken involving smoothing of the data resulting in improved graphical presentation of the flux v time data. The smoothed data can also be used to give a better estimate of the average and standard deviation.

Smoothing allows the analyst to check for relationships between X and Y with the error redistributed; that is; the error is minimized. At any point the errors are redistributed around the real value with equal probability of being high or low.

Two approaches were used: moving means and exponential smoothing(or filtering), Soper and Lee(1987). Moving means is a method of smoothing a time series by averaging successive groups of data. The simplest involves calculating the mean for overlapping groups of three data points. These averages give estimates of the trend values associated with adjacent data values. As the number of data points incorporated in calculating the moving mean increases, the smoothing effect is greater but the number of means is less. The disadvantage of this approach is that equal weight is given to all constituents even though they are of different ages and possibly relevance. Moving means of three and five were used here.

Exponential smoothing avoids the above disadvantage by weighting using the smoothing parameter, a, which lies between 0-1, (commonly 0.05-0.3) and frequently set to 0.2. Values close to 0 give the most smoothing; values close to 1 the least. In this case, a prediction for one period beyond the end of the data can be made. The formula used to evaluate the smoothed value is:

$$Smooth_{t+1} = a\,data_t + (1-a)\,Smooth_t \quad \text{(A1.2)}$$

where smooth and data refer to the smoothed and raw data points respectively and t is a counter.

The first data point is usually taken as the initial smooth. This means that the trends shown by the smooth can be distorted by this first point if it differs from the remaining data. Two situations in the experiments where this can occur are in the initial rapid flux decay at the start of a filtration experiment where flux values 20-30s apart can be significantly different and at the start of each snapshot

frame if new steady state conditions have not been obtained. The first situation is not a cause of concern as after several minutes any displacement of the smoothed curve from the actual data is eliminated. In addition, it is the data from the last six min of this first period that is used to calculate an average flux value. The latter situation is more important-often the first(and sometimes the second and third) data points seemed to be inconsistent with the remaining data. In these cases the initial starting value used in smoothing was either the second or the average of the first 2 points. Exponential smoothing with a=0.1 and 0.2 was used here.

(B) Results and Discussion:

These methods were first applied to two concentration experiments: Expts 43 and 44 for **DI**1.6 and **DI**1.6**P** respectively. The flux v time data for Expt 44 has been included here in Fig A1.3(a)-(e) to illustrate these different smoothing methods. The spread in the data decreases in the order: raw; means(3); means(5); exponential smoothing(0.2); exp smoothing(0.1) as shown in Fig A1.3(a)-(e).

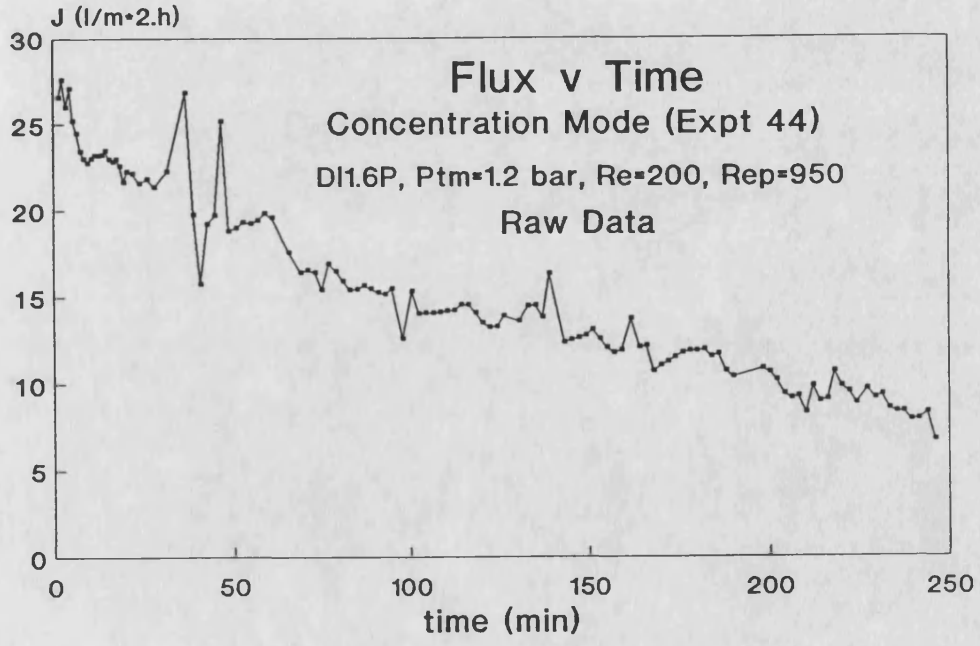

Fig A1.3a: Flux v time data for Expt 44 showing the raw data.

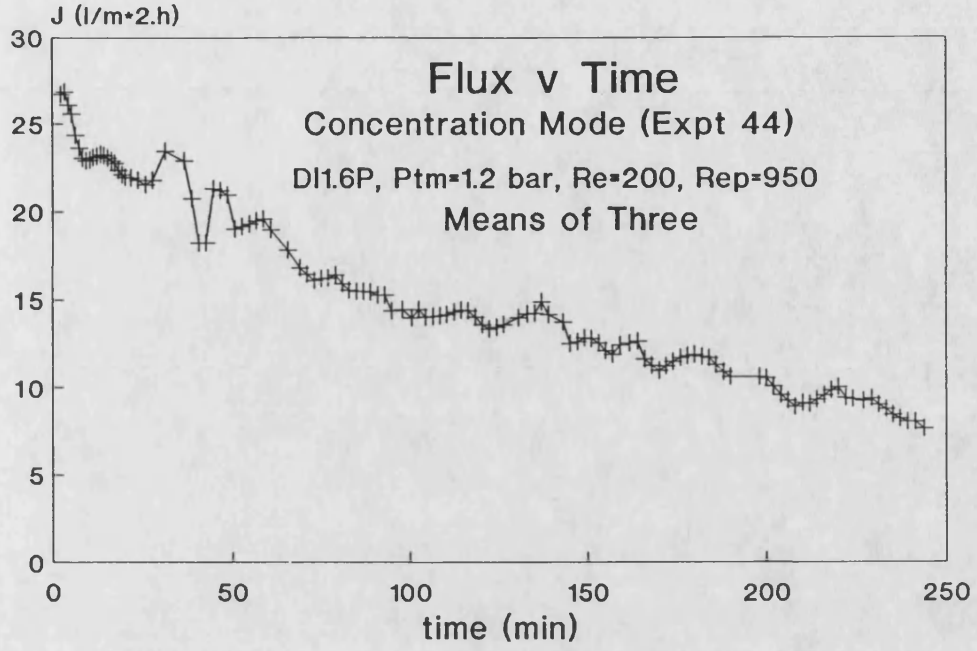

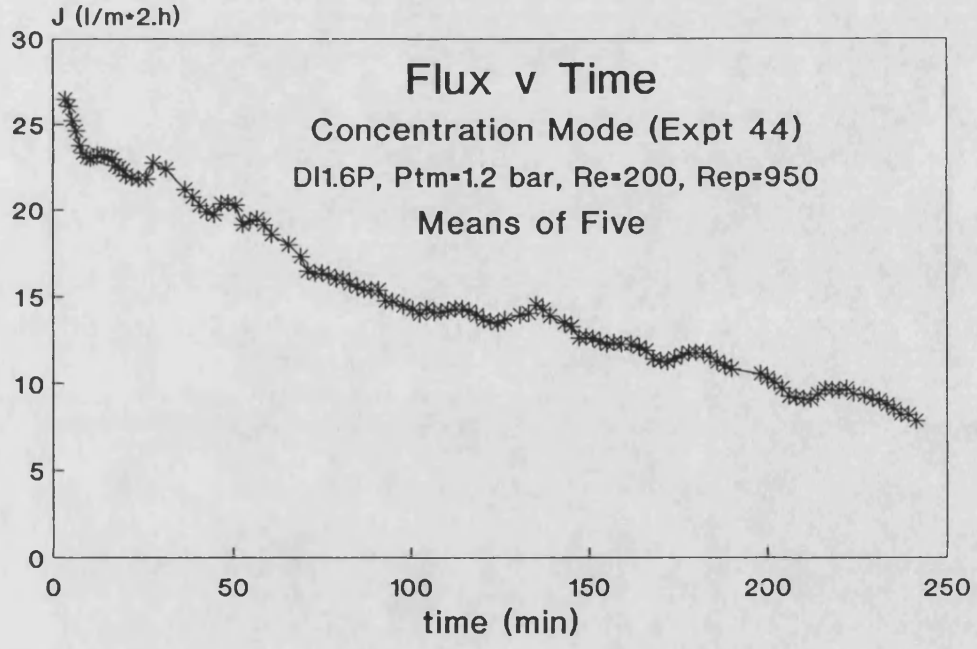

Fig A1.3: Flux v time data for Expt 44 showing smoothed data using b) means of 3; c) means of 5.

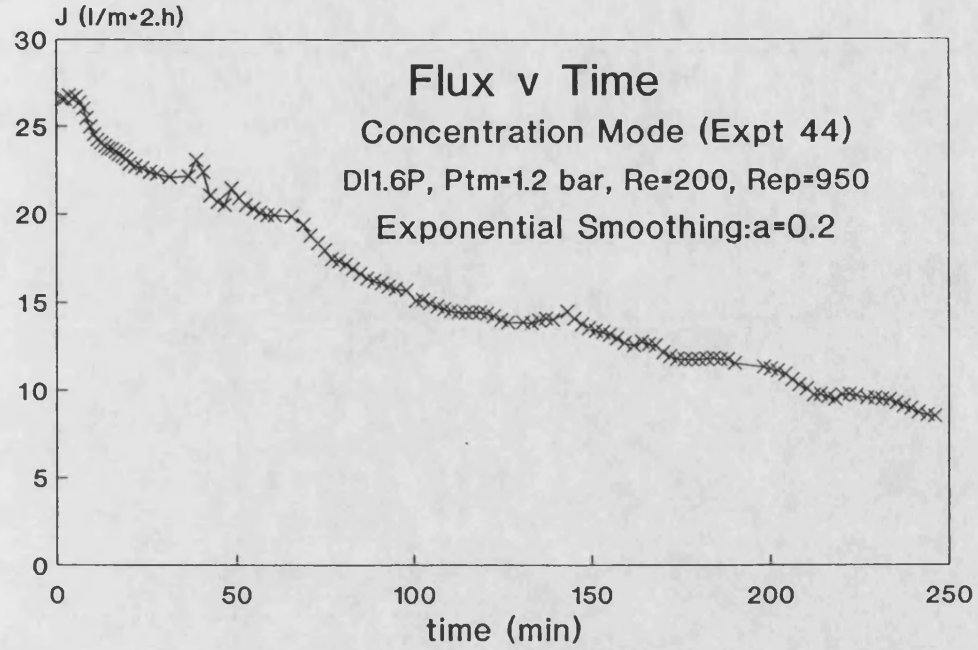

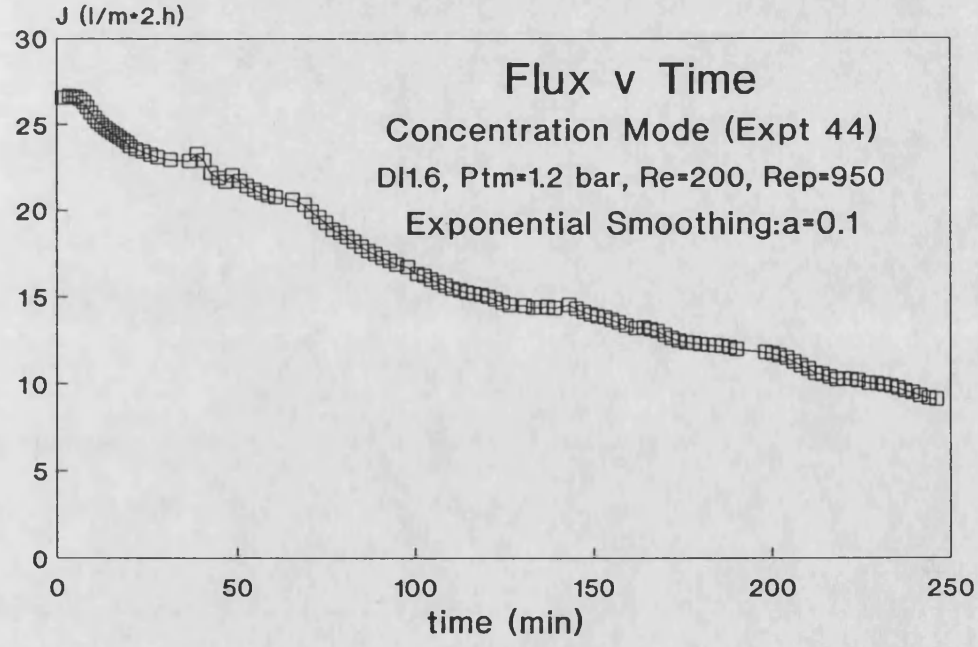

Fig A1.3: Flux v time data for Expt 44 showing exponentially smoothed data with d) a=0.2; e) a=0.1.

Smoothing is easier to apply to the experimental data than the leaf and stem analysis and this was subsequently adopted in Stage 2 to check the validity of the raw average flux values with the smoothing parameter, a, set to 0.2. The logging interval was increased to 30s and although this reduces the number of data points used to calculate the average, the longer time interval reduces the data scatter resulting in a smaller standard deviation. Fig A1.4(a)-(b) shows the flux v time data for a steady flow snapshot experiment for **DI**3.2 from Stage 2A. Fig A1.4b shows how exponential smoothing(a=0.2) eliminates most of the data scatter demonstrated by the raw data(Fig A1.4a). Table A1.4 shows how the smoothed average values agree very well with corresponding raw values and the standard deviation is correspondingly reduced, further validating the use of this method. In plotting the flux/P_{tm}/Re graphs the raw average values have been used. On the basis of these analyses the error in the flux is estimated to be ±5% in both Stages 1 and 2.

A1.4 Single Snapshot Analysis:

The average flux value obtained from any frame of a snapshot experiment should be representative of the steady state flux from a long term fouling experiment performed under identical operating conditions. This is true if:

a) the time dependent flux decay is insignificant compared with the variation in process fluxes between different frames.

b) the fluxes are starting condition independent.

c) the initial period is of sufficient duration for fluxes to stabilize after the rapid inital flux decay so that the flux decline over a 6 min period is negligible.

These 3 points are discussed in this section and a comparison is made of steady state fluxes from long term fouling experiments with snapshot fluxes corresponding to identical operating conditions.

Long term fouling experiments of 2 hours duration were carried out in Stage 1. The steady state fluxes(averaged over the last 40 and 60 min of operation for **DO**2.2 and **DI**1.6 respectively) and corresponding snapshot fluxes

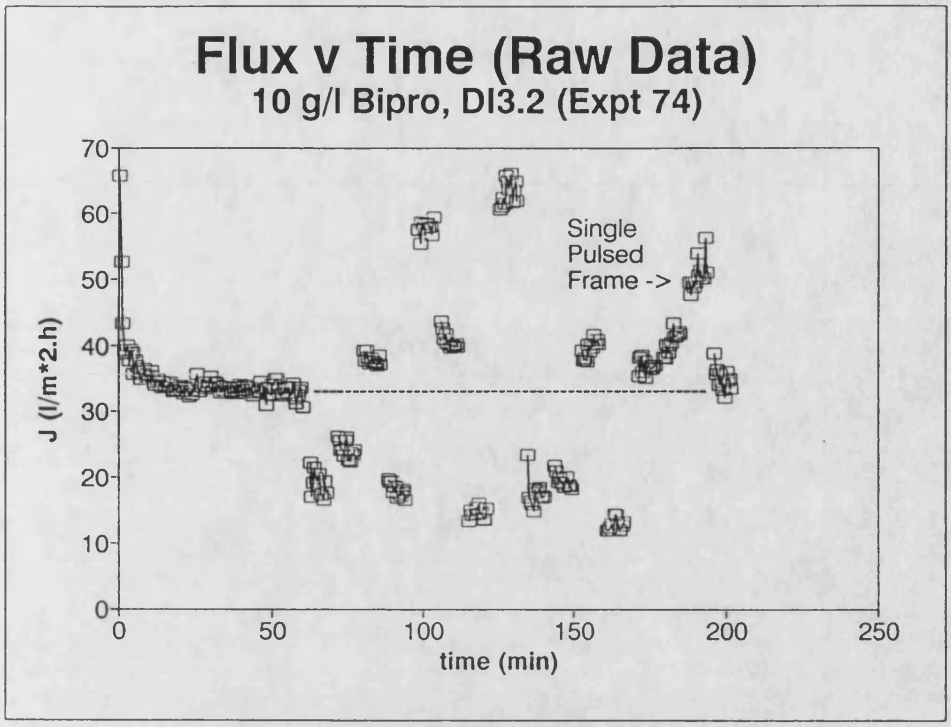

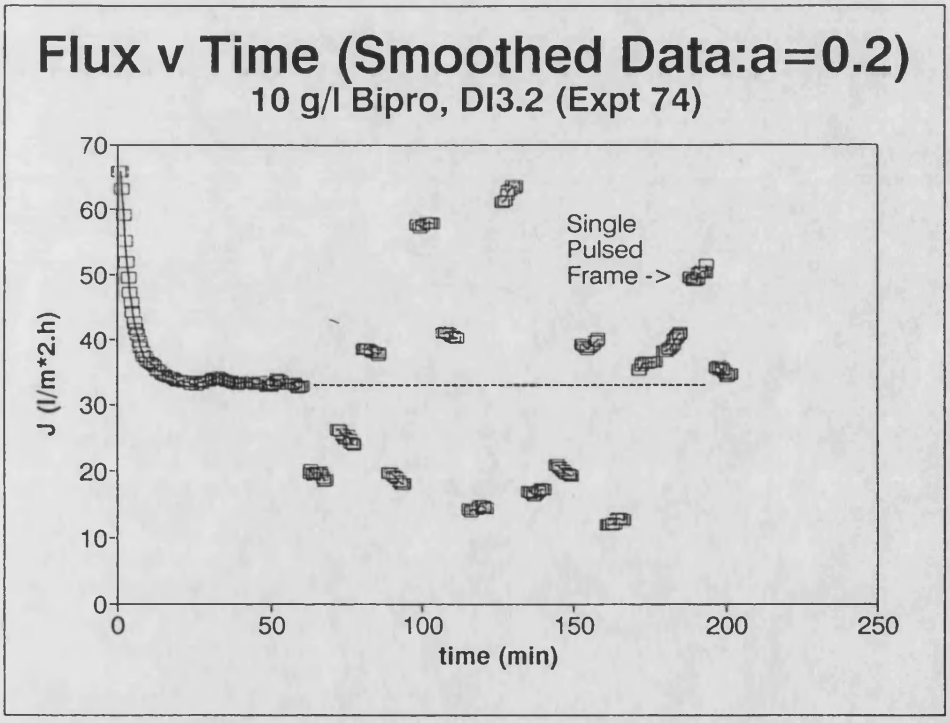

Fig A1.4: Flux v time data for a "snapshot" ultrafiltration experiment(No.74) for **DI**3.2 from Stage 2A showing a) the raw data; b) the exponentially smoothed data using a=0.2.

			Flux values ($lm^{-2}h^{-1}$)					
No.	P_{tm}	Re	raw			smoothed		
	(bar)		J	σ	%err	J	σ	%err
1	2.1	750	32.7	1.1	3	33.1	0.3	1
2	5.6	100	19.0	1.8	9	19.5	0.5	3
3	1.0	2200	24.3	1.3	5	25.2	0.8	3
4	3.2	750	37.9	0.8	2	38.2	0.3	1
5	3.2	100	18.1	1.0	6	18.9	0.7	4
6	3.2	2200	57.9	1.0	2	57.7	0.3	1
7	5.7	750	40.8	1.3	3	40.7	0.3	1
8	2.1	100	14.5	0.8	6	14.4	0.3	2
9	4.9	2200	63.2	1.9	3	62.4	1.0	2
10	0.9	750	17.0	1.1	6	16.9	0.3	2
11	3.9	100	19.4	1.1	6	20.1	0.6	3
12	2.0	2200	39.6	1.3	3	39.2	0.5	1
13	1.0	100	12.7	0.9	7	12.3	0.4	3
14	4.1	750	36.8	1.0	3	36.2	0.5	1
15	2.1	2200	40.6	1.6	4	39.4	1.1	3
16	2.1P	750	50.7	2.4	5	49.9	0.8	2
17	2.2	750	34.6	1.3	4	35.1	0.5	1

Table A1.4: Summary of raw and exponentially smoothed(a=0.2) averages and the corresponding standard deviations for the flux data obtained from Expt 74. % err=σ/J*100%.

are compared in Table A1.5 for the 2 sets of baffled systems and show reasonable agreement. Most flux values agree within one standard deviation of each other. The agreement is worst for the baffled systems under pulsed flow conditions. The long term fouling values are consistently less than the snapshot values.

Consider the 3 criteria stated at the start of this section. For (a), the time dependent flux decay was considered to be acceptable if the flux decline in any experiment was less than 15% as variations based on the major parameters of influence were greater than 300%. The flux decline was calculated from the average flux values corresponding to the last 6 min of the initial period and the

Expt	Re	Long Term Fouling		Snapshot	
		J_{ss}	σ	J_{ss}	σ
ET	1050	9.1	0.7	9.5	0.5
DO2.2	1050	17.5	0.5	18.4	1.4
DO2.2P	1050	18.3	0.2	22.5	1.0
ET	350	6.8	0.5	8.9	0.9
ETP	350	9.8	0.6	10.1	1.1
ET	1200	8.8	0.4	9.1	0.8
DI1.6	350	14.1	0.6	14.8	1.5
DI1.6P	350	17.6	0.9	20.9	0.9
DI1.6P	1200	20.2	0.9	22.9	0.9
ET	700	7.5	0.7	7.6	1.0
ETP	700	8.7	0.4	8.9	0.6
DI1.6	700	18.1	0.3	20.0	0.8
DI1.6P	700	19.7	0.9	22.1	0.3

Table A1.5: Comparison of long term fouling steady state and "snapshot" fluxes for the two baffled systems at $P_{tm} = 1.2$ bar. σ is the standard deviation in the flux.

6 min final period, for which the operating conditions were the same. This was satisfied in all but 5 cases; the results from these 5 experiments are not included here. Fig A1.4 shows how the extent of flux decay during a typical snapshot experiment is very small as the starting and end fluxes, connected by the horizontal line, are almost identical in this experiment. Hence criterion (a) is satisfied.

No systematic study was made of the dependency of snapshot fluxes on the initial operating conditions. However, comparison of different experimental results from Stage 1 and 2 showed no such dependency existed, thus satisfying criterion (b).

Finally the long term fouling results from Stage 1(see Section 3.3.5) suggest that the initial period of 20 min should be extended to 60 min to ensure that the flux has stabilized after the initial period of rapid decay. It was also felt that these long term fouling experiments had been too short as some snapshot experiments took up to 3 hours to complete. Fouling behaviour can change with time and it is possible that rapid flux decay could occur after 2 hours.

Consequently a long term fouling experiment of 5 hours duration was carried out in Stage 2. This is shown in Fig A1.5. Average flux values calculated over 20 min intervals are equal within one standard deviation over the period 50-300 min. Thus, an initial period of one hour is sufficient to satisfy criterion (c). This longer time period was used in all Stage 2 experiments. Again, the long term fouling average is lower than the corresponding snapshot data and there is no obvious reason for this result, unless it is simply that continuous changing of flow conditions itself reduces fouling. However, the agreement between corresponding snapshot and long term fouling fluxes is sufficient to conclude that the snapshot fluxes are representative of steady state fluxes from long term fouling experiments performed under identical operating conditions.

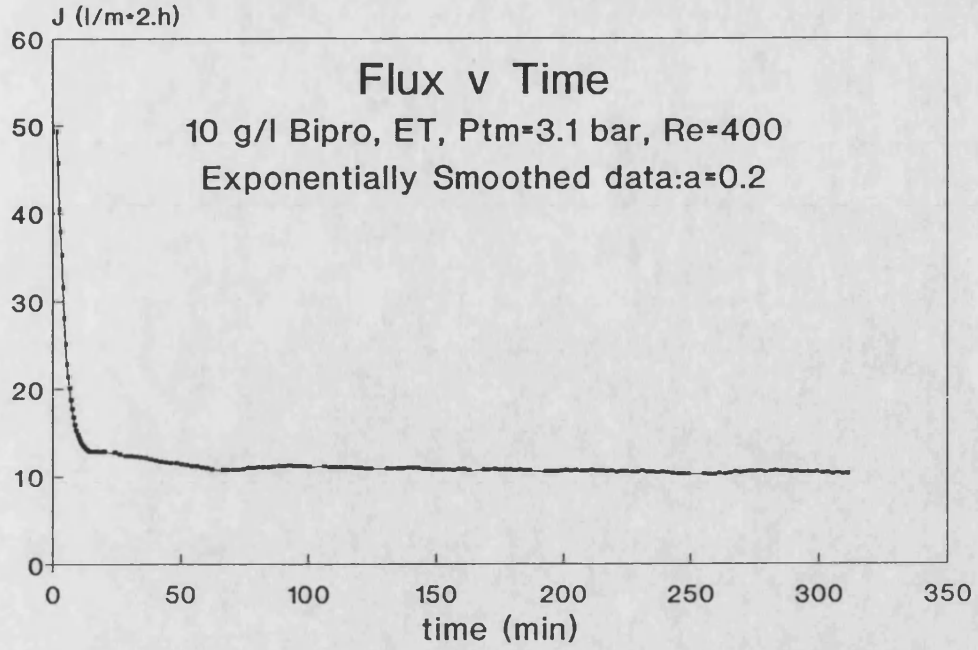

Fig A1.5: Long term fouling experiment of 5 hours duration for **ET** at P_{tm} = 3.1 bar and Re = 400. The data has been exponentially smoothed with a = 0.2.

A1.5 Modified Snapshot Technique:

A series of snapshot experiments were carried out in Stage 2 for **ET**, **ETP**, **DI**1.6 and **DI**1.6**P** using new FP100 membranes with an initial period of 60 min and logging interval of 30s. Although the results of each snapshot experiment appeared to be consistent, the fluxes were much lower than expected and more importantly, there was a lack of consistency between individual experiments. Long term fouling steady state fluxes did not agree well with corresponding snapshot values. The water flux behaviour was also erratic. It was felt that one possible cause for this behaviour may be the more severe operating conditions used in Stage 2 which could result in greater fouling, rendering the snapshot technique invalid. However, further experiments led to the conclusion that these membranes were faulty. No further problems were experienced when these membranes were replaced.

The problems experienced here led to further modifications of the snapshot technique used in Stage 2 of the experiments. These are described

below and also in Section 4.2.2. The cleaning cycle was also modified as described in Section 2.3.5.

For each system two experiments were carried out for both steady and pulsed flow conditions. Each half of a pair had identical starting and end conditions. For a steady flow snapshot experiment, a single pulsed flow frame was included to see if the pulsed flow flux, calculated for this frame, was consistent with corresponding fluxes from pulsed flow snapshot experiments: this pulsed flow frame is identified in Fig A1.4. The other frames in this graph all correspond to steady flow conditions. Similarly in a pulsed flow snapshot experiment, one steady flow frame was included. The 2 halves could be combined to give the overall flux/pressure relationship.

Fig A1.6(a)-(d) illustrates the individual snapshot experiments for pulsed and steady flow from Stage 2A for **DI3.2**. The numbers refer to the order in which the operating conditions were changed as explained in Section A1.2; the letter suffix P or S attached to the data points refers to pulsed or steady flow respectively. The steady flow data(Fig A1.6a, A1.6b) and pulsed flow data(A1.6c, A1.6d) is combined to give the overall flux v pressure relationship for this system under these conditions of pulsed and steady flow in Fig A1.7. Only the pulsed flow data for an amplitude of 30.5 mm(100%) from Fig A1.6d has been used in the combined graph. The agreement between the 4 data sets is excellent. Fluxes corresponding to the same conditions of P_{tm} for pulsed flow and P_{tm} and Re for steady flow (No.1 and 17 only in Fig A1.6a and A1.6b) are almost identical. Similarly the pulsed flow frame from each steady flow snapshot experiment (No.16**P** in Fig A1.6a and A1.6b) agree well with the corresponding pulsed flow snapshot results. The converse is also true. It is important to note that the change in flux in going from pulsed to steady flow or vice-versa is rapid and reversible, as demonstrated by the pulsed flow frame shown in Fig A1.4(a-b).

The compatability of these results illustrates the validity and usefulness of the snapshot method. A considerable amount of information concerning the membrane performance under different conditions of P_{tm}, Re and Re_p has been generated in only 4 experiments.

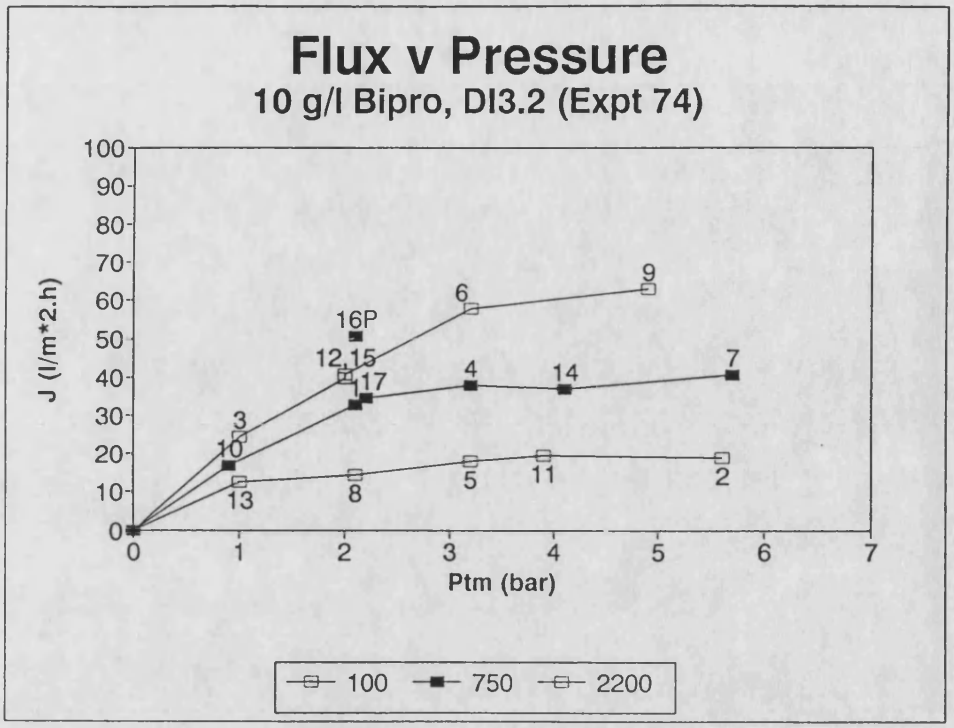

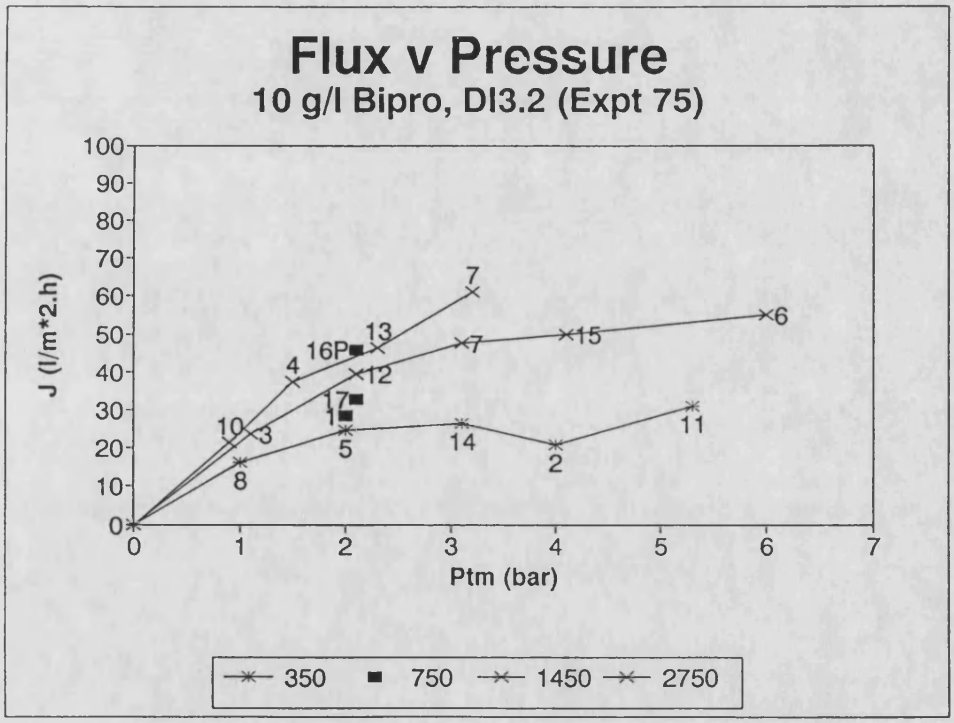

Fig A1.6: Individual snapshot experiments for **DI**3.2 from Stage 2A corresponding to steady flow at the Re values indicated in the legend for a) Expt 74 and b) Expt 75.

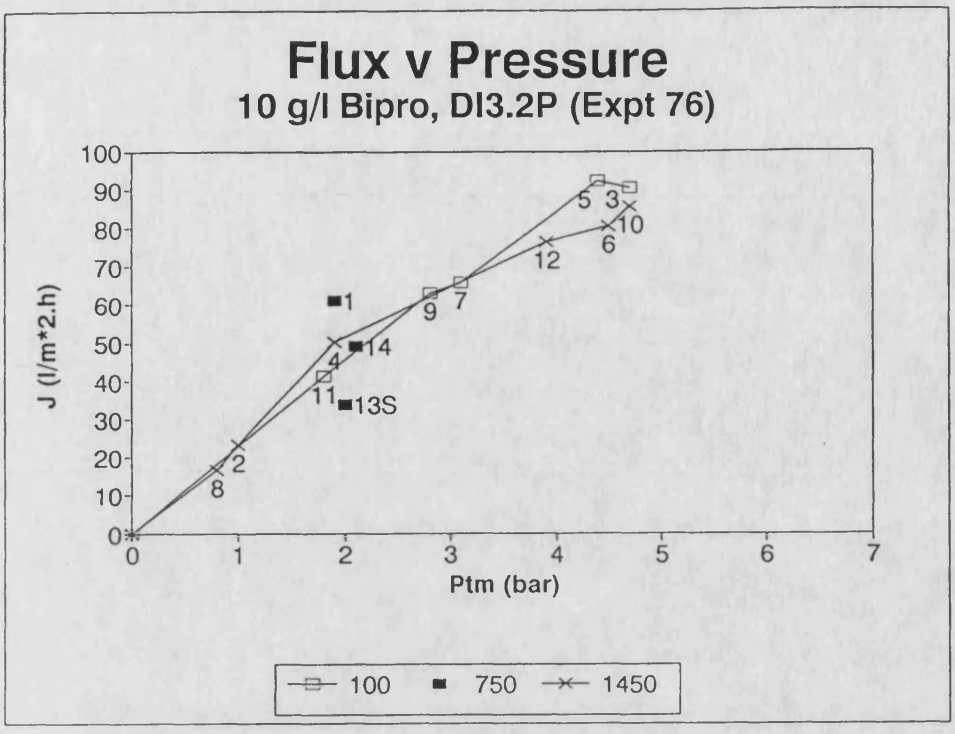

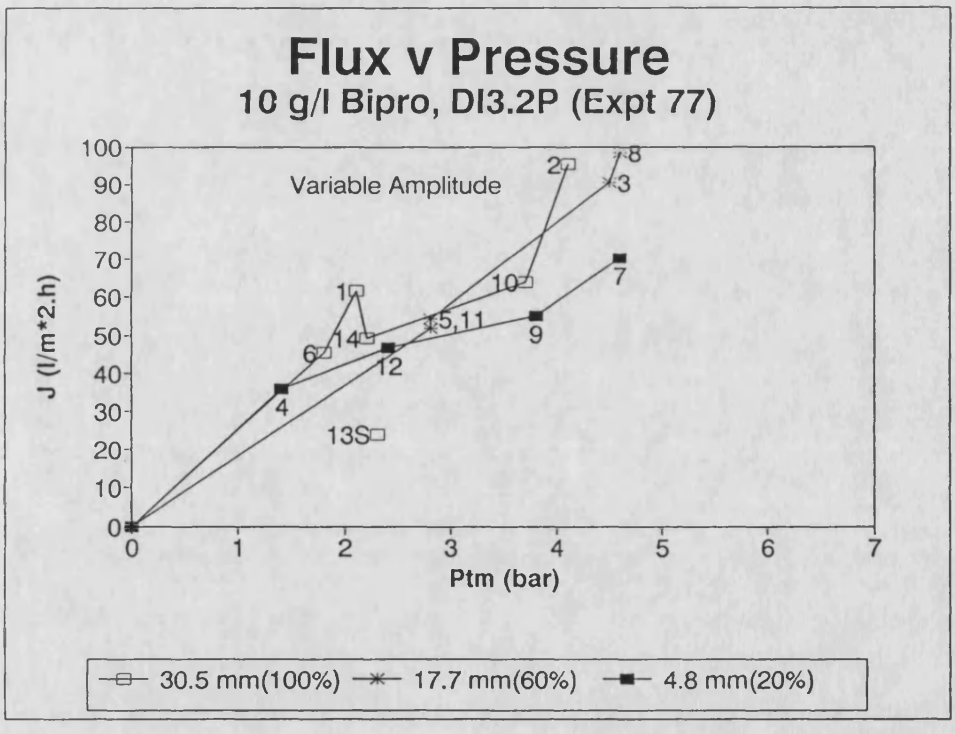

Fig A1.6: Individual snapshot experiments for **DI3.2P** from Stage 2A corresponding to pulsed flow at the Re and X values indicated in the legend for c) Expt 76 and d) Expt 77.

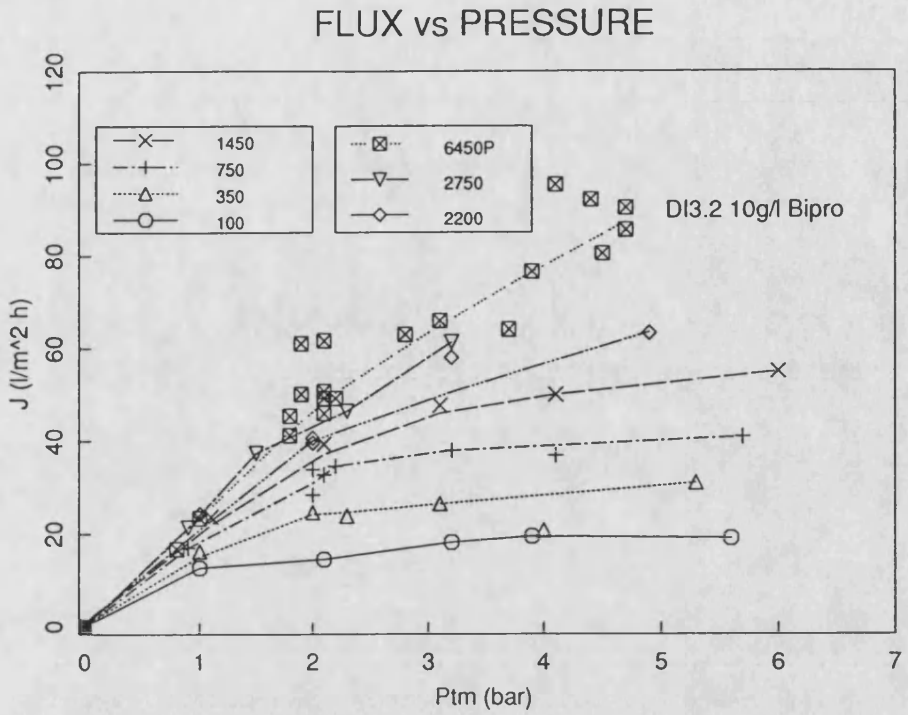

Fig A1.7: The combined snapshot ultrafiltration results for **DI**3.2 for steady and pulsed flow conditions for the Re values indicated in the legend. This graph has been constructed from the 4 individual graphs of Fig A1.6.

A1.6 Smoothing Stage 2 Flux/Pressure Data:

Fig A1.8(a)-(d) show the variation in the flux for different baffled systems under the same conditions of pulsed flow. The numbers in the legend refer to: Expt No.(Re). Re values without the suffix P in the legend refer to pulsed flow frames from a steady snapshot experiment. This data agrees well with the pulsed snapshot data in all cases.

The variation in the flux values is greater than for steady flow for Stage 2A, especially at high P_{tm} values. More data has also been collected for pulsed flow. For these 2 reasons, smoothing has been used to generate a curve to represent all the data using the lowess function in the S software package. S is an interactive environment for data analysis and graphics. Lowess(x,y,f,iter,delta)

generates a smoothed curve from a scatter plot of (x,y) points. It uses the method of robust locally weighted regression(Cleveland, 1979). The procedure involves fitting values, y_i, at each x using a polynomial fit to the data using weighted least squares. A different set of weights are then defined for each (x,y) based on the size of the residual $y-y_i$. Large residuals result in small weights and small residuals in large weights. New fitted values are then computed and this is repeated iter times. The assumption of smoothness allows points in the neighbourhood of (x,y) to be used in forming y_i. Increasing f, the fraction of data used for smoothing at each point, increases the neighbourhood and the smoothness of the fit. The default values for f and iter are 2/3 and 3 respectively. Delta is the interval size and the default value is 1% of the range of x.

The smoothed curves fit the data well. In Fig A1.8b and A1.8c, data from Stages 2A and 2B has been plotted together. Different membranes were used in each stage. Smoothed curves have been plotted for each stage and for the combined data. The agreement is satisfactory especially for **DI**1.6.

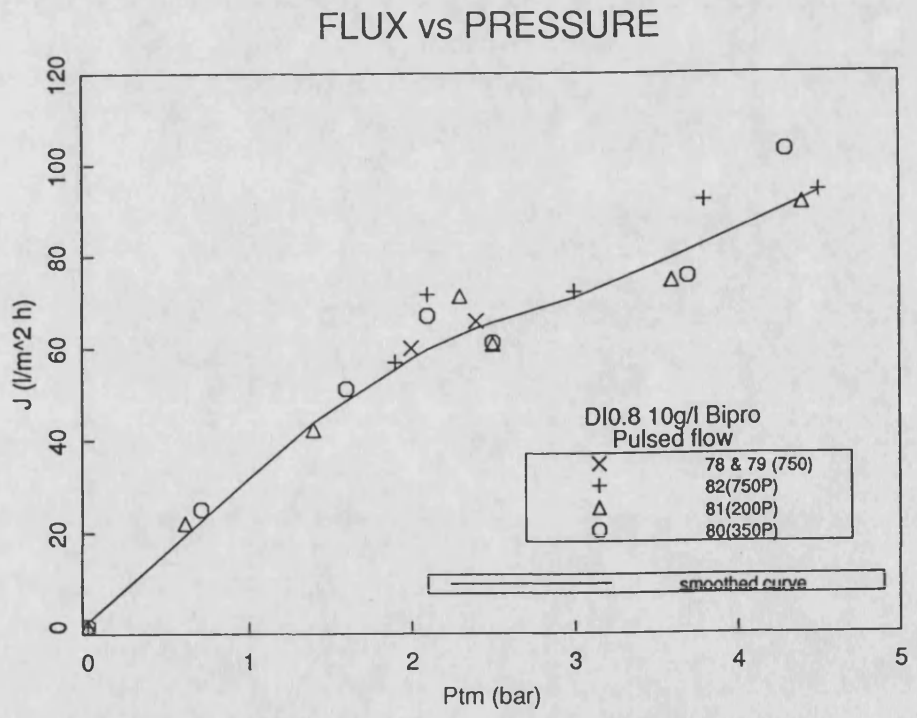

Fig A1.8a: Variation in the flux for **DI**0.8 under the same conditions of pulsed flow between different experiments. The data is represented by a smoothed curve as described in the text.

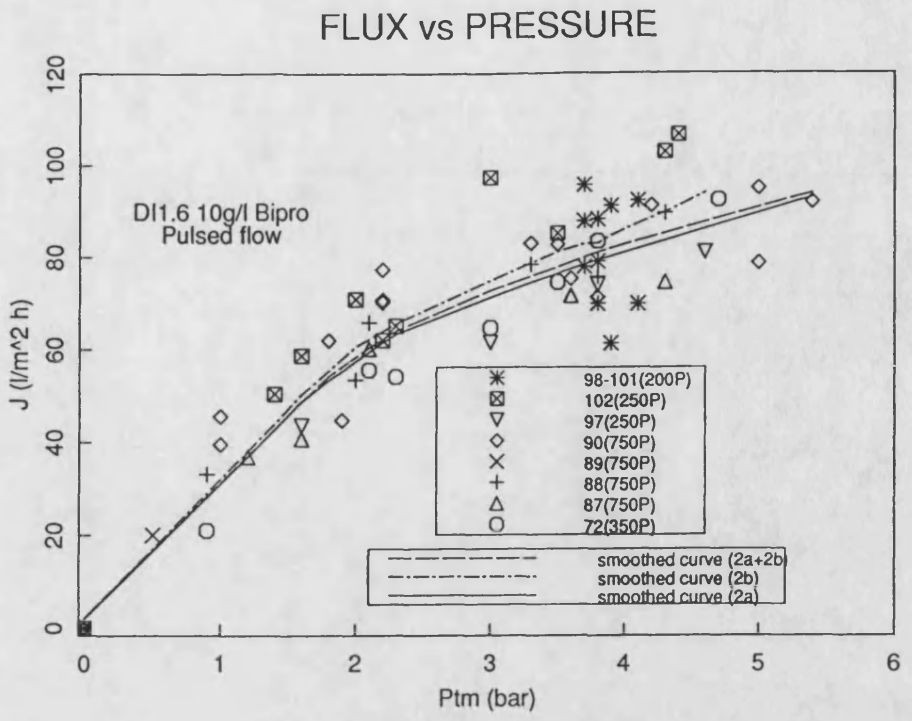

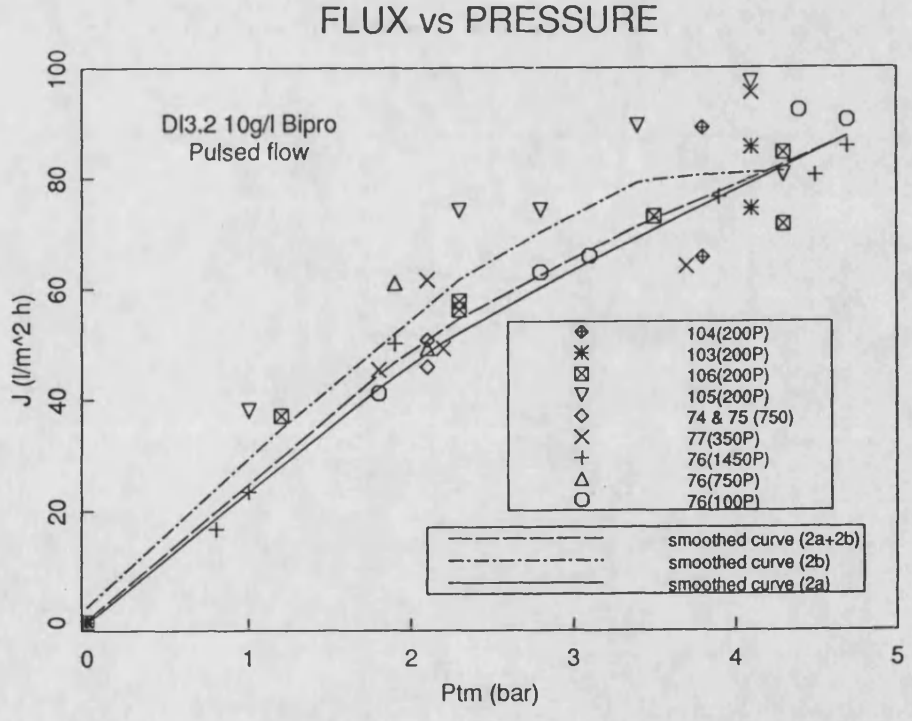

Fig A1.8: Variation in the flux for b) **DI**1.6 and c) **DI**3.2 under the same conditions of pulsed flow. Experiment numbers in the range 72-90 and 97-106 correspond to Stages 2A and 2B respectively.

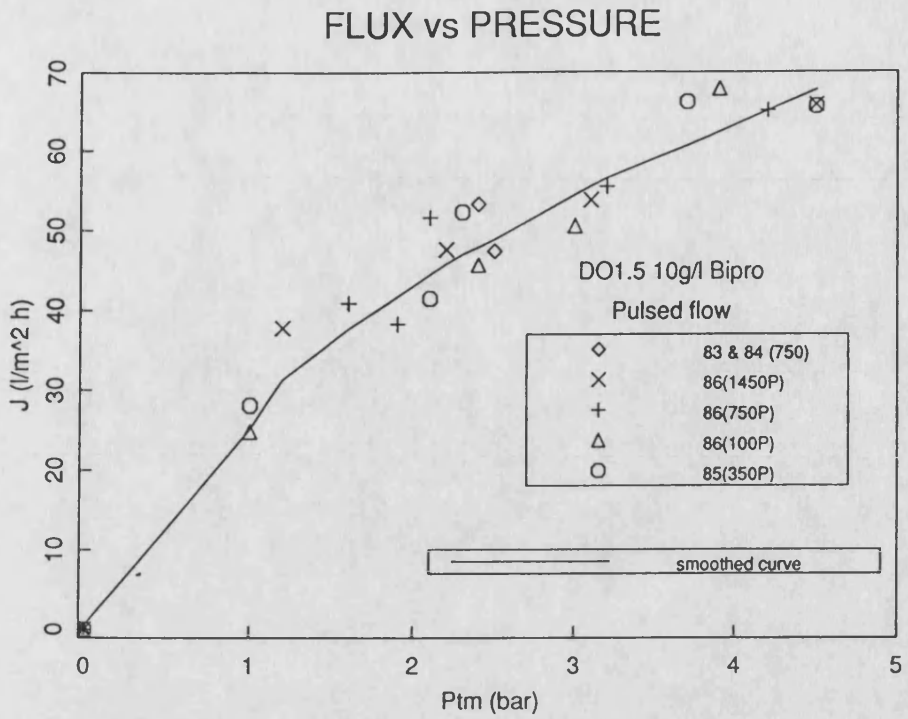

Fig A1.8d: Variation in the flux for **DO**1.5 under the same conditions of pulsed flow between different experiments.

In Fig 4.3 and 4.4 of Section 4.2.3, the data points and smoothed curves are plotted along with the steady flow data in the same graphs. The steady flow data is also represented by a smoothed curve generated using lowess-This is particularly relevant for Stage 2B where the data scatter is greater than in Stage 2A due to the more turbulent flow conditions used in the former case. This form of graphical presentation is simpler than that used in Stage 1.

A1.7 Weaknesses of The Snapshot Method:

The weaknesses of the snapshot method are:

a) long term fouling steady state flux values are consistently less than corresponding snapshot values.

b) this technique is only applicable to systems where the extent of long term fouling is insignificant compared with the variation in process fluxes and "steady

state" snapshot fluxes are starting condition independent. Bipro was the only feed solution used in the snapshot experiments at C=5-25 gl^{-1} and appears to satisfy these criteria with the FP100 membranes used here. Each system may respond differently; certainly the snapshot method will not be universally applicable.

c) in the pressure dependent region the data becomes quite scattered especially at high P_{tm} and for pulsed flow or turbulent steady flow. Variations in membrane resistance between different experiments is one factor causing this data scatter as under these conditions the membrane resistance constitutes a greater proportion of the total resistance to permeation. Another factor is the variation in P_{tm} due to P_p(see Section 4.2.3(C).

If the extent of flux decline is significant it may be possible to correct the data to compensate for this. Two approaches are suggested:

a) The method of Devereux and Hoare(1986) for correcting fluxes to compensate for the effects of flux decline may be applicable. They observed the decline in flux with time over a period of 1-2 hours during the processing of a nonwashed protein precipitate suspension for ultrafiltration PM50 and microfiltration 0.2 micron membranes. They used these flux decline(FD) curves to correct for the experimental time involved in measuring the flux/P_{tm} characteristics. The corrected flux is given by the measured flux divided by the fractional decline observed in these FD curves for equivalent time span of the experiment.

b) This approach is similar to (a). However, instead of collecting additional long term flux decay data as done by Devereux and Hoare(1986), the extent of flux decay may be fitted by a model and the model predictions can be used to correct the flux. Wu et al(1990) developed an empirical method for modelling the flux decline with time for protein ultrafiltration. This is particularly suitable for applying to the snapshot method as the model requires knowledge of the initial rapid flux decay period until fluxes stabilize and the long term steady state flux. These periods correspond to the initial and final frames of a snapshot experiment and hence this data is readily accessible. Once the model parameters are determined from the experimental data, the model can be applied to calculate the flux at any time, t.

The experimental fluxes can then be corrected to t=60 min(or any arbitrary time)

using:

$$J_c(60) = J(t)\frac{J_m(60)}{J_m(t)} \qquad \text{(A1.3)}$$

where J(t) is the experimental raw average flux value at time, t; $J_m(60)$ and $J_m(t)$ are the model fluxes at time 60 min and t respectively and $J_c(60)$ is the corrected experimental flux at t=60 min.

This model was applied to experimental data obtained with the dud membranes, discussed in Section A1.5, where the flux decline during a snapshot experiment was greater than 15% in some cases. It fitted the data well, suggesting that this approach is feasible.

A1.8 Membrane Variability:

The other main cause of experimental error is the membrane itself. The filtration performance may differ:

a) between different membranes.

b) due to deterioration in the membrane performance as demonstrated by changing rejection behaviour and membrane resistance.

c) if the system is not sealed properly so that leaks occur.

A1.8.1 Different membranes:

The manufacturer acknowledges that there can be considerable variability in the filtration performance of their FP100 membranes even when they come from the same 10 ft length and this was observed experimentally. The water flux behaviour of the 2 membranes to be used in each side of the ultrafiltration module was measured over the experimental P_{tm} range. If the variation was less than 5%, the membranes were considered suitable for use. Once new membranes have been fouled, differences in behaviour are less significant as virgin

performance is never regained on chemically cleaning the membrane. More importantly, in process runs, the filtration performance will be governed by the fouling layer, referred to as the secondary membrane which forms on the membrane surface. Experimentally, after fouling and chemically cleaning the membrane once or twice, reproducible data could be obtained. Consequently, the first and sometimes the second experiments were used to obtain qualitative information only.

A1.8.2 Deterioration in Membrane Performance:

The membrane resistance and rejection behaviour was monitored to check for any deterioration in performance. A natural deterioration with time will occur. In this work, there is also potential for the baffles damaging the membrane during the filtration experiments and more probably on their installation and removal. The rejection behaviour is controlled primarily by the secondary membrane(Murkes and Carlsson, 1988) formed on the surface and will not detect any deterioration in the membrane performance unless this affects the nature of the secondary membrane itself. No systematic changes in rejection behaviour or post-experiment membrane resistance were observed. This suggests that baffles and/or pulsed flow do not affect the extent of fouling. The pre-experiment membrane resistance gives a better indication of any change in the membrane performance. The variation in the pre-experiment membrane resistance was a maximum of 20% for each set of membranes used. No systematic decline or rise occurred, indicating the baffles have not damaged the membrane. Changes that did occur may have been due to ineffective chemical cleaning. These changes did not affect the flux performance, again this being attributed to the secondary membrane controlling the filtration process.

A1.8.3 Leaks:

These two parameters can also be used to check if any leaks occurred resulting in false flux values being obtained. In 4 pulsed flow experiments under conditions of high P_{tm} up to 50% more permeate was collected from the outlet permeate chamber than from the inlet. This was supported by rejection measurements. The pre and post water flux measurements did not reproduce these results presumably because the water flux is measured at P_{tm}=1-1.2 bar. This behaviour was attributed to a leaky seal and the flux data from these experiments was rejected. In all experiments if the variation in the amount of permeate collected from both tubes was less than 10%, the flux data was considered acceptable.

A1.9 Summary and Conclusions:

The snapshot technique has been validated in this section:

a) For each frame of a snapshot experiment, the raw average flux value has been shown to be a valid criterion for data representation despite the relatively large magnitude of the standard deviation in some cases. Two statistical methods were used to verify this: leaf and stem analysis and exponential smoothing(a=0.2). Increasing the logging interval from 20 to 30s in Stage 2 reduced the data scatter. The error in the flux was estimated to be 5%.

b) Negligible long term fouling was judged to have occurred over the duration of an experiment if the overall flux decline within any experiment was less than 15%. Only 5 experiments did not satisfy this criteria and these results were rejected.

c) Snapshot fluxes appeared to be independent of the starting conditions used.

d) An initial operating period of 20 min was used in Stage 1 for fluxes to stabilize after the initial period of rapid flux decay before changing the operating conditions. This period was extended to 60 min in Stage 2. In both cases, the flux decline over any subsequent 6 min period was negligible.

e) Flux values were consistent between different steady and pulsed flow snapshot

experiments.

f) The average flux values obtained from any frame of a snapshot experiment were representative of but consistently greater than steady state fluxes from long term fouling experiments performed under identical operating conditions.

g) The snapshot technique is not universally applicable but depends on conditions a-d being satisfied. When operating in the pressure dependent region, the data is likely to be more scattered, especially for pulsed flow. Differences in the filtration performance of different FP100 membranes can also be a source of experimental variation.

h) The use of baffles and/or pulsed flow does not appear to affect the nature of the fouling layer formed on the membrane surface. Baffles were installed and removed without damaging the membrane.

i) It may be possible to apply the snapshot method to situations where the overall flux decline is significant but measurable, by correcting for the extent of flux decay either using experimental long term flux/time data or an empirical flux decline model.

j) The snapshot technique generates a considerable amount of data on the membrane filtration behaviour under different operating conditions of P_{tm} and Re for both steady and pulsed flow in relatively few experiments.

APPENDIX A2

RAW REYNOLDS NUMBER DATA

Table A2.1a and A2.1b shows the measured values of the volumetric flow rate, Q, for Stages 1 and 2 of the experiments and values of the velocity, v and Reynolds number, Re calculated from Q. Two Reynolds numbers are tabulated: the raw value, used in all calculations; and the rounded Re value, which is stated in the text.

Stage 1: C_b=25 gl^{-1}; Density=1002.8 $kg.m^{-3}$; viscosity=9.802E-04$kg.m^{-3}$

Q($l.min^{-1}$)	v(ms^{-1})	Re(raw)	Re(text)
0.005	0.00068	9	10
0.025	0.0034	43	50
0.05	0.0068	87	100
0.1	0.014	174	200
0.2	0.027	347	350
0.3	0.041	521	500
0.4	0.054	695	700
0.6	0.081	1042	1050
0.69	0.094	1198	1200
0.9	0.12	1563	1550
1.6	0.22	2779	2800
1.9	0.26	3300	3300
0.5P	**0.073P**	**934P**	**950P**

Table A2.1a: Q data used for calculation of v and Re for Stage 1. Raw and rounded Re values are shown here.

Stage 2: $C_b = 10\ gl^{1-1}$; Density = 999.2 $kg.m^{-3}$; viscosity = 9.278E-04$kg.m^{-3}$

Flow Visualization: H_2O at 18°C Density = 998.5 $kg.m^{-3}$; viscosity = 10.556E-04$kg.m^{-3}$

		Filtration Re values		FV Re values	
Q($l.min^{-1}$)	v(ms^{-1})	raw	text	raw	text
0.05	0.0068	91	100	---	---
0.1	0.014	---	---	160	150
0.2	0.027	366	350	321	300
0.4	0.054	731	750	642	650
0.8	0.11	1463	1450	1285	1300
1.2	0.16	2194	2200	1927	1950
1.5	0.20	2742	2750	---	---
2.4	0.32	---	---	3853	3850
3.5	0.48	6462	6450	5717	5700
5.9	0.80	---	---	9458	9450
8.8	1.2	16154	16000	---	---
14	1.9	25578	26000	---	---
19.3	2.7	---	---	31056	31000
22.1	3.0	40386	40000	---	---
27.2	3.7	49809	50000	---	---
3.5P	0.48P	6462P	6450P	5717P	5700P

Table A2.1b: Q data used for calculation of v and Re for Stage 2 and for the flow visualization experiments. Raw and rounded Re values are shown here.

NOMENCLATURE

Dimensions are given in terms of mass[M], length[L] and time[T]. The section where each term is first used or defined is also stated.

A_b	baffle cross-sectional flow area	L^2	1.4.1
A_{ct}	cross-sectional area of the empty tube	L^2	1.4.1
A_m	Membrane Surface area	L^2	5.2.1
a	smoothing parameter	--	A1.3.2
C_b	bulk concentration	ML^{-3}	3.3.2
D	membrane tube internal diameter	L	1.4.1
D_{hy}	hydraulic diameter	L	1.4.1
d_i	inner diameter of baffle	L	1.4.1
d_o	outer diameter of baffle	L	1.4.1
d	channel height(Colman and Mitchell, 1990)	L	1.4.1
dP	pressure drop	$ML^{-1}T^{-2}$	5.1.1
dP_p	pulsing pressure drop	$ML^{-1}T^{-2}$	5.1.1
E	specific power consumption	MT^{-3}	5.2.1
E_n	specific net forward flow power consumption	MT^{-3}	5.2.1
E_p	specific pulsed flow power consumption	MT^{-3}	5.2.1
f	frequency	T^{-1}	1.4.1
h	half the minimum channel width(Sobey, 1980)	L	1.4.1
J	permeation flux	LT^{-1}	3.3.1
J_c	corrected experimental permeation flux	LT^{-1}	A1.7
J_m	permeation flux calculated from model	LT^{-1}	A1.7
J_{ss}	steady state permeation flux	LT^{-1}	3.3.5
K_c	Keulagen Carpenter number	--	1.4.3
L	centre to centre baffle spacing	L	1.4.3

L	lower hinge	--	A1.3.1
M	median	--	A1.3.1
$m_{i/o}$	inlet/outlet permeate ratio	--	4.2.3
N	total count	--	A1.3.1
NFR	net to peak flow ratio	--	1.4.1
P_p	pulsing pressure	$ML^{-1}T^{-2}$	4.1.1
P_{th}	threshold pressure	$ML^{-1}T^{-2}$	3.3.1
P_{tm}	transmembrane pressure	$ML^{-1}T^{-2}$	2.3.2
PuRe	Pulsatile Reynolds number(Colman and Mitchell, 1990)	--	1.4.1
Q	volumetric flow rate	L^3T^{-1}	1.4.1
Q_p	pulsed volumetric flow rate	L^3T^{-1}	5.1.1
R_m	membrane resistance	L^{-1}	2.3.6
Re	Reynolds number	--	1.4.1
Re_{crit}	critical Reynolds number	--	1.4.1
Re_{bp}	Baffled Pulsed Reynolds number	--	1.4.1
Re_o	Peak Reynolds number(Sobey, 1980)	--	1.4.1
Re_p	Pulsed Reynolds number	--	1.4.1
Re_0	Reynolds number at t=0 in a concentration experiment	--	4.4.3
Re_t	threshold Reynolds number	--	3.3.3
r	radius of curvature	L	1.4.3
St	Strouhal number	--	1.4.1
T	trimean	--	A1.3.1
Th	Thomson number(Colman and Mitchell, 1990)	--	1.4.1
t	baffle thickness	L	2.2.3
U	upper hinge	--	A1.3.1
Va	Valensi number	--	1.4.1
V_p	pulsed velocity waveform	L^3	4.1.1
v	velocity	LT^{-1}	1.4.1
v_{bp}	baffled pulsed flow velocity	LT^{-1}	1.4.1
v_p	pulsed flow velocity	LT^{-1}	1.4.1
X	peak-centre amplitude	L	1.4.1
X_o	peak-centre amplitude(Sobey, 1980)	L	1.4.1

Greek Letters

α^2	Pulsatile Reynolds number(Sobey, 1980)	--	1.4.1
ϕ	phase difference between dP_p and Q_p	--	5.1.1
σ	standard deviation	--	3.3.5
μ	dynamic viscosity	$ML^{-1}T^{-1}$	1.4.1
ρ	density	ML^{-3}	1.4.1

REFERENCES

Abel, K., Jeffree, M.A., Bellhouse, B.J., Bellhouse, E.L., Haworth, W.S., (1981), "A Practical Secondary-Flow Hemodialyzer", **Trans. Am. Soc. Artif. Intern. Organs**, 27, 639-643

Aimar, P. and Sanchez, V., (1985), "Membrane Fouling and Limiting Phenomena in Ultrafiltration", in **Fouling and Cleaning in Food Processing**, Second International Conference on Fouling and Cleaning in Food Processing, ed. D. Lund, E. Plett, C. Sandu, Wisconsin, 466-475

Aref, H., (1984), "Stirring by Chaotic Advection", **J. Fluid Mech.**, 143, 1-21

Bauser, H., Chmiel, H., Stroh, N., Walitza, E., (1982), "Interfacial Effects with Microfiltration Membranes", **J. Memb. Sci.**, 11, 321-332

Bauser, H., Chmiel, H., Stroh, N., Walitza, E., (1986), "Control of Concentration Polarization and Fouling in Medical, Food and Biotechnical Applications", **J. Memb. Sci.**, 27, 195-202

Belfort, G., (1977), "Pretreatment and Cleaning of Hyperfiltration (Reverse Osmosis) Membranes in Municipal Wastewater Renovation", **Desal.**, 21, 285-300

Belfort, G. and Marx, B., (1979), "Artificial Particulate Fouling of Hyperfiltration Membranes", **Desal.**, 28, 13-30

Belfort, G., (1988), "Membrane Modules: Comparison of different Configurations Using Fluid Mechanics", **J. Memb. Sci.**, 35, 245-270

Bell, G., (1985), "Membrane Separation Processes", presented at **Downstream Separation Processes in Biochemical Engineering**, IChemE, Glasgow, Nov 21

Bellhouse, B.J., Bellhouse, F.H., Curl, C.M., MacMillan, T.I., Gunning, A.J., Spratt, E.H., MacMurray, S.B., Nelems, J.M., (1973), "A High Efficiency Membrane Oxygenator and Pulsatile Pumping System, and its Application to Animal Trials", **Trans. Am. Soc. Artif. Intern. Organs**, 19, 72-79

Benzinger, W.D., Toal, M.G., Sprout, O.S., Hinde, G.M., (1980), "Development of Non-Fouling Piezoelectric Ultrafiltration Membranes", **Final Report to the Office of Water Research and Technology**, Aug, 35pg

Bowen, W.R. and Sabuni, H., (1987), "Electrically Enhanced Membrane Filtration", in **Proceedings from the Workshop on Concentration Polarization and Membrane Fouling**, Twente University, Enschede, May

Bradley, S.E., Fryer, P.J., Griffin, T.A., Wilson, D.I., (1989), "Use of an Oscillatory Flow Heat Exchanger in Food Processing", in **Proceedings 3rd Int. Conf. on Fouling and Cleaning in the Food Industry**, Prien , Germany, June

Brunold, C.R., Hunns, J.C.B., Mackley, M.R., Thompson, J.W., (1989), "Experimental Observations on Flow Patterns and Energy Losses for Oscillatory Flow in Ducts Containing Sharp Edges", **Chem. Eng. Sci.**, 44(5), 1227-1244

Charm, S.E. and Lai, C.J., (1971), "Comparison of Ultrafiltration Systems for Concentration of Biologicals", **Biotech. and Bioeng.**, 13, 185-202

Cleveland, W.S., (1979), "Robust Locally Weighted Regression and Smoothing Scatterplots", **J. Amer. Stat. Assoc.**, 74(368), 829-836

Cloake, W.T., (1988), **Statistical Modelling Using 1-2-3:Release 2**, MIS:Press, Portland, Oregon

Colman, D.A. and Mitchell, W.S., (1990), "Enhanced Mass Transfer for Membrane Processes", **I. Chem. E. Symp. Ser.**, 118, 87-103

Copas, A.L. and Middleman, S., (1974), "Use of Convection Promotion in the Ultrafiltration of a Gel-Forming Solute", **Ind. Eng. Chem. Process Des. Develop.**, 13(2), 143-145

Coulson, J.M. and Richardson, J.F., (1977), **Chemical Engineering Vol 1: Fluid Flow, Heat and Mass Transfer**, 3rd edition, Pergamon Press, Oxford

de Boer, R. and Hiddink, J., (1980), "Membrane Processes in the Dairy Industry", **J. Food. Sci.**, 35, 169-192

de Wit, J.N., Klarenbeek, G., de Boer, R., (1978), "Ultrafiltration-Technique for Up-grading Dairy Products", Brief Communication in **20th International Dairy Congress**, 919-920

Delaney, R.A.M., and Donnelly, J.K., (1975), "Ion Exchange/ Ultrafiltration Studies on Whey. Complimentary Aspects", Presentation **International Symp. Separation Processes by Membranes, Ion Exchange and Freeze Concentration in the Food Industry**, Paris, Mar, March 13-14

Devereux, N. and Hoare, M., (1986), "Membrane Separation of Protein Precipitates: Studies with Cross Flow in Hollow Fibres", **Biotech. and Bioeng.**, 28, 422-431

Dickens, A.W., Mackley, M.R., Williams, H.R., (1989), "Experimental Residence Time Distribution Measurements for Unsteady Flow in Baffled Tubes", **Chem. Eng. Sci.**, 44(7), 1471-1479

Dorrington, K.L., Ralph, M.E., Bellhouse, B.J., Gardez, J.P., Sykes, M.K., (1985), "Oxygen and CO_2 Transfer of a Polypropylene Dimpled Membrane Lung with Variable Secondary Flows", **J. Biomed. Eng.**, 7, 89-99

Edwards, M.F. and Wilkinson, W.L., (1971), "Review of Potential Applications of Pulsating Flow in Pipes", **Trans. Instn. Chem. Engrs.**, 49, 85-93

Fairbanks, H.V., (1973), "Use of Ultrasound to Increase Filtration Rate", **Ultrasonics Int. Conf. Proc.**, Imperial College, London, 11-15

Fane, A.G., (1983), "Factors affecting Flux and Rejection in Ultrafiltration", **J. Sep. Proc. Technol.**, 4(1), 15-23

Fane, A.G., Fell, C.J.D, Kim, K.J., (1985), "The Effect of Surfactant Pretreatment on the Ultrafiltration of Proteins", **Desal.**, 53, 37-55

Field, R.W. and Finnigan, S.M., (1988), "Modelling of Membrane Fouling-A Guide Towards Improved Hydrodynamic Design", to be published in **Proceedings Int. Conf. on Fouling in Process Plant**, Oxford University, July 25-29

Finnigan, S.M. and Howell, J.A., (1989A), "The Effect of Pulsatile Flow on Ultrafiltration Fluxes in a Baffled Tubular Membrane System", **Chem. Eng. Res. Des.**, 67(3), 278-282

Finnigan, S.M. and Howell, J.A., (1989B), "The Effect of Pulsed Flow on Ultrafiltration Fluxes in a Baffled Tubular Membrane System", in **The Membrane Alternative-Energy Implications for Industry Conference**, University of Bath, March 29-30, Elsevier, in press.

Finnigan, S.M. and Howell, J.A, (1989C), "The Effect of Pulsed Flow on Ultrafiltration Fluxes in a Baffled Tubular Membrane System", in **Proceedings 3rd Int. Conf. on Foulng and Cleaning in the Food Industry**, Prien, Germany, June, in press.

Finnigan, S.M. and Howell, J.A., (1989D), "The Effect of Pulsed Flow on Ultrafiltration Fluxes in a Baffled Tubular Membrane System", presented at **6th Int. Symp. on Synthetic membranes in Science and Industry**, Tubingen, Sept 4-8, to be published in J. Memb. Sci.

Gregor, H.P. and Gregor, C.D., (1978), "Synthetic Membrane Technology", **Scientific American**, 239, 88-101

Hallström, B. and López-Leiva, M., (1978), "Description of a Rotating Ultrafiltration Module", **Desalination**, 24, 273-9

Hanemaaijer, J.H., (1987), "Fouling of Ultrafiltration Membranes. The Role of Protein Adsorption and Salt Precipitation", in **Proceedings from the workshop on Concentration Polarization and Membrane Fouling**, Twente University, Enschede, May

Harper, W.J., (1980), "Factors Affecting the Application of Ultrafiltration Membranes in the Dairy Industry", in **Ultrafiltration Membranes and Applications**, ed. A.R. Cooper, Plenum Press, New York, 321-342

Hayes, J.F., Dunkerley, J.A., Muller, L.L., Griffin, A.T., (1974), "Studies on Whey Processing by Ultrafiltration. 2. Improving Permeation Rates by Preventing Fouling", **Aust. J. Dairy Technol.**, 29, 132-140

Hermann, C.C., (1982), "High Frequency Excitation and Vibration Studies on Hyperfiltration Membranes", **Desal.**, 42, 329-338

Hickey, M.W., Hill, R.D., Smith, B.R., (1980), "Investigations into Ultrafiltration and Reverse Osmosis of Wheys. 1) The Effect of Certain Pretreatments", **N.Z. J. Dairy Sci. Technol.**, 15(2), 109-121

Hickey, M.W. and Hill, R.D. (1980), "Investigations into Ultrafiltration and Reverse Osmosis of Wheys. 2) The Effects of Some Minor Constituents", **N.Z. J. Dairy Sci. Technol.**, 15(2), 123-130

Hiddink, J., Kloosterboer, D., Bruin, S., (1980), "Evaluation of Static Mixers as Convection Promoters in the Ultrafiltration of Dairy Liquids", **Desal.**, 35, 149-167

Hiddink, J., de Boer, R., Nooy, P.F.C., (1981), "Effect of Various Pretreatments on Ultrafiltration of Sweet Cheese Whey at about 55°C", **Milchwissenschaft**, 36(11), 657-663

Howell, J.A. and Velicangil, O., (1977), "Protease Coupled Membranes for Ultrafiltration", **Biotech. and Bioeng.**, 19, 1891-1894

Howell, J.A. and Velicangil, O., (1981), "Self-Cleaning Membranes for Ultrafiltration", **Biotech. and Bioeng.**, 23, 843-854

Howell, J.A. and Velicangil, O., (1982), "Theoretical Considerations of Membrane Fouling and its Treatment with Immobilized enzymes for Protein Ultrafiltration", **J. Appl. Poly. Sci.**, 27, 21-32

Howes, T., (1988), **On the Dispersion of Unsteady Flow in Baffled Tubes**, PhD thesis, Department of Chemical Engineering, Cambridge University

Kennedy, T.J., Merson, R.L., McCoy, B.J., (1974), "Improved Permeation Flux by Pulsed Reverse Osmosis", **Chem. Eng. Sci.**, 29, 1927-1931

Kroner, K.H. and Nissinen, (1988), "Dynamic Filtration of Microbial Suspensions Using an Axially Rotating Filter", **J. Memb. Sci.**, 36, 85-100

Le, M.S. and Howell, J.A., (1983), "The Fouling of Ultrafiltration Membranes and its Treatment", in **Progress in Food Engineering**, Foster Publ, Switzerland, 321-326

Le, M.S. and Howell, J.A., (1985), "Ultrafiltration", in **Comprehensive Biotechnology**, ed. M. Moo-Young, Ch. 25, 383-409

Lee, D.N. and Merson, R.L., (1976), "Prefiltration of Cottage Cheese Whey to Reduce Fouling of Ultrafiltration Membranes", **J. Food Sci.**, 41, 403-410

Lee, D.N. and Merson, R.L., (1976), "Chemical Treatments of Cottage Cheese Whey to Reduce Fouling", **J. Food Sci.**, 41, 778-786

Lozier, J.C. and Sierka, R.A., (1985), "Using Ozone and Ultrasound to Reduce Reverse Osmosis Membrane Fouling", **J. AWWA**, Aug, 60-65

Mackley, M.R., (1987), "Using Oscillatory Flow to Improve Performance", **The Chem. Engr.**, Feb, 18-20

Mackley, M.R, Tweedle, G.M., Wyatt, I.D., (1990), "Experimental Heat Transfer Measurements for Pulsatile Flow in Baffled Tubes", **Chem. Eng. Sci.**, 45(5), 1237-1242

McGregor, W.C., (1986), "Selection and Use of Ultrafiltration Membranes", in **Membrane Separations in Biotechnology**, ed. W.C. McGregor, Marcel Dekker Inc, USA, Ch. 1, 1-36

McKeever, F.M. and Kemp, J.S., (1986), **Flow Oscillations and Ultrafiltration**, Department of Chemical Engineering, Cambridge University, Part 2 Project

Melling, J., (1974), "Application of Ultrafiltration-Modifying Factors", **Proc. Biochem.**, Sept, 7-10

Merin, U. and Cheryan, M., (1980), "Factors Affecting the Mechanism of Flux Decline During Ultrafiltration of Cottage Cheese Whey", **J. Food Processing and Preservation**, 4, 183-198

Merzkirch, W., (1974), **Flow Visualization**, Academic Press, New York

Michaels, A.S., (1968), "New Separation Techniques for the CPI", **Chem. Eng. Prog.**, 64, 31-43

Michaels, A.S., Robertson, C.R., Reihanian, H., (1983), "Recent Developments in Ultrafiltration: A Solution to the Polarization/Fouling Problem", **IMTEC Conference Proceedings**, Australia, Nov 8-10, 59-63

Milisic, V. and Bersillon, J.L., (1986), "Anti-fouling Techniques in Cross Flow Microfiltration", **4th World Filtration Congress**, Ostend, April, 11.19-11.23

Muller, L.L., Hayes, J.F., Griffin, A.T., (1973), "Studies on Whey Processing by Ultrafiltration. 1. Comparative Performance of Various Ultrafiltration Modules on Whey From Hydrochloric Acid Casein and Cheddar Cheese", **Aust. J. Dairy Technol.**, 28, 70-77

Murkes, J., (1978), "Some Viewpoints on the Industrial Application of Membrane Technology", **Desal.**, 24, 225-233

Murkes, J. and Carlsson, C.G., (1988), **Crossflow Filtration**, John Wiley & Sons Ltd, New York

Nakao, S., Nomura, T., Kimura, S., (1979), "Characteristics of Macromolecular Gel Layer Formed on Ultrafiltration Tubular Membrane", **AIChE J.**, 25(4), 615-622

Peri, C. and Dunkley, W.L., (1971), "Reverse Osmosis of Cottage Cheese Whey. 2. Influence of Flow Conditions", **J. Food Sci.**, 36, 395-396

Poyen, S., Quemeneur, F., Bariou, B., (1987), "Improvement of the Flux of Permeate in Ultrafiltration by Turbulence Promoters", **Int. Chem. Eng.**, 27(3), 441-447

Racz, I.G., Wassink, J.G., Klaasen, R., (1986), "Mass Transfer, Fluid Flow and Membrane Properties in Flat and Corrugated Plate Hyperfiltration Modules", **Desal.**, 60, 213-222

Ralph, M.E., (1985), **Flows in Wavy-Walled Tubes**, PhD thesis, Oxford University

Ralph, M.E., (1986), "Oscillatory Flows in Wavy-Walled Tubes", **J. Fluid Mech.**, 168, 515-540

Ralph, M.E., (1987), "Steady Flow Structures and Pressure Drops in Wavy-Walled Tubes", **J. Fluids Eng.**, 109, 255-261

Randerson, D.H., (1983), "Principles Governing Flux Rate in Membranes for Blood-Plasma Separation", **IMTEC Conference Proceedings**, Australia, Nov 8-10, 44-46

Rebsamen, E., (1981), "Fundamentals and Engineering Concept of a Pressure Filter for Dynamic Filtration", **Proceedings Symposium Societe Belge de Filtration**, Louvain-la-Neuve, 247-270

Reed, I.M. and Dudley, L.Y., (1987), **Adsorption of Proteins to Membranes,** BIOSEP report, Chemical Engineering Division, AERE Harwell

Savvides, C.N. and Gerrard, J.H., (1984), "Numerical Analysis of the Flow through a Corrugated Tube with Application to Arterial Prostheses", **J. Fluid. Mech.,** 138, 129-160

Semmelink, A., (1973), "Ultrasonically Enhanced Liquid Filtering", in **Ultrasonics Int. Conf. Proc.**, Imperial College, London, 7-10

Sergeev, S.I., (1966), "Fluid Oscillations in Pipes at Moderate Reynolds Numbers", **Fluid Dynamics,** 1, 121-122

Sobey, I.J., (1980), "On Flow Through Furrowed Channels. Part 1. Calculated Flow Patterns", **J. Fluid. Mech.,** 96(1), 1-26

Sobey, I.J., (1985), "Dispersion Caused by Separation During Oscillatory Flow Through a Furrowed Channel", **Chem. Eng. Sci.,** 40(11), 2129-2134

Soper, J.B. and Lee, M.P., (1987), **Statistics with Lotus 1-2-3,** Chartwell-Bratt (Publishing and Training Ltd)

Speaker, L.M., (1985), "Antifouling technology for Membranes and Non-permeable Surfaces", in **Fouling and Cleaning in Food Processing,** Second International Conference on Fouling and Cleaning in Food Processing, ed. D. Lund, E. Plett, C. Sandu, Wisconsin, 454-465

Stephanoff, K.D., Sobey, I.J., Bellhouse, B.J., (1980), "On Flow Through Furrowed Channels. Part 2. Observed Flow Patterns", **J. Fluid Mech.,** 96(1), 27-32

Suki, A., Fane, A.G., Fell C.J.D., (1986), "Modelling Fouling Mechanisms in Protein Ultrafiltration", **J. Memb. Sci.,** 27, 181-193

Thomas, D.G. and Watson, J.S., (1968), "Reduction of Concentration Polarization of Dynamically Formed Hyperfiltration Membranes by Detached Turbulence Promoters", **Ind. Eng. Chem. Process Des. Develop.**, 7(3), 397-401

Tukey, J.W., (1977), **Exploratory Data Analysis**, Addison-Wesley Publishing Company Inc., Phillipines

Turker, M. and Hubble, J., (1987), "Membrane Fouling in Constant Flux Ultrafiltration Cells", **J. Memb. Sci.**, 34, 267-281

Ury, J.F., (1962), "Viscous Damping in Oscillatory Viscous Columns", **Int. J. Mech. Sci.**, 4, 349-369

Van Der Waal, M.J. and Racz, I.G., (1989), "Mass Transfer in Corrugated-Plate Membrane Modules. 1. Hyperfiltration Experiments", **J. Memb. Sci.**, 40, 243-260

Van Der Waal, M.J., Stevanovic, S, Racz, I.G., (1989), "Mass Transfer in Corrugated-Plate Membrane Modules. 2. Ultrafiltration Experiments", **J. Memb. Sci.**, 40, 261-275

Velicangil, O., (1979), **Self-Cleaning Membranes for Ultrafiltration**, PhD thesis, Department of Chemical Engineering, University of Wales, Swansea

Wakeman, R., (1986), "Electrofiltration: Microfiltration and Electrophoresis", **The Chem. Engr.**, June, 65-70

Wallace, R.A. and Gable, R.J., (1974), "The Electret Effect in Cellulose Acetate Reverse Osmosis Membranes", **Polym. Eng. Sci.**, 14(2), 92-97

Wang, S.S., Davidson, B., Gillespie, C., Harris, L.R., Lent, D.S., (1980), "Dynamics of Enhanced Protein Ultrafiltration Using an Immobilized Protease", **J. Food. Sci.**, 45, 700-702

Winfield, B.A., (1986), "Waste Treatment with Reverse Osmosis Membranes", in **Membrane Separations in Biotechnology**, ed. W.C. McGregor, Marcel Dekker Inc, USA, Ch. 13, 355-373

Wu, D., Turner, N.M., Howell, J.A., (1990), "A New Method for Modelling the Time-Dependence of Permeation Flux in Ultrafiltration", to be published

Wyatt, I.D., (1988), **Heat Transfer During Oscillatory Flow in a Baffled Tube**, Department of Chemical Engineering, Cambridge University, Part 2 Project

Wyatt, J.M., Knowles, C.J., Bellhouse, B.J., (1987), "A Novel Membrane Module for Use in Biotechnology that has High Transmembrane Flux Rates and Low Fouling", in **Proceedings of International Conference on Bioreactors and Biotransformations**, ed. G.W. Moody and P.B. Baker, Gleneagles, Scotland, 166-172

Zahka, J. and Leahy, T.J., (1985), "Practical Aspects of Tangential Flow Filtration in Cell Separations", Advances in Chemistry Series, **Amer. Chem. Soc. Symp. Ser.**, 271, 51-69